

The Manufacture and Evaluation of Ceramic Membranes

By

Nelke C. Van de Ven

Thesis presented in partial fulfillment
of the requirements for the degree



of
MASTERS OF SCIENCE IN ENGINEERING
(CHEMICAL ENGINEERING)

In the department of Chemical Engineering
at the University of Stellenbosch.

Supervisors:

Professor L. Lorenzen

Professor I. Nieuwoudt

December 2001

Declaration

I, the undersigned, hereby declare that the work contained in this thesis is my own original work and has not previously in its entirety or in part been submitted at any university for a degree.

Nelke C. Van de Ven

12 April 2001

Summary

Inorganic membranes offer numerous advantages, such as stability at high temperatures and a long lifetime. Two Russian professors invented and patented a method for manufacturing a tubular ceramic membrane [Linkov & Belyakov, 1996]. Their membranes were used in the water purification industry and in gas separation research at the University of Stellenbosch [Keuler, 2000], but the performance of the membranes have been reported to be inconsistent. This project investigates the manufacturing process for these membranes in an attempt to improve their inconsistent performance. It also provides useful insight into relevant methods of evaluation.

Thirty-two ceramic membranes were successfully manufactured according to the patent by Linkov and Belyakov [1996], with slight modifications to the original manufacturing process. It was found for example that, to obtain membranes with a thickness of 1 mm, the casting suspension should contain 1.85 grams of water per gram of oxides, instead of the 1.15 grams of water per gram of oxides according to Linkov and Belyakov [1996]. The quality of the gypsum mould and the drying of the green body were found to be the most difficult steps in the manufacturing process.

Gas permeabilities for the manufactured membranes were typically 1×10^{-5} mol/m²sPa for argon and nitrogen and 4.5×10^{-5} mol/m²sPa for hydrogen. Water permeabilities for the manufactured membranes were typically 600 l/m²hbar. Gas permeability coefficients for the manufactured membranes were typically 5×10^{-15} m² for nitrogen and argon and 8×10^{-15} m² for hydrogen. The water permeability coefficients were typically 1.7×10^{-15} m².

The gas and water permeabilities for the manufactured membranes were typically 5 and 10 times higher than the permeability values for membranes manufactured by Linkov. Gas and liquid permeability coefficients for the manufactured membranes, taking into account the thickness of the membranes, were 7 and 14 times higher than those achieved with Linkov's membranes. Linkov's membranes were on average thinner than the manufactured membranes, while the permeability of the manufactured membranes was higher, explaining the high permeability coefficients.

The nitrogen and argon permeabilities, as well as their permeability coefficients were found to increase linearly with increasing pressure difference. However, the hydrogen permeability and permeability coefficients as well as the water permeability coefficients, were pressure independent.

The gas permeability results also indicated that the permeability of the manufactured membranes increased with increasing sintering time and temperature. Combining the gas permeability results with the selectivity results, manufactured membranes with higher gas permeability had the same selectivity as Linkov's membrane. Therefore the manufactured membranes had a higher capacity than Linkov's membranes, with the same selectivity. For the manufactured membranes, however, a lower mechanical strength was reported, typically 9 N/mm^2 , compared to the mechanical strength of Linkov's membrane which was roughly 10 times higher.

To further improve the membranes, a number of options can be investigated:

- The influence of a higher zirconia content on the ceramic membranes (between 29w% and 36.6w% for best mechanical strength).
- Increasing of the sintering time and temperature for a more sintered and mechanically stronger membrane.
- Examining the relationship between the permeability and mechanical strength of the membranes.

Opsomming

Anorganiese membrane besit 'n aantal voordele, soos stabiliteit by hoë temperatuur toepassings en 'n langer leeftyd. Twee Russiese professore het 'n vervaardigingsmetode vir buisvormige keramiekmembrane uitgevind en gepatenteer [Linkov and Belyakov, 1996]. Hulle membrane was gebruik in die watersuiwerings industrie sowel as in 'n gasskeidings ondersoek by die Universiteit van Stellenbosch [Keuler, 2000], maar die prestasie van die membrane was wisselvallig. Hierdie projek ondersoek die vervaardigings metode vir hierdie keramiekmembrane in 'n poging die wisselvallige prestasie van die membrane te verbeter. Die projek gee ook bruikbare insig in relevante toetsmetodes vir die vervaardigde membrane.

Twee en dertig keramiekmembrane was suksesvol vervaardig volgens die patent van Linkov en Belyakov [1996], met klein veranderings. Dit was byvoorbeeld gevind dat, om membrane te vervaardig met 'n dikte van 1 mm, die gietsuspensie 1.85 gram water per gram oxide moet bevat in plaas van een gram water per een gram oxides soos volgens Linkov en Belyakov [1996]. Die kwaliteit van die gips vorm en die droog van die groen liggaam was die moeilikste beheerbare stappe in die vervaardigingsproses.

Die gasdeurlaatbaarheid van die vervaardigde membrane was tipies 1×10^{-5} mol/m²sPa vir argon en stikstof en 4.5×10^{-5} mol/m²sPa vir waterstof. Waterdeurlaatbaarheid van die vervaardigde membrane was 600 l/m²hbar. Gasdeurlaatbaarheidskoeffisiente vir die vervaardigde membrane was tipies 5×10^{-15} m² vir argon en stikstof en 8×10^{-15} m² vir waterstof. Die waterdeurdringbaarheidskoeffisiente was tipies 1.7×10^{-15} m².

Die gas- en waterdeurlaatbaarheid vir die vervaardigde membrane was tipies 5 en 10 maal hoër as die deurlaatbaarheid waardes vir membrane wat deur Linkov vervaardig is. Gas- en waterdeurlaatbaarheidskoeffisiente vir die vervaardigde membrane, wat deur die dikte van die membrane beïnvloed word, was 7 en 14 maal hoër as die bereik met Linkov se membrane. Linkov se membrane was gemiddeld dunner as die vervaardigde membrane, terwyl die deurlaatbaarheid van die vervaardigde membrane hoër was, wat die hoë deurlaatbaarheidskoeffisiente verklaar.

Daar was gevind dat die argon- en stikstofdeurlaatbaarhede sowel as hulle deurlaatbaarheidskoeffisiente lineêr toeneem met toenemende drukverskil. Die waterstofdeurlaatbaarheid en -deurlaatbaarheidskoeffisiente sowel as die waterdeurlaatbaarheidskoeffisiente egter, was onafhanklik van die drukverskil.

Die gasdeurlaatbaarheid resultate het ook aangedui dat die deurlaatbaarheid van die vervaardigde membrane toeneem met toenemende sintertyd en -temperatuur. Wanneer die gasdeurlaatbaarheid resultate gekombineer word met die selektiwiteit resultate blyk dit dat, terwyl dat die vervaardigde membrane 'n hoër gasdeurlaatbaarheid het as Linkov se membrane, hulle nog steeds dieselfde selektiwiteit het. Dit beteken dat die kapasiteit van die vervaardigde membrane hoër is, terwyl die selektiwiteit van die skeidingsproses behou word. Vir die vervaardigde membrane was 'n laer meganiese sterkte gevind, tipies 9 N/mm^2 , terwyl die meganiese sterkte van Linkov se membrane omtrend 10 keer hoër was.

Verskeie opsies kan ondersoek word om die membrane te verbeter:

- Die invloed van 'n hoër zirkonia inhoud op die keramiekmembrane (tussen 29m% en 36.6m% vir beste meganiese sterkte).
- Verlenging van die sintertyd en -temperatuur om 'n meer gesinterde en meganies sterker keramiekmembraan te verkry.
- Ondersoek na die verhouding tussen deurlaatbaarheid en die sterkte van die membraan.

Acknowledgements

I would like to express my gratitude to the following people:

- Prof. L. Lorenzen, my supervisor, for his guidance and support over the past two years,
- Mr. D.N. Steenkamp of the Department of Physics at the University of Stellenbosch, for helping me with the vacuum oven and SEM,
- Mr. F.P.J. Muller for his “electrical assistance” but especially for making it possible to perform the three point bend tests on the membranes,
- Dr. E.P. Jacobs and Mr. D. Koen of the Department of Polymer Science at the University of Stellenbosch, for making it possible to perform water permeability tests on the membranes,
- Mrs. H. Divey of the Department of Chemical Engineering of the University of Cape Town for the Malvern particle analysis,
- Mnr. F.E. Greef, Dr. D.G. Bessarabov and Prof. M.F.C. van de Ven for always patiently listening to my problems and questions during my project, and always being prepared to help me with any of them,
- The staff from the technical workshop at the Department of Chemical Engineering at the University of Stellenbosch, for always being there if I needed them, and
- Everybody in the Department of Chemical Engineering, who made the past two years so interesting, I’ll never forget you!

Table of Contents

| | | |
|-----------|---|-----------|
| 1. | INTRODUCTION | 1 |
| 2. | LITERATURE STUDY AND BACKGROUND | 3 |
| 2.1 | Ceramics | 3 |
| 2.1.1 | <i>Structures of Ceramic Materials</i> | 4 |
| 2.1.1.1 | The Covalent Bond | 4 |
| 2.1.1.2 | The Ionic Bond | 5 |
| 2.1.1.3 | The Metallic Bond | 5 |
| 2.1.1.4 | <i>The Secondary Bond</i> | 5 |
| 2.1.1.5 | Crystal Structures | 6 |
| 2.1.2 | <i>Properties of Ceramic Materials</i> | 6 |
| 2.2 | Ceramic Membranes | 8 |
| 2.2.1 | <i>Design and Shape of the Ceramic Membrane</i> | 9 |
| 2.2.2 | <i>Porosity</i> | 10 |
| 2.2.3 | <i>Permselectivity and Permeability</i> | 11 |
| 2.2.4 | <i>Uses of Ceramic Membranes</i> | 12 |
| 2.3 | Manufacturing Ceramic Membranes | 14 |
| 2.3.1 | <i>Materials</i> | 14 |
| 2.3.2 | <i>Particle Shapes and Sizes</i> | 15 |
| 2.3.3 | <i>Sol-Gel Technique</i> | 16 |
| 2.3.4 | <i>Sintering</i> | 17 |
| 2.3.4.1 | <i>Sintering Mechanisms</i> | 18 |
| 2.3.4.1.1 | Evaporation-Condensation | 19 |
| 2.3.4.1.2 | Diffusion | 19 |
| 2.3.4.2 | Sintering Stages | 20 |
| 2.3.4.3 | Sintering and Porosity | 21 |
| 2.4 | Evaluating Ceramic Membranes | 22 |
| 2.4.1 | <i>Gas Permeation</i> | 23 |
| 2.4.2 | <i>Liquid Displacement Techniques</i> | 23 |
| 2.4.3 | <i>Permporometry</i> | 24 |
| 2.4.4 | <i>Bubble Point Technique</i> | 24 |
| 2.4.5 | <i>Microscopy Observation</i> | 25 |
| 2.4.5.1 | Atomic Force Microscopy (AFM) | 25 |
| 2.4.5.2 | Scanning Electron Microscopy (SEM) | 26 |
| 2.4.6 | <i>Nitrogen Adsorption-Desorption and Mercury Penetration</i> | 27 |
| 2.4.6.1 | Nitrogen Adsorption-Desorption | 27 |
| 2.4.6.2 | Mercury Porosimetry | 28 |

| | | |
|------------|---|-----------|
| 2.4.7 | <i>Thermoporometry</i> | 28 |
| 2.4.8 | <i>Transport Models</i> | 29 |
| 2.5 | Introduction to the Method of Membrane Manufacture | 30 |
| 2.5.1 | <i>Example 1 from Linkov's Patent</i> | 31 |
| 2.5.2 | <i>Outline of the Membrane Manufacturing Process</i> | 32 |
| 2.6 | Summary | 33 |
| | | |
| 3. | Raw Material Preparation | 34 |
| 3.1 | Raw Materials | 34 |
| 3.1.1 | <i>Gamma-Alumina (γ-Al₂O₃)</i> | 34 |
| 3.1.2 | <i>Zirconia</i> | 35 |
| 3.1.3 | <i>Alumina and Zirconia as a Composite Ceramic</i> | 36 |
| 3.2 | Burn Out of Organic Impurities | 37 |
| 3.2.1 | <i>TGA-Analysis</i> | 38 |
| 3.2.2 | <i>The Crystal Structure</i> | 39 |
| 3.3 | Separate Wet Milling | 39 |
| 3.3.1 | <i>The Influence of Milling Properties on the Size Distribution</i> | 40 |
| 3.3.1.1 | <i>Milling Time</i> | 41 |
| 3.3.1.2 | <i>Ball Ratio</i> | 41 |
| 3.3.2 | <i>Characterisation of the Milled Materials</i> | 43 |
| 3.4 | Summary | 45 |
| | | |
| 4. | Manufacture of Ceramic Membranes | 48 |
| 4.1 | Roller Stirring and Mixing-Obtaining a Stable Casting Suspension | 48 |
| 4.1.1 | <i>Water Removal</i> | 49 |
| 4.1.2 | <i>Amount of Water in the Casting Suspension</i> | 50 |
| 4.2 | Forming of the Green Body | 52 |
| 4.2.1 | <i>Background on Slip Casting</i> | 52 |
| 4.2.2 | <i>Forming of an Asymmetrical Green Body</i> | 53 |
| 4.2.3 | <i>The Gypsum Mould</i> | 55 |
| 4.2.4 | <i>Membrane Deposition</i> | 57 |
| 4.2.4.1 | <i>Method of Slip Casting</i> | 58 |
| 4.2.4.2 | <i>Slip Casting Time and Thickness</i> | 59 |
| 4.3 | Drying in a Constant Humidity Chamber | 60 |
| 4.4 | Sintering of the Green Body | 60 |
| 4.5 | The Manufactured Membranes | 62 |
| 4.6 | Summary | 63 |

| | | |
|------------|--|------------|
| 5. | Methods for the Evaluation of the Ceramic Membranes | 66 |
| 5.1 | Chosen Evaluation Methods | 66 |
| 5.2 | Evaluation of the Permeability | 67 |
| 5.2.1 | <i>Membrane Testing Module</i> | 67 |
| 5.2.2 | <i>Gas and Liquid Permeability Coefficients, K_g and K_l</i> | 68 |
| 5.2.3 | <i>Gas Permeability Tests</i> | 69 |
| 5.2.3.1 | Experimental Set Up | 70 |
| 5.2.3.2 | Permeability | 71 |
| 5.2.3.3 | Selectivity | 71 |
| 5.2.3.4 | Gas Permeability Model | 72 |
| 5.2.4 | <i>Liquid Permeability Tests</i> | 75 |
| 5.2.4.1 | Experimental Set Up | 75 |
| 5.2.4.2 | Liquid Permeability Modelling | 76 |
| 5.3 | Evaluation of Mechanical Strength | 77 |
| 5.3.1 | <i>Experimental Set Up for the 3-Point Bend Test</i> | 78 |
| 5.3.2 | <i>Determination of the Flexural Strength</i> | 79 |
| 5.4 | Scanning Electron Microscopy (SEM) Evaluation | 80 |
| 5.5 | Summary | 81 |
| | | |
| 6. | Evaluation of the Manufactured Ceramic Membranes | 82 |
| 6.1 | Gas Permeability Results | 82 |
| 6.1.1 | <i>Variance Between the Manufactured Membranes</i> | 83 |
| 6.1.2 | <i>Influence of Sintering Time on Gas Permeability</i> | 84 |
| 6.1.3 | <i>Influence of Sintering Temperature on Gas Permeability</i> | 86 |
| 6.1.4 | <i>Comparison to Linkov's Membranes and Other Commercial Membranes</i> | 88 |
| 6.1.5 | <i>Applying the Gas Permeability Model</i> | 91 |
| 6.2 | Selectivity Results | 92 |
| 6.2.1 | <i>Influence of Sintering Time and Temperature on Ideal Selectivity</i> | 94 |
| 6.2.2 | <i>Influence of Permeability on Ideal Selectivity</i> | 96 |
| 6.2.3 | <i>Comparison to Theoretical Selectivity and Linkov's Membrane</i> | 97 |
| 6.2.3.1 | Comparison to the Theoretical Selectivity | 98 |
| 6.2.3.1 | Comparison to the Selectivity Values for Linkov's Membrane | 99 |
| 6.3 | Water Permeability Results | 99 |
| 6.4 | Permeability Coefficients | 102 |
| 6.4.1 | <i>Gas Permeability Coefficients</i> | 102 |
| 6.4.2 | <i>Water Permeability Coefficients</i> | 106 |
| 6.5 | Mechanical Strength | 108 |
| 6.6 | SEM Results | 110 |
| 6.7 | Conclusions | 111 |

| | | |
|------------|--|------------|
| 6.7.1 | <i>Gas Permeability</i> | 111 |
| 6.7.2 | <i>Selectivity</i> | 113 |
| 6.7.3 | <i>Water Permeability</i> | 113 |
| 6.7.4 | <i>Permeability Coefficients</i> | 114 |
| 6.7.4.1 | Gas Permeability Coefficient | 114 |
| 6.7.4.2 | Water Permeability Coefficient | 115 |
| 6.7.5 | <i>Mechanical Strength</i> | 115 |
| 6.8 | Summary | 116 |
| 7. | Conclusions and Future Work | 117 |
| 7.1 | Conclusions | 117 |
| 7.2 | Recommendations for Future Work | 121 |
| 8. | List of Symbols | 123 |
| 9. | References | 124 |
| Appendix A | Linkov's Patent | A-1 |
| Appendix B | Raw material Specifications and Phase Diagrams | B-1 |
| Appendix C | TGA Results | C-1 |
| Appendix D | Particle Size Distribution | D-1 |
| Appendix E | Slip Casting | E-1 |
| Appendix F | List of Tested Manufactured Membranes | F-1 |
| Appendix G | Gas Permeability Results | G-1 |
| Appendix H | Mathematical Derivation of K_i and K_g | H-1 |
| Appendix I | Water Permeability Results | I-1 |
| Appendix J | 3-Point Bend Test Results | J-1 |
| Appendix K | Some SEM Results | K-1 |

List of Tables

| | | |
|------------|--|-----|
| Table 2.1 | Pores, pore sizes and filtration types | 11 |
| Table 2.2 | Advantages and disadvantages of ceramic membranes | 13 |
| Table 3.1 | Alumina phases observed with increasing temperature | 35 |
| Table 3.2 | Zirconia phases observed with increasing temperature | 36 |
| Table 3.3 | Phase content and properties of Al ₂ O ₃ -ZrO ₂ composites | 37 |
| Table 3.4 | Powder-size distribution properties | 45 |
| Table 4.1 | Influence of H ₂ O content on the thickness of the green body | 51 |
| Table 4.2 | Sintering temperatures and times | 61 |
| Table 4.3 | Manufactured membranes summarised | 62 |
| Table 4.4 | Number of membranes sintered, cracked and tested | 63 |
| Table 5.1 | Maximum flexural strength at a certain force for a membrane | 80 |
| Table 6.1 | Variance between the gas permeability of the manufactured membranes and commercial membranes | 83 |
| Table 6.2 | Highest and lowest permeability values at P _m = 105 kPa | 88 |
| Table 6.3 | Permeability values for alumina ceramic membranes found in literature | 89 |
| Table 6.4 | Highest and lowest ideal selectivity values at P _m = 105 kPa, all for a sintering temperature of 1300°C | 95 |
| Table 6.5 | Table of selectivity values | 97 |
| Table 6.6 | Typical water permeability values for tubular ceramic membranes at 20°C and the water permeability values for Linkov's membrane and the manufactured membranes 38b and 53a | 101 |
| Table 6.7 | Comparing gas permeability coefficients | 105 |
| Table 6.8 | Water permeability coefficients for the two manufactured membranes, Linkov's membrane and two coefficients found in literature | 106 |
| Table 6.9 | Liquid permeability coefficients compared to the coefficients obtained from the gas permeability coefficients | 107 |
| Table 6.10 | Summarised mechanical strength results | 109 |

List of Figures

| | | |
|-------------|--|----|
| Figure 2.1 | Dependence of Intrinsic Properties | 7 |
| Figure 2.2 | Four different microstructures of ceramics | 8 |
| Figure 2.3 | Cross-section view of a tubular cross-flow filtration membrane | 9 |
| Figure 2.4 | Typical asymmetric membrane | 10 |
| Figure 2.5 | A production route for a typical asymmetric ceramic membrane | 14 |
| Figure 2.6 | The ceramic membrane and approximate particle sizes based on the globular model of ceramic materials composition | 16 |
| Figure 2.7 | The sintering process: decrease in pore volume and increase in density, with time, during sintering | 18 |
| Figure 2.8 | The four sintering mechanisms | 18 |
| Figure 2.9 | Transport models | 29 |
| Figure 2.10 | Schematic diagram of the ceramic membrane manufacturing process | 32 |
| Figure 2.10 | Schematic diagram of the ceramic membrane manufacturing process | 34 |
| Figure 3.1 | A model of the spinel structure | 34 |
| Figure 3.2 | Heating and cooling curves for the vacuum furnace | 37 |
| Figure 3.3 | Particle size distribution results at certain times for the ratios oxide:balls:water of 1:2:1 and 1:4:1 | 42 |
| Figure 3.4 | Cumulative mass distributions of the alumina before milling and after 80 h of milling | 42 |
| Figure 3.5 | Cumulative mass distributions of the zirconia before milling and after 60 h of milling | 43 |
| Figure 3.6 | Alumina powder before and after milling | 44 |
| Figure 2.10 | Schematic diagram of the ceramic membrane manufacturing process | 48 |
| Figure 4.1 | Influence of the amount of water in the casting suspension on the membrane thickness | 51 |
| Figure 4.2 | The casting suspension | 54 |
| Figure 4.3 | Stainless-Steel contra mould of the gypsum mould | 56 |
| Figure 4.4 | Drawing and picture of a typical gypsum mould | 56 |
| Figure 4.5 | Influence of the time the casting suspension is in the gypsum mould on the membrane thickness | 59 |
| Figure 4.6 | Typical ramp sintering profile for sintering the manufactured green bodies | 61 |
| Figure 5.1 | Schematic diagram of the evaluation of ceramic membranes | 66 |
| Figure 5.2 | Picture of tested membrane mounted between 2 perspex tubes | 67 |
| Figure 5.3 | Schematic cross-section drawing of the testing module with the membrane | 68 |
| Figure 5.4 | Testing module, with mounted membrane inside, coupled to the gas permeability set-up | 68 |
| Figure 5.5 | Experimental set-up for the gas permeability tests | 70 |

| | | |
|--------------|--|-----|
| Figure 5.6 | Experimental set-up of the liquid permeability tests | 76 |
| Figure 5.7 | Schematic diagram of 3-point bend tests | 77 |
| Figure 5.8 | Picture of bend-test set-up | 78 |
| Figure 6.1 | Argon, nitrogen and hydrogen permeabilities for membrane 53a | 83 |
| Figure 6.2 a | Average hydrogen permeabilities for different sintering times at a sintering temperature of 1300°C and an average pressure of 105 kPa | 85 |
| Figure 6.2 b | Average argon and nitrogen permeabilities for different sintering times at a sintering temperature of 1300°C and an average pressure of 105 kPa | 85 |
| Figure 6.3 a | Average hydrogen permeabilities for different sintering temperatures at a sintering time of 1 hour and an average pressure of 105 kPa | 87 |
| Figure 6.3 b | Average argon and nitrogen permeabilities for different sintering temperatures at a sintering time of 1 hour and an average pressure of 105 kPa | 87 |
| Figure 6.4 | Average nitrogen permeability of the manufactured membranes (sintered at 1300°C for 1 hour) compared to some nitrogen permeabilities from table 6.2, as well as to the nitrogen permeability of Linkov's membrane. | 90 |
| Figure 6.5 | Comparison of the $Q_i P_i / A \Delta P$ vs. P_m plot and the F_o vs. P_m plot | 92 |
| Figure 6.6 | Ideal selectivity results for membrane 53a over the hydrogen pressure range | 93 |
| Figure 6.7 | Average ideal selectivities for different sintering times at a sintering temperature of 1300°C and an average pressure of 105 kPa | 94 |
| Figure 6.8 | Average ideal selectivities for different sintering temperatures at a sintering time of 1 hour and an average pressure of 105 kPa | 95 |
| Figure 6.9 | Nitrogen/argon selectivity as a function of nitrogen permeability | 96 |
| Figure 6.10 | Theoretical and Linkov's selectivities compared to the average selectivities for the manufactured membranes at $P_m=105$ kPa and to the average of the highest selectivities | 97 |
| Figure 6.11 | Water permeability for membrane 53a | 100 |
| Figure 6.12 | Gas permeability coefficients for membrane 53a | 103 |
| Figure 6.13 | Average gas permeability coefficients for different sintering times at a sintering temperature of 1300°C | 104 |
| Figure 6.14 | Average gas permeability coefficients for membranes sintered for 1 hour at different sintering temperatures | 105 |
| Figure 6.15 | Increasing force applied on membrane 54 with a bend test until fracture occurs | 108 |
| Figure 6.16 | Maximum force and maximum flexural strength of three manufactured membranes compared | 109 |
| Figure 6.17 | SEM photos of Linkov's membrane | 111 |

1. Introduction

A membrane can be defined as a selective barrier between two phases. In recent years, the use of inorganic membranes in separation technologies has given rise to much interest. Inorganic membranes offer numerous advantages, such as, stability at high temperatures and pressure resistance (no compression of the membrane), chemical stability, insensitivity to bacterial action and longer lifetime.

Commercially available ceramic membranes are generally of the cross-flow design and are tubular in shape. They consist of a support layer, and a thin membrane layer. The support provides strength and makes a sufficiently high flow rate possible, while the membrane layer acts as the functional part of the membrane. In order to facilitate a high permeate flow rate through the membrane wall and yet obtain the required pore size at the membrane-filtrate interface, a series of graded membranes is usually laid down.

The manufacturing of these asymmetric membranes generally entails two separate steps, viz. the preparation of the support followed by the coating of the support with the thin membrane layer by a process such as, for example, sol-gel deposition. This manufacturing method requires high precision operations and clean room conditions and, when applied to large membrane surfaces, has low reproducibility and is extremely labour intensive due to a large number of technological operations involved [Linkov & Belyakov, 1996]. It is therefore an objective of this project to investigate the manufacture of an asymmetrical ceramic membrane in one technological operation, combining the support and membrane layer steps into one single “step”.

Two Russian researchers, Prof. Linkov and Prof. Belyakov, have invented and patented such a manufacturing method for a ceramic membrane [Linkov & Belyakov, 1996]. The membranes have been used in the water purification industry, as well as in gas separation research at the University of Stellenbosch, but the strength and performance of the membranes have been reported to be inconsistent and unreliable. Also an aim in this project is therefore to examine a manufacturing method for these ceramic membranes, both to determine whether it is possible to manufacture the

membranes as well as to gain information and possibly improve on the poor and varying performance of these membranes.

Summarised the three main objectives of this project are:

- To manufacture ceramic membranes as described in the patent by Linkov and Belyakov.
- To investigate and possibly improve this manufacturing method of the ceramic membrane.
- To test the permeability, strength and structure of the manufactured ceramic membranes.

As such, the findings from this study provide insight in a manufacturing method of an asymmetric ceramic membrane with support- and membrane layer, in one technological operation, as well as insight in the methods to evaluate such a ceramic membrane.

2. Literature Study and Background

In this chapter, the background and literature overview related to ceramic membrane manufacturing and the evaluation of ceramic membranes is discussed. It includes information about the properties of ceramic materials and ceramic membranes, the manufacturing of ceramic membranes and a number of evaluation methods to characterise (ceramic) membranes. Lastly it shortly introduces the manufacturing method that was implemented to manufacture the membranes for this project.

2.1 Ceramics

Many of the membranes that are used in industry are polymeric membranes. Recently the use of ceramic materials to manufacture membranes has received much attention. To better understand the advantages of ceramic materials, this paragraph discusses ceramics.

Originally, ceramics were made from minerals like clay, bauxite (an impure hydrated aluminium oxide), quartz, slate-stone and feldspar. During the past 35 years, a large diversity of synthesised combinations has emerged [Burggraaf and Keizer, 1991].

Technically, ceramics consist of two groups:

- Functional ceramics: these ceramics can be used in electrical, magnetic, di-electric or optical applications.
- Structural ceramics (or engineering ceramics): these ceramics are used because of their mechanical properties, like hardness, stiffness and stability - including chemical stability, as well as their thermal properties.

The ceramic materials that are used to manufacture ceramic membranes are always structural ceramics. A typical engineering ceramic is an inorganic compound consisting of one or more metals with a non-metallic element like oxygen, carbon, nitrogen, borium and silicium. Ceramics are therefore, often called oxides, carbides, nitrides, etc [Welles et al., 1988].

The boundaries of materials like metals are pretty much reached and the realisation of a number of new products is impossible with these materials [Van de Ven et. al, 1988]. People are therefore willing to spend money on ceramic materials research and technical development.

2.1.1 Structures of Ceramic Materials

Ceramic membranes will have a very different structure than polymeric membranes. To better understand ceramic membranes, the materials these membranes are made of and their structure, this paragraph is dedicated to the structures of ceramic materials

All materials contain chemical elements. The construction of the atoms of these elements is mostly responsible for the behaviour of the atoms towards other atoms or towards atoms of another element. All of this influences the formation and structure of materials.

Atoms strive to a completely filled outer orbit, which represents a stable situation for an atom. This stable situation can also be accomplished by bonding with other atoms. The type of bond between the different atoms determines the characteristics of materials. There are three types of *primary* bonds, the covalent, the ionic and the metallic bonds. *Secondary* bonds like the Van der Waals bond are also present. Ceramic materials have ionic as well as covalent characteristics, sometimes even combined with Van der Waals bonds. Mixtures of these bonding types provide ceramics their hardness, stiffness and stability [Van de Ven et al., 1988].

2.1.1.1 *The Covalent Bond*

An atom can reach a stable situation in its outer orbit by sharing one or more electrons with an adjacent atom. Three-dimensional structures of pure covalent bonds can only be formed when a minimum of four electrons are shared. The negative charges of these bonds will provide repulsive forces between them and the bonds will be positioned in such a way that the distance between them is maximised. This positioning partly determines the structure. The extremely directed bonding strength

of covalent ceramic materials results in high melting points, hardness and a very strong material.

2.1.1.2 *The Ionic Bond*

When one atom provides an electron and the other atom receives an electron, an ionic bond originates. This way, both atoms obtain electron-orbits of the noble gas type. The ionic character of a bond is linked to the electron-negativity of the atom. The electron-negativity of an atom is the ability of the atom to attract electrons in the molecule. The larger the difference in electron-negativity between two atoms, the more ionic the bond becomes to eventually turn into a pure ionic bond. Characteristics of the ionic bond are the following [Van de Ven et al., 1988]:

- The radius and the charge of the ion determine the structure. Preferably the structure should be as closely packed as possible.
- Bonding forces are not directed, but evenly spread over all neighbouring ions.
- Only a little electrical conduction is possible since the electrons are bound to the ions.
- They have reasonably high melting points.

2.1.1.3 *The metallic bond*

A characteristic of the metallic bond is that the valence electrons are not bound to a certain atom, but they can move around freely in the metal-structure. The bond exists because of the attraction of free electrons by the metal electrons and vice versa. The bonding force is not directed. The good heat conduction and low electrical resistance is as a consequence of the moving electrons. In ceramics this bond is almost non-existing, but it is still able to differentiate between metal and ceramic properties.

2.1.1.4 *The secondary bond*

Molecules that are close to one another will attract one another, i.e. the Van der Waals force. The Van der Waals force increases with molecule mass and at the same time

the melting and boiling point will become higher. The Van der Waals bonds are relatively weak bonds (they are secondary bonds).

In ceramic materials, Van der Waals bonds can, next to primary bonds, play an important role. They are especially significant in plate structures, like clay and graphite. These materials have strong primary bonds in the plate direction, and are kept together by the Van der Waals forces, resulting in anisotropy.

2.1.1.5 *Crystal Structures*

Ions and atoms want to be in a state of minimal internal energy, leading to a regularly ordered structure. When such an ordered structure repeats itself over large distances, it is called a crystal structure.

2.1.2 Properties of Ceramic Materials

Materials in the “engineering ceramics” group always have one or more of the following properties [Van de Ven et al., 1988]:

- hardness,
- high wear resistance,
- resistance to high temperatures,
- low specific weight,
- low ductility,
- low thermal expansion coefficient,
- chemically inert, and
- low electrical conduction.

The crystal structures of ceramics are complex since they accommodate more than one element of widely different atomic sizes. Besides crystals, a ceramic also often has a glass-phase and pores. The kind and amount of phases and pores, as well as their size, form, orientation and distribution are known as the so-called microstructure of the ceramic material.

The mechanical properties of technical ceramics depend, via the production technology, to a large extent on the microstructure. The intrinsic properties (expansion, heat-conduction) depend on parameters like composition, chemical bonding and crystal structure, on atomic scales. The dependence of the properties of a membrane on the chemical composition and the production technology is shown in **figure 2.1**.

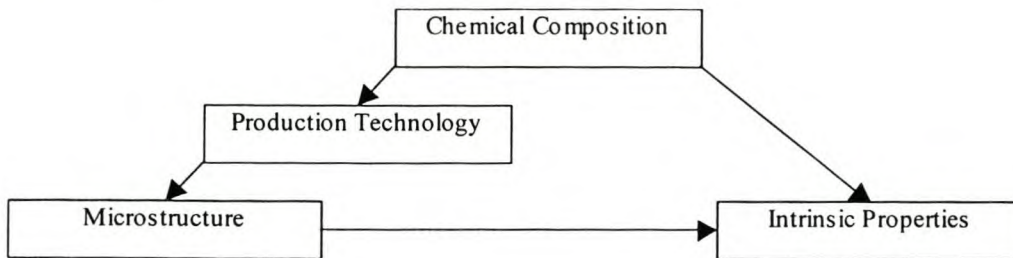


Figure 2.1: Dependence of Intrinsic Properties [Welles et al., 1988]

When using ceramic materials for technical applications, however, these materials have the following restrictions:

- difficulties considering production with *reproducible* quality,
- mechanical properties, *brittleness*, and
- *non-destructive inspection*.

The first two points, reproducibility and brittleness, are determined by how well the microstructure of the material can be controlled. Controlling the raw materials and the manufacture process controls the microstructure. Non-destructive inspection can be applied to the final product, where the product is inspected for the presence of, for example, cracks or holes. However, it is important to if possible, inspect the product before it reaches it's final stage to prevent wasting time and or money [Welles et. al., 1988].

Ceramic materials are becoming increasingly important in the modern industry, and they are new with regards to certain applications. Therefore, it is important to know what the properties of the final product are or can be. The microstructure has a big influence on the properties of the final product. **Figure 2.2** shows four different kinds of microstructures.

Prominent features in **figure 2.2** are the grain boundaries and the pores. Especially the pores and mistakes like scrapes and cracks will have a negative impact on the mechanical properties.

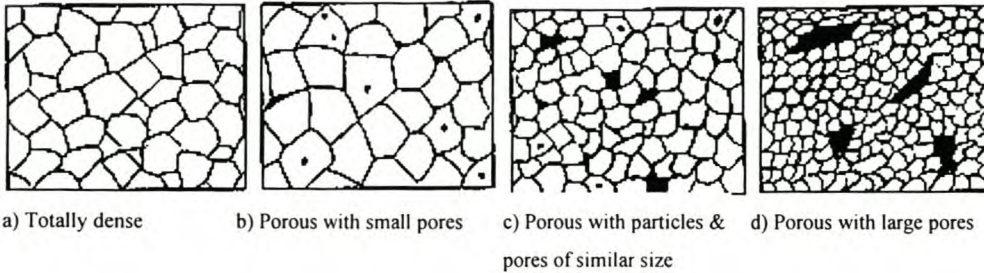


Figure 2.2: Four different microstructures of ceramics [Van de Ven et al., 1988]

The bonding types of ceramic materials make them very resistant to chemicals. Since many ceramics are composed of metal oxides, further oxidation is prevented (they are already oxidised). The strength of the bonds provides ceramics with hardness, a high melting point and stiffness. This strength also makes it almost impossible for the ceramic to deform while a stress is applied; the ceramic material will, therefore, keep its form until a certain stress has been reached, after which fracture will occur.

Ceramic materials can resist high-pressure stresses much better than shear stresses because of their low ductility. Small cracks existing in the ceramic are pressed together by pressure stresses, whereas a shear stress will pull the crack apart and thus increase it [Van de Ven et al., 1988 and Welles et al., 1988].

2.2 Ceramic Membranes

The use of inorganic membranes in separation technologies is relatively new, and has given rise to much interest in recent years. This is due the inherent properties of inorganic membrane materials that are generally more stable chemically, structurally and thermally than organic membranes. Ceramic membranes represent a distinct class of inorganic membranes. Other “new” membrane materials are materials such as glasses, carbon, metals and organic-inorganic polymers.

2.2.1 Design and Shape of the Ceramic Membrane

Commercially available ceramic membranes are generally operated in cross-flow fashion, and are tubular in shape, see **figure 2.3**. The filtrate or feed is pumped under pressure into one end of the tube. The pressure difference generated across the membrane wall will cause some of the feed to pass through it as permeate, leaving a concentration of the feed particles in the remaining fluid (the retentate). The retentate exits through the opposite end of the tube containing the filtered particles. The feed thus flows parallel to the membrane surface, while the permeate flows in the transverse direction, hence the term 'cross-flow' filtration.

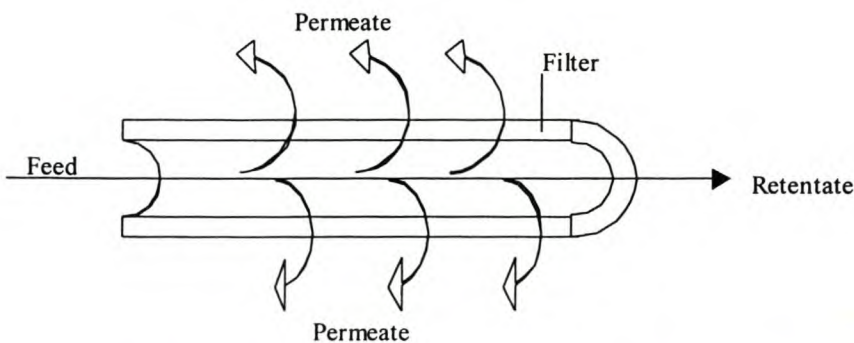


Figure 2.3: Cross-section view of a tubular cross-flow filtration membrane.

This flow geometry reduces 'fouling' of the membrane surface compared with that in other orientations because filtered particles are removed in the retentate. The inner surface of the tube performs the filtration action. A thin porous layer, the *membrane layer*, of sintered ceramic material on this surface acts as the functional part of the membrane, see **figure 2.4**. In order to facilitate a high permeate flow through the membrane wall and yet obtain the required pore size at the membrane-filtrate interface, a series of graded membrane-layers are often laid down. This grading of pore size leads to the term 'asymmetric' being applied to the membrane. The thickness of this composite membrane should be minimised in order to maximise the permeate-flow. The membrane support structure, the *support layer*, should be strong but highly permeable since its function is to strengthen the membrane without hindering fluid flow [Clark et al., 1988].

Recent efforts have been directed towards the development of ceramic membranes in which the microstructure is tailored to application, well characterised and reproducible.

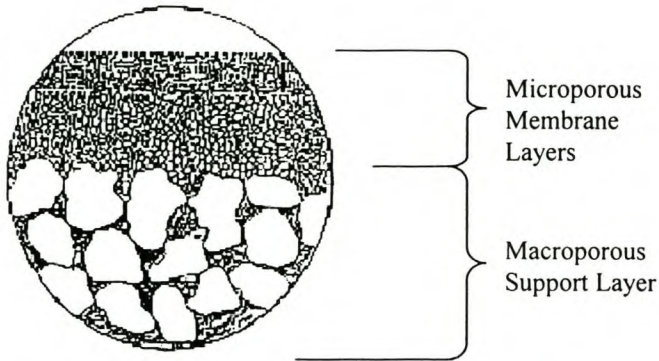


Figure 2.4: Typical asymmetric membrane [Clark et al., 1988]

2.2.2 Porosity

In separation technologies based on permselective membranes, the difference in filtered species ranges from micron sized particles to nano-sized molecules such as gas molecules. As indicated in **table 2.1**, one can see that the porosity of the membrane has to be adapted to the products to be separated.

The porosity, or void- or fluid volume fraction, of a porous medium is defined by the ratio fluid volume (U_f), over total volume (U_0):

$$\epsilon = \frac{U_f}{U_0} \quad (2.1)$$

Although the production of porous ceramics with controlled pore size and porosity is not well documented yet [Clark et al., 1988], much information is present concerning different pore sizes and filtration types.

Table 2.1. Pores, pore sizes and filtration types

| Pores | Filtration Type* | Pore Sizes IUPAC** [nm] | Adsorption Mechanism** | Operating Pressure *** [bar] |
|----------------------------|--|-------------------------|---|------------------------------|
| Macro-pores | Micro-filtration | > 50 | Multilayer adsorption | 0.07 - 1.7 |
| | | $10^2 - 10^4$ **** | | |
| Meso-pores | Ultra-filtration | 2 – 50 | Capillary condensation | 0.7 – 6.9 |
| | | $1-10^2$ **** | | |
| Micro-pores/ Nano-pores | Nano-filtration, Pervaporation, Gas separation | < 2 | Liquid filling | < 13 |
| | Reverse osmosis | 0.1-1 **** | Rejects 99.9+% of viruses, bacteria and pyrogens. *** | 13.8 - 68.9 |

* Cot et al., 1994, ** Calvo et al., 1997, *** Osmonics, 1992, **** Larbot et al., 1987.

2.2.3 Permselectivity and Permeability

Two of the most important parameters that describe the separation performance of a membrane are its permselectivity and permeability. Permselectivity is the ability of the membrane to separate the permeate from the retentate, and for ultra filtration this is usually expressed in terms of rejection or retention coefficients:

$$R = 1 - C_p/C_r \quad (2.2)$$

C_p and C_r represent the concentrations of the rejected species in the permeate and retentate respectively. Essentially the rejection coefficient, R , gives a fraction of the rejected species that “leaks” through the membrane.

Liquid permeability is typically used to provide an indication of the capacity of a membrane; a high flux equals a high throughput. The flux through a porous medium is proportional to the fluid pressure gradient in that particular direction. Darcy’s law, a purely empirical law introduced in 1876, states that if discharge through a porous medium is in the x -direction, then:

$$q = -\frac{k}{\mu} \cdot \frac{dP}{dx} \quad (2.3)$$

with μ the dynamic viscosity of the fluid and k the hydrodynamic permeability coefficient, or Darcy-permeability coefficient. The dynamic viscosity of the fluid (μ) and the permeability coefficient of the porous medium (k) are constants for each fluid and porous media indicating a linear relationship between the pressure gradient (dP/dx) and the superficial velocity, (q):

$$-\frac{dP}{dx} = \frac{\mu}{k} \cdot q = A \cdot q \quad (2.4)$$

At high fluid-flow velocities a non-linear deviation from equation (2.4) was experimentally observed. Forchheimer then in 1937 proposed the following empirical equation [du Plessis, 2000]:

$$-\frac{dP}{dx} = A \cdot q + B \cdot q^2 \quad (2.5)$$

The coefficients A and B of equations (2.3) and (2.4) are expressed in terms of measurable parameters with the Carman-Kozeny equation (for A) and the Burke-Plummer equation (for B):

$$A = \frac{150 \cdot (1 - \epsilon)^2}{D^2 \cdot \epsilon^3} \mu \quad (2.6)$$

$$B = \frac{1.75 \cdot (1 - \epsilon)}{D \cdot \epsilon^3} \rho \quad (2.7)$$

with D the effective diameter of the solid grains of the porous medium and ϵ the porosity.

2.2.4 Why Ceramic Membranes

Natural membranes are used by all life forms for separation of nutrients, selective protection from toxins, photosynthesis, etc. The commercial application of micro-

porous ceramic membranes began in the late 1970's, focussing mostly on liquid phase micro- and ultra-filtration [Burggraaf and Keizer, 1991]. As a result of their superior mechanical-, thermal-, and chemical properties compared to polymeric membranes, considerable attention has been focussed on high-temperature-gas-phase-applications including filtration, gas separation and ceramic membrane reactors [Gallaher & Liu, 1994]. Besides their advantages, however, ceramic membranes do have some disadvantages. As an overview, **table 2.2** shows the advantages and disadvantages of ceramic membranes.

Table 2.2: Advantages and disadvantages of ceramic membranes [Burggraaf and Keizer, 1991]

| Advantages: | Disadvantages: |
|---|---|
| 1) Stability at high temperatures | 1) Sealing for high-temperature applications may be complicated |
| 3) Mechanical Stability | 2) Brittle character |
| 2) Chemical Stability | 3) Relatively high capital installation costs |
| 4) Long lifetime | 4) Relative high modification costs in case of defects |
| 5) High flux and less fouling | |
| 6) Rigorous cleaning allowable | |
| 7) Good control of pore dimensions and pore size distribution | |
| 8) Low energy costs | |

The rate of advances toward industry-scale applications of porous inorganic membranes has been rapid in recent years [Hsieh, 1996]. Much attention has been paid to ceramic membranes exhibiting a nano-porous structure with the aim of new membrane processes for the nano-filtration of liquids [Guizard et al., 1990], pervaporation [Ulhorn & Burggraaf, 1991], gas separation [Ulhorn & Burggraaf, 1991 and Klein & Giszpenc, 1990] and catalysis [Armor, 1989].

The increasing energy costs have made membrane processes even more economically attractive. Generally, membrane technology is a competitive separation method for small to medium volumetric flow-rate applications and for either primary separation or when the purity level required is in the 95 to 99% range [Hsieh, 1996].

2.3 Manufacturing Ceramic Membranes

Ceramic membranes can be prepared by conventional methods such as pressing, extrusion, and slip casting. These techniques are usually preceded by e.g. powder preparation and mixing, and then followed by sintering.

A common production route for a ceramic membrane is presented in **figure 2.5** [Clark et al., 1988]. The manufacture of ceramic membranes is normally carried out in two stages: the production of the support structure, 1(a-e) in **figure 2.5**, and the application of the membrane layer, 2(a-b) in **figure 2.5**. Methods such as coating, chemical vapour deposition and sol-gel techniques are techniques frequently used for the application of the membrane layer. One of these techniques, the sol-gel technique, will be discussed in more detail in paragraph 2.4.3.

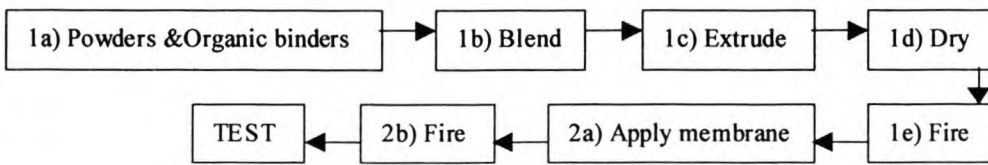


Figure 2.5: A production route for a typical asymmetric ceramic membrane [Clark et al., 1988]

2.3.1 Materials

Membranes have to work in liquid or gaseous media, usually under harsh conditions. The major type of ceramics used in ceramic membrane manufacturing therefore consists of refractory oxides: alumina, zirconia or titania [Anderson et al., 1988, Larbot et al., 1989, Doyen et al., 1996, and Bae et al., 1997]. Nevertheless, many other ceramic materials can be used [Cot et al., 1994]. The membranes manufactured and evaluated in this project contained 70% alumina, 29% zirconia and 1% yttria.

Reasons for the addition of zirconia to the alumina are that zirconia-dispersed alumina ceramics exhibit better thermal and mechanical properties, such as fracture toughness and fracture strength, than conventional alumina ceramics [Wang, 1996]. Galaj et al.

[1990] argued that it is essential to match the nature of the membrane surface with the fluid, or gas for that matter, to be filtrated.

2.3.2 Particle shapes and sizes

Characteristics of the starting powder such as particle shape and size-distribution obviously influence the characteristics of the membrane. The size and size-distribution of the starting particles, for example, are essential in the sintering step [Cot et al., 1994].

Generally, ideal packing of mono-sized quasi-spherical particles generates inter-particle voids for which the size, shape and porous volume (porosity) will depend on the chosen arrangement model. Particle packing in ceramic membranes can be assumed as randomly arranged with a tortuous porosity in the 30-40% range. When particles deviate from the spherical shape, different porous structure can be obtained [Cot et al., 1994]. According to the patent by Maebashi [1990], selecting the particle diameter of the coarse alumina could readily control the average pore size of the membrane.

Figure 2 in Appendix A shows a globular model of the ceramic material compositions [Linkov and Belyakov, 1996]. According to this model a substantial increase in milling time affects in the first place, not particle sizes but packing modes of the particles. For instance, more dense packing in agglomerates consisting of 5 particles give pores of smaller diameter than in a (less dense packing) 6 particle agglomerate. According to Linkov's patent the spherical particles with a diameter of 4 nm packed in 5- and 6-member agglomerates are responsible for the formation of 2,6 and 4 nm pores.

This phenomenon is explained also by Reed [1988]: "The void fraction increases with a decrease in particle size in the small-size range. This behaviour apparently arises because large, heavy particles exert a sufficiently great force through their points of contact, when vibrated or otherwise distributed, to breakdown arching and bridging effects. Small particles on the other hand, do not exert such a force since the number of contacts per particle remains the same as long as the same type of packing is preserved."

Figure 2.6 indicates what type of packing may be expected from the larger particles in the support part (A) and the smaller particles in the membrane part (B) of the membrane. The particle sizes in both parts can now be approximated. This approximation is based on a model and on the assumption that all particles are round which is unlikely.

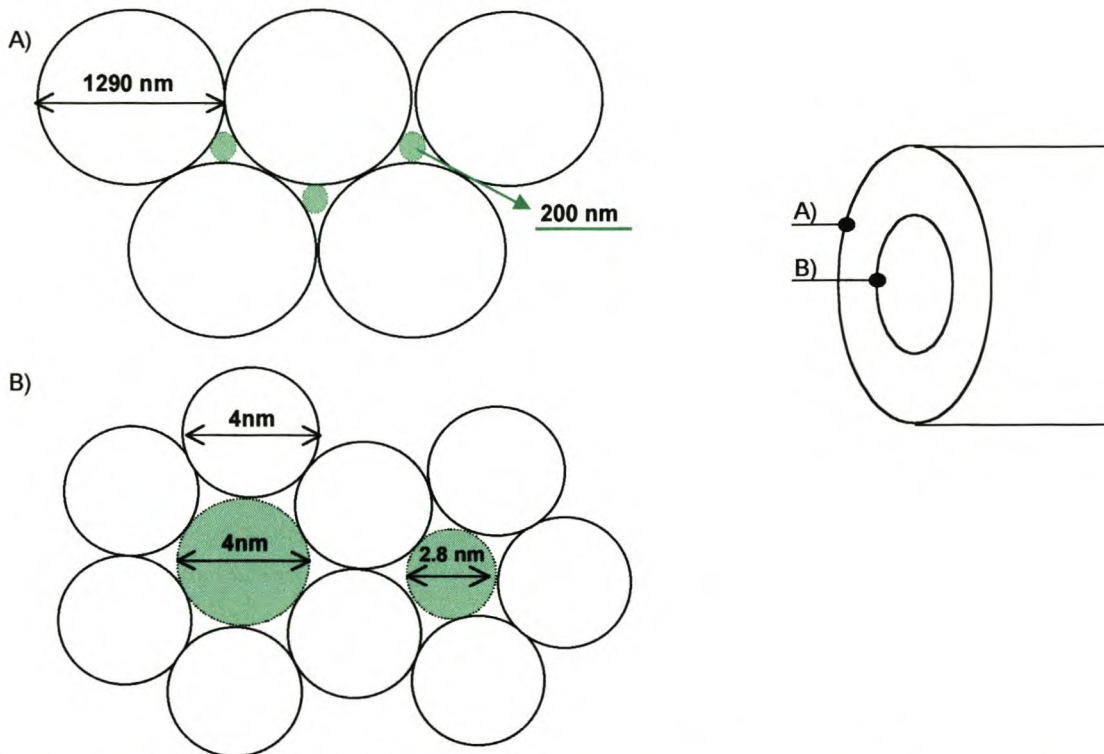


Figure 2.6: The ceramic membrane and approximate particle sizes based on the globular model of ceramic materials composition

2.3.3 Sol-gel-technique

There are a number of techniques to deposit a membrane layer upon the support layer, some of which were mentioned already. Only one of them, the sol-gel technique, is discussed here briefly. Information on some of the other techniques can be found in the literature [Cot et al., 1994, Ulhorn et al., 1992(b), Tayaa et al., 1992, Maebashi, 1990, Kiyoshi & Noahito, 1991, Galaj et al., 1990, Terpstra et al., 1988, Larbot et al., 1987 and 1988].

The sol gel process is used to produce and consolidate exceptionally fine, pure ceramic powders. The basic steps of the sol gel process are as follows:

- starting materials are typically alkoxides, hydrolysed with water or hydrated oxides,
- the sol is obtained by peptization,
- organic binders are added followed by a viscosity control of the sol,
- by slip casting, a thin layer is set down on the surface of the support, where the gel deposits, and
- the final steps are the drying and sintering steps.

As Ulhorn [1992(b)] states, details of the preparation of layered ceramic membranes are not given by industrial organisations. Ulhorn also explains how the membrane layer is often “slip-casted” upon a support using a sol-gel: “If a dry support is brought into contact with a sol, capillary forces are present inside the support pores. Water of the sol is sucked into the support. A layer is formed by concentration of the sol particles at the boundary of support and sol.” This technique, the sol-gel technique, is often used to deposit a membrane layer on a support and described in various articles and patents [Hsieh, 1996, Cot et al., 1994, Ulhorn et al., 1992(b), Tayaa et al., 1992, Maebashi, 1990, Kiyoshi & Naohito, 1991 and Cot, 1988]. The sol-gel method also allows for the subsequent coating of a support with several porous ceramic layers, each containing pores of a smaller size. The disadvantages of this method are that it requires high precision operations and clean room conditions and, when it is applied to large membrane surfaces, has low reproducibility and is extremely labour intensive due to the large number of technological operations involved [Linkov & Belyakov, 1997)].

2.3.4 Sintering

The final step in ceramic membrane manufacturing is to sinter the membrane. Sintering is a high-temperature treatment used to join small particles, see **figure 2.7**.

The precursor or green body, is a body of packed, fine, ceramic particles, usually with a large inner surface (between 10 and 600 m²/g). During sintering, diffusion of atoms

to points of contact takes place, causing bridges to form between the particles. The inner surface and the volume of pores are drastically reduced by particles that melt together, see **figure 2.7**. The longer the sintering time, the less the pore volume. Defects and irregularities in the precursor will remain after- or even increase during sintering. The driving force of the process is the decrease in free enthalpy of the system by a decrease in the surface energy. [Van de Ven et al., 1988, Welles et al., 1988 and Askeland, 1996]

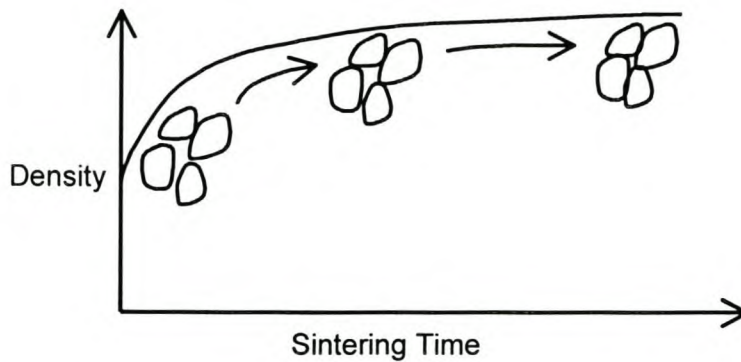
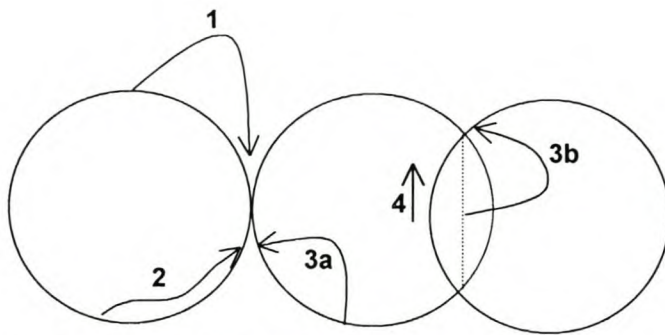


Figure 2.7: The sintering process: decrease in pore volume and increase in density, with time, during sintering

2.3.4.1 Sintering Mechanisms

To sinter a green body the transport of material is required. There are several different ways to transport materials during sintering, called sintering mechanisms, as shown also in **figure 2.8**.

- 1) Evaporation-condensation; relies on the difference between the vapour pressures above surfaces with differing curved radii.
- 2) Surface diffusion; diffusion of atoms along surfaces such as cracks or particle surfaces.
- 3) Volume diffusion; diffusion of atoms via grid defects such as vacancies and interstitial sites.
- 4) Particle-boundary diffusion; diffusion via the boundary between two particles.



1. Evaporation-Condensation
2. Surface Diffusion
- 3a. Volume Diffusion-from surface
- 3b. Volume Diffusion-from particle boundary
4. Particle Boundary Diffusion

Figure 2.8: The four sintering mechanisms [Van de Ven et al., 1988]

2.3.4.1.1 Evaporation-condensation

Material on the surface of the particles will evaporate as a consequence of a difference in vapour pressures at differently curved (concave and convex) surfaces. This material will be deposited in between the particles as shown in **figure 2.8**. Shrinkage does not occur in this mechanism since the total volume stays the same but the form of the pores does change. The particles at least have to be smaller than 10 μm . This mechanism plays only an inferior role during sintering and does not occur at low vapour pressures.

2.3.4.1.2 Diffusion

Diffusion plays the most important role during sintering. Concave curved surfaces have an elevated concentration of vacancies while convex curved surfaces have a reduced concentration of vacancies compared to a flat surface ($r = \infty$). Where particles touch each other there is an elevated vacancy concentration while there is a reduced concentration below the free surface [Van de Ven et al., 1988].

$$\frac{\Delta C}{C_o} = \frac{\tau \cdot V_o}{R \cdot T \cdot r} \quad (2.8)$$

where C_o is the vacancy concentration of a material with a flat surface, τ is the surface-energy, V_o is the molar surface, and r the curve radius.

Material transport will then take place because of the diffusion of vacancies from the concave curved surfaces to the surface. This diffusion can take place through the interior of the particles, along the particle boundaries and from the surface of the particles. Shrinkage occurs in both particle boundary diffusion and volume diffusion. It can be seen as two particles moving towards each other.

With a decreasing particles size, the difference in vacancy concentration (ΔC) and vapour pressure increases linearly with $1/r$, while the transport distance between the particles and pores decreases. Fick's first law describes the mass transport:

$$J = D \cdot \left[\frac{\Delta C}{\Delta x} \right] \quad (2.9)$$

$$D = D_o \cdot \exp\left(\frac{E_{act}}{k \cdot T}\right) \quad (2.10)$$

Where D is the diffusion coefficient, D_o a constant determined by the jumping distance and the co-ordination number of the ions and E_{act} is the energy required moving an atom from one lattice site to another.

Following from equation (2.8), ΔC will decrease with increasing temperature while the diffusion coefficient increases with increasing temperature. The diffusion coefficient will increase faster than the vacancy concentration decreases and therefore the sintering speed will increase with temperature.

2.3.4.2 Sintering Stages

There are three different sintering stages, i.e. [Van de Ven et al., 1988]:

- 1) The beginning-stage: neck-forming and neck-growth, sharp decrease of the specific surface, little shrinkage, number of pores stays constant.

- 2) The middle-stage: this stage starts when the necks have grown to be 0.3 times the particle diameter. The particles draw near with above described mechanisms where shrinkage occurs, there are changes in the pores, canal-like pores develop, the specific surface decreases to almost zero and there is only slight particle growth. The canal-pores reduce until they become unstable and start becoming closed pores. This phenomenon starts when the open porosity is about 15-20% and stops when the closed porosity has become about 5-8%. This is where the end-stage starts.
- 3) The end-stage: in the end-stage the pore volume decreases even more. Theoretically, sintering ends when all pores have disappeared and the density equals the theoretic density.

When ceramic materials are sintered to obtain a porous structure, as is the case for the sintering of ceramic membranes, the sintering rarely goes beyond initial stage sintering.

2.3.4.3 *Sintering and Porosity*

The porosity in ceramic supports and membranes results from a process in which no pressure assistance is provided during sintering. According to Cot [1994], and Galaj [1990], porosity is directly related to the size, size distribution and arrangement of individual particles in the fired material. It has to be kept in mind that ceramic membranes are not prepared with ideal particles and so, when the starting particles have a broad size distribution, smaller particles are “swallowed” by larger ones during the sintering process [Cot et al., 1994].

The particles size evolution during sintering is a function of temperature and time. Generally, individual ceramic grains and pores, increase in size with increasing temperature and time [Galaj et al., 1990 and Larbot et al., 1987]. The required sintering temperatures are lower than in other sintering processes because of the active state of the fine particulate materials used [Hsieh, 1996].

In the patent by Maebashi [1990], a mixture of alumina and zirconia was added to the alumina as a sintering aid. This makes it possible to obtain a ceramic membrane having a high durability and given pore size even if the sintering temperature is low.

2.4 Evaluating Ceramic Membranes

Membrane technology provides an economical and reliable separation process in many industrial applications. Tailoring membranes with better separation characteristics for specific industrial applications is important to the continued development of this technology. A key need in such research is the improvement of the characterisation methods of fundamental properties such as pore size, pore size distribution, surface area and tortuosity [Jakobs & Koros, 1997].

The structural characterisation techniques for ultra-filtration membranes that are available now cover a broad range of physical methods divided into two groups: a group giving parameters related to the membrane permeation and another of methods that directly obtain morphological properties.

The permeation parameter techniques (liquid and gas flux measurements, solute retention test, liquid displacement methods, permoporometry, etc.) allow pore size distribution determination only for the pores open to flux. These techniques are especially suitable for characterising the thin membrane layer in asymmetric membranes but they do not provide any insight into the remaining support structure [Calvo et al., 1997].

The morphology related techniques on the other hand; (gas adsorption-desorption, mercury porosimetry, electron microscopy, thermoporometry, etc.) can give complete information on the porous structure.

According to Jakobs [1997], characterisation methods for fundamental properties such as pore size, pore size distribution, surface area and tortuosity give insight into fundamental membrane properties. They do not necessarily allow prediction of more application-oriented characteristics such as flux, the selectivity or rejection and the molecular weight cut-off.

Much has been written about different membrane characterisation methods, but no uniform nomenclature exists and various names are used for related tests. Here follows a description of a number of characterisation techniques. Paragraphs 2.4.1 to 2.4.4 are permeation parameter techniques, and the techniques described in paragraphs 2.4.5 to 2.4.7 are morphology related.

2.4.1 Gas Permeation

The gas permeation method can be used as a non-destructive comparable test for the selection of a suitable support for the deposition of a micro- or ultra-filtration separation layer [Uchytel, 1994].

The mechanisms for gas transport vary primarily with pore size and to some extent with chemical interactions between the diffusing species and the membrane material. At the largest pore size, transport is governed by Poiseuille flow and no separation occurs for multi-component streams. When the pore size is approximately less than 1/10 that of the mean free path of the diffusing species, collisions between the gas molecules and the pore wall control the transport of species through the membrane. This is known as Knudsen diffusion and separation between species is inversely proportional to the square root of their molecular weights. When pore dimensions approach those of the diffusing species, separations can occur by size exclusion or molecular sieving [Gallaher & Liu, 1994].

2.4.2 Liquid Displacement Techniques

Liquid Displacement Techniques have proved to be useful and they are widely used for characterisation of especially micro-filtration membranes. A number of characterisation methods are rather similar and all rely on the same principle of displacement of a wetting liquid.

The membrane is wetted with a liquid that is held in the pores by capillary forces (fluid A). Another less wetting fluid (fluid B), liquid or gas, acts at increased pressure on one side of the membrane and eventually displaces fluid A. Until the pressure

difference over the filter reaches the capillary pressure of the largest pores, fluid A acts like a barrier and no flow can occur. After increasing the pressure over this limit, fluid A is expelled from the largest pores and fluid B permeates. By successively increasing the pressure, smaller and smaller pores are opened for permeation of fluid B. The ideal flow versus pressure drop curve generated in this fashion is usually 'S-shaped' and is often referred to as the flow-pressure curve [Jakobs & Koros, 1997]. Calvo [1997], claims that analysis of ultra-filtration membranes requires the use of appropriate liquid-liquid interfaces or excessively high-applied pressures. Permporometry, described next, is a gas-liquid equilibrium method but it can also be seen as liquid displacement technique.

2.4.3 Permporometry

Permporometry is based on the capillary condensation of liquids in micro-pores. The vapour pressure of a liquid is dependent on the radius of curvature of its surface, therefore, the vapour pressure of the liquid in a capillary increases with increasing capillary radius. By capillary condensation, pores of a certain size are blocked with liquid by setting the relative pressure. Measuring the gas flow of the free diffusive transport through the open pores (through the membrane) while decreasing the relative pressure, the size distribution of the active pores can be obtained. Similar measurements can be carried on during the adsorption process, but it is more difficult to obtain equilibrium with these measurements, so the desorption process is preferred. Comparing the nitrogen adsorption/desorption technique with permporometry, nitrogen adsorption/desorption measures the size (distribution) of the active as well as the passive pores. Permporometry measures only the active pores [Nakao, 1994].

2.4.4 Bubble Point Technique

Originally, the bubble point measurement method was done by semi-automatic incrementing of differential gas pressure applied to one side of a test material until a "steady stream of bubbles" is observed from the downstream side of the material.

This technique and all similar techniques suffer from inherent subjectivity; they rely upon human observation and judgement.

A more sophisticated and sensitive technique resulted from concerns about repeatability and accuracy of the bubble point. In this technique the bubble point is detected by monitoring pressure versus time at a constant flow. Any deviation of the pressure time curve from linearity would then be taken as an indication of the bubble point. This method still did not correlate to the true largest pore size.

Despite its disadvantages and problems the bubble point technique is one of the most widely used testing standards for membranes. The technique is described in detail in several articles including [Advances in Pore Size Characterisation, 1998 and Jakobs & Koros, 1997].

2.4.5 Microscopy Observation

Microscopy observation can be used for both pore size and particle size distribution. This method directly gives visual information about the sample such as shape and size, distribution, cross-sectional structure of pores and/or particles. A disadvantage of microscopy is that it is not possible to obtain an indication of pore length or tortuosity; only the surface pores can be seen [Nakao, 1994]. It is also possible to sample only a very small area fraction. It is destructive but it is still a very important and valuable method [Jakobs & Koros, 1997].

2.4.5.1 Atomic Force Microscopy (AFM)

The AFM [Bottino et al., 1994, Bowen et al., 1996, and Bowen et al., 1998] gives topographical images by scanning a sharp tip over the surface of a material. It works with an optical lever system and uses micro-fabricated cantilevers to minimise forces between tip and membrane surface [Dietz et al., 1992]. The resolution can reach atomic dimensions for flat surfaces [Albrecht & Quate, 1988]. One of AFM's most important properties is that it can image surfaces in air and even under liquids without special surface preparation [Bowen et al., 1996]. The AFM software allows

quantitative determination of the diameter of pores by use of the images, in conjunction with digitally stored line profiles. The simultaneous use of images and profiles greatly facilitates identification of the entrance of individual pores. The diameter deep in the membrane may not be determined directly by surface AFM due to convolution between the tip shape and the pore. The AFM image analysis software allows roughness analysis on both selected areas and membranes [Calvo et al., 1997].

Bottino et al. [1994] successfully applied AFM to surface studies of ceramic membranes. They suggest that the AFM capability to reconstruct the three-dimensional image of the membrane surface can be exploited to obtain quantitative information about the surface roughness, which is useful for explaining the behaviour of membrane performance during the ultra-filtration process.

2.4.5.2 *Scanning Electron Microscopy (SEM)*

The scanning electron microscope generates electron beams and then forms an image from the emitted electrons as a result of interaction between the bombarding electrons and the atoms of the specimen. SEM's can generate higher-resolution information than reflected light microscopes, since electrons have a much shorter wavelength than light photons. They have become a basic surface and micro-structural characterisation tool in membrane separations. Theoretically the maximum magnification of SEM's can be beyond 800,000x. Practical magnification and resolution limits, however, are less than 100,000x due to instrumental parameters [Hsieh et al., 1988].

Besides using the SEM to characterise the microstructure of ceramic membranes it can also be used for analytical purposes when coupled with an X-ray generation unit. The asymmetric structure of ceramic membranes can easily be observed under a SEM, but due to its limited resolution, SEM cannot always be used to perform a proper analysis on the selective membrane layer [Bottino et al., 1994].

2.4.6 Nitrogen Adsorption-Desorption and Mercury Penetration

Nitrogen adsorption-desorption and mercury penetration methods are well known and widely accepted but unsatisfactory for asymmetric ceramic membranes. Both methods have as a disadvantage that they cannot distinguish dead end pores and pores available for permeation. They are both based on artificial and simple models of the porous structure (e.g. straight cylindrical non-intersecting pores of uniform and invariable radii). These methods can therefore, only give adequate results for these unique types of porous structures, which in reality do not reflect the porous structure of any sample.

Asymmetric membranes with two or more different layers represent very complicated systems and for that reason the results gained by measured data does often significantly differ from the real membrane structure [Jakobs & Koros, 1997 and Rocek & Uchytel, 1994].

2.4.6.1 Nitrogen Adsorption-Desorption

The nitrogen adsorption/desorption method, based on the widely used BET theory, is a standard procedure (also for ceramic membranes) for pore size distribution and surface area determination. This measurement technique, however, is good only for pore diameters ranging from 1.5 nm to 100 nm (= 0.1 micron). For composite membranes with the support having pores larger than 100 nm, the nitrogen adsorption/desorption method is not suitable. A possible but cumbersome solution suggested by Hsieh et al. [1988], is to “shave” most of the bulk support layer to increase the pore volume percentage of the thin membrane film. Knowing the amount of bulk support layer removed and the mercury porosimetry data of the shaved membrane sample, it is possible to combine the two pieces of information to arrive at the pore size distribution of a multiple-layered composite membrane. Application of the nitrogen adsorption/desorption method to the membrane field is thus restricted, according to Calvo [Calvo et. al., 1997], mainly due to the lower porosities usually found in these materials as well as due to the difficulty to correctly interpret the results in many cases.

2.4.6.2 Mercury Porosimetry

A mercury penetration study employs high pressures. Mercury Porosimetry measures the mercury uptake into the previously evacuated porous material under increasing pressure of mercury. The method is based on the assumption that only cylindrical pores are presented in the sample. Commercial mercury porosimeters can usually provide pore diameter distribution data in the range of 4 nm to 7.5 microns. Nowadays, mercury porosimetry is used for the rough characterisation of samples of (asymmetric) ceramic membranes [Hsieh et al., 1988 and Rocek & Uchytíl, 1994].

2.4.7 Thermoporometry

When pores of a porous material are totally filled with a liquid, the thermodynamics of the divided phases show that the curvature of the liquid-solid interface can be linked to the change of state temperature. The radius of the pores is linked to the decrease in the solidification temperature, and for each change in temperature, the amount of energy released per gram of sample is measured. The output of a differential scanning calorimeter (DSC) that monitors the temperature and energy is in the form of freezing or melting diagrams. The pore size and pore volume and their distribution can then be calculated from these diagrams with the equations as outlined by Nakao [Nakao, 1994].

Thermoporometry allows pore structures to be measured in wet environments in which they are used. This technique is therefore, extremely attractive for the structural analysis of membranes since the structure change during sample preparation and observation can be minimised. However, most materials that have been analysed by this method, were inorganic, isotropic and with a large pore volume making pore size analysis easier [Nakao, 1994].

Zeman [Zeman et. al., 1987], indicates that in both thermoporometry and nitrogen adsorption-desorption methods the pores in the sub-layer of the asymmetric filter are measured, and therefore, these methods give pore sizes much larger than the size of the pores in the membrane layer.

Cuperus [Cuperus et. al., 1987 and Cuperus et al., 1992] measured the pore size distribution of alumina ultra-filtration membranes by thermoporometry. Good agreement was obtained in calculated mean pore radius and distribution between thermoporometry and the nitrogen adsorption-desorption method. They also confirmed a liquid-solid transition of water in a small pore followed by a volume expansion which damaged the alumina membranes. According to Nakao [Nakao, 1994], thermoporometry may be the best technique to obtain information on the subject of deformation of the membrane porous structure.

2.4.8 Transport Models

In solute separation experiments volumetric permeate flux and solute rejection can be obtained. Both the flux and rejection are strongly dependent on the structure of the membrane. Membrane structures such as thickness, tortuosity, pore size, pore density and so on can be characterised, if the relationship between flux, rejection, and the membrane structure is known. Here follows a short description of the three major approaches (see **figure 2.9**). For more details the references should be consulted.

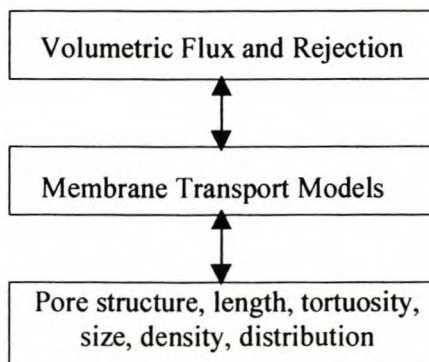


Figure 2.9: Transport models

- 1) Based on irreversible thermodynamics [Kedem & Katchalsky, 1958 and Spiegler & Kedem, 1966]

This model relates fluxes, the volume flux and solute flux in filter processes, and driving forces, the mechanical pressure applied and osmotic pressure. They are applied to a black box representing the membrane using linear phenomenological equations with phenomenological coefficients.

- 2) Stefan-Maxwell multi-component diffusion equations [Peppas & Meadows, 1983 and Robertson & Sydney, 1988]

This model has often been applied to multi-component gaseous diffusion processes, but is also applicable to liquid processes. This model is shown to be equivalent to the irreversible thermodynamic model described above.

- 3) Hydrodynamic model or pore model [Solomon, 1968, Verniory et al., 1973, Bean, 1972, Nakao & Kimura, 1981 and Nakao & Kimura, 1982]

Hydrodynamic models have been developed to account for the trans-capillary transport of spheres and they were applied to the analysis of solute permeation through biological membranes. The validity of some of the assumptions on which the application of the modified hydrodynamic model to ultra-filtration membranes relies are uncertain. In more modern pore models some of the flaws in the older models are corrected.

2.5 Introduction to the Method of Membrane Manufacture

As stated in Chapter 1 it is an objective of this project to investigate the manufacture of an asymmetrical ceramic membrane in one technological operation, combining the support and membrane layer steps into one single “step”. The aim of this project is to research the manufacture and evaluation of a ceramic membrane. A recipe to manufacture an γ -alumina-zirconia membrane as described in the patent of Linkov [Linkov & Belyakov, 1996] was used as a basis, see **Appendix A**. Linkov's patent describes the manufacture of an asymmetrical ceramic membrane, support and membrane layer, in one technological operation. Example 1 in the patent of Linkov was used as a guideline for the manufacturing procedure described in Chapters 3 and 4.

The following recipe from the patent of Linkov is the manufacturing method that was investigated in this project.

2.5.1 Example 1 from Linkov's Patent

γ - Al_2O_3 and ZrO_2 stabilised with Y_2O_3 was heated at 900°C in a vacuum furnace for 2 hours in order to remove organic pollutants. This operation was followed by a separate milling in a wet ball mill using steel balls with a diameter of 15 mm. The oxide/balls/water ratio was maintained as close as possible to 1/2/1 throughout the whole milling operation. The milling time for Al_2O_3 was 80 hours and for ZrO_2 – 60 hours. The dense precipitate formed in the mill was placed into the polyethylene drum, 15 % water was added to it and the mixture was roller stirred over 4 hours. The casting suspension was prepared by mixing milled Al_2O_3 and ZrO_2 in the same drum for 1 hour. The composition of the casting suspension attributed to the best mechanical properties and highest chemical stability of resulting ceramic membranes was as follows:

Al_2O_3 – 70%,

ZrO_2 – 29 %, and

Y_2O_3 – 1%

The casting suspension was poured into specially designed tubular gypsum moulds where precursors for the ceramic membranes formed during 1 minute. The moulds were drained and membrane precursors were removed from them and placed into a drying chamber. The drying temperature was maintained at 20°C , the humidity at 40 %, the drying time was 3 days. After the drying operation the membrane precursors were placed in an oven, heated up to 1300°C at a heating rate of 100°C and calcined at this temperature for 1 hour. The resulting ceramic membranes possessed uniform pore-size distribution in the macro pore support layer with a mean pore diameter of 0.15 μm . A thin mesoporous layer was formed on the inner surface of the ceramic membranes. The mean pore diameters of mesopores in this layer were 2.6 and 4,0 nm.

2.5.2 Outline of the Membrane Manufacturing Process

The “recipe” as described in the previous paragraph, paragraph 2.5.1, was followed as close as possible during this reasearch project, and when necessary changes were made. The flow diagram in **figure 2.10** shows the manufacturing procedure as described in paragraph 2.5.1. The first 3 blocks up to the separate wet milling are discussed in Chapter 3 as raw material preparation. These steps were kept constant. The rest of the steps are discussed in Chapter 4 as the manufacture of the ceramic membrane.

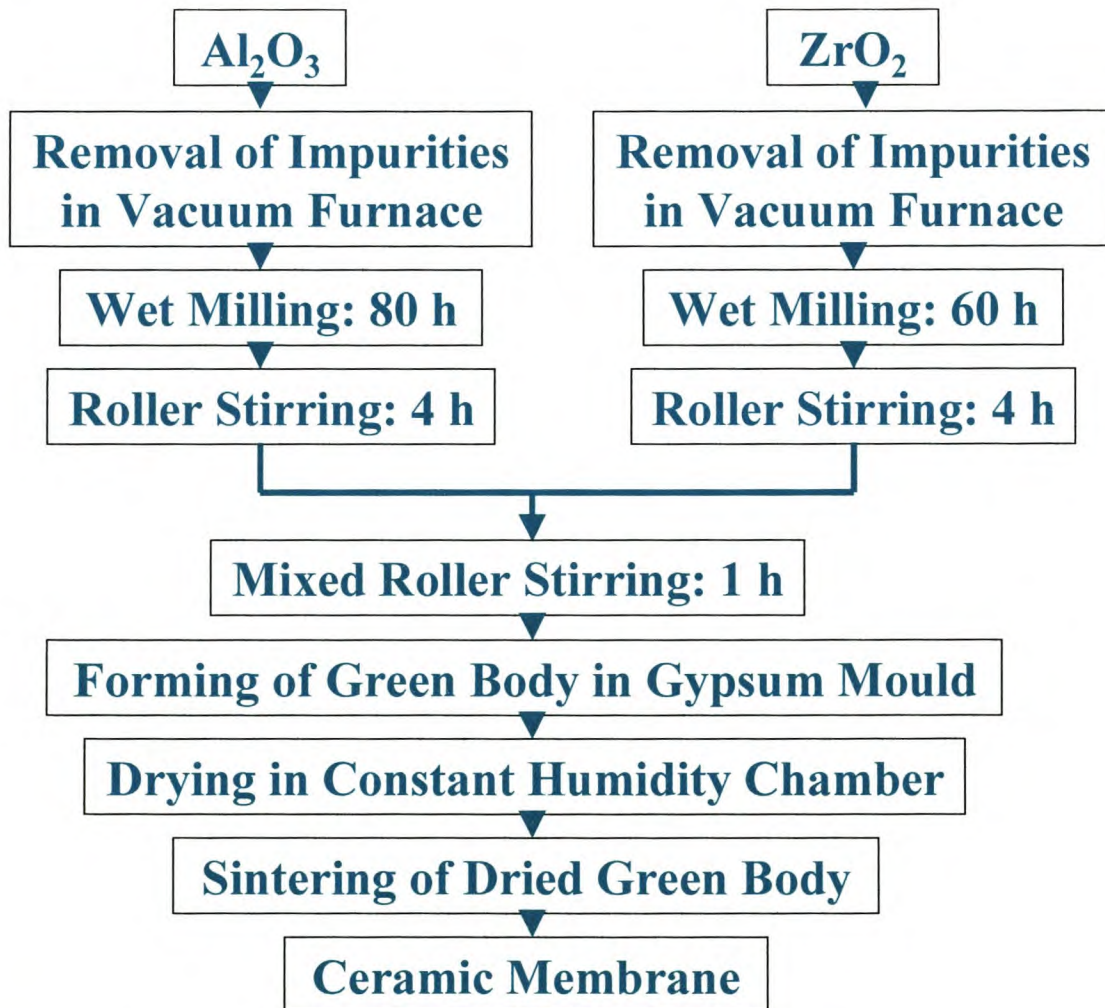


Figure 2.10: Schematic diagram of the ceramic membrane manufacturing process

2.6 Summary

The objective of this chapter is to provide background on ceramic materials, ceramic membranes, the manufacture of ceramic membranes, and evaluation methods to characterise ceramic membranes.

The use of inorganic membranes, especially ceramic membranes, in separation technologies is relatively new. The main advantage of using ceramic membranes in separation processes is their stability (chemically, structurally and thermally). The main disadvantage of ceramic membranes is their brittleness. Recent efforts have been directed towards the development of ceramic membranes in which the microstructure is tailored to application, well characterised and reproducible.

The most common production route for ceramic membranes is a method that consists of two steps: the manufacture of the support structure followed by the application of one or more membranes layers. The manufacturing method that is examined in this project reduces this procedure to one technological step where the support structure and membrane layer are manufactured at the same time.

A number of different evaluation methods for membranes exist. Depending on the type of membrane (polymeric or ceramic) and the pore sizes of the membrane, certain methods are more applicable than others are.

3. Raw Material Preparation

Paragraph 2.5 shortly introduces the manufacturing method used for the manufacture of the membranes for this research project. Chapter 4 discusses the research results of the various steps of the manufacture method. The raw material preparation, the highlighted part in **figure 2.10**, is discussed in this chapter. Firstly, the properties of the raw materials are discussed and secondly the preparation of these materials for manufacturing ceramic membranes is discussed.

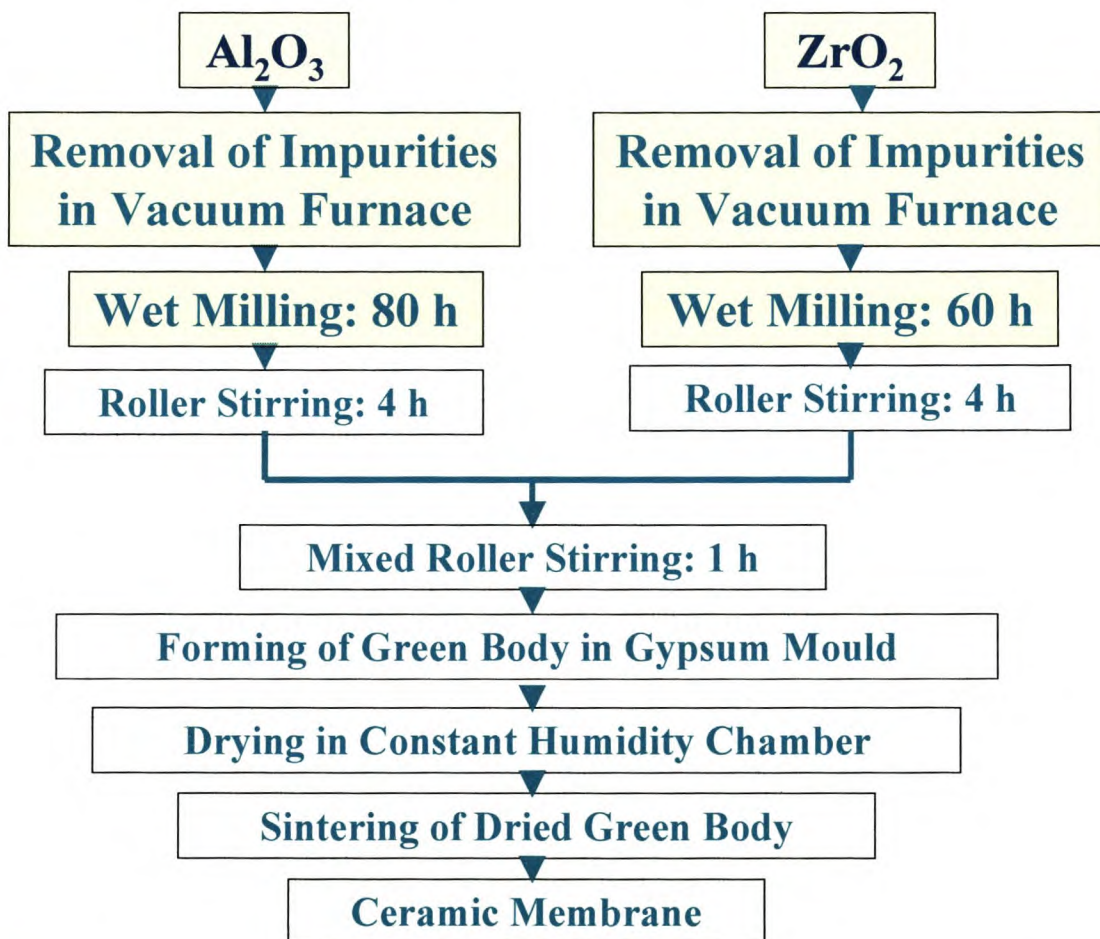


Figure 2.10: Schematic diagram of the ceramic membrane manufacturing process

3.1 Raw Materials

The raw materials used in the manufacturing process for the ceramic membrane are γ -alumina and yttrium-stabilised-zirconia. These two materials are discussed separately, after which their composite properties are discussed. The raw material specifications of the γ -alumina, zirconia and yttria can be found in **Appendix B**.

3.1.1 Gamma-Alumina (γ - Al_2O_3)

The stable crystalline alumina form is corundum (α -alumina). γ -Alumina is one of several structurally related, metastable forms. These occur in "active-alumina" and are being studied extensively due to their importance in adsorbents and catalysts. Larbot et al., 1987, observed the three phases after thermal treatment of γ -alumina as shown in **table 3.1**.

| Temperature [°C] | 400 | 900 | 1100 | 1200 |
|---------------------|------------------------------------|------------------------------------|------|------------------------------------|
| Structure | γ - Al_2O_3 | θ - Al_2O_3 | | α - Al_2O_3 |

"Low-temperature" γ - and μ -alumina have similar X-ray diffraction patterns and the term γ - Al_2O_3 has been applied to either form and as a generic term for all low temperature forms. γ - and μ -Alumina are often poorly crystallized and difficult to distinguish. The low-temperature forms are obtained by dehydrating at temperatures not exceeding 600°C and it can change irreversibly to "high-temperature" forms (δ , θ , or κ) at 600°C to 900°C [Chase et al., 1986]. γ - Al_2O_3 is generally believed to be a defective spinel phase of alumina with cation site vacancies randomly distributed. Its structure and properties are not well understood. There has been long-standing controversy as to whether the cation vacancies are located at the tetrahedral sites or the octahedral sites. Based on an empirical pair potential calculation and first-principles electronic structure studies, Mo et al. [1997], concluded that the cation vacancies are preferentially located at the octahedral sites in bulk γ - Al_2O_3 . **Figure 3.1** shows a spinel structure that is similar to the γ - Al_2O_3 structure.

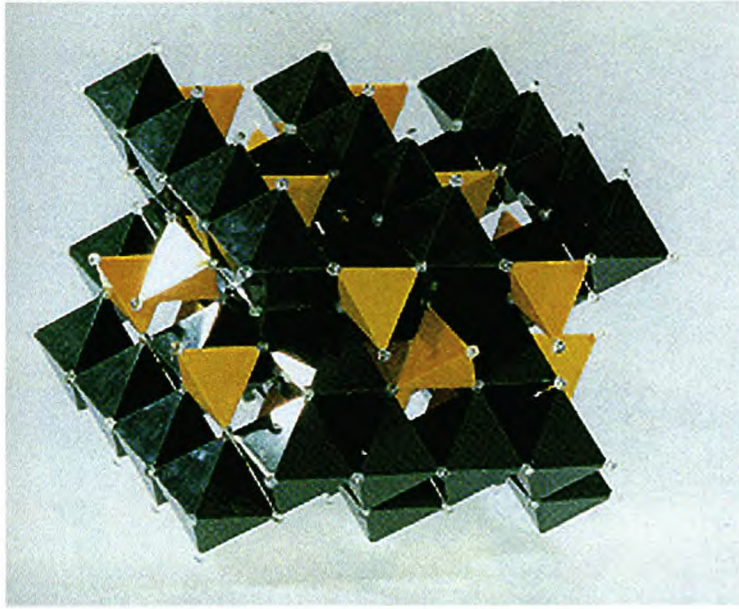


Figure 3.1: A model of the spinel structure.

3.1.2 Zirconia

Cracks or stress concentrations may be introduced by phase transformations when a ceramic is heated or cooled. Zirconia transforms from a tetragonal structure to a monoclinic structure on cooling, which leads to a large volume change. This volume change can be as large as 3% to 5% volume-increase. The resulting stresses cannot be relieved by plastic deformation; therefore they initiate or propagate cracks in the part. By adding stabilisers like MgO, CaO and Y₂O₃ to the zirconia, the tetragonal structure is maintained on cooling (see **Appendix B** for phase diagrams). Addition of Y₂O₃ provides the best properties [Van de Ven et al., 1988]. This product, then called PSZ (Partially Stabilised Zirconia), eliminates the phase transformation and makes it possible to use the material as a refractory. However, the fracture toughness is still only about 2 MN/m^{3/2}. The structures of zirconia at their respective temperatures are shown in **table 3.2**.

| Temperature [°C] | 25 | 1227 | 2327 | 2677 |
|------------------|------------|------------|-------|---------------|
| Structure | Monoclinic | Tetragonal | Cubic | Melting point |

3.1.3 Alumina and Zirconia as a Composite Ceramic

The patent of Linkov [Linkov & Belyakov, 1996] suggests that the composition of the suspension should range from 60 to 80 m% for alumina and 20 to 40 m% for zirconia. For the manufacture of the membranes the following composition was chosen: 70 m% γ -alumina, 29 m% zirconia and 1 m% yttria (almost 2 mol%). This composition (29 m% which is 23.4 vol% zirconia) was also used in Example 1 in the patent by Linkov [Linkov & Belyakov, 1996].

Holz et al. [1994] show that a 30 vol% (=37 m%) ZrO_2 in an Al_2O_3 / ZrO_2 composite produces ceramic materials with superior mechanical properties. The choice of composition (23 vol% or 29 m% ZrO_2) was decided upon by considering the data in table 3.3 [Lange, 1982].

| ZrO ₂ content (w%) | Y ₂ O ₃ content (mol%) | Sintering Temperature (°C) | Sintering Time (h) | Density (g/cm ³) | Volume-fraction ZrO ₂ phase (%)* | Hardness H (GPa) | K _c (MPam ^{1/2}) |
|-------------------------------|--|----------------------------|--------------------|------------------------------|---|------------------|---------------------------------------|
| 12.4 | 0 | 1600 | 2 | 4.15 | ~80t | 15.8 | 6.73 |
| 24.8 | 0 | 1600 | 2 | - | < 20t | 10.1 | (5.25) |
| 22.6 | 2 | 1600 | 2 | 4.38 | 100t | 16.1 | 6.58 |
| 29.6 | 2 | 1600 | 2 | 4.50 | 100t | 16.4 | 6.38 |
| 36.6 | 2 | 1600 | 2 | 4.62 | 100t | 15.7 | 7.43 |
| 55.8 | 2 | 1600 | 2 | 4.89 | tr-m | 15.1 | 8.12 |
| 24.8 | 7.5 | 1600 | 2 | 4.46 | 100c | 15.8 | 4.54 |

* t = tetragonal, tr-m = trace monoclinic, c = cubic

Table 3.3, although the fabrication conditions are not the same as those in the manufacture of the ceramic membranes, gives a good indication of the ZrO_2 and Y_2O_3 content that provides Al_2O_3 / ZrO_2 composites with the best mechanical properties:

- When no Y_2O_3 is added to the composite the volume fraction tetragonal ZrO_2 as well as the composition's hardness, decreases rapidly with increasing ZrO_2 content.

- When 2 mol% Y_2O_3 is added, all of the ZrO_2 stays in the tetragonal phase until the ZrO_2 content increases beyond 55.8 m% where a trace of the monoclinic ZrO_2 appears. Beyond this point, the hardness also starts decreasing rapidly.
- When 7.5 mol% Y_2O_3 is added, the ZrO_2 keeps its cubic phase instead of the tetragonal.

The best properties in terms of Hardness and K_c in **table 3.3** were found for a zirconia content of between 29.6 m% ($H=16.4$, $K_c=6.38$) and 36.6 m% ($H=15.7$, $K_c=7.43$). A 29 m% zirconia content was used for the manufacture of the ceramic membranes. As an additional experiment the zirconia content could be increased up to 36-37 m% to examine the influence of the zirconia content on the manufactured membranes.

3.2 Burn Out of Organic Impurities

The γ -alumina and zirconia as received from the supplier may contain impurities. To obtain a strong ceramic product it is generally important to work with substances that are as pure as possible. Linkov [Linkov & Belyakov, 1996], suggests the burn out of organic impurities using a vacuum furnace at a temperature of 900°C. The heating and cooling profiles of the vacuum furnace are shown in **figure 3.2**.

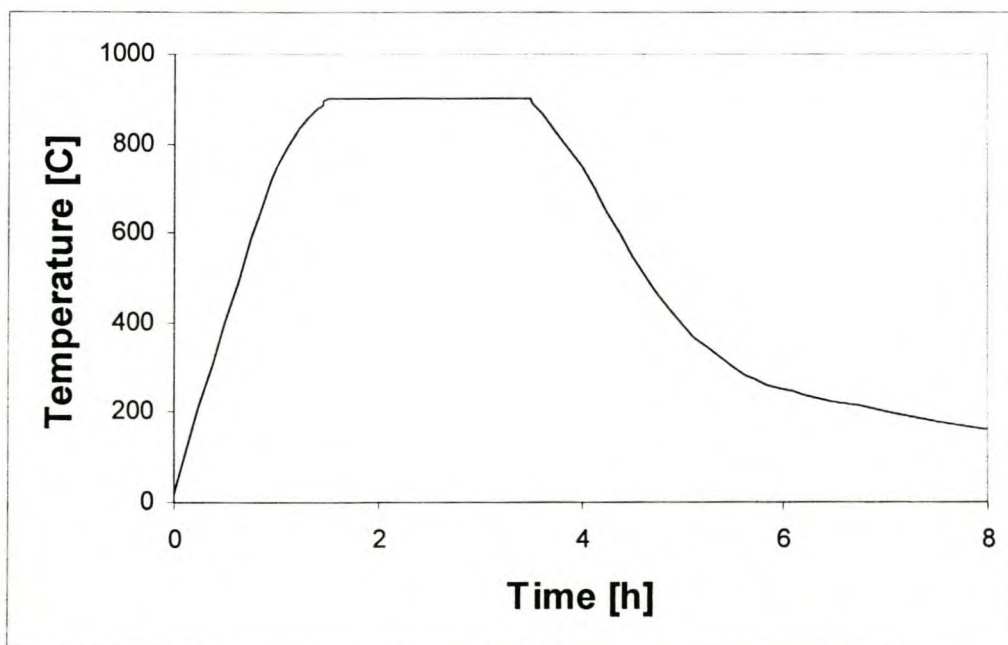


Figure 3.2: Heating and cooling curves for the vacuum furnace

For this step in the manufacturing process of the ceramic membrane a high temperature vacuum furnace was used (Vacuum Furnace, Department of Chemical Engineering, University of Stellenbosch). The space inside the vacuum furnace was particularly small. Therefore two special containers were designed and manufactured.

3.2.1 TGA-Analysis

To determine to what extent a burn-out of impurities takes place during treatment in a vacuum furnace, the decrease in mass of the alumina and zirconia powders before and after the vacuum-heating treatment was measured. The temperature profile of the vacuum furnace was simulated and the weight-loss recorded with a TGA (TGA-50, Shimadzu, Thermo-Gravimetric Analyser with a Nitrogen gas-flow of 20 ml/min). The results are shown in **Appendix C**. The results show a weight loss of 2.5 m% for the original alumina powder at a temperature of 900°C, but the weight increases by 1.5 m% when the sample is cooled down. The alumina sample tested with the TGA after vacuum treatment shows a weight loss of almost 7 m%, but the weight does not increase during the cooling process. For the original zirconia sample first a slight weight loss is observed after which the weight increases again.

For the zirconia sample that was treated in the vacuum oven on the other hand, an increase in weight by almost 2 m% is shown in **Appendix C**. These findings seem inaccurate. They may be explained by the fact that both the zirconia and alumina powder are able to absorb and desorb gasses under certain conditions. It is clear, however, that the vacuum oven treatment does have an influence on the two powders.

3.2.2 The Crystal Structure

Besides burning out organic impurities the effect of this treatment on both the alumina and zirconia powders depends largely on the presence of phase changes with increasing temperature in the two powders. **Tables 3.1** and **3.2** display the temperatures at which phase changes normally occur in alumina and zirconia powders:

- **Table 3.2** indicates that for zirconia, the first phase change (that of monoclinic to tetragonal zirconia) only appears at 1227°C. A phase change in the zirconia therefore is unlikely since the maximum vacuum furnace temperature is 900 °C.
- For the alumina powder **table 3.1** indicates that the phase change of $\gamma\text{-Al}_2\text{O}_3$ to $\theta\text{-Al}_2\text{O}_3$ is occurring at 900 °C (Chase et al. [1986] actually claims the phase change occurs *between* 600 and 900 °C). The alumina powder after the vacuum furnace treatment is therefore likely to at least be partly in a different phase from the original $\gamma\text{-Al}_2\text{O}_3$.

3.3 Separate Wet Milling

The next step in the manufacture of the ceramic membrane is the separate wet milling of both the alumina and zirconia powders. The patent [Linkov & Belyakov, 199] proposes the use of steel ball mills for this step with a ratio of oxide:balls:water of 1:2:1 and with steel balls, 15 mm in diameter. In order to prevent steel contamination and to ensure a good recovery, it was decided to use ceramic ball mills with ceramic balls instead. Thus, during the milling of both powders, ceramic ball mills with alumina balls ($d \approx 15$ mm, mass approximately 10g) were used while the oxide:balls:water ratio was kept at 1:2:1.

According to the patent [Linkov & Belyakov, 1996], the mean pore diameter of the macropores (the support layer of the ceramic membrane) should be between 120 – 240 nm. The mean pore diameter of the mesopores (the membrane layer of the ceramic membrane) should be between 2.6 – 4 nm. The globular model of ceramic materials composition, which is described in paragraph 2.3.1, explains the formation of these small pores (between 2.6 - 4nm). Example 1 in Linkov's patent suggests milling times of 80 and 60 hours for alumina and zirconia respectively. **Appendix A** indicates that these milling times should lead to a mean macro-pore diameter of 150 nm. The milling times of 80 and 60 hours for the alumina and zirconia powders were used and kept constant during the manufacture of the ceramic membranes.

3.3.1 The Influence of Milling Properties on the Size Distribution

During the wet milling of metal oxides, an increase in the milling time (after certain time elapsed from the start of the milling operation) does not affect the size of the particles. The same applies for dry milling as described by Sarkar [1975], who found that after 8 hours of milling, the crystallite size as well as the strain had reached their ultimate values (see **Appendix D, figure D1**).

Linkov [Linkov & Belyakov, 1996] claimed that “*Although an increase in milling time is not accompanied by a decrease in particle sizes, a decrease in pore sizes of the ceramic material can still be obtained*”. Linkov states that, although an increase in milling time after a certain time does not reduce the particle size, it does result in the occurrence of a so called “*bi-disperse suspension*”. A bi-disperse suspension is a suspension where, together with large particles, particles of considerable smaller size are present. Linkov claims that this bi-disperse property leads to the formation of the asymmetrical porous structure during the manufacture of porous ceramic materials by means of slip casting.

Linkov also claims that it is possible to precisely control the pore sizes in the support- as well as in the membrane layer of the membrane by controlling the milling times. In Linkov’s patent a table is found (see **Appendix A**), in which the mean-pore-diameter of the macropores is displayed as a function of the milling time of alumina and zirconia. However, Linkov’s patent does not give any information on the particle size distribution before or after milling.

To examine the influence of milling properties on the particle size distributions, there are basically three variables that can be evaluated during wet milling;

- milling time,
- ball ratio, and
- water ratio.

The effect of these variables on the *particle size distribution* (not on the ceramic membranes) was examined and will be discussed in the next three paragraphs. The experiments could be extended by also examining the influence of these variables on the *final product*, the ceramic membranes, but this was not part of this project.

3.3.1.1 Milling Time

To examine the change in particle size distribution with milling time, both alumina and zirconia powders were milled while small samples were taken at certain intervals and analysed with the Malvern. The particle size distributions at these intervals are depicted in **Appendix D** and selected results are shown in **figure 3.4**. Both graphs in **figure 3.4** show a decreasing particle size distribution with milling time. It is also clear that with increasing milling time the decrease in particle size is smaller, until it does not affect the size distribution anymore (as stated also by Sakar [1975] and Linkov & Belyakov [1997]).

3.3.1.2 Ball Ratio

To examine the influence of a higher ratio of balls on the particle size distribution during milling, a batch of both alumina and zirconia was also milled with an oxide:balls:water ratio of 1:4:1. The results are shown in **figure 3.3** as well as more extensively in **Appendix D**.

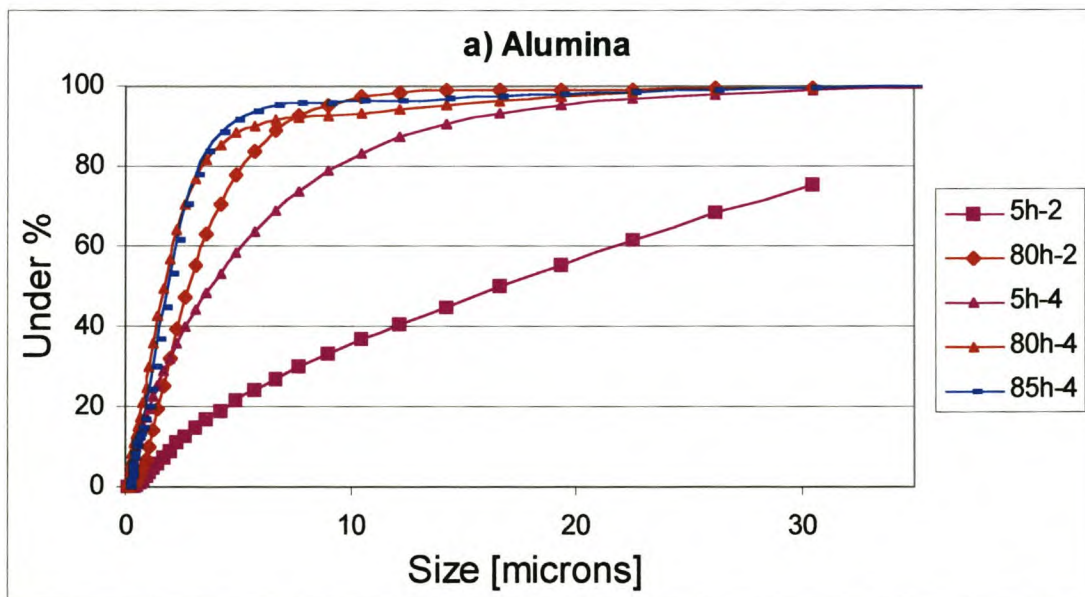


Figure 3.3 a: Particle size distribution results for alumina at certain times for the ratios oxide:balls:water of 1:2:1 (-2) and 1:4:1 (-4).

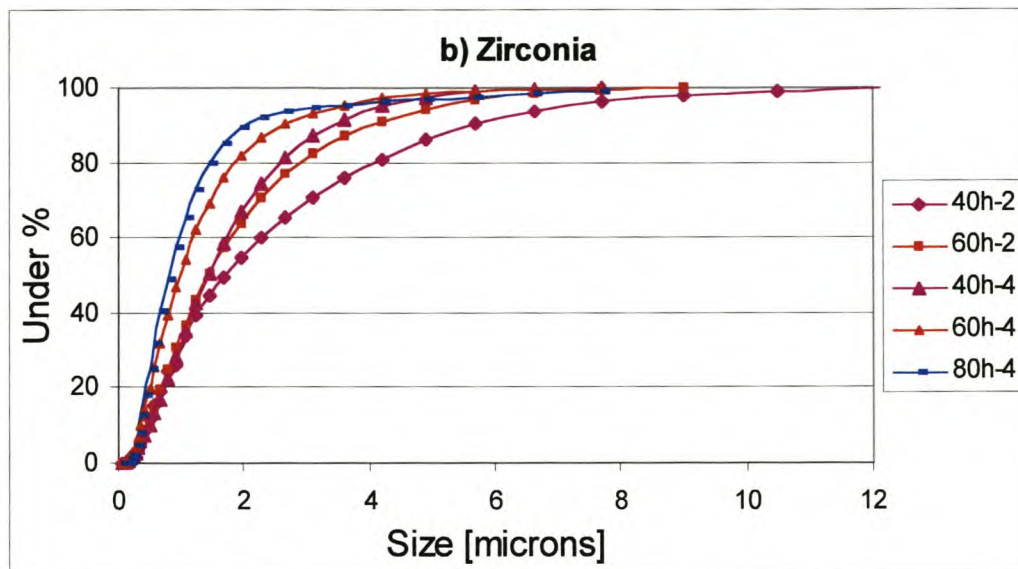


Figure 3.3 b: Particle size distribution results for zirconia at certain times for the ratios oxide:balls:water of 1:2:1 (-2) and 1:4:1 (-4)

Figure 3.3 shows that for a ratio of 1:4:1, the particle size distribution decreases faster with increasing milling time than that for a ratio of 1:2:1. A certain particle size distribution can be reached in a shorter period of time when more balls are used. Both these observations imply that the milling times as well as the oxide:balls:water ratio can be increased to obtain a slightly smaller particle size distribution. The effect of such a smaller particle size distribution on the manufacture of the membrane is not pursued further in this project. Instead the milling time is kept to the 80 hours for the alumina and 60 h for the zirconia while the oxide:balls:water ratio is kept at 1:2:1. The influence of changing the water ratio on the membranes is discussed in chapter 4.

The mass of the ceramic balls was measured before and after milling. The mass loss was less than 0.1 grams after 80 hours of milling (less than 0.1 m%).

3.3.2 Characterisation of the Milled Materials

The particle-size distributions of the alumina and zirconia powders were determined using a Malvern particle-size analyser (Malvern Mastersizer S long bench version 2.15, Department of Chemical Engineering, UCT, Cape Town). For the analysis of

the powders, stable suspensions were prepared using a dispersing agent (1g/l tetrasodium pyrophosphate and 1g/l calgon solutions) as the liquid phase.

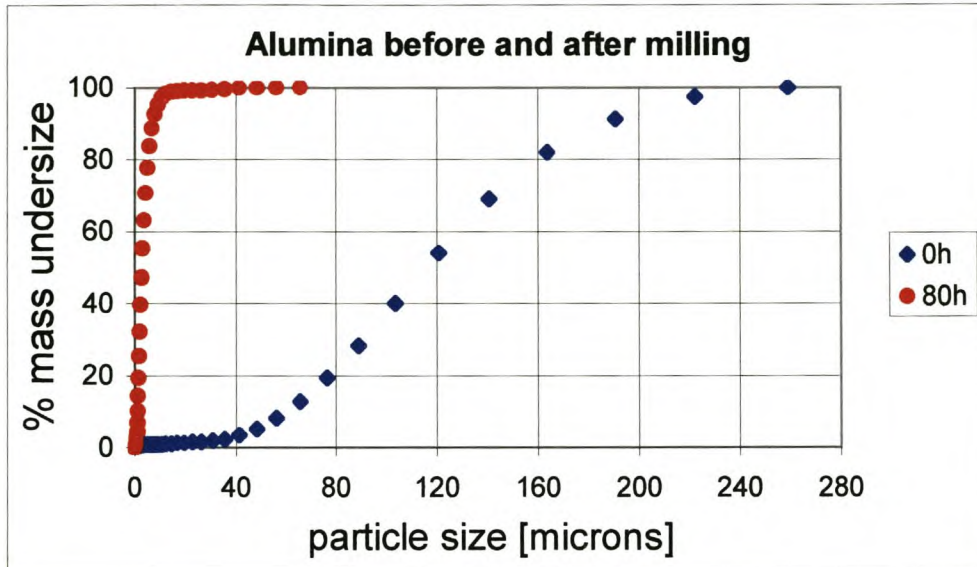


Figure 3.4: Cumulative mass distributions of the alumina before milling and after 80 h of milling

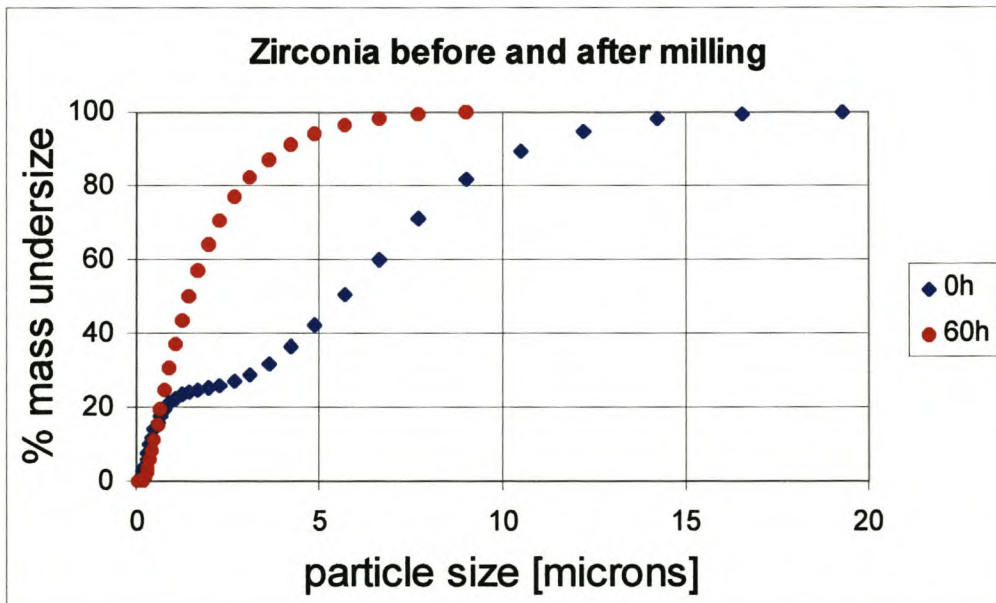


Figure 3.5: Cumulative mass distributions of the zirconia before milling and after 60 h of milling

The cumulative particle-size distributions of the starting powders before and after milling are shown in **figure 3.4** and **figure 3.5**. After milling the alumina powder for

80 h, the size distribution changed considerably. The change after the zirconia powder was milled for 60 h was less pronounced, since the zirconia particles were smaller before milling. **Appendix D** shows the change in particle-size distribution during milling for both powders.

Table 3.4 provides additional data describing the zirconia and alumina powders. The specific surface area was determined by BET (BET micrometrics, ASAP 2010, Department of Chemical Engineering, University of Stellenbosch). To obtain a visual picture of the alumina both before and after milling, Scanning Electron Microscope (Department of Physics, University of Stellenbosch) was used. **Figure 3.6** shows pictures of alumina-powder samples before and after milling.

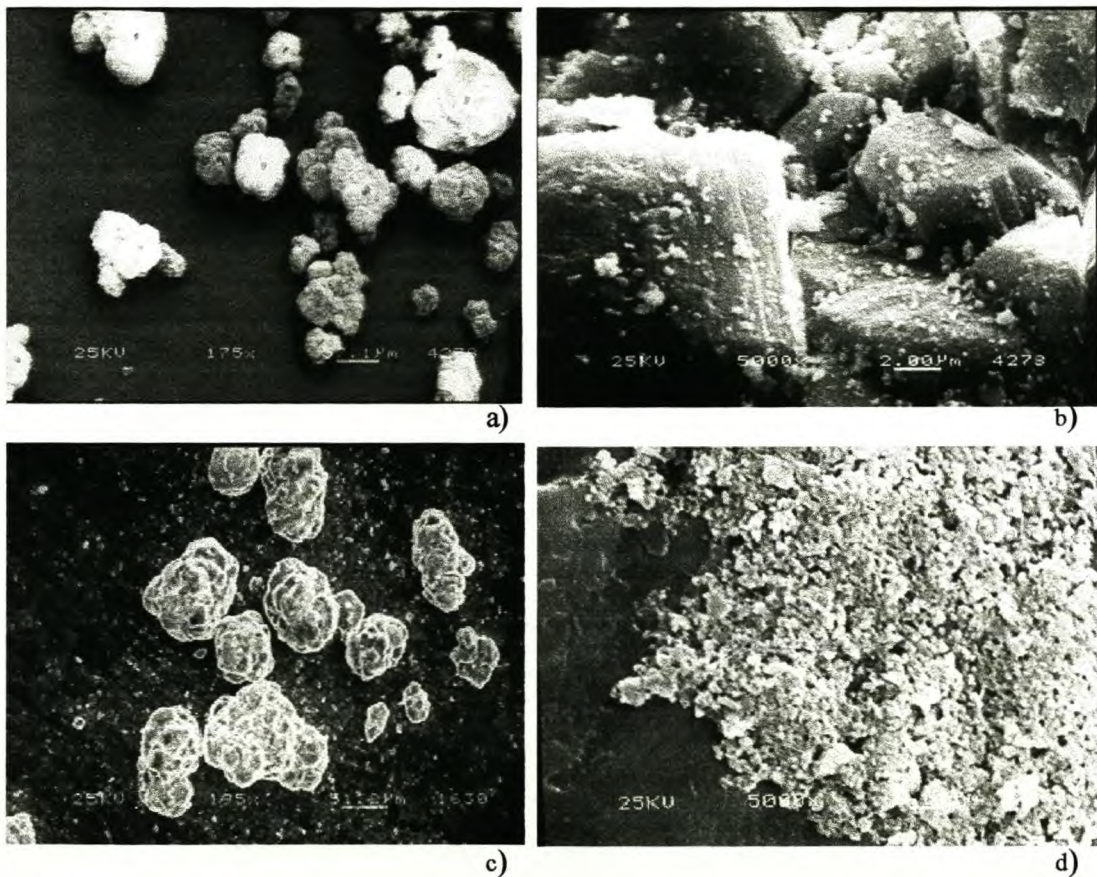


Figure 3.6: Alumina powder before milling a) 175x and b) 5000x, enlarged, Alumina powder after milling c) 195x and d) 5000x, enlarged.

Table 3.4 Powder-size distribution properties before (0h) and after (80h) milling

| Powder | D_{50} (μm) | $D_{10} - d_{90}$ (μm) | Specific surface area (m^2/g) |
|-----------------|----------------------------|-------------------------------------|---|
| Alumina (0 h) | 115.83 | 60.1-186.0 | 167.7 |
| Zirconia (0 h) | 5.65 | 0.37-10.6 | 6.7 |
| Alumina (80 h) | 2.79 | 1.05-6.93 | - |
| Zirconia (60 h) | 1.43 | 0.46-4.01 | - |

Before milling the alumina powder consisted of large particles and barely contained any particles smaller than 60 μm (see **table 3.4** and **figure 3.6a**). The close-up of one of these particles (**figure 3.6b**) does show some smaller particles on one of the large particles. **Figure 3.6c** is a picture of some of the still relatively large alumina particles that were still present in the milled alumina, whereas **figure 3.6d** clearly shows how the particle size has decreased.

3.4 Summary

In this chapter the raw material preparation, entailing the first two steps of the membrane manufacturing process, is discussed. The constant parameters, modifications, and unknown parameters of the raw material preparation are summarised shortly.

The following parameters were kept constant throughout the raw material preparation:

- Raw Materials Used:
 - 70 m% alumina
 - 29 m% zirconia
 - 1 m% yttria

The same raw materials were used for all ceramic membranes manufactured during this project.

- Separate Wet Milling:
 - oxide:balls:water-ratio: 1:2:1
 - milling time for alumina: 80 h
 - milling time for zirconia: 60 h

The following modification was made during the project to the original raw material preparation of Linkov [Linkov and Belyakov, 1996]:

- A ceramic ball mill with ceramic balls was used instead of a steel ball mill with steel balls

Uncontrollable Parameters:

- Linkov and Belyakov gave no information on the initial size distribution or on the size distribution after milling in their patent.

The cumulative mass distributions before and after milling, of the alumina and zirconia powders used as the raw materials for the membranes manufactured in this project, were determined and are shown in **figure 3.4** and **figure 3.5**.

4. Manufacture of Ceramic Membranes

The quality of the ceramic membranes depends both on the starting materials as well as on the manufacturing procedure. Chapter 3 discusses the preparation of the raw materials. The method of manufacture, the highlighted part in **figure 2.10**, is discussed in this chapter.

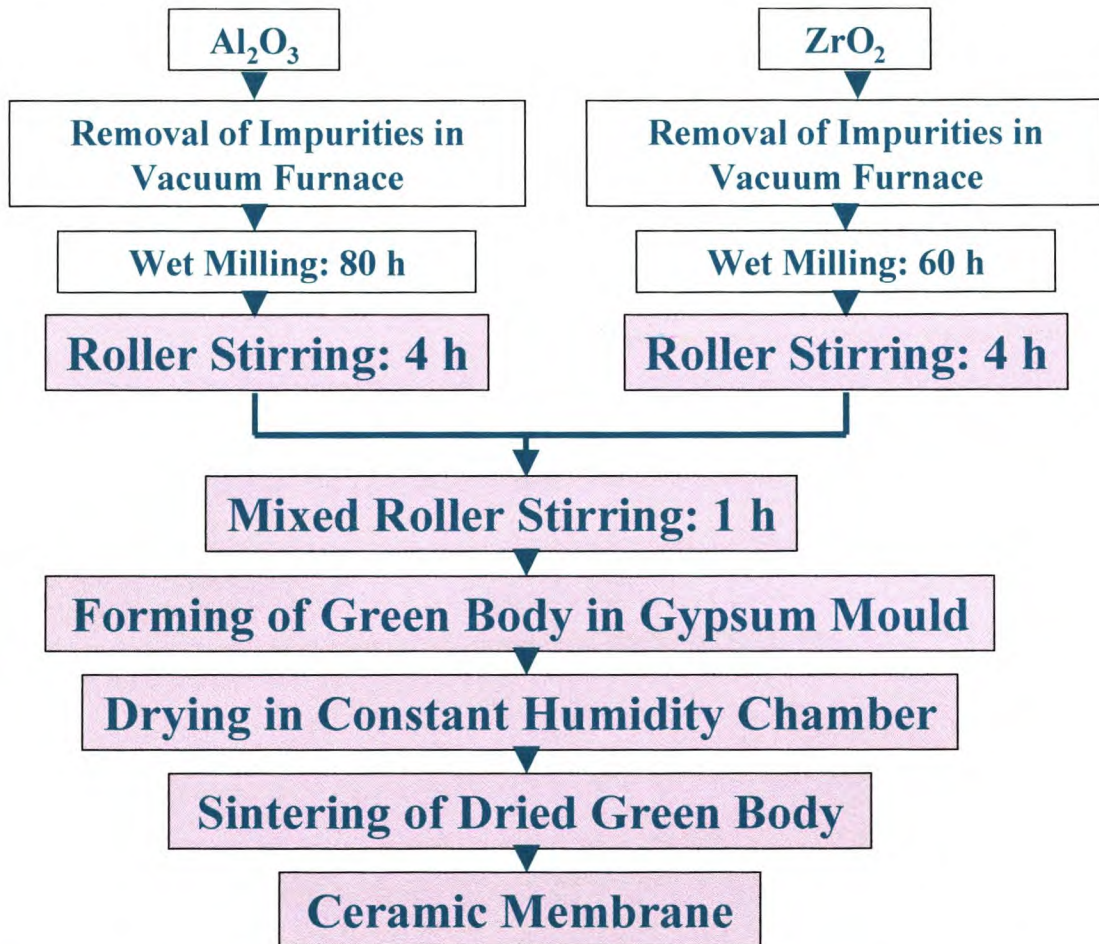


Figure 2.10: Schematic diagram of the ceramic membrane manufacturing process

4.1 Roller Stirring and Mixing –A Stable Casting Suspension.

The patent by Linkov and Belyakov [1996] suggests that after removing the alumina and zirconia from the mills, it should be placed into two polyethylene drums, where 15 m% water is added. The two drums are then roller-stirred for 4 hours.

Subsequently, the casting suspension is prepared by mixing the alumina and zirconia suspensions in the same drum for 1 hour. The resulting casting suspension should, according to Linkov, have a density of between 2.2 and 2.4 g/cm³.

4.1.1 Water Removal

The patent by Linkov and Belyakov does not describe how to remove the wet alumina and zirconia powders from the mills or how to place them in the polyethylene bottles. For this project, a small syringe connected to a flexible tube was used to remove the wet alumina and zirconia powders from the ceramic mills. To remove as much as possible of the milled powder some water was added. The amount of water added for this purpose exceeded the amount (add 15 m%) suggested by Linkov and Belyakov [1996]. After sucking the suspension from the mill it was immediately squirted into a polyethylene bottle.

The amount of water in the casting suspension at this point exceeded the prescribed amount (it is best to add as little water as possible when removing the oxides from the mills). To remove the excess water from the suspension (after removal from the mills) two options were considered, viz.

- Evaporation of the water in a warm water-bath at a low ($\approx 40^{\circ}\text{C}$) temperature. The advantage of this method is that the suspension is left in the polyethylene bottle but the disadvantage is the elevated temperature that might influence the suspension.
- The second method was centrifugal separation (Department Chemical Engineering, University of Stellenbosch) of the powder from the water, followed by removal of excess water. The advantage of this method is that the mixture is not exposed to an elevated temperature. Disadvantages are that the suspension is removed from the polyethylene bottle resulting in a loss of the casting suspension, as well as the break-up of the suspension by the centrifugal actions.

Evaporating water at a low temperature was found not to influence the stability of the suspension and no losses of the oxides occurred and therefore, this method of water

removal was preferred. The next paragraph discusses the influence of the water in the casting suspension on the green body.

4.1.2 Amount of Water in the Casting Suspension

The amount of water in the casting suspension is very important for the structure and strength of the green body and thus the ceramic membrane. As Darcovich and Cloutier [1999] explains: "*The colloidal phase-state of a suspension that forms the consolidated green body has a direct influence on the eventual microstructure of the sintered solid object.*"

The properties of the casting suspension influence a number of different aspects of the formation of the green body by slip casting:

- The thickness of the membrane; too much water in the casting suspension resulted in a very thin green body (and very fragile) whereas too little water resulted in a thick (viscous) casting suspension and a thick green body, as well as a membrane surface that was less smooth. The amount of water in the casting suspension thus has an influence on the membrane thickness and smoothness.
- How well slip casting can be executed; when the casting suspension is too thick it was found that it was difficult to remove the excess slip. When the casting suspension is too thin however, it was found that it was difficult to remove the (very thin) green body from the mould.
- The structure of the green body, the smoothness of the membrane (as mentioned in the previous points) as well as how easily cracks will form in the green body and the sintered product also are related to the amount of water in the casting suspension.

Linkov and Belyakov [1996] suggests a suspension density of 2.2-2.4 g/cm³, but it was found in this research project that suspensions with this density were very difficult to slip cast because of the thickness, or high "viscosity" of the suspension. To examine the influence of the amount of water in the casting suspension on membrane thickness a number of experiments were performed, where different

amounts of water was evaporated in the warm water bath, and the results are shown in **table 4.1**. The first two columns are a summary of the results for the different mixtures that were prepared. The next two columns show the influence of the water content on the membrane thickness for the membranes of one specific mixture only.

Table 4.1: Influence of H₂O content on the thickness of the green body

| Summary of the results for all mixtures | | Results for one specific mixture only | |
|--|--|--|--|
| Ratio: <i>g Water</i> <i>g Mixture</i> | <i>Membrane thickness</i> <i>after 60s</i> <i>[mm]</i> | Ratio: <i>g Water</i> <i>g Mixture</i> | <i>Membrane thickness</i> <i>after 60s</i> <i>[mm]</i> |
| 1.3 | 1.25 | 1.5 | 1.2 |
| 1.45 | 1.2 | 1.77 | 1.07 |
| 1.65 | 1.1 | 1.8 | 1.05 |
| 1.75 | 1.07 | 1.89 | 1 |
| 1.8 | 1.05 | 2.01 | 0.85 |
| 1.85 | 1 | 2.13 | 0.5 |
| 1.95 | 0.9 | | |
| 2 | 0.85 | | |
| 2.1 | 0.6 | | |

The results from **table 4.1** are also shown in **figure 4.1**. This figure shows a large increase in membrane thickness for a small initial decrease in the water content of the mixtures (up to a water content of twice as much water).

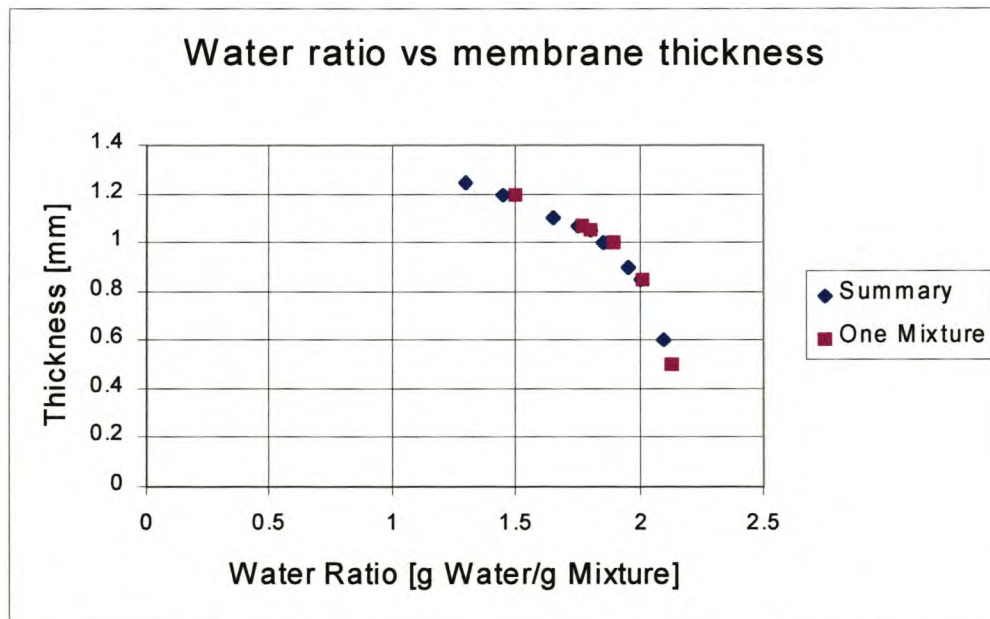


Figure 4.1: Influence of the amount of water in the casting suspension on the membrane thickness. (A water ratio of 1 corresponds to equal mass amounts of water and oxides; a water ratio of 2 corresponds to twice as much water.)

Figure 4.1 shows that decreasing the water content in the mixture continues to increase the membrane thickness, but the increase in thickness becomes less prominent. The increase is fairly constant for a water ratio decrease between 2 and 1.8. For water ratios less than 1.8, the increase in membrane thickness with decreasing water ratio became even less. To obtain a membrane thickness of 1 mm the water ratio is between 1.8 and 1.9 grams of water per gram of oxides.

The influence of membrane thickness on permeability and mechanical strength will be discussed in chapter 5 and 6, where gas and liquid permeability coefficients are discussed.

4.2 Forming of the Green Body

To form the green body for the ceramic membrane, Linkov and Belyakov [1996] suggest slip casting using a gypsum mould. When the bi-disperse casting suspension comes into contact with the mould surface, the larger metal oxide particles precipitate at a higher rate than the smaller ones. As a result, the portion of the ceramic green body formed next to the mould surface consists of larger particles and thus, has larger pores. The deposition of the smaller particles then takes place onto the newly formed green body, which at that point, serves as a support for the thin membrane layer consisting of smaller particles with smaller pores.

4.2.1 Background on Slip Casting

Slip casting or mould casting [Bridger and Massuda, 1987, and Tiller and Tsai, 1986] is a common method for the production of hollow ceramic products (see **Appendix E**). Slip casting consists of suspending powdered raw materials in liquid, this is the casting suspension. The casting suspension is poured into a porous mould, usually made of gypsum. The mould absorbs the liquid from the casting suspension, leaving a layer of solid material on the mould surface. The excess slip is removed after the desired shell thickness has formed, producing a hollow component (green body). The slip casting process is especially economical for short production runs. The main

disadvantages of the process are poor dimensional accuracy and slow rates of production.

4.2.2 Forming of an Asymmetrical Green Body

A French patent by Guendjian [1965] further explains this formation of both the support and the membrane layer simultaneously in the slip casting process of an alumina powder suspension. This patent states that when the excess solution is removed from the membrane, the deposit still consists of a large amount of liquid, and the colloidal particles in the deposit move to the deposit-air interface, eventually forming the thin membrane-layer. To understand this process, it is described in detail below. Note that the slip casting method is also used to deposit a membrane layer on a support in the sol-gel-technique as described in paragraph 2.3.2.

- (a) A stable suspension of milled material is obtained, containing a small amount of colloidal particles.
- (b) The suspension is poured into a micro-porous mould, preferably gypsum.
- (c) After the required deposition thickness is obtained, holding the mould upside down pours out the rest of the suspension.
- (d) Then, after slow drying of the mould the deposited body will shrink slightly and let loose its grip on the mould.

The green body then looks like an agglomeration of reasonably large particles, *the support layer*, with on the inside (the inside was not in contact with the gypsum mould) a very thin layer of colloidal mineral particles, *the membrane layer*.

The *membrane layer* then consists of the same material as the *support layer*, and is uniformly porous but has pores that are much smaller than those of the *support layer*. The stable suspension (**figure 4.2a**) consists of particles with certain dimensions, and a certain portion of colloidal particles with much smaller dimensions. The two different porous structures apparently evolve as a consequence of the movement of helicoidal particles from the suspension to the surface. This phenomenon can be explained as follows:

Consider a solution consisting of particles (1) of which the diameters are more than approximately ten Angstroms. Where these particles are in equilibrium in the liquid and on the surface of this solution (**figure 4.2b**) one finds a film of pure fluid (2 in **figure 4.2b**).

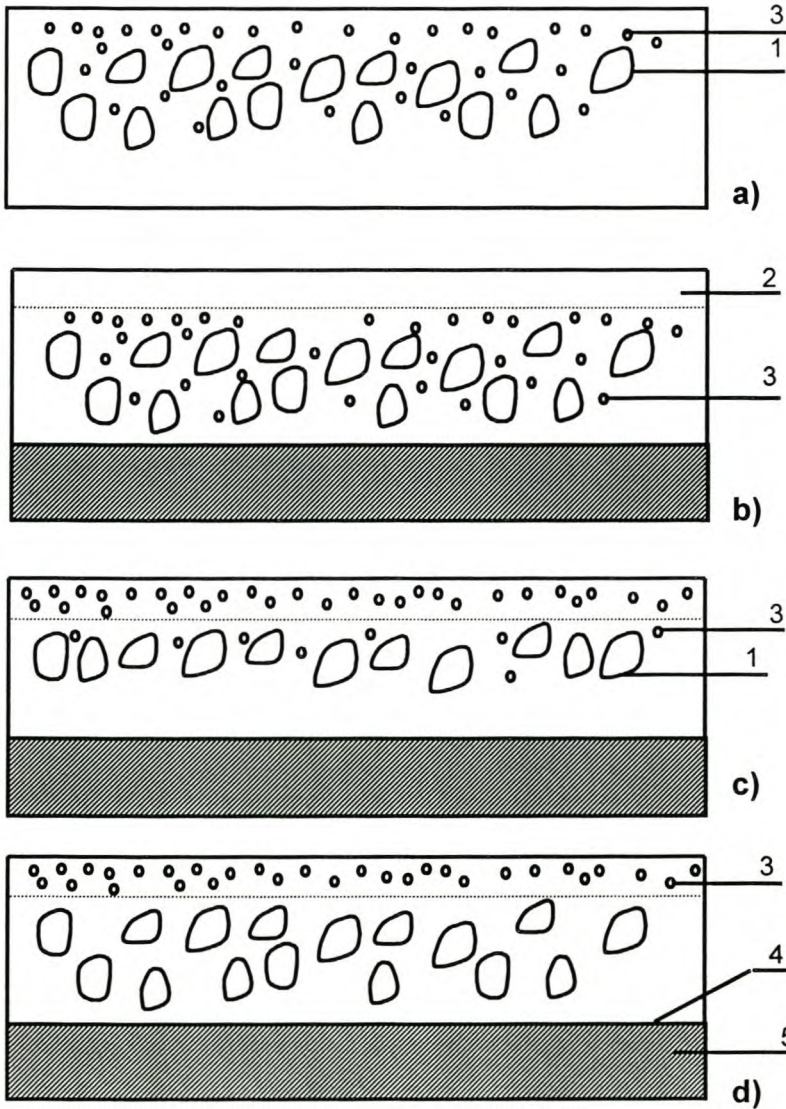


Figure 4.2: a) The stable casting suspension containing a certain amount of colloidal particles, b) A casting solution with a film of pure liquid on the surface, c) A suspension containing a certain percentage of colloidal particles, and d) The suspension after some of the water from the suspension has leaked into the gypsum [Guendjian, 1965]

Now consider the case of a suspension (**figure 4.2 a and c**) containing a certain percentage of colloidal particles (3) that is particles with dimensions in the order of the liquid molecule's dimensions. The liquid-surface-bed (2), that

according to Laplace's theory, has properties that can be approximated as a stretched membrane, will stop these particles from moving into the liquid-membrane. The colloidal particles, on the other hand, move with a Brownian movement and are the only kind that can "fall" through this liquid-membrane. After a certain time, practically all of the colloidal particles have "fallen" through the liquid-membrane.

The composition, as depicted in **figure 4.2d**, is then obtained by leakage of the water in the suspension into the gypsum as follows:

The solution is poured into a gypsum mould (5) that absorbs the liquid (water) of the solution, and the particles attach to the inside wall (4) of the gypsum mould. As soon as the desired thickness is obtained (between 1 and 2 mm) the mould is simply turned upside down and the resulting solution is poured out. At that point, the deposit still consists of a large amount of liquid, and the colloidal particles (3) move to the deposit-air interface. After complete drying, one can verify the thin film of **figure 4.2d**.

4.2.3 The Gypsum Mould

For the formation of the green body a tubular gypsum mould, **figure 4.4**, for the slip casting was designed and made using a stainless-steel contra-mould, **figure 4.3** (for specific gypsum information, see **Appendix E**). The gypsum moulds were made according to the following procedure:

The gypsum powder was mixed with distilled water (mass-ratio gypsum:water \approx 1.025:1) and cast in the stainless steel contra mould (**figure 4.3**). The gypsum mould was left to dry for 12 hours after which it was fired in an oven at 200°C for another 12 hours. The gypsum moulds were kept at a constant humidity of 40% at a temperature of 20°C until they were used.

Removing the gypsum mould from the stainless-steel contra mould initially caused problems until the stainless steel contra mould was modified slightly. The gypsum initially used for the moulds ran out of stock and other gypsum was ordered. Most of the gypsum moulds made with the initial gypsum cracked. A few of them (their water

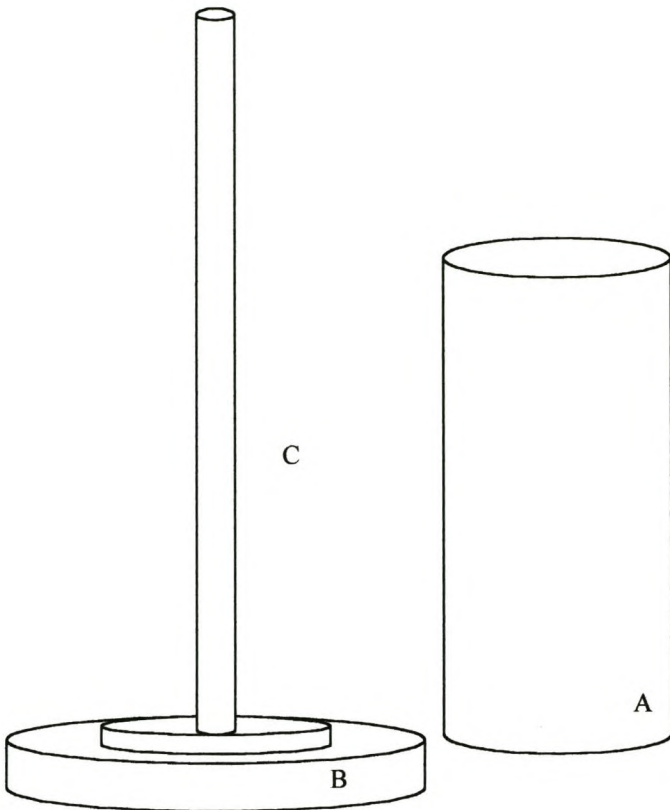


Figure 4.3: Stainless-Steel contra mould of the gypsum mould. Piece A is placed over C after which the gypsum is cast in between A and C resulting in a gypsum mould as displayed in figure 4.4

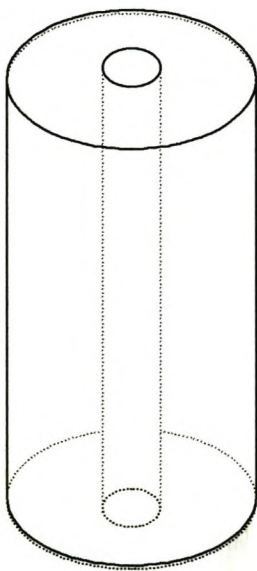


Figure 4.4: Drawing and picture of a typical gypsum mould

ratio was 2.3:1) however were still used for the manufacture of the ceramic membranes. The specific information for the gypsum that was used is found in **Appendix E** and the gypsum moulds used for each membrane is indicated with the specifics of each membrane in **Appendix F**.

The porosity of the mould determines how much and how fast water is drawn into the mould and “sucked” out of the casting suspension. The smoothness of the inside of the gypsum mould was also found to be important for obtaining a smooth green body. Some of the moulds had small cavities on the inside, which resulted in corresponding cavities in the green bodies also. For gypsum moulds that were irregular on the inside, the green body would form with uneven dimensions.

To obtain better membranes, i.e. more regular and dimensionally accurate and reproducible membranes, one should have gypsum moulds as close as possible to perfect [Tilborg and Veringa, 1989].

4.2.4 Membrane Deposition

According to the literature, the thickness of the layer, L_g , of a product manufactured by slip casting increases linearly with the square root of the dipping time [Burggraaf & Keizer, 1991]. Leenaars and Burggraaf [1985] and Ulhurn et al. [1989] found that for alumina and titania, the rate of membrane deposition increases with the *slip concentration* or with *decreasing support-pore size*:

$$L_g = \left(\frac{2 \cdot K_m \cdot \Delta P_g \cdot t}{\mu \cdot \alpha} \right)^{1/2} \quad (4.1)$$

where L_g is the permeability constant of the gel layer, μ the viscosity of the slip “liquid”, K_m a constant related to the reciprocal of solid concentration and ΔP_g the pressure drop across the gel layer.

From equation (4.1), it can be seen that the viscosity of the casting suspension plays an important role. It regulates the formation rate of the gel layer and helps to prevent the slip from penetrating the porous support system. The influence of the viscosity on the casting suspension can be modified by the addition of binders. These binders can

also play an important role in the prevention of cracks in the layer. However, for this project, binders were not used for the manufacture of the ceramic membranes. To improve the membrane strength and performance, experiments can be done with adding binders.

4.2.4.1 *Method of Slip Casting*

Two different slip casting “techniques” were used to slip cast the green body into the gypsum mould:

- 1) - The mould is filled with casting suspension.
 - During 60 seconds the mould containing the casting suspension is slowly rotated horizontally.
 - After the 60 seconds of rotating, the excess suspension is discarded.

When the casting suspension contains too little water, proper removal of excess suspension becomes extremely difficult (since most of the liquid of the suspension was sucked into the mould). When the casting suspension contains too much water on the other hand, the green body became extremely thin and fragile. This occurs due to the fact that in this technique only a limited volume of casting suspension is used and therefore, when all the oxides in this limited volume has deposited, there simply is no material left to deposit and form a thicker green body.

- 1) - The casting suspension is continuously added to the mould for 60 seconds in such a way that the mould is completely filled with the casting suspension at any period during the 60 seconds.
 - After 60 seconds the excess suspension is discarded.

This method provided smoother inside surfaces and a more equal thickness of the membranes. Also, this technique decreased both the problems occurring in the first technique with casting suspensions that contained too much or too little water.

4.2.4.2 Slip Casting Time and Thickness

According to the literature [Burggraaf and Keizer, 1991], the thickness of a membrane should increase linearly with the square root of slip casting time. For the last few membranes manufactured, two additional casting times were used (90 and 120 seconds). The membrane thickness versus the square root of time is plotted in **figure 4.5**, and indeed shows a linear relationship.

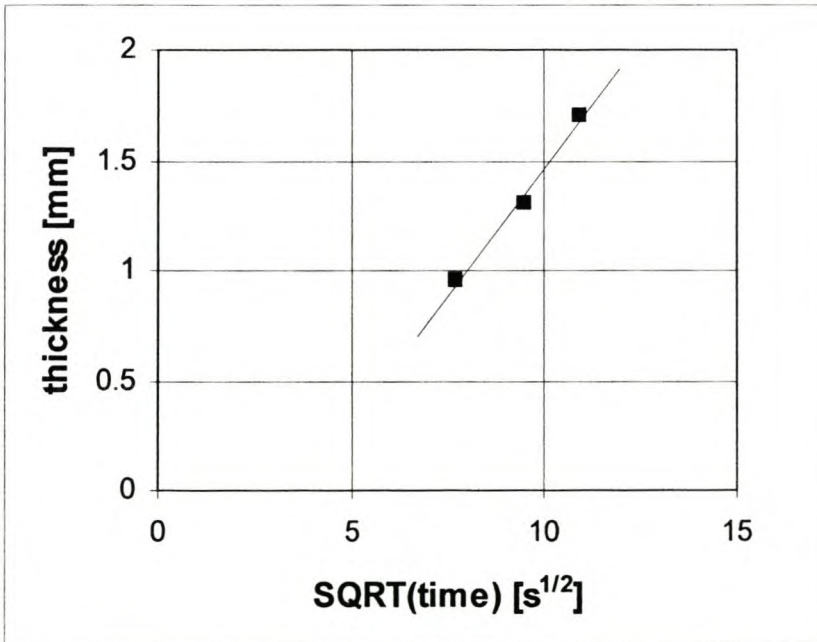


Figure 4.5: Influence of the time the casting suspension is in the gypsum mould on the membrane thickness (the real times are 60, 90 and 120 seconds)

The verification of this relationship is important if membranes of a certain thickness should be manufactured; their slip casting time can then be calculated beforehand:

$$th_{mem} = 0.2328 \cdot \sqrt{t} - 0.8702 \quad (4.2)$$

However, equation (4.2) will only be valid for a mixture with 1.85g water per 1 gram oxides. Since only 3 data points have been obtained so far, it is recommended that more data points be generated to validate this linear relationship.

4.3 Drying in a Constant Humidity Chamber

Linkov and Belyakov [1996] suggest that the green bodies be dried in a constant humidity chamber after the slip casting. Products made by slip casting are liable to undergo large shrinkage during drying because the green density obtained by this method is only about 70% of the theoretical density. To prevent severe shrinkage, for this project the green bodies were dried in a constant humidity chamber (Votch Constant Humidity Chamber, Department Chemical Engineering, University of Stellenbosch) for 72 hours at a temperature of 20°C and a humidity of 40%.

4.4 Sintering of the Green Body

The sintering of a green body, more specifically the sintering temperature and time, are expected to have an influence on the porosity and thus the permeability as well as the strength of the ceramic product. Generally the strength of the body will increase with decreasing porosity.

Sintering generally does not begin until the heating temperature exceeds 0.5 to 0.7 of the melting temperature, which is sufficient to cause significant atomic diffusion for (solid state, i.e. without a liquid phase) sintering. The heating prior to sintering induces material changes such as drying, vaporisation of chemically combined water or water in crystal structures as well as pyrolysis of contaminations introduced during the manufacturing process.

Linkov and Belyakov [1996] suggest that the green body, or precursor, be sintered in a furnace at a rate of 100°C per hour up to 1300°C, and fired at that temperature for 60 minutes. For the sintering of the manufactured ceramic membranes in this project, this sintering profile, as shown in **figure 4.6** was initially used.

To examine the influence of and possibly optimise the sintering temperature and time, the selected temperatures and times are shown in **table 4.2**. The influence of sintering time on the membranes is examined at 1300°C for 6 different sintering times. In the case of a sintering time of 0h the membrane is heated up to 1300°C and then

immediately cooled down again. The influence of sintering temperature is also examined at four different temperatures, 1250, 1300, 1350 and 1400°C.

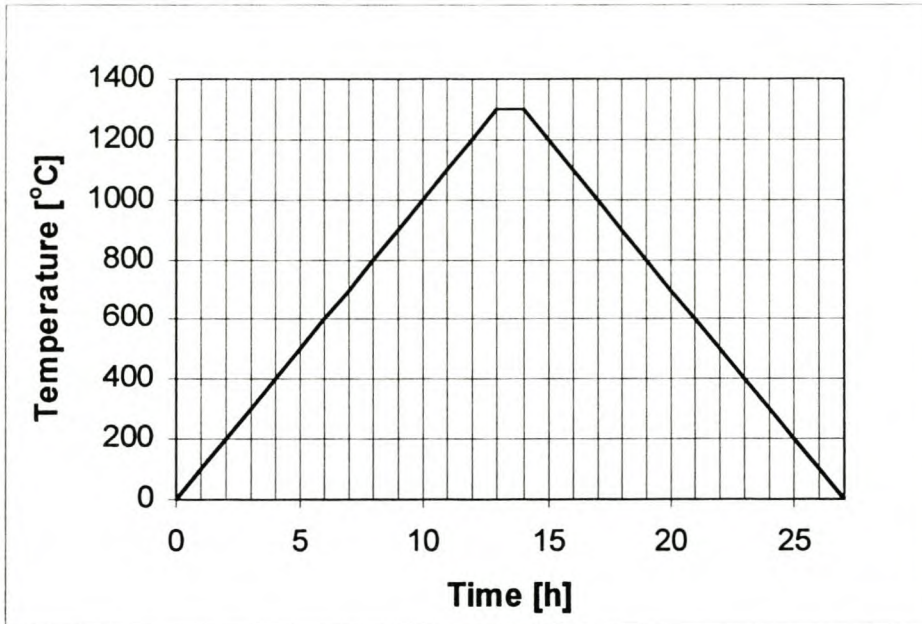


Figure 4.6: Typical ramp sintering profile for sintering the manufactured green bodies

Table 4.2: Sintering temperatures and times

| | t = 0 h | t = 0.5 h | t = 1 h | t=1.5 h | t = 2 h | t = 4 h |
|-------------|---------|-----------|---------|---------|---------|---------|
| T = 1250°C | | | ✓ | | | |
| T = 1300°C | ✓ | ✓ | ✓ | ✓ | ✓ | ✓ |
| T = 1350°C | | | ✓ | | | |
| T = 1400 °C | | | ✓ | | | |

Sintering temperature and time strongly influence the phase compositions (e.g. alumina, titania and zirconia membranes). At phase transitions (γ - θ - α alumina) there is a strong increase in pore size [Larbot et al., 1987, and Keizer et al., 1988]. According to Keizer et al. [1988] the pore diameters of a membrane can be regulated by heat treatment to values as small as 3-6 nm and up to 50-200 nm depending on the material.

All membranes sintered at 1250 °C were very fragile, and all of them broke before their permeability could be tested. This could be due to the zirconia, which changes from the monoclinic phase to the tetragonal phase at 1227°C.

The methods to evaluate the manufactured membranes are discussed first in chapter 5. The membranes manufactured under the other sintering times and temperatures are evaluated in Chapter 6.

4.5 The Manufactured Membranes

In total 32 membranes of the total manufactured membranes were suitable for testing. **Table 4.3** summarises the total number of membranes that were dried, sintered and tested. Of the 75 membranes that were dried only 89% was also sintered. The 10% of the dried membranes that were not sintered were the membranes that broke completely when removed from the gypsum mould. Membranes that were cracked but not broken after removal from the gypsum mould were still sintered. Of the sintered membranes, 44 membranes did not have cracks and could be considered for evaluation tests. Of these 44 membranes eventually only 32 membranes were strong enough or suitable enough to test.

| Table 4.3: Manufactured membranes summarised | |
|---|------|
| <i>Total Number of Membranes Dried:</i> | 75 |
| <i>% With Cracks:</i> | 40 % |
| <i>% Sintered:</i> | 89 % |
| <i>Total Number of Membranes Sintered:</i> | 67 |
| <i>Membranes Sintered without Cracks:</i> | 44 |
| <i>Total Number of Membranes Tested:</i> | 32 |
| <i>% Tested:</i> | 73 % |

Table 4.4 indicates how many membranes were sintered, cracked and tested at each sintering temperature and time. For each sintering temperature and time at least 4 membranes were sintered.

| Table 4.4: Number of membranes sintered, cracked and tested | | | | | | | | | |
|--|----------|------|------|------|-----|-----|---------|------|------|
| | @ 1300°C | | | | | | for 1 h | | |
| | 0 h | 0.5h | 1 h | 1.5h | 2 h | 4 h | 1350 | 1400 | 1250 |
| Sintered: | 7 | 6 | 20 | 4 | 8 | 6 | 5 | 6 | 6 |
| Cracked: | 2 | 2 | 9 | 1 | 3 | 2 | 1 | 2 | 1 |
| Tested: | 4 | 4 | 8 | 3 | 3 | 4 | 2 | 4 | 0 |
| NoCrack/Tested | 5/4 | 4/4 | 11/8 | 3/3 | 5/3 | 4/4 | 4/2 | 4/4 | 4/0 |

The last row in **table 4.4** compares the number of sintered membranes without cracks to the number of sintered membranes that were tested. This ratio is good in all cases except for the membranes sintered for 1 hour at 1250 °C, which all broke during testing, as discussed already.

4.6 Summary

In this chapter the membrane manufacture process is discussed. In total, 32 ceramic membranes were successfully manufactured with modifications to the manufacturing process. The modifications, constant parameters and uncontrollable parameters of the manufacturing process are first summarised shortly.

The following modifications were made during the project to the original manufacturing process of Linkov and Belyakov, [1996]:

- Instead of only adding 15 m% water after wet milling, up to 200 m% water was added to remove the milled suspension from the ceramic mills.
- A small syringe with a flexible tube was used to remove the wet powder from the ceramic mills.
- Excess water was removed by evaporation in a warm water bath at 40 °C. (Centrifugal separation proved to be inefficient.)
- To obtain membranes with a thickness of 1 mm for a slip casting time of 60 seconds, it was found that the casting suspension should contain 1.85 grams of water per grams of oxides compared to the 1.15 prescribed by Linkov and Belyakov [1996].

- The second casting method, continuously adding casting suspension for 60 seconds, provided a more smooth inside surface and a more equal thickness compared to the first casting method, where the casting suspension is poured into the gypsum mould and the gypsum mould manually rotated for 60 seconds.
- The membranes were sintered at 1300 °C. for 1 hour as Linkov and Belyakov [1996] suggest, but membranes were also sintered at 5 other sintering times and 3 other sintering temperatures.

The following parameters were kept constant throughout the manufacture of the ceramic membranes:

- Separate Roller Stirring: - 4 hours for the alumina and the zirconia suspensions in a polyethylene bottle at 25 °C.
- Mixed Roller Stirring: - 1 hour in a polyethylene bottle at 25 °C.
- Evaporation: - In a warm water bath at 40 °C until enough water has evaporated (measured in mass).
- Slip Casting:
 - Membranes are all slip-cast for 60 seconds unless noted otherwise.
 - Gypsum moulds are all made with a gypsum:water mass ratio of 1.025:1.
- Drying: - All membranes were dried in a Vötsch constant humidity chamber for 72 hours at a temperature of 20°C and a humidity of 40%.

Uncontrollable Parameters:

- The quality of the gypsum moulds was not fully controllable. Also the quality of the gypsum that the mould are made with was not fully controlled.
- Dimensions of the manufactured membranes were very difficult to control accurately. They depend on the composition of the casting suspension as well as on the quality of the gypsum mould.

It was found that, as stated in literature, the membrane thickness increases with the square root of slip casting time, which allows one to predict the membrane thickness for a certain slip casting time.

The membranes sintered for 1 hour at 1250°C were mechanically too weak to evaluate them.

Chapters 5 and 6 discuss the evaluation methods for and the evaluation of the manufactured membranes.

5. Selected Methods for Evaluating the Ceramic Membranes

The separation efficiency (e.g. selectivity and permeability) of the ceramic membranes depends mostly on micro-structural features of the membrane layer as well as the support layer. Such micro-structural features include pore size and distribution, pore shape and tortuosity.

To determine the separation efficiency and the strength of the membrane a large variety of evaluation methods exist, most of which are described in chapter 2.

5.1 Chosen Evaluation Methods

The task of analysing thin asymmetric or graded-structure membranes with a wide range of pore sizes is quite challenging. The difficulty lies in the very small percentage of pore volume contributed by the thin membrane film relative to that of the support layer [Hsieh, 1991].

The evaluation methods decided upon for the evaluation of the membranes in this project are shown in **figure 5.1**.

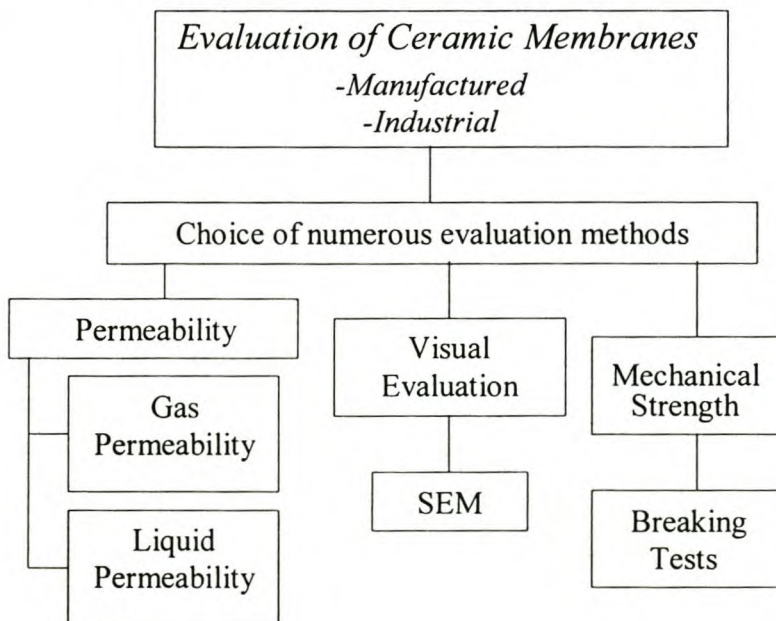


Figure 5.1: Schematic diagram of the evaluation of the ceramic membranes

5.2 Evaluation of the Permeability

The permeability of a membrane is perhaps one of the most important performance criteria for cost effective membrane technology, particularly for large-scale separations. In cross-flow membrane separation processes, permeability may be influenced by factors such as cross-flow velocity, trans-membrane pressure difference, temperature and feed characteristics.

For evaluation of the manufactured membranes more application-oriented characteristics such as permeability were preferred to compare the results with those of commercial membranes. Therefore both gas- and liquid permeability tests were conducted. Permeability tests are typically used to provide an indication of the capacity of a membrane; a high permeability equals a high throughput.

For both the gas and the liquid permeability tests the same membrane-testing module was used. This membrane-testing module is described first.

5.2.1 Membrane Testing Module

To protect the membrane and to be able to mount the membrane airtight into the testing module, it was mounted between two perspex tubes. The ceramic membrane was mounted between 2 perspex tubes using Pattex super gel to initially attach the two tubes. Fibroglas casting resin was then casted around and on the glued surface giving the attachment some strength (**figure 5.2**).



Figure 5.2: Picture of the tested membrane mounted between 2 perspex tubes

The mounted membrane was then inserted into the testing module. The testing module, shown schematically in **figure 5.3**, is coupled to either the gas or the liquid permeability test set-up with rubber tubes. **Figure 5.4** shows a picture of the testing

module, with the mounted membrane inside, coupled to the gas permeability set-up. O-rings (**figure 5.3**) between the red screw-on pieces and the rest of the testing module, prevent the gasses and liquid from leaking.

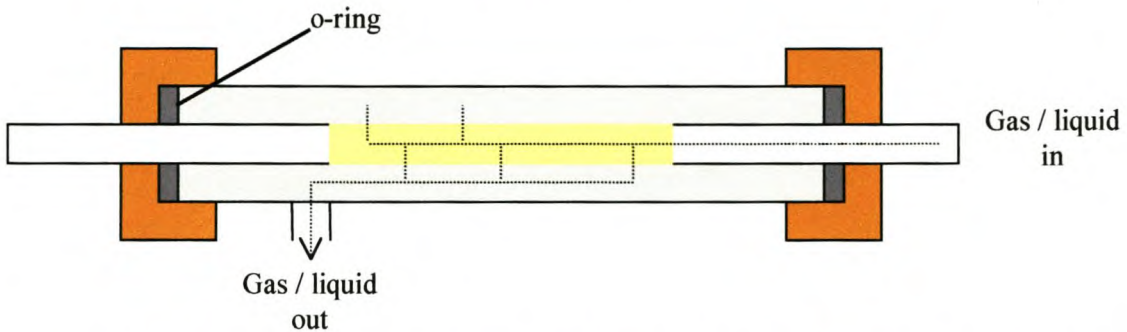


Figure 5.3: Schematic cross-section drawing of the testing module with the membrane (yellow)

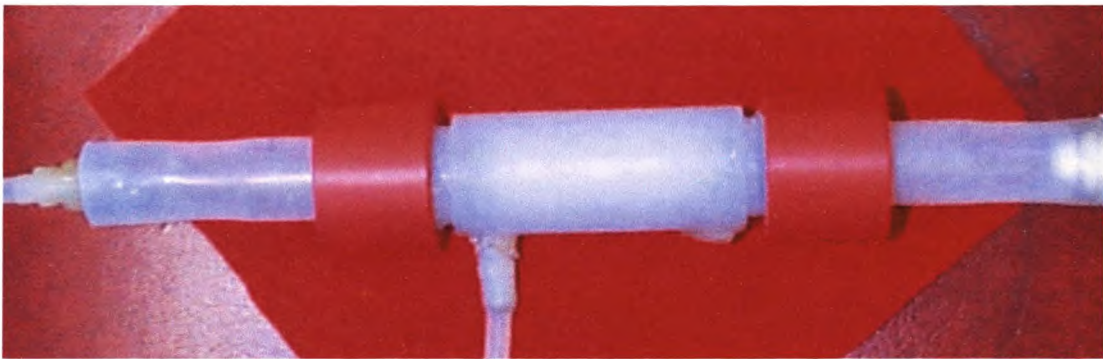


Figure 5.4: Testing module, with mounted membrane inside, coupled to the gas permeability set-up

This Membrane Testing Module was also used for the liquid permeation tests as described in paragraph 5.2.4.

5.2.2 Gas and Liquid Permeability Coefficients, K_g and K_l .

Darcy's law (see equation 2.3) describes viscous flow of a Newtonian fluid through a porous medium. Force fields such as gravity are ignored and a uni-directional pressure gradient is assumed. Darcy's law is valid for compressible as well as incompressible media.

Darcy's law and the equations of continuity and motion (assume a steady state situation, neglecting the accumulation term) are used to obtain equations for the liquid and gas permeability coefficients. For a liquid, the dependence of ρ and μ on the pressure is minor and therefore ignored. For a gas, ρ is a function of pressure and described by the ideal gas law. All permeability tests are performed at 25 °C.

After implementation of Darcy's law and integration of the equation of continuity for a cylindrical geometry, the following equations are obtained (see **Appendix H** for detailed mathematics):

For a cylindrical geometry, the liquid permeability coefficient K_l :

$$K_l = \frac{\dot{m} \cdot \mu \cdot \ln\left(\frac{r_2}{r_1}\right)}{\rho \cdot 2 \cdot \pi \cdot H \cdot \Delta P} \quad (5.1)$$

For a cylindrical geometry, the gas permeability coefficient, K_g :

$$K_g = \frac{\dot{m} \cdot \mu \cdot \ln\left(\frac{r_2}{r_1}\right) \cdot R \cdot T}{2 \cdot \pi \cdot H \cdot \Delta P \cdot P_m \cdot M_i} \quad (5.2)$$

5.2.3 Gas Permeability Tests

The measurement of the permeability of a gas through a porous medium as a function of the mean pressure across a porous medium characterizes the membrane and also provides good comparative data. Several authors have applied the gas flux data to characterise microporous and asymmetric ultra filtration membranes, as well as to determine a mean pore radius of the membrane.

The manufactured membranes were tested with three gasses, argon and nitrogen and hydrogen. Different gasses have different molecular sizes and, depending on the pore size of the membrane layer, gasses are able to permeate through the membrane at certain rates. The experimental set-up for the gas permeability tests is discussed in the next paragraph.

5.2.3.1 Experimental Set Up

The experimental set-up for the gas permeability tests is shown in **figure 5.4**. The gas-flow is controlled and measured by the mass-flow-controller, which was calibrated with the bubble-flow-meter (see **Appendix G**).

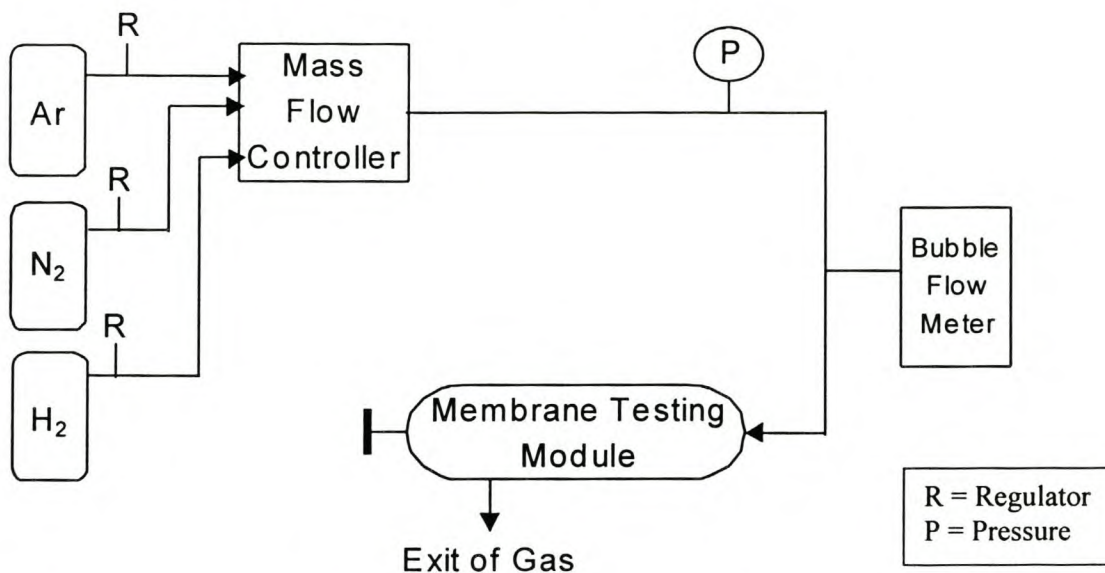


Figure 5.5: Experimental set-up for the gas permeability tests

The experimental procedure for the gas permeability experiments consisted of the following steps:

- The gas bottle was opened and the gas-regulator of the gas set to the regulated pressure.
- The mass flow controller is set to 100, which is equivalent to a gas flow of 1,2 cm³/s for Nitrogen and 1,67 cm³/s for Argon at 25 °C and atmospheric pressure (see **Appendix G-I**).
- The only point at which gas can escape the testing module (gas out point in **figure 5.5**) is closed off to test the set-up for any leaks. If the pressure increases and the mass flow controller (that also displays the measured mass flow) decreases to 0, the set-up is leak proof.
- The gas out point is then opened to gas flow again and the gas flow is incrementally increased while the pressure for each increase is recorded.

5.2.3.2 Permeability

To understand the performance of the membranes, the terms permeability and selectivity are briefly explained next. It is important to note that the gas and liquid permeabilities are each defined differently:

The (molar) gas permeability, F_o , is determined by dividing molar permeate flux by the trans-membrane pressure difference. It indicates the membrane's molar flow per unit area (flux) per unit pressure difference over the membrane, therefore, gas permeability $\Leftrightarrow F_o \equiv [\text{mol}/(\text{m}^2\text{sPa})]$.

The water permeability, F_w , on the other hand, is determined by dividing permeate flux, Q_w ($\text{litre}/\text{h}^1\text{m}^2$) by the backpressure over the membrane. It indicates the membrane's volume flow per unit area (flux) per unit pressure difference over the membrane, thus water permeability $\Leftrightarrow F_w \equiv [1/(\text{m}^2\text{hbar})]$.

5.2.3.3 Selectivity

The selectivity is a measure of the amount of separation that occurs between two gasses while they permeate through the membrane. For a certain membrane, the degree of separation between gasses depends on the relative permeabilities of the gasses to be separated. There are three definitions for the degree of separation, or selectivity:

For a binary mixture, the *actual* selectivity is defined as follows [Bhave, 1991]:

$$S_{12}^* = \frac{y_1/x_1}{(1-y_1)/(1-x_1)} \quad (5.3)$$

Where gas 1 is the more permeable gas and y and x are the mole fractions of the gas species downstream and upstream of the membrane, respectively.

The *ideal* selectivity is the separation factor given by the ratio of the individual permeabilities of the two gasses through the membrane:

$$S_{12} = \frac{F_{o1}}{F_{o2}} \quad (5.4)$$

It is important to keep in mind that the actual separation factor will usually be smaller than the ideal separation factor. The two become equal when the downstream pressure is much lower than the upstream pressure.

Then lastly there is the *theoretical* selectivity, which is the reciprocal ratio of the square root of the molecular masses of the two gasses:

$$S'_{12} = \frac{\sqrt{M_2}}{\sqrt{M_1}} \quad (5.5)$$

According to literature, if the theoretical selectivity equals the ideal selectivity, it can be deduced that Knudsen diffusion occurs [Germic et. al., 1997, and Lin et al., 1994]. To achieve higher separation selectivity than that in the Knudsen regime, requires a membrane with a smaller pore size

5.2.3.4 Gas Permeability Model

The measurement of the gas flow through a porous medium can provide a means of determining a mean pore radius of the porous material. The gas flow is a linear function of the mean pressure across the membrane. The mean pore radius that is calculated may not have a precisely defined physical meaning, but it is considered a useful tool when comparing membranes.

The determination of the porous structure of a membrane with supported layers is rather difficult. Common methods, such as mercury porosimetry and nitrogen adsorption are, without special modifications, only partly suitable [Uchytíl, 1994]. Uchytíl developed a simple permeation method as a complementary possibility:

To characterise the porous structure of a membrane using gas permeation it is necessary to introduce two simplifying assumptions:

- The membrane layer (subscript m) and the support (subscript s) are considered to be mono-disperse porous layers with tubular parallel pores of radii, r_m and r_s , respectively.
- The flow of non-adsorbing gas through the pores is assumed to be the sum of the Knudsen and Poiseuille flows; the contribution of surface diffusion is not considered.

The following equation is then used for the volumetric gas flow rate, Q , through the membrane:

$$Q = \frac{A \cdot \Delta P}{R_t} \quad (5.6)$$

with R_t the total resistance of the ceramic membrane to the gas flow, ΔP the pressure drop across the membrane and A the membrane area.

The total resistance of the ceramic membrane consists of R_s , the resistance of the support to the gas flow and R_m , the resistance of the membrane layer to the gas flow:

$$R_t = R_s + R_m \quad (5.7)$$

In homogeneous porous media with a pore radius larger than 1.5 nm, combined Knudsen and Poiseuille flow occurs. The mean free path of a molecule is the average distance between collisions. Knudsen diffusion takes place when the mean free path of the molecules is *larger* than the mean pore radius of the porous medium. Poiseuille flow, or laminar flow, on the other hand takes place when the mean free path of the molecules is *smaller* than the mean pore radius of the porous medium. For any one of the layers the following equations can be written: ($x = m$ or s)

$$\frac{1}{R_x} = \frac{1}{R_x^k} + \frac{1}{R_x^p} \quad (5.8)$$

where R_x is the total resistance with the superscripts k and p indicating the Knudsen and Poiseuille parts of the total resistance. For modelling purposes both resistances are defined independent of the pressure conditions [Uchytel, 1994]:

$$R_x^k = \frac{3 \cdot th \cdot \theta \cdot \left[\frac{\pi \cdot M}{8 \cdot R \cdot T} \right]^{\frac{1}{2}}}{2 \cdot r \cdot \epsilon} \quad (5.9)$$

and,

$$R_x^p = \frac{8 \cdot th \cdot \theta \cdot \mu}{r^2 \cdot \epsilon} \quad (5.10)$$

Where th is the layer thickness, θ is the tortuosity (pore length, $l_r = \theta \cdot th$), r is the mean pore radius, ϵ the porosity, R the gas constant, T the temperature, μ the gas viscosity and M the molecular weight of the gas.

The gas flow of gas i , in the support can be obtained by substituting equations 5.7-5.10 into equation 5.6. After rearrangement:

$$\frac{Q_i \cdot P_o}{A \cdot \Delta P_s} = \frac{1}{R_{s,i}^k} + \frac{P_{m,s}}{R_{s,i}^p} \quad (5.11)$$

The values on the left-hand side of equation 5.11 are a linear function of $P_{m,s}$, the arithmetic mean gas pressure in the layer. By plotting equation 5.11, the values of the Knudsen and Poiseuille resistances can be determined, which can then be used to calculate the mean pore radius of the support:

$$r_s = \frac{16 \cdot \mu_i \cdot \left[\frac{8 \cdot R \cdot T}{\pi \cdot M_i} \right]^{\frac{1}{2}} \cdot R_{s,i}^k}{3 \cdot R_{s,i}^p} \quad (5.12)$$

The geometric factor $\psi_s = \epsilon_s / \theta_s$ can be calculated by substituting the calculated r_s , into either one of the resistances.

The equations above are suitable to determine the mean pore radius of a support. The membrane layer is then applied to the support, after which the gas flow through the membrane plus the support layer is measured. Combining this data provides information on and a mean pore radius for both the membrane and the support layer according to Uchytel [1994]. However this model cannot be used in such a way for

the manufactured membranes, since the membrane layer and the support are formed together in one step. Uchytel model is discussed further in chapter 6.

Similar gas permeability models can be found [Altena et. al., 1983 and Nakao, 1994], that are based on gas flux measurements by pressure decay in a gas ballast chamber.

5.2.4 Liquid Permeability Tests

Water permeability experiments are generally used to determine intrinsic membrane properties. With a liquid such as pure water, the transport resistance due to gel layer and concentration polarization is generally negligible or absent and the permeate flux values therefore, vary linearly with the pressure drop over the membrane. The pure water permeability of a membrane is one of the most important performance criteria for cost effective membrane technology. In practical situations the observed permeate flux values at the operating pressure difference are seldom comparable to the water permeability data. This is due to increased hydraulic resistance to transport across the membrane structure as a result of particle deposits or the formation of a gel layer on the membrane [Bhave, 1991]. The obtained water permeability results therefore, were mostly used to compare different membranes.

5.2.4.1 *Experimental Set Up*

For the liquid permeability tests, a laboratory water-filtration pilot plant with RO (reverse osmosis) water was used. The experimental set-up for the liquid permeability tests is shown in **figure 5.6**. All measurements were done at ambient temperature conditions ($T = 25\text{ }^{\circ}\text{C}$).

A rotary pump pumps water from the RO water tank to the membrane module. Valve V3 is a backpressure valve that can be adjusted to set the pressure over the membrane. The pressure P2 is atmospheric pressure as the set-up is open to the atmosphere. The pressure over the membrane is then measured with the pressure gauge, P1. The water permeation through the membrane is determined by weighing the mass of the water, collected on the scale at a set time.

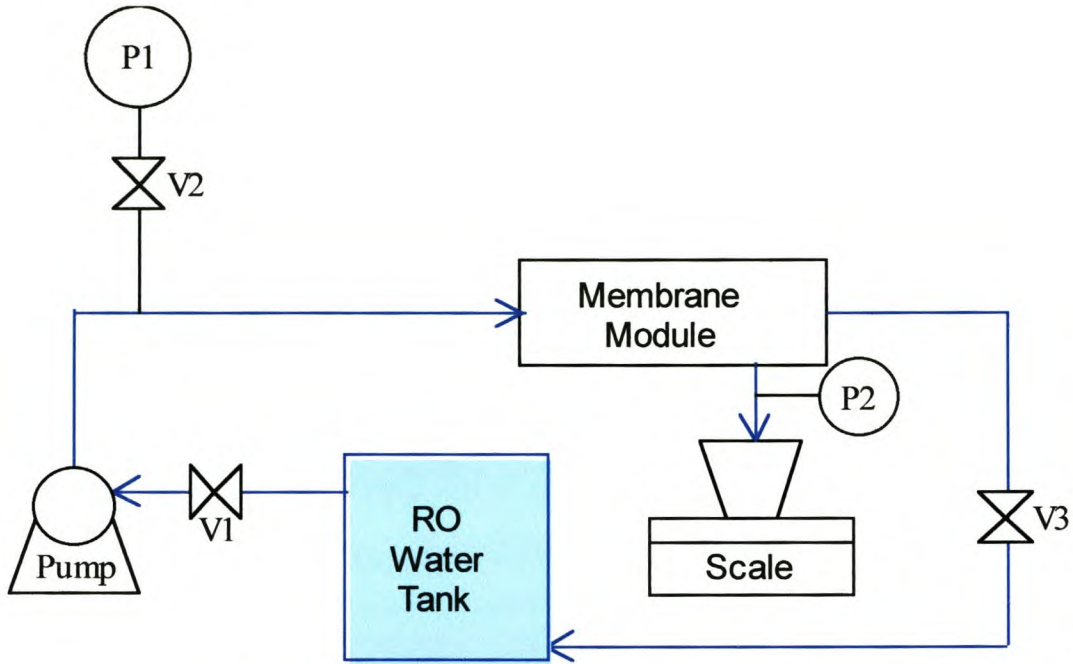


Figure 5.6: Experimental set-up of the liquid permeability tests

5.2.4.2 Liquid Permeation Modelling

Fluid flow in homogeneous porous materials can be described on a macroscopic level as Darcy did. Adjusting equation 2.3 for permeate flux related to the membrane resistance; the superficial velocity through the membrane, q , is proportional to the pressure drop over the membrane and inversely proportional to the membrane thickness, L :

$$q = \frac{\dot{m}}{\rho \cdot A_{mem}} \quad (5.13)$$

$$q = \frac{K \cdot \Delta P}{\mu \cdot L} \quad (5.14)$$

with K the intrinsic permeability coefficient, which describes the capacity of the porous medium to transmit fluids. The permeability coefficient, K , incorporates all of the boundary conditions relating to the flow resistance and is independent of the liquid and therefore considered a material property. The permeability in equation

(5.14) is determined under steady state conditions. These equations are acceptable when the superficial velocity (q) is very small.

For a higher permeability flux the Poiseuille equation for viscous flow is adapted for a porous medium. Liquid permeability is then described by the Carman-Kozeny equation (see also equations 2.4 and 2.6).

5.3 Evaluation of the Mechanical Strength

Generally the mechanical characteristics of ceramic materials are a high intrinsic strength and a low toughness; they are very brittle. The strength of the membranes depends on the porosity and the size of the largest flaw in the membrane. When the flaw size is reduced to the order of the particle size the maximum tensile strength is obtained. Since ceramic membranes are very brittle, when a stress is applied the ceramic material will fracture at a relatively low strain. To be able to compare the mechanical strength of the manufactured membranes to Linkov's membranes and to obtain a general indication of the strength of the ceramic membranes, the evaluation of the mechanical strength of the membranes is very important.

In many brittle materials, the normal tensile strength tests cannot easily be performed because of the presence of flaws at the surface. Often, just placing the brittle material in the grips of the tensile testing machine causes cracking [Askeland, 1996]. Therefore to test their mechanical strength a 3-point bend test is used (see **figure 5.7**).

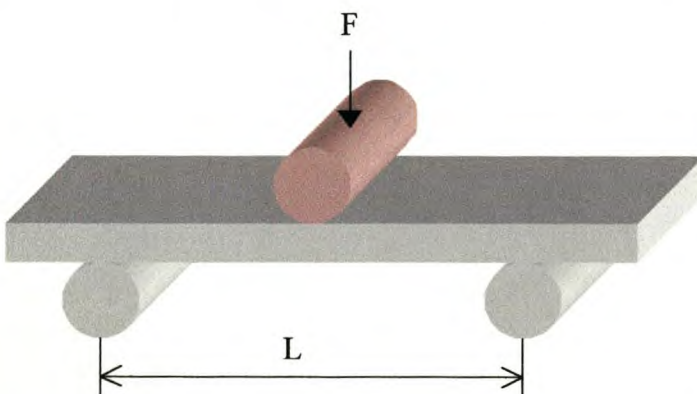


Figure 5.7: Schematic drawing of 3-point bend tests

By applying the load at three points and causing bending, a tensile force acts on the material opposite the midpoint. Fracture then begins at this point. The experimental set up for this test is now discussed.

5.3.1 The Experimental Set-Up for Mechanical Testing

To perform the 3-point bend test the Zwick-bench [Department of Civil Engineering, University of Stellenbosch] had to be modified. This bench is normally used for loads in the order of tons; (approximately 10.000 N). To perform a bend test on the membranes, a 50 kg (500 N) load cell had to be attached to the Zwick-bench as shown in **figure 5.8**. The bench had to be modified to be able to use this relatively small load cell. **Appendix J** shows the full picture of the Zwick bench with the modifications. The modified part of the Zwick-bench with a membrane in the testing position is shown in **figure 5.8**.

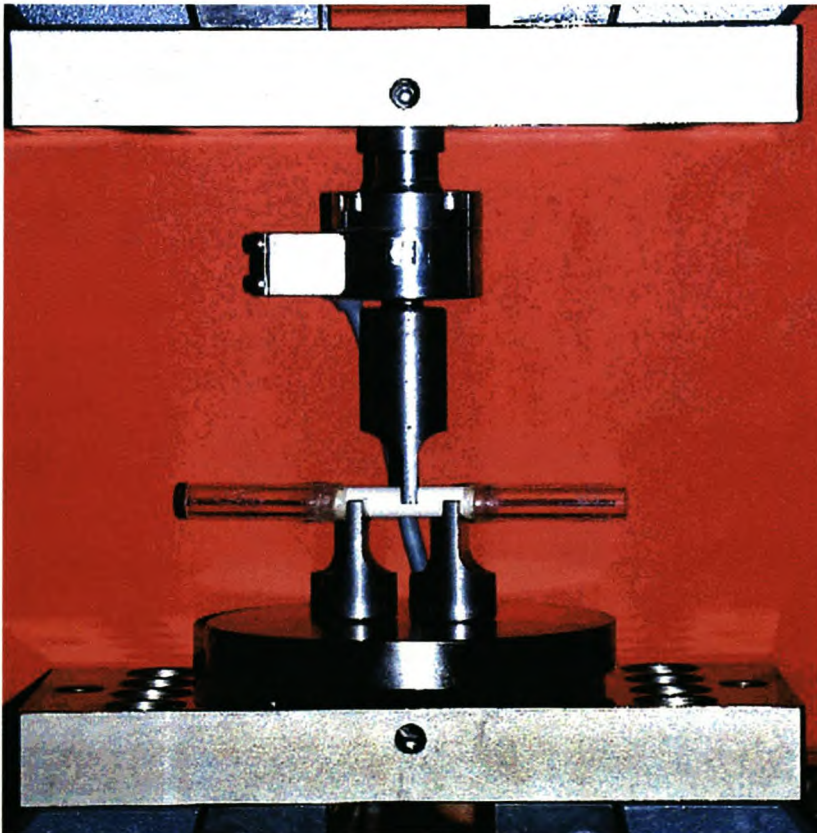


Figure 5.8: Picture of bend-test set-up

The total membrane length, L , over which the bend tests took place, was 29 mm, and the distance between the point where the load was applied and the end point of each membrane was thus, 14.5 mm. The load was lowered onto the membrane at a rate of 1mm per minute and the force on the membrane was recorded digitally. The load increased with time until fracture occurred. With the data of these experiments the breaking strength could be determined as described in the next paragraph.

5.3.2 Determination of the Flexural Strength

The test piece, the membrane, is a hollow cylinder, which has to be considered in the calculations of the breaking, or flexural strength. The moment inertia for a hollow cylinder is first calculated:

$$I = \frac{\pi}{64} \cdot (d_2^4 - d_1^4) \quad (5.15)$$

With the moment of inertia, the moment of resistance is calculated:

$$W = \frac{I}{r_2} \quad (5.16)$$

The flexural strength under bending, or modulus of rupture, describes the materials strength and can then be calculated as follows:

$$\sigma = \frac{M}{W} = \frac{F \cdot \frac{1}{2}L}{W} \quad (5.17)$$

From these equations, it can be seen that the flexural strength depends on the force the membrane can withstand as well as on the dimensions of the membrane. **Table 5.1** gives an indication of the maximum flexural strength at a certain force for a typical membrane.

| Table 5.1: Maximum flexural strength at a certain force for a membrane with an outside diameter: $d_2 = 11$ mm and inside diameter: $d_1 = 9$ mm | |
|---|----------|
| σ_{\max} [N/mm ²] | F [N] |
| 1 | 5.0 |
| 5 | 24.9 |
| 10 | 49.7 |
| 20 | 99.5 |
| 50 | 248.7 |
| 60 | 298.4 |
| 70 | 348.1 |
| 80 | 397.9 |
| 100 | 497.3 |
| 110 | 547.1 |

5.4 Scanning Electron Microscopy (SEM) Evaluation

Microscopy observation directly provides visual information on the membrane morphology. A disadvantage of SEM is the high electron beam energy that is applied to the sample, which can damage the sample surface. The sample is therefore, covered with a thin layer of gold. However, the gold layer may have an influence on the observed structures because of clustering effects of the gold. For the SEM evaluation, two different SEMs were made use of:

- The Scanning Electron Microscope at the University of Stellenbosch (SEM, Topcon ABT 60, Department of Physics, University of Stellenbosch). The used acceleration voltage was 25 kV and the working distance 10 mm. The samples were sputter coated with gold for pictures and with carbon for X-Ray analysis (making use of the Link EDS system and A N 1000 X-Ray analyser).

Although this SEM is not as accurate and precise as the SEM at UCT, it still provides important information and most pictures are taken with this SEM.

- The Scanning Electron Microscope at UCT (SEM, Detector: SE1, I-Probe: 50-500 pA, Electron Microscope Unit, UCT). The used acceleration voltage was 15 kV and the working distance 15 to 25 mm. The samples were sputter coated with

gold. For analysis the XPP/ASAP Quantification Method was used with an acceleration voltage of 20 kV, a beam current of 1000 pA a working distance of 25 mm and a take-off angle of 35 degrees.

This SEM and analysis apparatus is more accurate but the costs are very high and although the analysing method is accurate it produces a very local analysis of the samples.

5.5 Summary

Although numerous different evaluation methods are described in literature, only few of them are applicable to evaluate the manufactured membranes. Many of the evaluation methods give only a small specific little “piece of the puzzle”. It is also important to keep into consideration that many of the evaluation methods give only comparative information.

The evaluation of the gas and liquid permeabilities was chosen because of its application-oriented value. The mechanical strength evaluation was chosen after the observation that the manufactured membranes seemed more fragile than Linkov’s membranes. Lastly, SEM evaluation was chosen to obtain a visual image of the membrane structures.

The next chapter will discuss the results of these four evaluation methods.

6. Evaluation of the Manufactured Ceramic Membranes

In 1997, Keuler received membranes made by Linkov and Belyakov according to the manufacturing method described in **Appendix A**. He used these membranes in research at the University of Stellenbosch [Keuler, 2000] but their strength and performance have been reported to vary. The manufacture procedures of the ceramic membranes according to Linkov's patent are discussed in Chapter 3 and 4. This chapter discusses the results of the evaluation tests performed on the manufactured membranes. Of all the membranes that after sintering, did not have cracks (44, see also paragraph 4.5), 32 membranes were strong enough to be evaluated. The manufactured membranes were evaluated together with one of the membranes purchased from Linkov and Belyakov.

6.1 Gas Permeability Results

To characterise and compare the manufactured membranes, gas permeability tests were performed on each of the 32 membranes. Gas permeability values for the manufactured membranes were typically in the order of 1×10^{-5} mol/m²sPa for argon and nitrogen and between 4×10^{-5} and 5×10^{-5} mol/m²sPa for hydrogen, as shown for membrane 53a in **figure 6.1**.

In cross-flow membrane separation processes, permeability may be influenced by factors such as cross-flow velocity, trans-membrane pressure difference, temperature and feed characteristics. The nitrogen and argon permeabilities were found to slightly increase linearly with increasing pressure difference, as is the case for membrane 53a in **figure 6.1**. The hydrogen permeability did not depend on pressure, for most manufactured membranes the hydrogen permeation was constant with slight deviations.

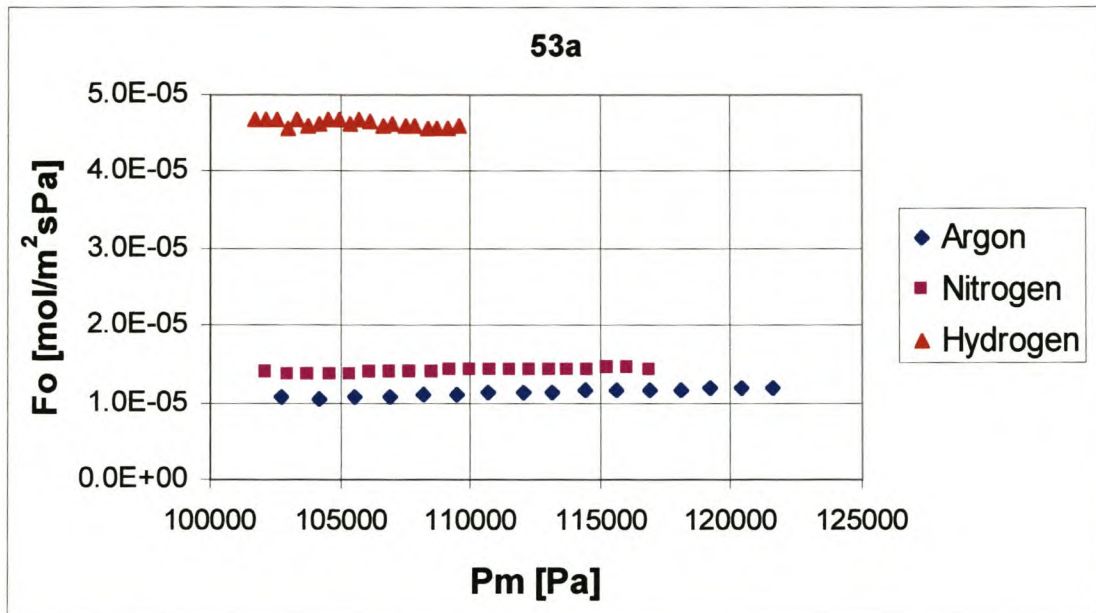


Figure 6.1: Argon, nitrogen and hydrogen permeabilities for membrane 53a

6.1.1 Variance Between the Manufactured Membranes

Variance in nitrogen permeability for the manufactured membranes sintered for 1 and 4 hours at 1300°C are displayed in **table 6.1**. **Table 6.1** indicates a mentionable variance between the nitrogen permeability values of the membranes sintered at these two sintering times. To put the importance of this variance into perspective it is compared to the variance found for commercial membranes, evaluated by Lin [Lin et al., 1994] and Gallaher [Gallaher et al., 1994].

| | <i>Lowest values</i> | <i>Highest values</i> |
|------------------------------|-----------------------|-----------------------|
| 4 nm [Lin et al., 1994] | 14.3×10^{-6} | 18.5×10^{-6} |
| 4 nm [Gallaher et al., 1994] | 6.2×10^{-6} | 8.6×10^{-6} |
| 1h @ 1300 °C | 10.5×10^{-6} | 13.8×10^{-6} |
| 4h @ 1300 °C | 10.1×10^{-6} | 14.2×10^{-6} |

The two values in **table 6.1** for the 4 nm pore diameter membranes [Lin et al., 1994, and, Gallaher et al., 1994] were determined from 14 similar membranes (evaluated by Lin) and 6 similar membranes (evaluated by Gallaher). **Table 6.1** indicates that a variance in gas permeabilities between membranes manufactured in a commercial process is common. The variance in gas permeability values found between the manufactured membranes that were sintered at a certain sintering time and temperature was similar to the variance found for commercial membranes.

Variance in gas permeability is increased by differences in membrane dimensions of the evaluated membranes, e.g. for thicker membranes the permeability is less. The dimensions of the manufactured membranes were not completely controllable, therefore some variance in gas permeability is expected. Accurately controlling the dimensions of the manufactured membranes will decrease the variance in gas permeabilities.

6.1.2 Influence of Sintering Time on Gas Permeability

The gas permeability was measured for six different sintering times at 1300°C as described in paragraph 4.4, namely: 0, 0.5, 1, 1.5, 2 and 4 hours. For each sintering time between three and eight membranes were tested (for the results of such a test, see e.g. **figure 6.1**), and the results are found in **Appendix G-II**. For each sintering time the average gas permeability values were calculated (see **Appendix G-III**), and **figure 6.2** shows the results for hydrogen permeabilities at 105 kPa.

Figure 6.2 indicates an initial increase in hydrogen permeability with sintering time, while the hydrogen permeability between 1 to 4 hours of sintering time is fairly constant. The hydrogen permeability is a maximum at a sintering time of 1.5 hours, after which the permeability appears to decrease again slightly. The nitrogen and argon permeabilities also increase with sintering time similar to the hydrogen permeability (see **figure 6.2 b**), but both nitrogen and argon permeabilities are maximum at a two hours sintering time.

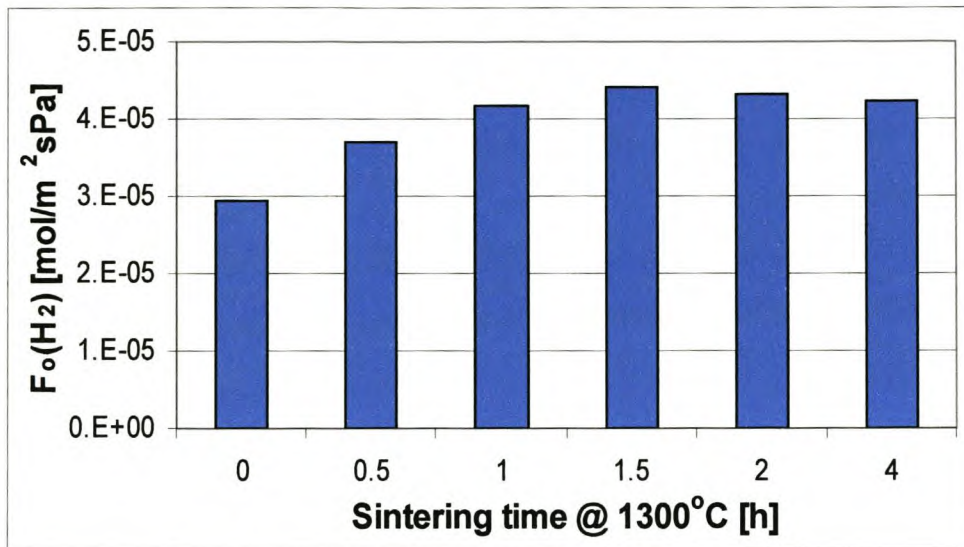


Figure 6.2 a: Average hydrogen permeabilities for different sintering times at a sintering temperature of 1300°C and an average pressure of 105 kPa

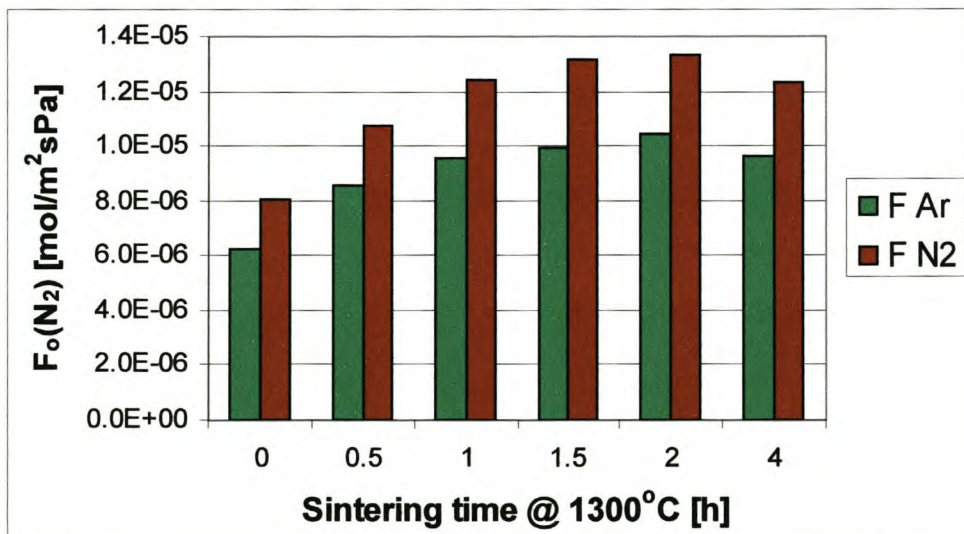


Figure 6.2 b: Average permeabilities of argon and nitrogen for different sintering times at a sintering temperature of 1300°C and an average pressure of 105 kPa

The initial increase in permeability can be explained by pore *growth* during initial-stage sintering [Akash and Merrilea, 1999]. In the initial stage of sintering, initial-stage pore growth is both qualitatively and quantitatively consistent with the well-known process of inter-particle neck formation (also see paragraph 2.4.4.2). Particle neck formation leads

to surface rounding of the pores. This causes a decrease in the surface area of the system without a concomitant decrease in pore volume, leading to an increase in pore size [Akash and Merrilea, 1999]. An increase in pore size will allow more moles of gas to flow through the membrane at a certain pressure, explaining the increase in permeability of the membrane.

6.1.3 Influence of Sintering Temperature on Gas Permeability

To examine the influence of sintering temperature on the gas permeability, the membranes were sintered at four different temperatures; 1250, 1300, 1350 and 1400°C. As already mentioned in paragraph 4.4, all membranes sintered at 1250°C were very fragile, and they all broke before their permeability could be tested. An explanation for this could be the fact that zirconia changes from the monoclinic phase to the tetragonal phase at about 1227°C...

For the remaining three different temperatures the average gas permeability values were calculated (see **Appendix G-III**), and **figure 6.3 a** and **b** shows the results for hydrogen and for argon and nitrogen permeabilities at 105 kPa. **Figure 6.3** appears to indicate an increase in permeability with sintering temperature. It must be noted that the calculated average permeability at 1350°C was calculated from only two values. Results that are more accurate would be obtained if more experiments were performed. Unfortunately, because of the limited amount of data in this particular section, it would be unwise to draw any definite conclusions from **figure 6.3** at this point. **Table 6.2**, which is discussed below also, indicates that the permeability increases with temperature but it is recommended that more membranes be manufactured, also at even higher temperatures to confirm a trend of increasing permeability with sintering temperature.

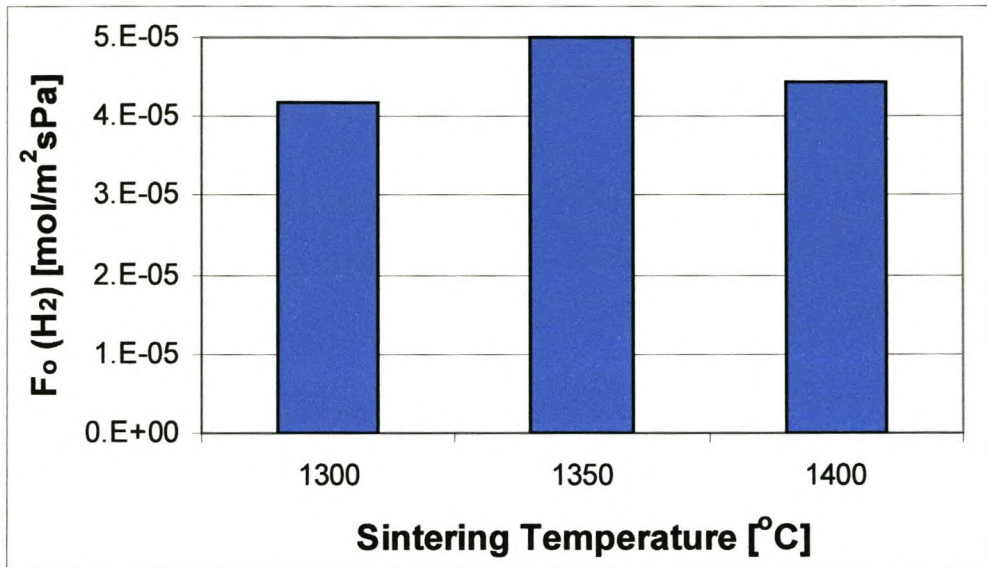


Figure 6.3 a: Average hydrogen permeabilities for different sintering temperatures at a sintering time of 1 hour and an average pressure of 105 kPa

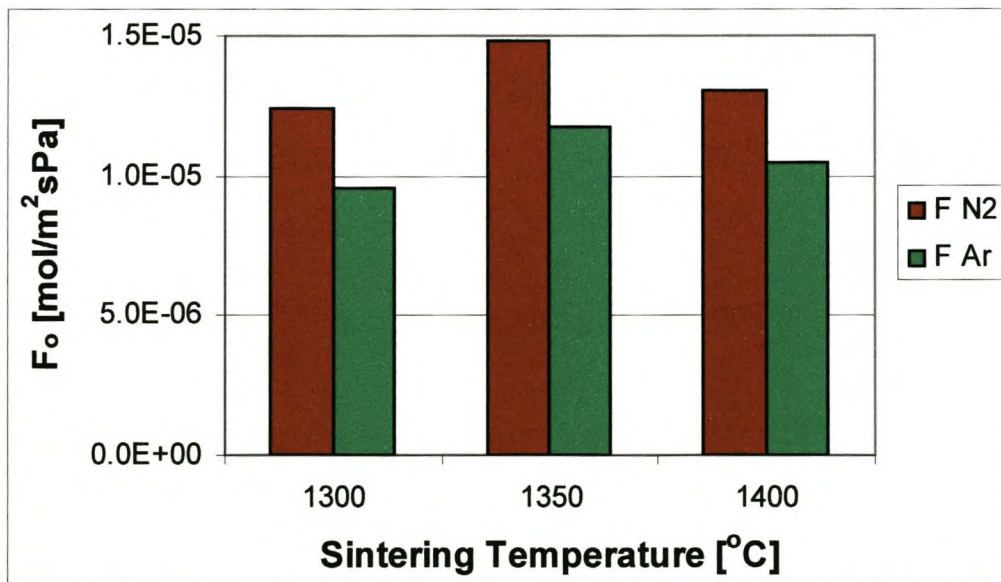


Figure 6.3 b: Average argon and nitrogen permeabilities for different sintering temperatures at a sintering time of 1 hour and an average pressure of 105 kPa

Table 6.2 shows the highest and lowest permeability values at an average pressure of $P_m=105000$ Pa.

| Table 6.2: Highest and lowest permeability values at $P_m = 105$ kPa | | | | | |
|--|--------------------------------|---|------------|-----------|-----------------------------|
| Membrane | Sintering time and temperature | Permeability $\cdot 10^{-6}$ [mol/m ² sPa] | | | |
| | | $F_o(H_2)$ | $F_o(N_2)$ | $F_o(Ar)$ | |
| 57f | 1 h @ 1400°C | 56.3 | | 13.5 | Highest permeability values |
| 34b | 1 h @ 1350°C | | 16.6 | | |
| 54 | 0 h @ 1300°C | 23.3 | 6.38 | 5.02 | Lowest permeability values |

Table 6.2 shows that the highest permeability values are found for the membranes sintered at a temperature higher than 1300°C. This is another indication that the permeability increased with increasing sintering temperature over the tested range. **Table 6.2** also shows the lowest permeability values. They were all found for membrane 54, which was sintered for 0 h at 1300°C. This complements the results in paragraph 6.1.1.

Eventually, after long sintering times at appropriate sintering temperatures, the permeability should decrease with sintering temperature and time (the material will become denser). For the manufacture of membranes, this is obviously not recommended.

6.1.4 Comparison of Result to those of Linkov's Membrane and Other Commercial Membranes

To compare the manufactured membranes to other (commercial) membranes is very important. It will give information on the performance of the manufactured membranes compared to commercial membranes and to Linkov's membrane. **Table 6.3** shows some permeability values that were found in literature. All these articles provided nitrogen permeabilities but unfortunately only one article was found providing hydrogen permeabilities and one providing an argon permeability value. It is important to notice that, for the 4 nm pore diameter membranes, for the one membrane a nitrogen permeability of 6.96×10^{-6} and for the other a 16.6×10^{-6} permeability was reported. This shows quite a large variance between membranes with the same pore diameter.

Table 6.3: Permeability values for alumina ceramic membranes found in literature

| Membrane Material | Pore diameter and other info. | Permeabilities $\cdot 10^{-6}$ [mol/m ² sPa] | | | Literature source (See References for detailed information) |
|---|-------------------------------|--|----------------------------------|---------------------|--|
| | | F _o (H ₂) | F _o (N ₂) | F _o (Ar) | |
| γ -Al ₂ O ₃ | 2 nm, tubular | 29 | 9 | | Terpstra et al., 1988 |
| γ -Al ₂ O ₃ | Tested at 263K* | | 4.2 | | Ulhorn et al., 1992 |
| γ -Al ₂ O ₃ | 4 nm | | 6.96 | | Gallaher et al., 1994 |
| γ -Al ₂ O ₃ | 4 nm | | 16.6 | | Lin et al., 1994 |
| SiO ₂ - γ -Al ₂ O ₃ | 0.5nm | | 0.276 | | Cao et al., 1996 |
| Al ₂ O ₃ | 5nm | | 5.51 | 4.29 | Leger et al., 1996b |

*All membranes except * are tested at a temperature of 25°C, at which the manufactured membranes are tested.*

The two values in **table 6.3** for the 4 nm pore diameter membranes [Lin et al., 1994, and, Gallaher et al., 1994] were the calculated average of 14 similar membranes (for Lin) and 6 similar membranes (for Gallaher). The variance between the gas permeability values of these membranes (obtained from membrane manufacturers) was between 14.3×10^{-6} and 18.5×10^{-6} mol/m²sPa for the membranes tested by Gallaher, and between 6.24×10^{-6} and 8.57×10^{-6} mol/m²sPa for the membranes tested by Lin (also see **table 6.2**). This indicates that a variance in gas permeabilities between membranes manufactured in a commercial process is common. A variance in gas permeabilities between the manufactured membranes is thus expected.

In **figure 6.4** the average nitrogen permeability of the manufactured membranes (sintered at 1300°C for 1 hour) is compared to some nitrogen permeabilities from **table 6.3**, as well as to the nitrogen permeability of Linkov's membrane (see **Appendix G-IV** for full permeability results). The permeability does not seem to be very consistent with pore diameter. An explanation for this inconsistency is that the methods that were used to determine the average pore diameters were not very compatible with each other. Sometimes the methods depend on the person executing the test and often the results are only comparative to membranes that have undergone the same test (with the same operator). It can be said, looking at **figure 6.4**, that the permeability of the manufactured membranes is in the same order of magnitude as that of other commercial membranes reported in literature although it is higher than most of them.

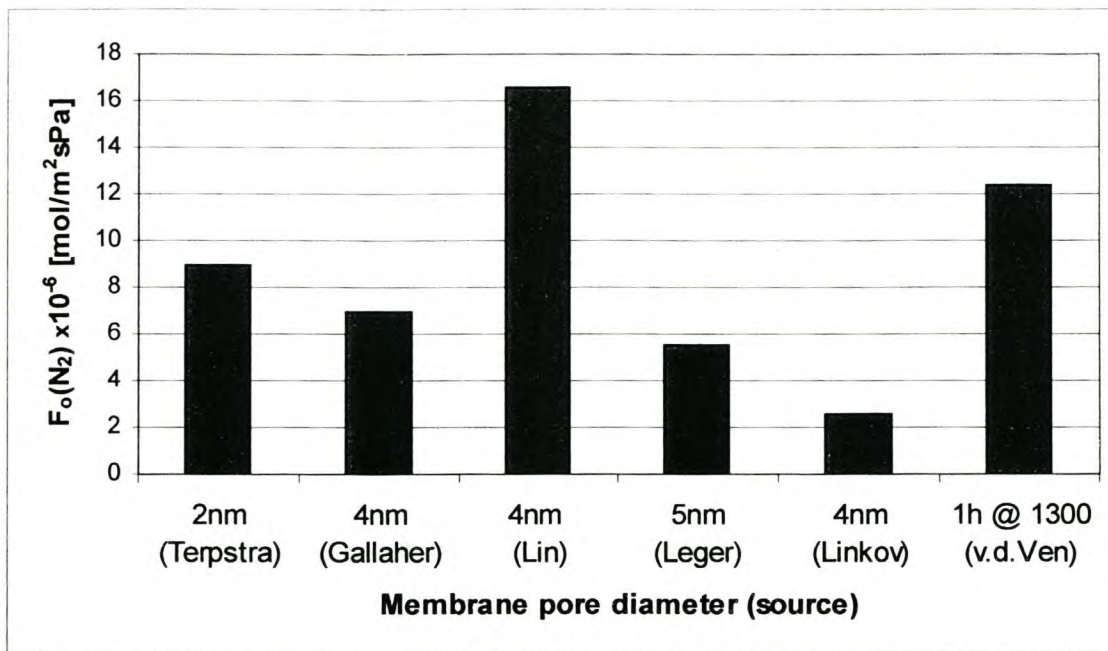


Figure 6.4: Average nitrogen permeability of the manufactured membranes (sintered at 1300°C for 1 hour) compared to some nitrogen permeabilities from table 6.2, as well as to the nitrogen permeability of Linkov’s membrane

Lastly, **figure 6.4** shows that the permeability of the manufactured membranes is about 4 times higher than that of Linkov’s membranes. Whether this is “good” or “bad” depends on, for example, what the membranes are used for, or their selectivity, which is discussed in paragraph 6.2.

The permeability, F_o , is calculated per inside-membrane-area unit. The permeability therefore, in fact does not take into account the thickness of the membrane. The gas permeability coefficient does take into account the thickness of the membrane. Gas permeability coefficients are thus an important tool to compare the different membranes, and are discussed in paragraph 6.4. The permeability, permeability coefficients, selectivity, and the mechanical strength of the membrane, are all factors that have to be considered together to determine the performance of the membrane.

6.1.5 Applying the Gas Permeability Model.

The model as described in paragraph 5.2.3.4 was designed to determine the average pore radius of supports. In essence, it therefore was not suitable for determination of the average pore size of the manufactured membranes. The model was applied to the manufactured membranes to determine whether it could be of value in comparing the average pore radius and/or the Knudsen and Poiseuille resistances.

The gas flow, $Q_i P_o / A \Delta P$ was plotted against the mean pressure P_m , and according to equation 5.11, the Knudsen and Poiseuille resistances as well as the average pore radius and total resistance of the membranes were determined. This method proved to be very ineffective due to the following reasons:

- For each gas, the Knudsen and Poiseuille resistances were different, which is explained by the fact that each gas molecule has a different mean free path. It was expected that hydrogen (the smallest molecule) would have the smallest total resistance and argon (the largest molecule) the highest. For some membranes this was true. However for other membranes the total resistance of nitrogen was much higher than for argon and hydrogen. The hydrogen resistance always had the smallest total resistance.
- Hydrogen didn't follow the common trend of increasing gas flow with increasing pressure. The Poiseuille resistance therefore became negative for some membranes, making the calculations for the average pore radius impossible and the calculations of the total resistance doubtful, which also confirms that the method was inaccurate.
- The average pore radius determined for each membrane was extremely high, even for Linkov's membrane it was calculated to be in the order of 700nm. The pore radius calculated for each different gas was also very different, making it difficult to decide on the "correct" radius.

What was interesting of the graphs obtained by plotting $Q_i P_o / A \Delta P$ vs P_m was that they were very similar to the graphs obtained for plotting F_o against P_m . This is shown for membrane 40 in figure 6.5.

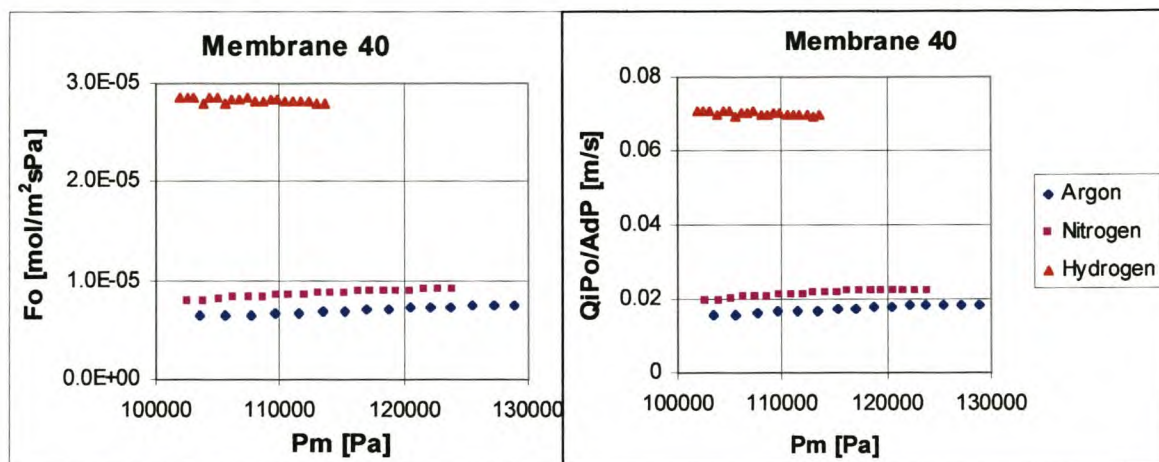


Figure 6.5: Comparison of the $Q_i P_o / A \Delta P$ vs P_m plot and the F_o vs P_m plot

According to the model as described in paragraph 5.2.3.4, the slope of the linear relationship between $Q_i P_o / A \Delta P$ and the mean pressure, P_m represents the Poiseuille resistance to permeability ($1/R^p$). The intercept of the same linear relationship represents the Knudsen resistance to permeability. The linear relationship between the permeability, F_o and the average pressure, P_m indicates that the slope and intercept of this linear relationship represent a similar Poiseuille and Knudsen resistance (with different units).

Unfortunately, however the model did not prove to be very accurate for above-mentioned reasons and the results of the modelling are therefore not discussed further. For the same reason adjusting the model to obtain Knudsen and Poiseuille resistances from the permeability (F_o vs P_m) plots was also not pursued any further.

6.2 Selectivity Results

As explained in paragraph 5.2.3.3, selectivity is a measure of the amount of separation that occurs between two gasses while they permeate through the membrane. Three

different definitions were also given. The *actual* selectivity can only be measured when a membrane separates two gasses.

The *ideal* selectivity is the separation factor given by the ratio of the individual permeabilities of the two gasses through the membrane, and this ideal selectivity is usually reported in the literature. As said before, it is important to keep in mind that the actual separation factor is usually smaller than the ideal separation factor.

The selectivity results obtained for the manufactured membranes are all ideal selectivity values. **Figure 6.6** shows the ideal selectivity results for membrane 53a.

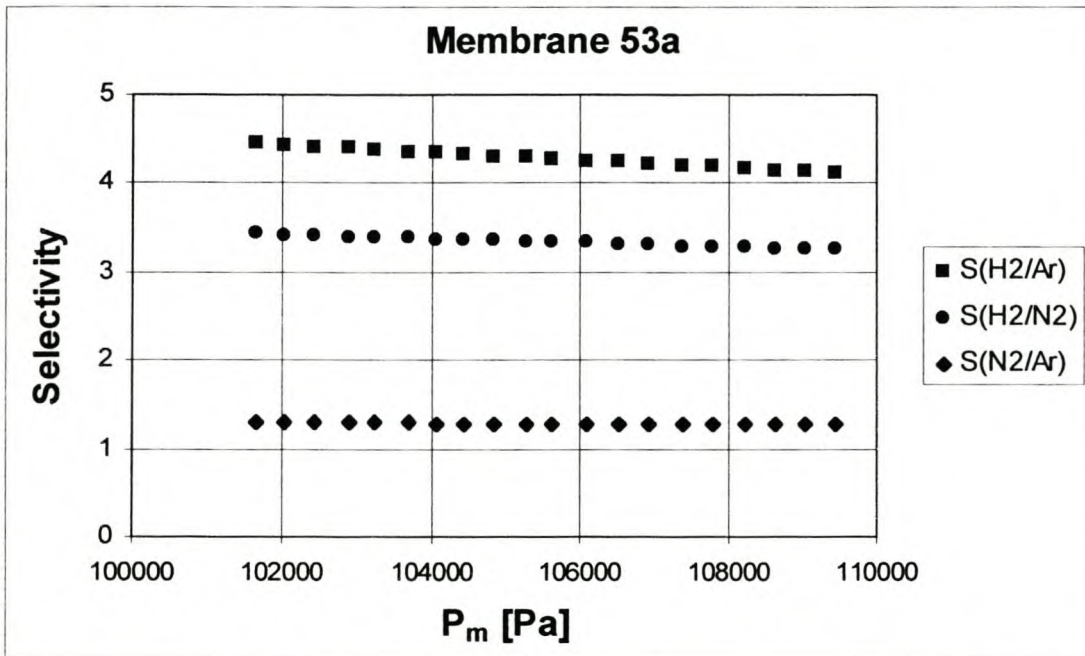


Figure 6.6: Ideal selectivity results for membrane 53a over the hydrogen pressure range

In **figure 6.6**, the nitrogen/argon selectivity is constant with pressure but the hydrogen/argon and hydrogen/nitrogen selectivities decrease with increasing average pressure, P_m. This is expected, since the ideal selectivity is only dependent on individual permeabilities and in **figure 6.1** it can be seen that the nitrogen and argon permeabilities increase slightly with pressure, while the hydrogen permeability stays constant.

For all the other manufactured membranes that were tested, hydrogen/argon and hydrogen/nitrogen selectivities also decreased with increasing average pressure, P_m , and the nitrogen/argon selectivity was constant with pressure.

6.2.1 Influence of Sintering Time and Temperature on Selectivity

For the six different sintering times and three different sintering temperatures, the average ideal-selectivity values were calculated (see **Appendix G-III**). **Figure 6.7** and **figure 6.8** show the results for each of the three different selectivities at 105 kPa.

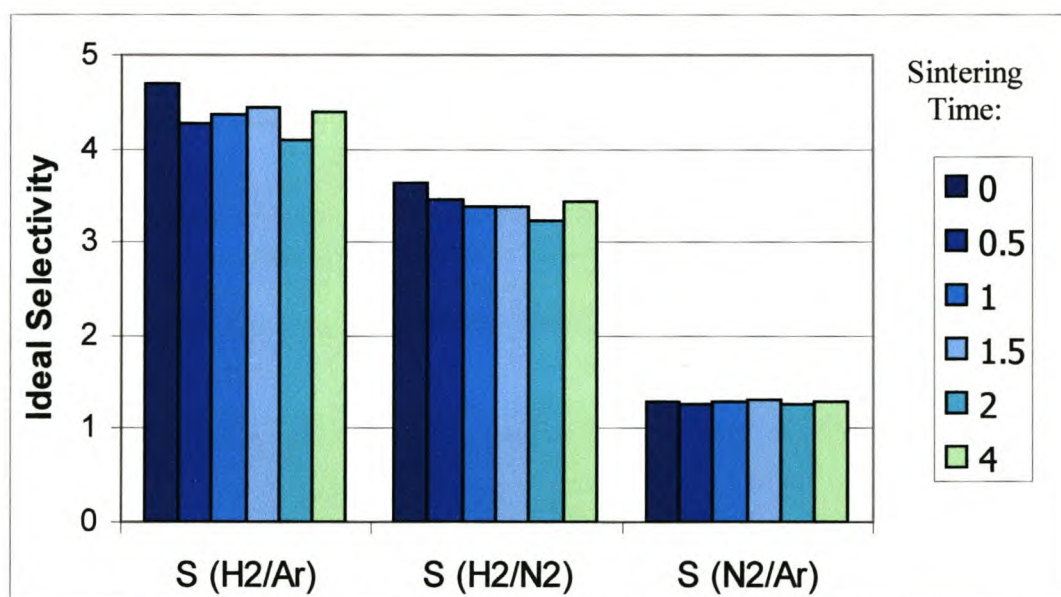


Figure 6.7: Average ideal selectivities for different sintering times at a sintering temperature of 1300°C and an average pressure of 105 kPa

There is some variance in selectivity for different sintering times, but there does not seem to be a real trend. **Figure 6.7** does not indicate a dependence of the ideal selectivity on the sintering time. The same can be said for **figure 6.8**. The average ideal selectivities for the three different sintering temperatures are very similar.

Figure 6.7 shows a larger variance between the different hydrogen/argon and hydrogen/nitrogen selectivities than between the nitrogen/argon selectivities. Table 6.4 gives an indication of the different selectivity values that were obtained.

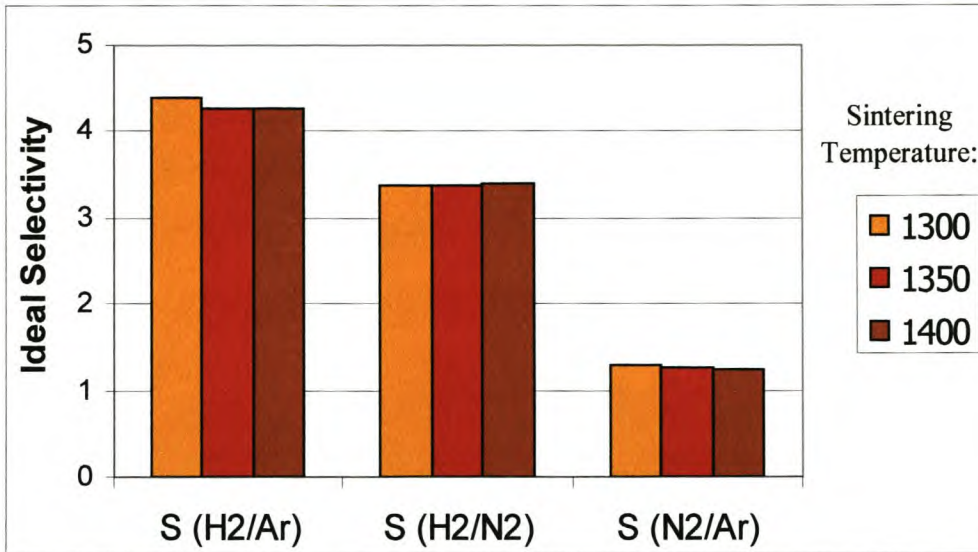


Figure 6.8: Average ideal selectivities for different sintering temperatures at a sintering time of 1 hour and an average pressure of 105 Pa

| Membrane | Sintering time | S(H ₂ /Ar) | S(H ₂ /N ₂) | S(N ₂ /Ar) | |
|----------|----------------|-----------------------|------------------------------------|-----------------------|----------------------------------|
| 56c | 0 h | 4.85 | 3.94 | | Highest ideal selectivity values |
| 45 | 1.5 h | | | 1.41 | |
| 36d | 2 h | 3.82 | 3.08 | | Lowest ideal selectivity values |
| 56c | 0 h | | | 1.23 | |

Table 6.4 shows something interesting. While the hydrogen/argon and hydrogen/nitrogen selectivity values for membrane 56c are the highest ideal selectivity values, the nitrogen/argon selectivity value for this membrane is actually the lowest ideal selectivity found for a mean pressure of 105000 Pa.

Although there was some variance in selectivity, the selectivity did not depend on the sintering time or temperature. The following paragraph discusses the influence of the permeability on the selectivity.

6.2.2 Influence of Permeability on Ideal Selectivity

Since the ideal selectivity is the ratio of the individual permeabilities of the two gasses, it would be interesting to see what influence the permeability has on the selectivity. The ideal selectivities of each membrane were therefore plotted against the individual permeabilities, see **figure h to m** in **Appendix G-V**. All figures in **Appendix G-V** were calculated, again for a mean pressure of $P_m=105$ kPa. These figures do not show any dependence on the permeability as shown in **figure 6.9**. As discussed already, **Figure 6.6** shows a linear dependence of ideal selectivity with pressure for the hydrogen/argon and hydrogen/nitrogen selectivities. This dependence on pressure is brought about by the dependence of the argon and nitrogen permeabilities on pressure. This indicates that, although the permeabilities for a certain membrane at a certain pressure differ, the ratio of the individual permeabilities stays constant.

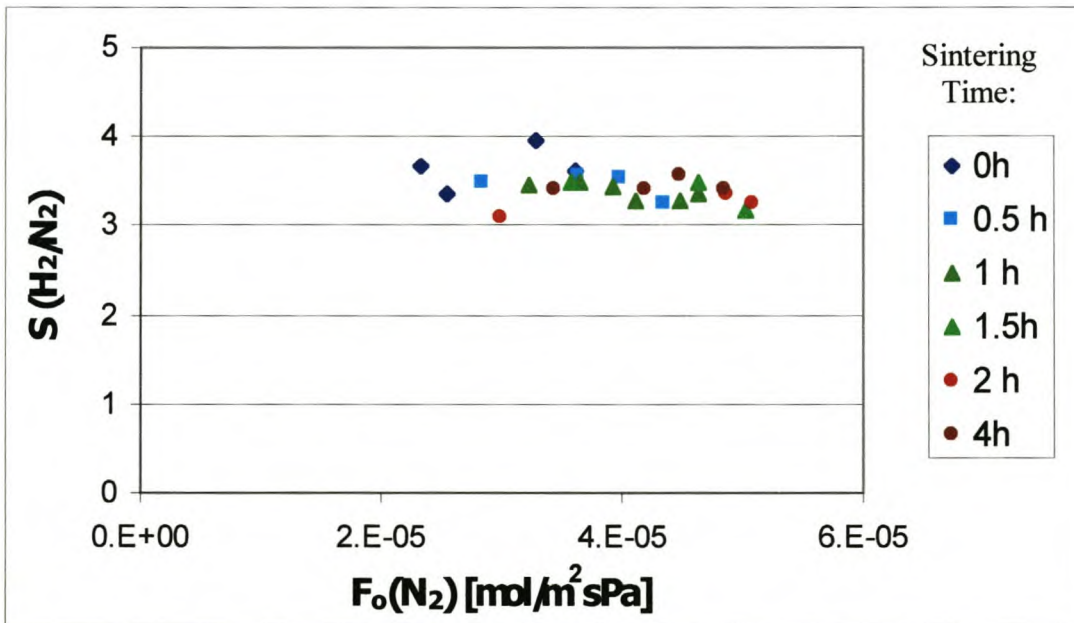


Figure 6.9: Nitrogen/argon selectivity as a function of nitrogen permeability

6.2.3 Comparison to Theoretical Selectivity and Linkov's Membrane

It is important to determine whether the selectivities obtained for the manufactured membranes compare well with their theoretical selectivities as well as with the selectivities obtained for Linkov's membrane. Comparison with the theoretical selectivity gives an indication of whether Knudsen diffusion occurs, while Linkov's membrane is a commercial membrane supposedly manufactured according to the investigated patent. **Figure 6.10** and **table 6.5**, compare the average ideal selectivity to its theoretical selectivities and to the selectivities obtained for Linkov's membrane, as discussed in paragraphs 6.2.3.1 and 6.2.3.2.

| Table 6.5: Table of selectivity values | | | |
|---|-----------------------|------------------------------------|-----------------------|
| | S(H ₂ /Ar) | S(H ₂ /N ₂) | S(N ₂ /Ar) |
| Theoretical selectivity | 4.45 | 3.73 | 1.19 |
| Linkov's membrane | 4.87 | 4.02 | 1.21 |
| Average selectivity @ P _m =105 kPa | 4.38 | 3.42 | 1.29 |
| Average selectivities of highest values* | 4.53 | 3.51 | 1.29 |
| Highest selectivities calculated* | 4.98 | 4.01 | 1.44 |

* P_m between 101.5 kPa and 102 kPa.

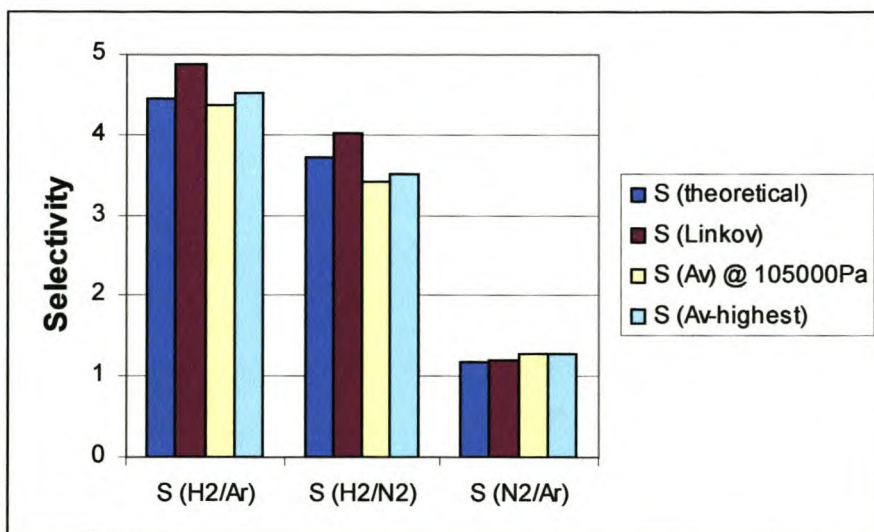


Figure 6.10: Theoretical and Linkov's selectivities compared to the average selectivities for the manufactured membranes at P_m=105 kPa and to the average of the highest selectivities

6.2.3.1 Comparison to the Theoretical Selectivity

According to literature, if the *theoretical* selectivity, (the reciprocal ratio of the square root of the molecular masses of the two gasses) equals the ideal selectivity, it can be deduced that Knudsen diffusion occurs [Germic et al., 1997, and Lin et al., 1994]. It is thus important to compare the ideal selectivity with the theoretical selectivity.

Figure 6.10 shows that the average ideal selectivity (at a mean pressure of $P_m = 105$ kPa) is less than the theoretical selectivity for the H_2/Ar and H_2/N_2 selectivities. The average ideal N_2/Ar selectivity, however, is higher than its theoretical selectivity (1.29 vs. 1.19, see **table 6.5**).

The highest selectivities for each membrane were obtained at low mean pressures since the nitrogen and argon permeabilities were lowest at these pressures and the hydrogen permeability constant. For low mean pressures (P_m between 101.5 kPa and 102 kPa) the average ideal selectivity was also calculated, resulting in higher values for the H_2/Ar and H_2/N_2 selectivities but the same value for the N_2/Ar selectivity. The H_2/Ar selectivity is now higher than the theoretical selectivity (4.53 vs. 4.45, see **table 6.5**), but the H_2/N_2 ideal selectivity is still less than its theoretical selectivity (3.51 vs. 3.73, see **table 6.5**). Although the average of the ideal H_2/N_2 selectivity for the lowest pressure was less than the theoretical selectivity, some of the highest ideal H_2/N_2 selectivity values did equal or were higher than the theoretical H_2/N_2 selectivity. The highest ideal selectivity values were obtained for membrane 56c and 45 (see also **table 6.4**), and their selectivity values are shown in **table 6.5** as the “highest selectivities calculated”.

Although the ideal selectivity values do not always equal the theoretical selectivity values, they are very close. This means that mostly Knudsen diffusion takes place. The subject of Knudsen diffusion was also discussed in paragraph 6.1.3: Applying the Gas Permeability Model.

6.2.3.2 Comparison to the Selectivity Values for Linkov's Membrane.

Comparing the selectivity of the manufactured membranes to the selectivity achieved by Linkov's membranes is important since firstly, Linkov's membrane is a commercial membrane. Secondly, the aim of the project was to investigate the manufacturing process and thus comparing the results of this investigation (the manufactured membranes) to their commercial "equivalent" is of great importance.

The ideal selectivities achieved by Linkov's membrane (see **figure 6.10** and **table 6.5**) were higher than the average ideal selectivities for the manufactured membranes, except in the case of the N₂/Ar selectivity. Linkov's membranes selectivities in all three cases also show higher ideal selectivities than their theoretical selectivities. According to Germic and Lin [Germic et al., 1997, and Lin et al., 1994], "to achieve a higher separation selectivity than that in the Knudsen regime, requires a membrane with a smaller pore size". This indicates that the pore size of Linkov's membranes is smaller than that of the manufactured membranes. This is confirmed when the permeabilities of these two membranes are compared; the permeability of the manufactured membranes is much higher than those of Linkov's membranes (see **table 6.3** and **figure 6.4**).

Some of the membranes, however, did have selectivities as high as (or even higher than) Linkov's membrane's selectivities (see **table 6.5** "highest selectivities calculated"). This indicates that some of the membranes with a much higher permeability still had the same selectivity as Linkov's membrane. A higher permeability for these manufactured membranes translates to a higher throughput, which means more gas is separated per unit time, with the same selectivity. This kind of membrane is an improvement on Linkov's membrane.

6.3 Water Permeability Results

Water permeability tests were only performed with a selected few (two) membranes for two reasons. Firstly, this test is partly a destructive test since the membranes cannot be

used afterwards for gas permeability tests (unless they are dried at a temperature over 200°C, removing all water in the ceramic structure).

Then secondly, the aim of this test was not to characterise each membrane as was the aim of the gas permeability tests. The aim was to investigate whether the manufactured membranes were suitable for use in liquid environments and how their water permeabilities compare to:

- the water permeability of Linkov's membrane, and
- the water permeabilities of other commercial membranes.

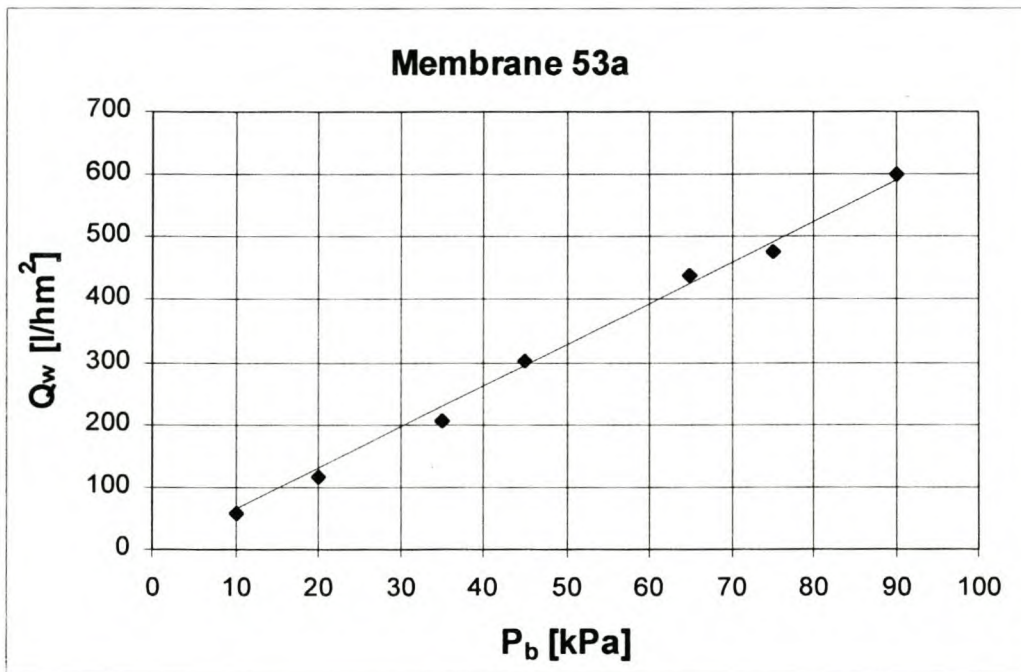


Figure 6.11: Water permeability for membrane 53a

Figure 6.11 shows the water permeate flux (Q_w) plotted against the backpressure over the membrane, P_b for membrane 53a. This figure shows that permeate water flux increases linearly with the pressure over the membrane as already predicted in paragraph 5.2.4. The water permeability, F_w , is determined (as defined in paragraph 5.2.3.2) by dividing, permeate flux, Q_w (Lh⁻¹m⁻²) by the pressure over the membrane, P_b (in bar). It indicates the membrane's volume flow per area unit (flux) per unit pressure difference over the membrane ($F_w \equiv$ [Lm⁻²h⁻¹bar⁻¹]). Note that although the pressure over the membrane, P_b ,

is measured in Pascal, the water permeability is defined as $F_w \equiv [Lm^{-2}h^{-1}bar^{-1}]$. The reason for this is firstly that most literature used these units for water permeability, but secondly, the water permeability calculated in Pascals become exponential numbers. Therefore, using bar-units is much more convenient. **Table 6.6** shows comparative water permeabilities for some inorganic membranes as well as the water permeabilities for the two tested manufactured membranes and Linkov's membrane.

Table 6.6: Typical water permeability values for tubular ceramic membranes at 20°C as well as the water permeability values for Linkov's membrane and the manufactured membranes 38b and 53a

| <i>Membrane Material</i> | <i>Pore size [nm]</i> | <i>Permeability [$Lm^{-2}h^{-1}bar^{-1}$]</i> | <i>Manufacturer (trade name)</i> |
|---|-----------------------|--|----------------------------------|
| α -Al ₂ O ₃ | 200 | 2000* | Alcoa/SCT (Membralox ®) |
| | 200 | 1500* | NGK |
| | 200 | 2500* | Norton (Ceraflo ®) |
| | 50 | 250 | TDK (Dynaceram ®) |
| γ -Al ₂ O ₃ | 50 | 300 | Alcoa/SCT (Membralox ®) |
| | 4 | 10* | Alcoa/SCT (Membralox ®) |
| ZrO ₂ | 140-200 | 600 | Tech Sep (Carbosep ®) |
| | 83 | 300 | Tech Sep (Carbosep ®) |
| | 23 | 70 | Tech Sep (Carbosep ®) |
| | 100 | 1500* | Alcoa/SCT (Membralox ®) |
| | 50 | 800* | Alcoa/SCT (Membralox ®) |
| | 20 | 400* | Alcoa/SCT (Membralox ®) |
| | 3 | 100 | [Larbot et al., 1989] |
| | 10 | 167 | [Larbot et al., 1989] |
| | 20 | 300 | [Larbot et al., 1989] |
| | 50 | 500 | [Larbot et al., 1989] |
| γ -Al ₂ O ₃ & ZrO ₂ | 4 | 60 | Linkov and Belyakov |
| | Unknown | 540 | van de Ven, membrane 38b |
| | Unknown | 630 | van de Ven, membrane 53a |

* Multichannel, tubular

Reference for all permeation values for the commercial membranes: Bhave R.R., Chapter 4, Table 4.1 and Table 4.3.

The permeabilities of the manufactured membranes 38b and 53a are about 10 times higher than the permeability of Linkov's membrane. The permeability values of the commercial membranes in **table 6.6** illustrate a general dependence of water permeability on the nominal pore size. The permeabilities of the manufactured membranes are in the

same order of magnitude as those of the commercial membranes that have a pore size of between 20 and 100 nm. The values in table 6.5 illustrate that the pore size of the manufactured membranes is probably between 20 and 100nm, compared to the pore size of Linkov's membrane, which is in the order of 5nm. It is recommended that the pore size distribution for the manufactured membranes be determined for a better comparison.

As said in paragraph 5.2.4, in practical situations the observed permeate flux values at the operating pressure difference are seldom comparable to the water permeability data. To find out how the manufactured membranes and Linkov's membrane perform in practical situations more tests should be performed, like measuring the flux decline over time while tap water is used as a liquid medium instead of clean reverse osmosis water, see also Lee et al. [1998]. Tests like these have not been performed, but they are highly recommended for future work.

6.4 Permeability Coefficients

The determined permeability coefficients of each membrane are derived material properties of the membrane; it is a characteristic of the membrane and the gas. Three gas permeability coefficients were determined for each membrane, as well as the liquid permeability coefficient for two manufactured membranes (53a and 38b) and Linkov's membrane. The permeability coefficient is an important tool to compare the different membranes since in calculating the permeability coefficient, the dimensions of the membrane are taken into account. The permeability, F_o , is calculated per inside-membrane-area unit, but the gas permeability coefficient takes into account the thickness of the membrane as well.

6.4.1 Gas Permeability Coefficients

For each manufactured membrane, the gas permeability coefficients for hydrogen, nitrogen and argon were determined from the data gained from the permeability experiments. The gas permeability coefficients were calculated using equation (5.2) (see

Appendix H for the derivation). **Figure 6.12** shows a typical graph of the gas permeability coefficients for the three gasses plotted against the reciprocal of the mean pressure over the membrane.

In **figure 6.12** the argon- and nitrogen permeability coefficients are almost equal and increase slightly with increasing mean pressure (decreasing $1/P_m$). The hydrogen permeability coefficient is about 150% higher than the other two permeability coefficients. With increasing mean pressure the hydrogen permeability coefficient sometimes increased or decreased slightly, and sometimes stayed constant.

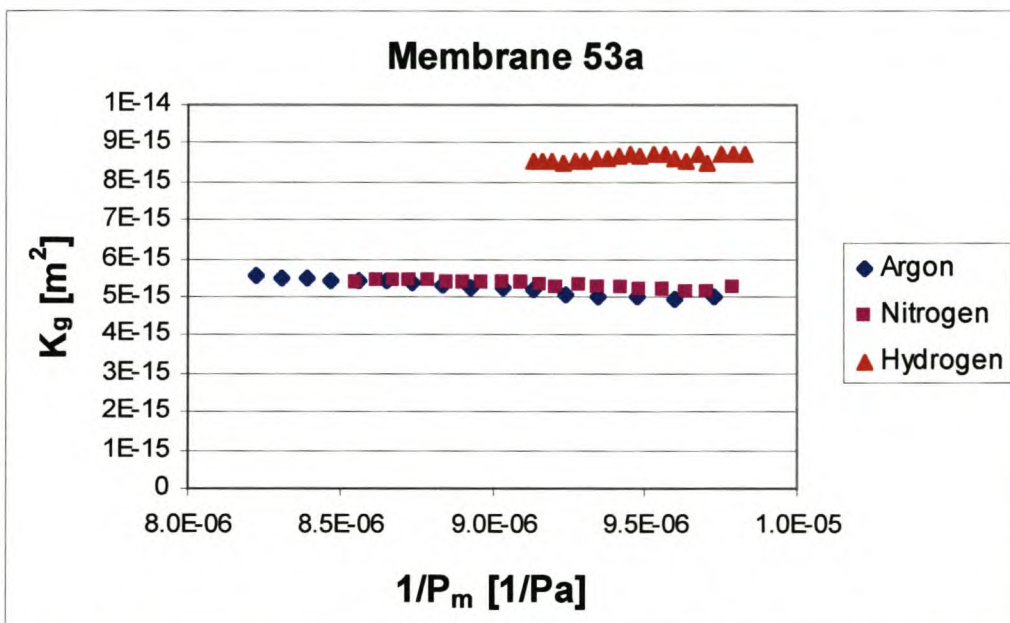


Figure 6.12: Gas permeability coefficients for membrane 53a

Permeability coefficients are usually reported as constants in literature. The results of the gas permeability experiments on the manufactured membranes indicate a definite dependence on pressure for the argon and nitrogen permeability coefficients. The gas permeability coefficients of the other manufactured membranes were all in the same order of magnitude as those of membrane 53a, shown in **figure 6.12**. For each membrane, its “constant” gas permeability coefficient was determined as the average of all the calculated coefficients. **Figure 6.13** shows the influence of different sintering times on the gas permeability coefficients.

The gas permeability coefficient appears to increase with increasing sintering time. The coefficients obtained for a sintering time of 0 hours at 1300°C is on average 20% less than the other permeability coefficients (and even 25% less than the membranes sintered at 2 and 4 hours). The coefficients for sintering times of 2 and 4 hours are only 5 to 10% higher than the coefficients at sintering times of 0.5, 1 and 1.5 hours.

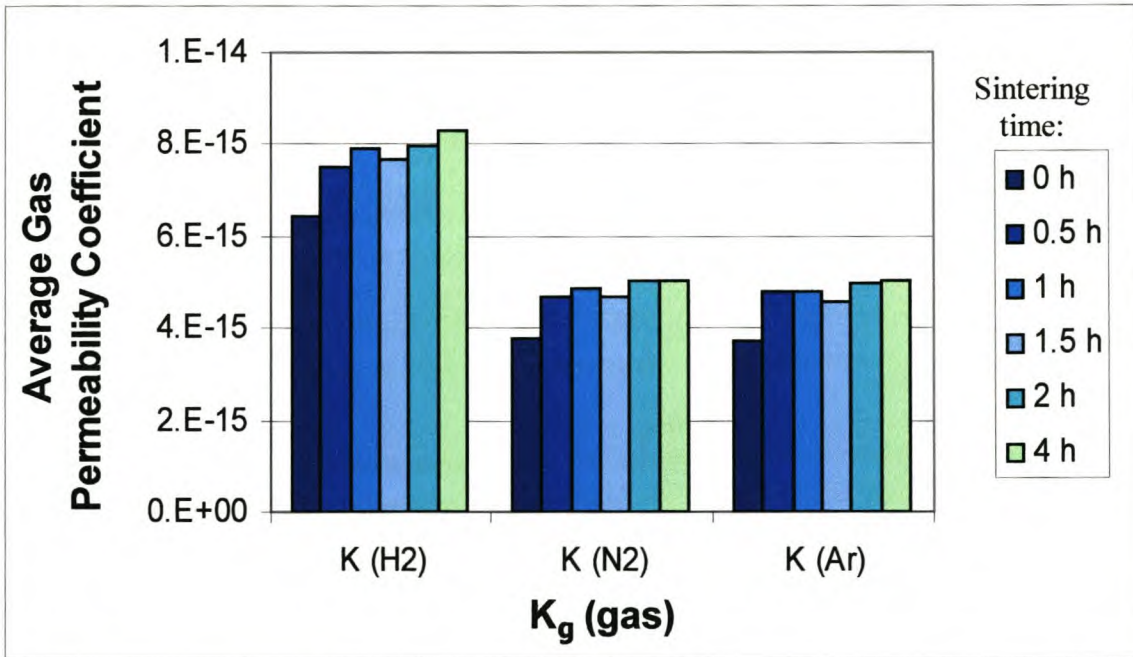


Figure 6.13: Average gas permeability coefficients for different sintering times at a sintering temperature of 1300°C

The permeability coefficients of the manufactured membranes that were sintered at higher temperatures (1350 and 1400°C) are compared to the permeability coefficients of the membranes sintered at 1300°C in **figure 6.14**. The permeability coefficients of the membranes sintered at higher temperatures are 20 to 40% higher than the coefficients of the membranes sintered at 1300°C.

The gas permeability coefficients for Linkovs membrane were also determined and **table 6.7** compares them to the highest (membrane 34b) and lowest (membrane 36d) gas permeability coefficients of the manufactured membranes. The highest gas permeability coefficients (membrane 34b) are 8 times higher and the lowest gas permeability

coefficients (membrane 36d) are about 3.5 times higher than the coefficients calculated for Linkov’s membrane.

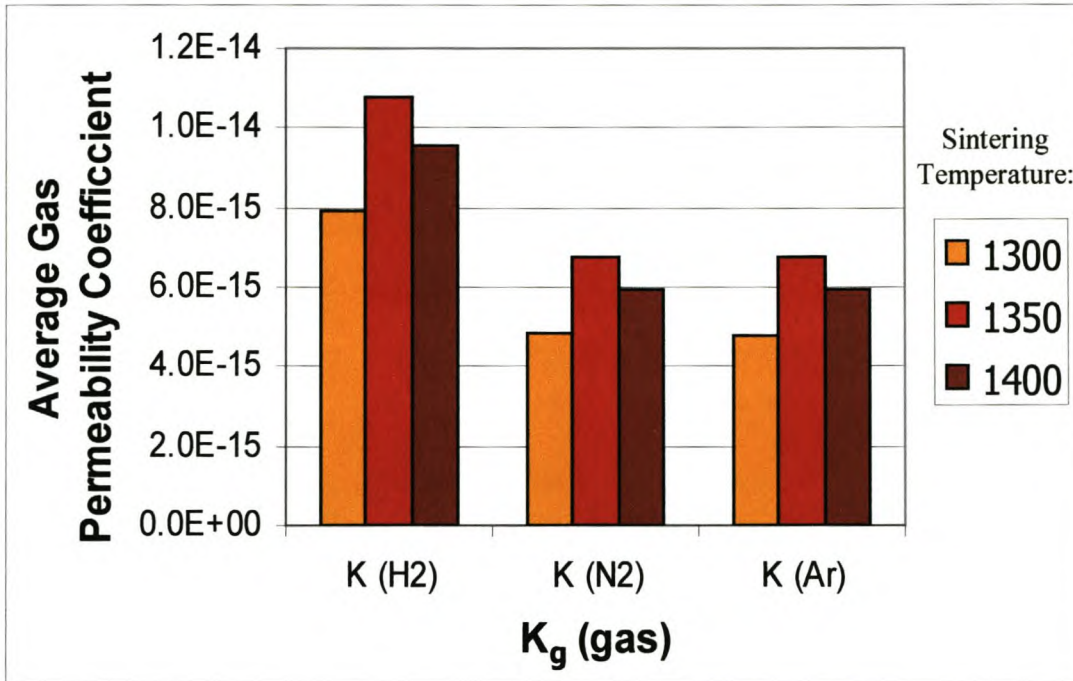


Figure 6.14: Average gas permeability coefficients for membranes sintered for 1 hour at different sintering temperatures

| Membrane | K(H ₂) x10 ⁻¹⁵ [m ²] | K(N ₂) x10 ⁻¹⁵ [m ²] | K(Ar) x10 ⁻¹⁵ [m ²] |
|----------|--|--|---|
| M34b | 11.2 | 7.05 | 7.03 |
| M36d | 4.84 | 2.98 | 2.97 |
| Linkov | 1.46 | 0.82 | 0.83 |

The permeability coefficients that are found in literature are often water permeability coefficients. Water permeability coefficients were calculated for the membranes that were tested for water permeation, that is, membranes 53a and 38b. The water permeability coefficients are discussed in paragraph 6.4.2.

6.4.2 Water Permeability Coefficients

The water permeability coefficients for the two manufactured membranes 53a and 38b were calculated with equation (5.1) (see **Appendix H** for the derivation). The water permeability coefficients does not depend on the pressure like the gas permeability coefficients. The average water-permeability coefficients for the two tested membranes and Linkov’s membrane are displayed in **table 6.8**. This table shows that the water permeability coefficients of the manufactured membranes 38b and 53a are 14.9 and 13.5 times higher than the water permeability coefficient of Linkov’s membrane respectively. The values found in literature were for flat membranes, and their water permeability coefficients are similar to that found for Linkov’s membrane.

Table 6.8: Water permeability coefficients for the two manufactured membranes, Linkov’s membrane and two coefficients found in literature

| Membrane | K_l [m ²] |
|---------------------|------------------------------------|
| M38b | $1.76 \times 10^{-15} \text{ m}^2$ |
| M53a | $1.59 \times 10^{-15} \text{ m}^2$ |
| Linkov | $1.18 \times 10^{-16} \text{ m}^2$ |
| Flat membrane, no1* | $6.99 \times 10^{-16} \text{ m}^2$ |
| Flat membrane, no5* | $1.35 \times 10^{-16} \text{ m}^2$ |

* from Table 2, Biesheuvel & Verweij, 1999

According to Glass and Green [1999], it is possible to obtain liquid permeability coefficients from gas permeability measurements. The gas permeability is plotted as a function of the reciprocal mean pressure, after which the liquid permeability coefficient is obtained by linear extrapolation of the gas permeability coefficient to infinite pressure. At high mean pressures, the mean free path of a gas is very small, and therefore, it behaves more like a liquid as molecule-molecule collisions dominate molecule-wall collisions. The relationship between the gas and the liquid permeability coefficients is:

$$K_g = K_l \cdot \left(1 + \frac{b}{P_m} \right) \tag{6.1}$$

with b the slippage factor. This slippage factor is also known as the Klinkenberg correction. This method is described in ASTM D4525-90e1 (Standard Test Method for Permeability of Rocks by Flowing Air). The liquid permeability coefficients as determined with this method are shown and compared to their liquid permeability coefficients in **table 6.9**.

For each membrane the liquid permeability coefficients determined from the gas permeability coefficients were 5 to 10 times higher than the actual liquid permeability coefficient. The argon- and nitrogen coefficients increased with increasing pressure when the gas permeability coefficients were plotted against the reciprocal of mean pressure. This is unlike the gas (helium) permeability coefficients of the specimens tested by Glass and Green, which decreased with pressure [Glass & Green, 1999]. Some, not all, of the hydrogen permeability coefficients decreased with increasing pressure, but the permeability coefficient determined for those cases were still much higher than the real liquid permeability coefficient.

| Table 6.9: Liquid permeability coefficients compared to the coefficients obtained from the gas permeability coefficients | | | | |
|---|---|--|--|---|
| Membrane | K_l $\times 10^{-15} \text{ [m}^2\text{]}$ | $K_l(\text{of } K_g(H_2))$ $\times 10^{-15} \text{ [m}^2\text{]}$ | $K_l(\text{of } K_g(N_2))$ $\times 10^{-15} \text{ [m}^2\text{]}$ | $K_l(\text{of } K_g(Ar))$ $\times 10^{-15} \text{ [m}^2\text{]}$ |
| M38b | 1.76 | 5.30 | 8.41 | 8.76 |
| M53a | 1.59 | 5.76 | 7.52 | 9.00 |
| Linkov | 0.12 | 1.84 | 1.66 | 1.37 |

While testing the manufactured membranes for their gas and liquid permeability, they appeared more fragile than Linkov's membrane. A couple of the manufactured membranes broke while they were being prepared for the tests. In addition, the manufactured membranes tested for liquid permeability easily broke while they were taken out of the membrane-testing module (quite a lot of force was needed to remove them). These observations as well as the differences in permeability led to the assumption that the breaking strength of the manufactured membranes should be less than that of Linkov's membrane. To verify and quantify this assumption, it was decided to test their mechanical strength. This is discussed in paragraph 6.5.

6.5 Mechanical Strength

The mechanical strength of membranes 24b, 46a and 54 as well as Linkov's membrane were tested with a three point bending test as described in paragraph 5.4. The main objective of this test was to compare the mechanical strength of the manufactured membranes to that of Linkov's membrane. This test is also a destructive test (apply force until fracture occurs) therefore, only three manufactured membranes were tested. The typical test results as obtained for membrane 54 are shown in **figure 6.15**.

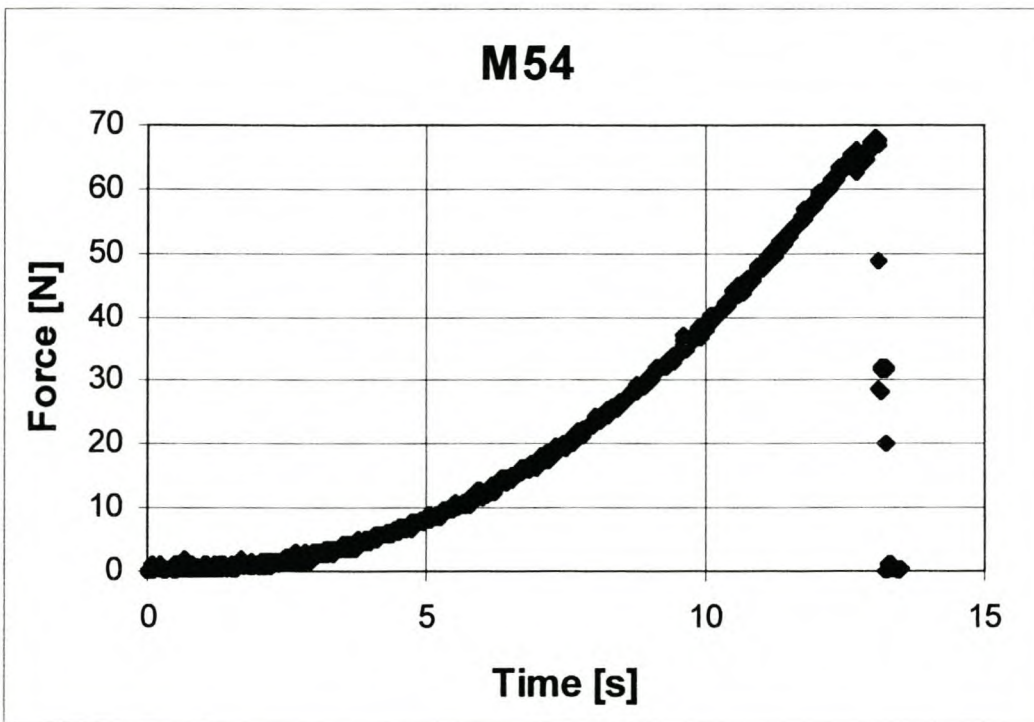


Figure 6.15: Increasing force applied on membrane 54 with a bend test until fracture occurs

Figure 6.15 shows the increasing force with time, until after 13 seconds at a force of 70 N, fracture of the membrane occurs. From these results, the maximum force that was applied to the membrane was obtained and with the maximum force and equation 5.17, the maximum flexural strength was calculated. The mechanical strength results for each tested membrane can be found in **Appendix J**.

To compare the tested membranes, their results are summarised in **figure 6.16** and **table 6.10**. The maximum force and maximum flexural strength of the three manufactured membranes are compared in **figure 6.16**.

The flexural strength can effectively be used in comparing the mechanical strength of membranes with different dimensions. To illustrate this, take a look at membranes 34b and 46a. The maximum force obtained for membranes 24b and 46a is almost equal, but the maximum flexural strength of membrane 24b is 20% higher (see **table 6.10**) than that of membrane 46a. This is due to the difference in membrane thickness and outside radius, which is taken into account by equations (5.15), (5.16) and (5.17).

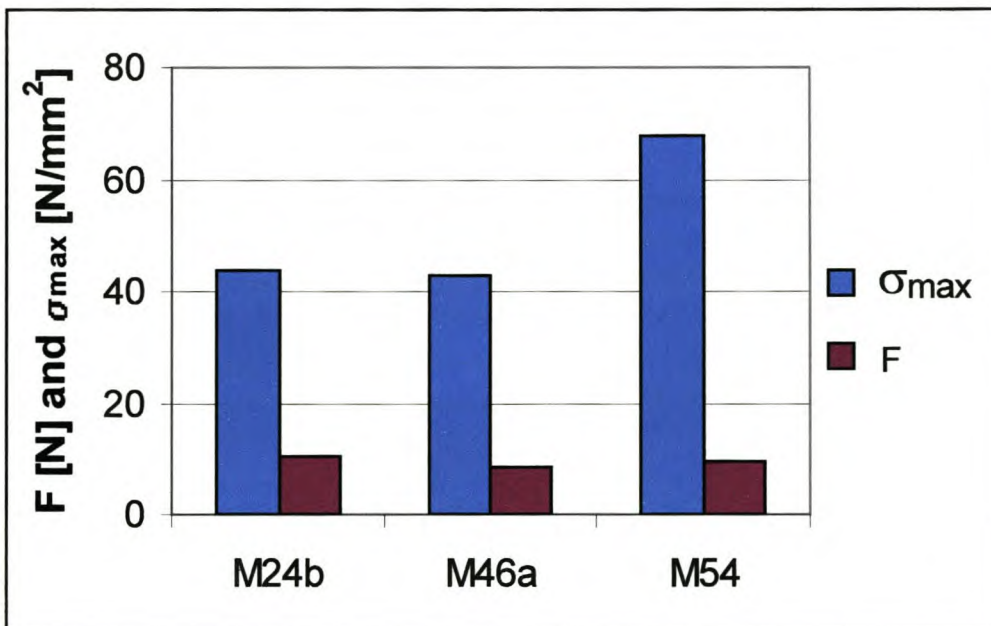


Figure 6.16: Maximum force and maximum flexural strength of three manufactured membranes compared

| Membrane | F [N] | σ max [N/mm ²] |
|----------|-------|----------------------------|
| Linkov | 323 | 107.1 |
| 24b | 44 | 10.4 |
| 46a | 43 | 8.6 |
| 54 | 68 | 9.3 |

Table 6.10 shows that Linkov's membrane indeed is mechanically stronger than the manufactured membranes. The maximum flexural strength of Linkov's membrane is roughly 10 times higher than the maximum flexural strengths of the manufactured membranes.

Comparing the results to the flexural strength of commercial membranes proved difficult. Despite the fact that ceramic membranes are, in general, mechanically more stable than organic membranes, available mechanical properties data for commercial ceramic membranes are sketchy and not yet standardised [Biesheuvel & Verweij, 1999].

6.6 SEM Results

Figure 6.17 shows SEM pictures of the inside and the outside of Linkov's membrane at 5.000x and 10.000x enlargement (see also **Appendix K**). The pictures of the outside of the membrane (**a** and **b** in **figure 6.17**) seem to have slightly larger particles than the pictures of the inside of the membrane (**c** and **d** in **figure 6.17**). SEM-pictures of the manufactured membranes were very similar see **Appendix K**.

The SEM analysis were found not to be very useful as a practical tool to characterise or compare the different membranes. The SEM results are very local and do not provide a good idea of what the membrane's performance is. Therefore, only **figure 6.17** is shown in this paragraph as an example of the results that were obtained. The SEM results of a few selected manufactured membranes can be found in **Appendix K**.

Lastly, X-ray analyses were also performed on both the inside and the outside of the membranes. The X-ray analysis on Linkov's membrane provided an interesting result: both the membrane and the support layers showed aluminium and zirconium, but the outside of the support layer also showed a calcium peak indicating that some of the gypsum mould was still attached to the outside of the membrane. Yttrium was not observed with the X-ray analysis.

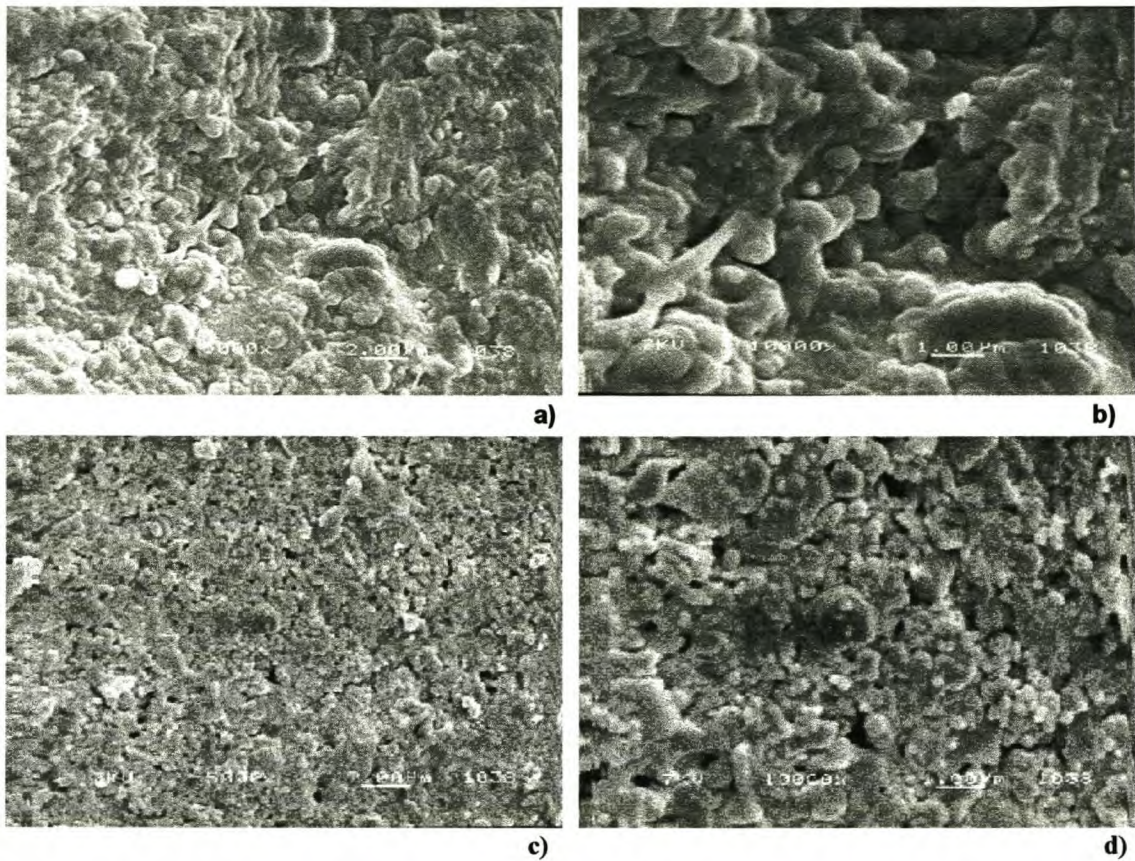


Figure 6.17: SEM photos of Linkov's membrane; the support layer at a) 5000x, and b) 10000x, and the membrane layer at c) 5000x, and d) 10000x enlargements

6.7 Conclusions

The permeability, permeability coefficients, selectivity, and the mechanical strength of a membrane, are all factors that have to be considered to determine the performance of a membrane. This paragraph summarises the results obtained in this chapter, taking these four points into consideration.

6.7.1 Gas Permeability

Gas permeabilities for the manufactured membranes were typically in the order of 1×10^{-5} mol/m²sPa for argon and nitrogen and between 4 and 5×10^{-5} mol/m²sPa for hydrogen.

The nitrogen and argon permeabilities were found to increase slightly, linearly with increasing pressure difference. For most manufactured membranes, the hydrogen permeation was constant, with slight deviations. The gas permeabilities of the manufactured membranes were in the same order of magnitude as those of other commercial membranes reported in literature with a pore size of 4 nm, and about four times higher than the gas permeabilities of Linkov's membrane.

An initial increase in gas permeability with increasing sintering time (0 to 1 hours) was observed after which the gas permeability was constant with increasing sintering time (between 1 to 4 hours). All membranes sintered at 1250°C were very fragile, and broke before their permeability could be tested. The permeability seems to increase with sintering temperature between 1300 and 1400°C, although the data was insufficient. Some additional points are:

- the lowest permeability values, were found for membrane 54, which was sintered for 0 h at 1300°C, and
- the highest permeability values were found for the membranes sintered at a temperature higher than 1300°C.

The obtained gas permeability coefficients discussed in paragraph 6.6.4, similarly also increased with sintering time and temperatures.

A large variance in gas permeability between commercial membranes with the same pore diameter and manufacturing procedure (tested with the same test) exists, indicating that a variance between membranes manufactured in a commercial process is common. A variance in gas permeability between the manufactured membranes was thus to be expected, and was indeed observed. Gas permeability was also found inconsistent with pore diameter for different commercial membranes. An explanation for this inconsistency is that the methods to determine the average pore diameter are not very consistent with each other. Sometimes the methods depend on the person executing the test and often the results are only comparative to membranes that have undergone the same test (with the same operator).

The gas permeability model as described in paragraph 5.2.3.4 is designed to determine the average pore radius of supports. In essence, it was therefore not suitable for determination of the average pore size of the manufactured membranes.

6.7.2 Selectivity

The nitrogen/argon selectivity was constant with pressure but the hydrogen/argon and hydrogen/nitrogen selectivities decreased with increasing average pressure, P_m . This was expected, since the ideal selectivity is calculated by dividing the individual permeabilities. Therefore, although the permeabilities for a certain membrane at a certain pressure differ, the ratio of the individual permeabilities stays constant.

There is some variance in selectivity for different sintering times and temperatures, but there is no indication of dependence of the ideal selectivity on the sintering time or temperature. The selectivity was also not dependent on the permeability; no increase in selectivity was observed if the membrane had a lower permeability or vice versa.

Although the ideal selectivity values did not always equal the theoretical selectivity values, they were very similar. Some of the membranes, however, did have selectivities as high as (or even higher than) Linkov's membrane. This indicates that mostly Knudsen diffusion takes place in the manufactured membranes. When combining the gas permeability results with the selectivity results, it was found that some of the manufactured membranes with higher gas permeability still had the same selectivity as Linkov's membrane. A higher permeability for these manufactured membranes translates to a higher throughput, meaning more gas is separated per unit time, with the same selectivity.

6.7.3 Water Permeability

The permeate water flux increases linearly with the pressure over the membrane as already described theoretically. The water permeabilities of the manufactured membranes

38b and 53a are about 10 times higher than the water permeability of Linkov's membrane. The permeability values of the commercial membranes illustrate a general dependence of water permeability on the nominal pore size. The permeabilities of the manufactured membranes are in the same order of magnitude as those of the commercial membranes that have a pore size of between 20 and 100 nm.

As said in paragraph 5.2.4, in practical situations the observed permeate flux values at the operating pressure difference are seldom comparable to the water permeability data. To find out how the manufactured membranes and Linkov's membrane perform in practical situations, more tests should be performed, like measuring the flux decline over time while tap water is used as a liquid medium instead of clean reverse osmosis water. Tests like these have not been performed, but they are highly recommended.

6.7.4 Permeability Coefficients

The gas and water permeabilities, F_o and F_w , are calculated per unit inside-membrane-area. These permeabilities therefore, in fact do not take into account the thickness of the membrane. The gas and liquid permeability coefficients do take into account the thickness of the membrane. For the manufactured membranes, the gas permeability coefficients were in the order of $5 \times 10^{-15} \text{ m}^2$ for nitrogen and argon, while the gas permeability coefficient for hydrogen was in the order of $8 \times 10^{-15} \text{ m}^2$. The liquid permeability coefficients were in the order of $1.7 \times 10^{-15} \text{ m}^2$ for water.

6.7.4.1 Gas Permeability Coefficients

The argon- and nitrogen permeability coefficients are almost equal and increase slightly with increasing mean pressure (decreasing $1/P_m$). The hydrogen permeability coefficient is about 150% higher than the other two permeability coefficients. Permeability coefficients are usually reported as constants in literature. The results of the gas permeability experiments on the manufactured membranes indicate a definite dependence on pressure for the argon and nitrogen permeability coefficients.

The gas permeability coefficients increase with increasing sintering time and temperature. The influence of sintering temperature on the gas permeability appears to be greater than that of the sintering time, but due to insufficient data no definite conclusions are made. Note that these results complement the permeability results in paragraph 6.6.1.

The highest gas permeability coefficients (membrane 34b) are 8 times higher and the lowest gas permeability coefficients (membrane 36d) are about 3.5 times higher than the coefficients calculated for Linkov's membrane.

6.7.4.2 *Water Permeability Coefficients*

The water permeability coefficients are not dependent on pressure, as was the case with the gas permeability coefficients. The water permeability coefficients of the tested manufactured membranes 38b and 53a are 14.9 and 13.5 times higher than the water permeability coefficient of Linkov's membrane respectively. The values found in literature are for flat membranes, and their water permeability coefficients are in the same order of magnitude of the water permeability determined for Linkov's membrane.

For each membrane the liquid permeability coefficients determined from the gas permeability coefficients are 5 to 10 times higher than the actual liquid permeability coefficient, indicating that this method is inaccurate.

6.7.5 Mechanical Strength

Linkov's membranes are found to be stronger mechanically (superior) than the manufactured membranes. The maximum flexural strength of Linkov's membrane is roughly ten times higher than the maximum flexural strengths of the manufactured membranes. The difference in mechanical strength is probably connected to the difference in permeability. A membrane with a higher permeability will have more pores or voids in its structure, which influences the strength of the structure in such a way that the structure, the membrane, becomes more fragile, or less strong mechanically.

6.6 Summary

The results of the permeability and strength tests in this chapter evaluate the membranes manufactured according to the manufacturing process described in the patent by Linkov and Belyakov [1997]. The manufactured membranes are characterised and compared to Linkov's membrane (a commercial membrane) by comparing their gas permeability, liquid permeability and mechanical strength results.

Comparing the manufactured membranes to Linkov's membranes, the manufactured membranes had a:

- Gas permeability of: 3 to 6 times higher
- Gas permeability coefficient of: 4 to 8 times higher
- Selectivity that is: slightly lower
- Water permeability of: 10 times higher
- Water permeability coefficient of: 14 times higher
- Flexural strength that is: 10 times lower

The gas and liquid permeabilities of the manufactured membranes are four and ten times higher than those of Linkov's membrane. The ideal selectivity calculated for Linkov's membrane is higher than most of the selectivities of the manufactured membranes, but the difference is small. Therefore the manufactured membranes show potential to have a high permeability (higher than Linkov's membrane) for the same selectivity.

The higher permeability of the manufactured membranes is probably the cause of the low mechanical strength. The flexural strength of Linkov's membrane is ten times higher than the flexural strength of the manufactured membranes. The manufacturing process should be optimised to obtain higher mechanical strength and a high permeability and selectivity as is obtained for the manufactured membranes.

7. Conclusions and Suggestions for Future Work

7.1 Conclusions

As described in chapter 1, it is an objective of this project to investigate the manufacture of an asymmetrical ceramic membrane in one technological operation, combining the support and membrane layer steps into one single “step”.

The three main objectives of the project therefore were:

- a) To manufacture a ceramic membrane as described in the patent by Linkov and Belyakov.
- b) To investigate and possibly improve this manufacturing method of the ceramic membrane.
- c) To test the permeability, strength and structure of the manufactured ceramic membranes.

Conclusions from the manufacturing method and the evaluation of the manufactured membranes are now summarised separately.

Manufacturing Method:

The manufacturing method for the ceramic membranes is discussed in chapters 3 and 4. With this manufacturing method 32 ceramic membranes strong enough to be evaluated, were successfully manufactured.

The following modifications were made during the project to the original manufacturing process of Linkov and Belyakov [1996]:

- A ceramic ball mill with ceramic balls was used instead of a steel ball mill with steel balls
- Instead of only adding 15 m% water after wet milling, up to 200 m% water was added to remove the milled suspension from the ceramic mills.

- A small syringe with a flexible tube was used to remove the wet powder from the ceramic mills.
- Excess water was removed by evaporation in a warm water bath at 40 °C (Centrifugal separation proved to be inefficient).
- To obtain membranes with a thickness of 1 mm for a slip casting time of 60 seconds, it was found that the casting suspension should contain 1.85 grams of water per gram of oxides instead of 1.15 prescribed by Linkov and Belyakov [1996].
- The second casting method, continuously adding casting suspension for 60 seconds, provides a more smooth inside surface and a more equal thickness compared to the first casting method, where the casting suspension is poured into the gypsum mould and the gypsum mould manually rotated for 60 seconds.
- The membranes were sintered at 1300 °C for 1 hour as Linkov and Belyakov [1996] suggest, but membranes were also sintered at 5 other sintering times and 3 other sintering temperatures.

The following parameters were kept constant throughout the manufacture of the ceramic membranes:

- Raw Materials Used:
 - 70 m% alumina
 - 29 m% zirconia
 - 1 m% yttria

The same raw materials were used for all ceramic membranes manufactured during this project.

- Separate Wet Milling:
 - oxide:balls:water-ratio: 1:2:1
 - milling time for alumina: 80 h
 - milling time for zirconia: 60 h
- Separate Roller Stirring: - 4 hours for the alumina and the zirconia suspensions in a polyethylene bottle at 25 °C.
- Mixed Roller Stirring: - 1 hour in a polyethylene bottle at 25 °C.
- Evaporation: - In a warm water bath at 40 °C until enough water has evaporated (measured in mass).
- Slip Casting: - Membranes are all slip-cast for 60 seconds.

- Gypsum moulds are all made with a gypsum:water mass ratio of 1.025:1.
- Drying:
 - All membranes were dried in a Vötsch constant humidity chamber for 72 hours at a temperature of 20°C and a humidity of 40%.

Uncontrollable Parameters:

- Linkov and Belyakov gave no information on the initial particle size distribution or on the particle size distribution after milling in their patent.
- The quality of the gypsum moulds was not fully controllable. Also the quality of the gypsum that the moulds are made with was not fully controlled.
- Dimensions of the manufactured membranes are very difficult to control accurately. They depend on the composition of the casting suspension as well as on the quality of the gypsum mould.

Evaluation of the Manufactured Membranes:

In chapter 5 the evaluation methods are discussed and in chapter 6 the evaluation of the manufactured membranes is discussed. The most important findings considering the evaluation of the manufactured membranes can be summarised as follows:

- Gas permeabilities for the manufactured membranes are typically in the order of 1×10^{-5} mol/m²sPa for argon and nitrogen and between 4 and 5×10^{-5} mol/m²sPa for hydrogen.
- Water permeabilities for the manufactured membranes are typically in the order of 600 l/m²hbar.
- Gas permeability coefficients for the manufactured membranes are typically in the order of 5×10^{-15} m² for nitrogen and argon and in the order of 8×10^{-15} m² for hydrogen. The liquid permeability coefficients were in the order of 1.7×10^{-15} m² for water.
- The maximum flexural strengths of the manufactured membranes are in the order of 9 N/mm².

Comparing the manufactured membranes to Linkov's membranes, the manufactured membranes had a:

- Gas permeability of: 3 to 6 times higher
- Gas permeability coefficient of: 4 to 8 times higher
- Selectivity that is: slightly lower
- Water permeability of: 10 times higher
- Water permeability coefficient of: 14 times higher
- Flexural strength that is: 10 times lower

- A variance in gas permeability between the manufactured membranes is observed. A similar variance in gas permeability between commercial membranes with the same pore diameter and manufacturing procedure exists, indicating that a variance between membranes manufactured in a commercial process is common,
- An initial increase in gas permeability with increasing sintering time (0 to 1 hours) is observed after which the gas permeability appears constant with increasing sintering time (between 1 to 4 hours). The permeability appears to increase with sintering temperature between 1300 and 1400°C.
- The gas permeability coefficients also increase with increasing sintering time and temperature. These results complement the permeability results.
- There is some variance in selectivity for different sintering times and temperatures, but there is no indication of dependence of the ideal selectivity on the sintering- time or temperature. The selectivity is also not dependent on the permeability; no higher selectivity is obtained for membranes with a lower permeability or vice versa.
- Combining the gas permeability results with the selectivity results, manufactured membranes with higher gas permeability still have the same selectivity as Linkov's membrane. A higher permeability for these manufactured membranes translates to a higher throughput, meaning more gas is separated per unit time, with the same selectivity,

- It was found that mostly Knudsen diffusion takes place in the manufactured membranes,
- The gas permeability model as described in paragraph 5.2.3.4, designed to determine the average pore radius of supports is not suitable for determination of the average pore size of the manufactured membranes,
- The liquid permeability coefficients determined from the gas permeability coefficients are 5 to 10 times higher than the actual liquid permeability coefficient, indicating that obtaining liquid permeability coefficients from gas permeability measurements is inaccurate.

Since the manufactured membranes have much higher permeabilities than Linkov's membrane while they have similar selectivities, they are in that aspect better than Linkov's membranes. On the other hand, probably as a consequence of their higher permeability (more pores), the manufactured membranes have a 10 times lower mechanical strength than Linkov's membrane. If the mechanical strength could be improved on or if the manufactured membranes are mounted on or in a strong carrier structure the manufactured membranes can be an interesting product.

7.2 Recommendations for Future Work

Recommendations for future work focus on the following aspects:

- Examining the influence of a higher zirconia content on the ceramic membranes (zirconia content should be between 29w% and 36.6w% for best mechanical strength).
- Examining the influence of different milling times and ball ratios on the *final product*, the ceramic membranes.
- To examine the influence of sintering temperature more intensely, more membranes should be manufactured at even higher temperatures to add to the current data and to confirm a trend of increasing permeability with sintering temperature.
- It is recommended that the pore size distribution for the manufactured membranes is determined for a better comparison.

- To examine how the manufactured membranes (and Linkov's membrane) perform in practical liquid permeability situations. More water permeability tests should be performed, like measuring the flux decline over time, while tap water is used as a liquid medium instead of clean-reverse-osmosis-water.
- Further improving the quality of the gypsum mould will improve the manufactured membranes and provide more accurate membrane dimensions.
- Then lastly the relationship between permeability and mechanical strength that possibly exists can be examined; Membranes with different permeabilities should be manufactured and their permeabilities plotted against their mechanical strength.

8. List of Symbols

| Symbol | Description | Units |
|--|---|--------------------------|
| A | Surface area | [m ²] |
| dp | Particle size | [m] |
| F | Force (3-point bending test) | [N] |
| F _o | Molar gas permeability | [mol/m ² sPa] |
| F _m | Molar flow rate | [mol/s] |
| F _w | Water permeability | [l/hm ² bar] |
| H | Tube length | [m] |
| I | Moment of inertia | [mm ⁴] |
| K | Permeability coefficient | [m ²] |
| K _g | Gas permeability coefficient | [m ²] |
| K _l | Liquid permeability coefficient | [m ²] |
| L | Length | [m] |
| l _r | Pore length | [m] |
| M | Molar mass | [kg/mol] |
| m | Massa | [kg] |
| \dot{m} | Mass flow rate | [kg/s] |
| M _m | Moment | [Nm] |
| P | Pressure | [Pa] |
| P _m | Mean pressure | [Pa] |
| P _o | Atmospheric pressure | [Pa] |
| q | Superficial velocity | [m/s] |
| Q | Volumetric flow rate | [m ³ /s] |
| Q _m | Mass flux | [kg/m ² s] |
| Q _w | Water flux | [L/hm ²] |
| R | Gas constant, 8.3144 | [J/molK] |
| r | Radius | [m] |
| R _t , R _s , R _m | Total, support layer, and membrane layer resistance | |
| S | Selectivity | |
| T | Temperature | [K] |
| th | Layer thickness | [m] |
| W | Resistance moment | [mm ³] |
| x | Distance | [m] |
| ε | Porosity | |
| μ | Viscosity | [Pas] |
| θ | Tortuosity | - |
| τ | Surface energy | [J/m ²] |
| ψ | Geometry factor | - |

9. References

Advances in Pore Size Characterization: New Techniques for Largest Pore Size and Pore Shape Determination, *Filtration & Separation*, 1998, 254-57.

Akash A. and J.M. Merrilea, 1999, Pore Growth during Initial-Stage Sintering, *J. Am. Ceram. Soc.*, 82, [11], 2948-52.

Albrecht T.R., and C.F. Quate, 1988, Atomic Resolution with the Atomic Force Microscope on Conductors and Non-Conductors, *J. Vac. Sci. Technol.*, 6, 271-75.

Altena F.W., H.A.M. Knoef, H. Heskamp, D. Bargeman and C.A. Smolders, 1983, Some Comments on the Applicability of Gas Permeation Methods to Characterize Porous Membranes Based on Improved Accuracy and Data Handling, *J. Mem. Sci.*, 12, 313-22.

Armor J.N., 1989, Catalysis with Permselective Membranes, *Applied Catalysis*, 49, 1-25.

Anderson M.A., M.J. Gieselmann and Q. Xu, 1988, Titania and Alumina Ceramic Membranes, *J. Mem. Sci.*, 39, 243-58.

Askeland D.R., 1996, *The Science and Engineering of Materials*, 3rd Edition, *Chapman & Hall*, 1-523.

Bae D.S., K.S. Han and S.H. Choi, 1997, Fabrication and Microstructure of TiO₂-ZrO₂ Composite Membranes, *J. Mat. Sci. Let.*, 16, 658-60.

Bean C.P., 1972, The Physics of Porous Membranes-Neutral Pores, in G. Eiseinan (Ed.), *Membranes*, Vol.1, Dekker, New York, 1-211.

Bhave R.R., 1991, Permeation and Separation Characteristics of Inorganic Membranes in Liquid Phase Applications, *Inorganic Membranes: Synthesis, Characteristics, and Applications*, Van Nostrand Reinold New York, 95-128

Biesheuvel P.M., and H. Verweij, 1999, Design of Ceramic Membrane Supports: Permeability, Tensile Strength and Stress, *J. Mem. Sci.*, 156, 141-52.

Bottino A., G. Capannelli, A. Grosso, O. Monticelli, O. Cavalleri, R. Rolandi, and R. Soria, 1994, Surface Characterization of Ceramic Membranes by Atomic Force Microscopy, *J. Mem. Sci.*, 95, 289-96.

Bowen W.R., N. Hilal, R.W. Lovitt, and P.M. Williams, 1996, Visualisation of an Ultrafiltration Membrane by Non-Contact Atomic Force Microscopy at Single Pore Resolution, *J. Mem. Sci.*, 110, 229-32.

Bowen W.R., N. Hilal, R.W. Lovitt, and C.J. Wright, 1998, A New Technique for Membrane Characterisation: Direct Measurement of the Force of Adhesion of a Single Particle Using an Atomic Force Microscope, *J. Mem. Sci.*, 139, 269-74.

Bridger K., and M. Massuda, 1987, Principles of Slip Casting/Pressure Filtration, Martin Marietta Laboratories Baltimore, Maryland, Ceramic Powder Science III.

Burggraaf A.J., and K. Keizer, 1991, Synthesis of Inorganic Membranes, *Inorganic Membranes, Synthesis, Characteristics, and Applications*, R.R. Bhave, Van Nostrand Reinold New York, 10-63.

Calvo J.I., P. Pradanos, A. Hernandez, W.R. Bowen, N. Hilal, R.W. Lovitt, 1997, and P.M. Williams, Bulk and Surface Characterization of Composite UF Membranes Atomic Force Microscopy, Gas Adsorption-Desorption and Liquid Displacement Techniques, *J. Mem. Sci.*, 128, 7-21.

Cao G., Y. Lu, L. Delattre, C.J. Brinker, and P.G. Lopez, 1996, Amorphous Silica Molecular Sieving Membranes by Sol Gel Processing, *Adv. Mater.*, 8, 588-91.

Chase M.W. Jr., C.A. Davies, J.R. Downey Jr., D.J. Frurip, R.A. McDonald, and A.N. Syverud, 1986, JANAF Thermodynamical Tables, Third Edition, 1-926.

Clark R.A., M.F. Hall, and J.N. Kirk, 1988, The Control of Pore Size in the Manufacture of Ceramic Filters, *Advanced Ceramics in Chemical Process Engineering*, British Ceramic Proceedings, 43, 425-36.

Cot L., 1988, New Inorganic Membranes, *British Ceramic Proceedings*, 43, 511-20.

Cot L., C. Guizard, A. Julbe, and A. Larbot, 1994, Preparation and Application of Inorganic Membranes, Membrane Processes in Separation and Purification, Kluwer Academic Publishers, 431-42.

Cuperus F.P., D. Bargeman, and C.A. Smolders, 1987, Thermoporometry and permoporometry applied to UF-membrane characterization, Proc. Int. Workshop on characterization of Ultrafiltration Membranes, 115-24.

Cuperus F.P., D. Bargeman, and C.A. Smolders, 1992, Critical Points in the Analysis of Membrane Pore Structures by Thermoporometry, J. Mem. Sci., 66, 45-53.

Darcovich K., and C.R. Cloutier, 1999, Processing of Functionally Gradient Ceramic Membrane Substrates for Enhanced Porosity, J. Am. Ceram. Soc., 82, [8], 2073-79.

Dietz P., P.K. Hansma, O. Inacker H.D. Lehmann, and K.H. Herrmann, 1992, Surface Pore Structures of Micro- and Ultrafiltration Membranes Imaged with the Atomic Force Microscope, J. Mem. Sci., 65, 101-11.

Doyen W., W. Adriansens, B. Molenberghs, and R. Leysen, 1996, A Comparison Between Polysulfone, Zirconia and Organo-Mineral Membranes for use in Ultrafiltration, Journal of Membrane Science, 113, 147-58.

Galaj S., M.P. Besland, A. Wicker, J. Gillot, and R. Soria, 1990, Membrane Filter, Ceramiques Tech. Soc. D., Patent No. US4946592 1-10.

Gallaher G.R., and P.K.T. Liu, 1994, Characterization of Ceramic Membranes I. Thermal and Hydrothermal Stabilities of Commercial 40 A Membranes, J. Mem. Sci., 92, 29-44.

Germic L., K. Ebert, R.H.B. Bouma, Z. Borneman, M.H.V. Mulder, and H. Strathmann, 1997, Characterization of Polyacrylonitrile Ultrafiltration Membranes, J. Mem. Sci., 132, 131-45.

Glass S.J., and D.J. Green, 1999, Permeability and Infiltration of Partially Sintered Ceramics, J. Am. Ceram. Soc., 82, [10], 2754-52.

Guendjian B., 1965, Elements Mineraux Simi-Permeables, Societe de Fabrication d'Elements Catalytiques resident en France (Seine), P.V. no. 13.371 No 1.440.105, 4p.

Guizard C., N. Ajaka, F. Garcia, A. Larbot, and L. Cot, 1990, New Membranes for the Hyperfiltration of Small Molecules. Influence of the Mesoporous Structure on Separation and Fractionation Performances, Proceed. Of Vth Filtration Congress, Nice, France, 143-45.

Holz D., M. Roger, R. Janssen, and N. Claussen, 1994, Mechanical Properties of Reaction-Bonded Al₂O₃/ZrO₂ Composites, Ceram. Eng. Sci. Proc., 651-58.

Hsieh, H.P., 1991, General Characteristics of Inorganic Membranes, Inorganic Membranes, Synthesis, Characteristics, and Applications, R.R. Bhave, Van Nostrand Reinold New York, 64-94.

Hsieh H.P., R.R. Bhave, and H.L. Fleming, 1988, Microporous Alumina Membranes, J. Mem. Sci., 39, 221-41.

Hsieh, H.P., 1996, Inorganic Membranes for Separation and Reaction, Elsevier Science Publishing Company, New York, 1-591.

Jakobs E., and W.J. Koros, 1997, Ceramic Membrane Characterization via the Bubble Point Technique, J. Mem. Sci., 124, 149-59.

Keuler J.N., 2000, PhD-thesis: Optimising Catalyst and Membrane Performance and Performing a Fundamental Analysis on the Dehydrogenation of Ethanol and 2-Butanol in a Catalytic Membrane Reactor, 1-420.

Kiyoshi Y., and W. Naohito, 1991, Ceramic Filter and Process for Making it. Patent no. EP0426546, TOTO LTD, 1-5.

Klein L.C., and N. Giszpenc, 1990, Sol-Gel Processing for Gas Separation Membranes, Ceramic Bull., 69, 1821-30.

Kedem O., and J. Katchalsky, 1958, Thermodynamic Analysis of the Permeability of Biological Membranes to Nonelectrolytes, *Biochim, Biophys. Acta*, 27, 229-46.

Keizer K., R.J.R. Uhlhorn, R.J. van Vuren, and A.J. Burggraaf, 1988, Gas separation mechanisms in microporous modified gamma-Al₂O₃ membranes, *J. Mem. Sci.* 39, 285-300.

Lange F.F., 1982, Transformation Toughening, part 4 Fabrication, Fracture Toughness and Strength of Al₂O₃-ZrO₂ Composites, *J. Mat. Sci.*, 17, 247-54.

Larbot A., J.A. Alary, C. Guizard, and L. Cot, 1987, New Inorganic Ultrafiltration Membranes: Preparation and Characterization, *Int. J. Hight. Tech. Ceram.*, 3, 143-51.

Larbot A., J.P. Fabre, C. Guizard, and L. Cot, 1988, Inorganic Membranes Obtained by Sol-Gel Techniques, *J. Mem. Sci.*, 39, 203-12.

Larbot A., J.P. Fabre, C. Guizard, L. Cot, and J. Gillot, 1989, New Inorganic Ultrafiltration Membranes: Titania and Zirconia Membranes, *J. Am. Ceram. Soc.*, 72, [2], 257-61.

Lee Y., and M.M. Clark, 1998, Modeling of Flux Decline During Crossflow Ultrafiltration of Colloidal Suspensions, *J. Mem. Sci.*, 149, 181-202.

Leenaars A.F.M, and A.J. Burggraaf, 1985, The Preparation and Characterization of Alumina Membranes with Ultra-Fine Pores, *J. Mem. Sci.*, 24, 261-70.

Leger C., H.D.L. Lira, and R. Paterson, 1996a, Preparation and Properties of Surface Modified Ceramic Membranes. Part II., *J. Mem. Sci.*, 120, 135-46.

Leger C., H.D.L. Lira, and R. Paterson, 1996b, Preparation and Properties of Surface Modified Ceramic Membranes. Part III., *J. Mem. Sci.*, 120, 187-95.

Lin C.L., D.L. Flowers, and P.K.T. Liu, 1994, Characterization of Ceramic Membranes II. Modified Commercial Membranes with Pore Size under 40 Å, *J. Mem. Sci.*, 92, 45-58.

Linkov V.M., and V.N. Belyakov, 1996, Ceramic Membranes, Application No.: 97/7639, Priority Claimed: ZA 96/5323 1996JUN24, RG & Co Ref: 514414, 13p.

Maebashi N., 1992, Ceramic Filter and Process for Making it, US-patent: US005098571A, 1-9.

Mo S.D., Y.N. Xu, and W.Y. Ching, 1997, Electronic and Structural Properties of Bulk γ - Al_2O_3 , J. Am. Ceram. Soc 80, [5], 1193-97.

Nakao S., 1994, Determination of Pore Size and Pore Size Distribution 3. Filtration Membranes, J. Mem. Sci., 96, 131-65.

Nakao S., and S. Kimura, 1981, Analysis of Solutes Rejection in Ultrafiltration, J. Chem. Eng. Jpn., 14, 32-37.

Nakao S., and S. Kimura, 1982, Models of Membrane Transport Phenomena and their Application for Ultrafiltration Data, J. Chem. Eng. Jpn., 15, 200-205.

Osmonics, 1992, Methods of Water Purification, National Development, <http://www.osmonics.com/products/Page716.htm>, 1-6.

Peppas N.A., and D.L. Meadows, 1983, Macromolecular Structure and Solute Diffusion in Membranes: an Overview of Recent Theories, J. Mem. Sci., 16, 361-77.

Plessis du J.P., 2000, Porous Media Modelling, University of Stellenbosch, 1-101.

Reed J.S., 1988, Introduction to the Principles of Ceramic Processing, *John Wiley & Sons*, 1-486.

Robertson B.C., and A.L. Sydney, 1988, A Stefan Maxwell Analysis of Protein Transport in Porous Membranes, Sep. Sci. Technol., 23, 1977-1811

Rocek J., and P. Uchytíl, 1994, Evaluation of Selected Methods for the Characterisation of Ceramic Membranes, J. Mem. Sci., 89, 119-29.

Sakar B.K., 1975, The Effect of Ball Milling on Alumina Powders, *Trans. Indian Ceram. Soc.*, 34, 8-12.

Solomon A.K., 1968, Characterization of Biological Membranes by Equivalent Pores, *J. Gen. Physiol.*, 15, 355.

Spiegler K.S., and O. Kedem, 1966, Thermodynamics of Hyperfiltration (Reverse Osmosis): Criteria for Efficient Membranes, *Desalination*, 1, 311-26.

Tayaa H., A. Mosset, and J. Galy, 1992, Effect of Chemical Additives in the Sol-Gel Processing of Aluminas. II. Structural Evolution During the Thermal Treatment. Specific Areas of γ -Alumina, *Eur. J. Solid State Inorg. Chem.*, 29, 27-38.

Terpstra R.A., B.C. Bonekamp, and H.J. Veringa, 1988, Preparation, Characterization and some Properties of Tubular Alpha Alumina Ceramic Membranes for MF and as a Support for UF and Gas Separation Membranes, *Desalination*, 70, 395-404.

Tilborg P.J., and H.J. Veringa, 1989, De Vervaardiging van Geavanceerde Keramische Materialen voor Technische Toepassingen, *Nationaal Keramisch Atelier*, 1-28.

Tiller F.M., and C.D Tsai, 1986, Theory of Filtration of Ceramics: I, Slip Casting, *J. Am. Ceram. Soc.*, 69, [12], 882-87.

Uchytel P., 1994, Gas Permeation in Ceramic Membranes, Part I. Theory and Testing of Ceramic Membranes, *J. Mem. Sci.*, 97, 139-44.

Ulhorn R.J.R., and A.J. Burggraaf, 1991, Gas Separation with Inorganic Membranes, *Inorganic Membranes*, (R.R. Bhave Ed.), Van Nostrand Reinhold, New York, 1-155.

Ulhorn R.J.R., K. Keizer, and A.J. Burggraaf, 1989, Gas and Surface Diffusion in Modified γ -Alumina Systems, *J. Mem. Sci.*, 46, 225-41.

Ulhorn R.J.R., K. Keizer, and A.J. Burggraaf, 1992a, Gas Transport and Separation with Ceramic Membranes, Part I. Multilayer Diffusion and Capillary Condensation, *J. Mem. Sci.*, 66, 259-69.

Uhlhorn B.J.R., M.H.B.J. Huis in't Veld, K. Keizer A.J. Burggraaf, 1992b, Synthesis of Ceramic Membranes, Part I. Synthesis of Non-Supported and Supported γ -Alumina Membranes without Defects, *J. Mat. Sci.*, **27**, 527-37.

Van de Ven M.F.C., A. Kruyt, W.L. In de Haak et al., 1988, Kernverslag Technische Keramiek en Mechanische Karakterisering van Zirconia, Universiteit van Twente, 1-11.

Verniory A., R. Du Bois, P. Decoodt, J.P. Gasee, and P.P. Lambert, 1973, Measurement of the Permeability of Biological Membranes, *J. Gen. Physiol.*, **62**, 489.

Wang J., 1996, Microcrack Coalescence in Alumina-Zirconia Composites, *J. Mat. Sci. Letters*, **15**, 442-44.

Welles W.H.A.M., W.L. In de Haak, A. Kruyt, J. H. Maas, M.F.C. van de Ven, and, A.J.A. Winnubst, 1988, Keramische Materialen, Diktaat, Universiteit van Twente, 1-63.

Zeman L., G. Tkacik, and P. Le Parlouer, 1987, Characterization of Porous Sublayers in UF Membranes by Thermoporometry, *J. Mem. Sci.*, **32**, 329-37.

Appendix A: Linkov's Patent

FORM P7

REG & CO. REF.

514414

COMPLETE SPECIFICATION

| | | | | |
|---|------------------------------|-------------------------|----|--------------|
| 01 | 01 | Official application No | 22 | Lodging Date |
| 51 | International classification | | | |
| B32B | | | | |
| 71 | Full Name(s) of Applicant(s) | | | |
| Prof. Dr. Vladimir Mikhailovich LINKOV Prof. Dr. Vladimir Nikolaevich BELYAKOV | | | | |
| 72 | Full name(s) of inventor(s) | | | |
| Prof. Dr. Vladimir Mikhailovich LINKOV Prof. Dr. Vladimir Nikolaevich BELYAKOV | | | | |
| 54 | Title of invention | | | |
| Ceramic Membranes | | | | |

Address for service

Dr GERNTHOLTZ
PATENT ATTORNEYS
30 UNION RD. MILNERTON 7441
P.O. BOX 8
CAPE TOWN 8000
SOUTH AFRICA

DrG REF 514414

TITLE OF INVENTION

Ceramic Membrane.

FIELD OF INVENTION

The present invention relates to ceramic membranes.

More particularly, the invention relates to ceramic membranes having an anisotropic porous structure.

BACKGROUND TO INVENTION

It is known from EP 0 426 546 A2 that a preparation of inorganic membrane materials with an asymmetrical porous structure can be carried out in two consecutive stages, namely the formation of a ceramic membrane support and the coating of the support with a thin ceramic layer (active layer) containing meso- or micropores. As a rule the preparation of a support is not described, as it is assumed that any porous ceramic material can be utilized, provided that it possesses required chemical and mechanical properties.

The most widely used method for the formation of thin porous ceramic layers is called a sol-gel technology. It involves deposition of a metal oxide sol onto the ceramic or metal porous support surface followed by the sol coagulation, drying and firing. This method allows for the subsequent coating of a support with several porous ceramic layers. Each consecutive layer may contain pores of a smaller size. Metal oxides used for the coatings can have different chemical natures to that of the porous support forming materials.

The described membrane manufacturing process requires high precision operations and clean room conditions and, when applied to large membrane surfaces, has low reproducibility and is extremely labour intensive due to a large number of technological operations involved.

5 It is an object of the invention to provide an asymmetrical ceramic membrane in one technological operation, which will combine the preparation of the membrane support and the coating of an active layer in a single procedure.

SUMMARY OF INVENTION

10 According to the invention, a method for preparing a ceramic membrane, includes the steps of preparing a binary mixture of Al_2O_3 and ZrO_2 ; of diminishing the binary mixture; of suspending the diminished binary mixture in water; of casting the suspension of the diminished binary mixture into a gypsum mould to obtain a casting; and of drying and subsequently
 15 calcinating the casting to obtain a membrane having a macroporous layer and a superimposed mesoporous layer.

The membrane may have a tubular shape, and the macroporous layer may be on the outside and the mesoporous layer on the inside.

The ZrO_2 may be stabilized with Y_2O_3 .

20 The binary mixture may be prepared to have the following ratio:

Al_2O_3 : 60–40% by weight

ZrO_2 : 20–40% by weight.

The density of the binary mixture may be 2,2 to 2,4 g/cm^3 .

The invention also extends to a ceramic membrane produced of Al_2O_3 and ZrO_2 .

BRIEF DESCRIPTION OF DRAWINGS

5 The invention will now be described by way of example with reference to the accompanying schematic drawings.

In the drawings there is shown in:

Figure 1 a schematic sectional side view of a ceramic membrane in accordance with the invention; and

10 Figure 2 a globular model of ceramic materials composition in accordance with the invention.

DETAILED DESCRIPTION OF DRAWINGS

Referring to Figure 1 of the drawings, a schematic sectional side view of a ceramic membrane in accordance with the invention is shown.

15 The ceramic membrane, shown in tubular form and generally indicated by reference numeral 10, includes a macroporous outer layer 12 and a mesoporous inner (or active) layer 14.

Figure 2 of the drawing shows a globular model of ceramic material compositions in accordance with the invention.

20 The possibility exists to precisely control the size of the macropores present in the support part of the membrane, which is formed by larger

metal oxide particles and that of mesopores in the active layer of the membrane, which is formed by smaller particles. This is due to the fact that although an increase in the milling time is not accompanied by a decrease in particle sizes, a decrease in pore sizes of the ceramic material is still present. This change in pore sizes occurs as a gradual process with a discrete step of 0,06 μm in the case of larger pores. This stepwise decrease in pore sizes when the particle sizes remain unchanged is explained by a so-called globular model of ceramic materials composition (Figure 2). According to this model a substantial increase in milling times affects in the first place not particle sizes but packing modes of the particles and, for instance, more dense packing in agglomerates consisting of 5 particles give pores of a smaller diameter than that in the case of a 6 particle agglomerate. It also should be noted that the highest porosity and specific surface area are characteristic of the membranes produced with short milling times when low density structures containing 6-particle agglomerates are formed. In the case of mesopores, the spherical particles with a diameter of 4 nm packed in 5- and 6-member agglomerates are responsible for the formation of 2,6 and 4 nm pores.

According to the invention, a membrane precursor is prepared from a binary mixture of Al_2O_3 and ZrO_2 . In this mixture ZrO_2 stabilized with Y_2O_3 can be used. The binary mixture described is ball-milled during different times.

During the wet milling of metal oxides used as precursors for ceramic materials an increase in the milling time, after certain time elapsed from the start of the milling operation, does not affect the size of particles obtained. At the same time an increase in the milling time results in the occurrence of

a so-called bi-disperse suspension. In such a suspension together with large particles those of considerably smaller size are present. This bi-disperse property of suspensions formed by particles of milled metal oxides leads to the formation of an irregular porous structure during the manufacturing of porous ceramic materials by means of the mould casting using gypsum moulds. This is due to the fact that when the suspension comes in contact with the mould surface, the larger metal oxide particles precipitate at a higher rate than the smaller ones. As a result a greater portion of the ceramic green body formed next to the mould surface consists of larger particles and has larger pore sizes respectively. On the later stage of the precipitation process the deposition of the smaller particles takes place and during this time the newly formed green body serves as a support for a thin layer consisting of smaller particles and thus having smaller pores.

The suspension used for the preparation of asymmetrical ceramic membranes according to the present invention consists of Al_2O_3 and ZrO_2 milled for different times. The composition of the suspension ranges from 60 % to 80 % for Al_2O_3 and from 20 % to 40 % for ZrO_2 . The selection of the proportions of the metal oxides present in the suspension was done according to, F.F. de Lange, J. Mater. Sci., 17(1) 247-54 (1982), where it was demonstrated that ceramic materials of such composition possessed best mechanical properties.

The wet milling of the metal oxides is carried out in a ball mill equipped with steel balls. A material : balls : water ratio is maintained at 1 : 2 : 1.

The milling time for each oxide is determined by milling conditions and a required particle size. For the above milling ration the milling of Al_2O_3 for

50 and 100 hours results in average particle sizes of 0,2 and 0,15 μm respectively. When ZrO_2 is milled under the same conditions for 100 and 200 hours the size of large particles remains unchanged and makes 0,15 μm . For the latter an increase in the milling time results in an increase in the number of small particles with a diameter of 4 nm.

On completion of the milling operation and the removal of excessive water, the metal oxides are transferred into a mixing bowl where a mixture of the described above composition is made. After the mixing, an amount of water necessary for achieving a density of 2,2 - 2,4 g cm^{-3} is added to the suspension under intensive stirring.

The casting suspension is poured into a dry gypsum mould and kept there until the formation of a ceramic green body of required thickness (1-2 mm). After the removal of an excessive suspension, the green body is extracted from the mould. The air drying of the green body is carried out during 72 hours followed by a gradual temperature increase up to 1300°C at a rate of 100°C min^{-1} and the firing at that temperature during 60 minutes.

Formation of a macroporous inner layer and mesoporous outer layer occurs simultaneously during contact of water suspension of mixture with the gypsum mould.

The ceramic membrane is obtained by drying and subsequent calcination of the cast material.

The mixture of Al_2O_3 and ZrO_2 is according to the following ratio:

60-80 %w of Al_2O_3 and

20-40 %w of ZrO_2 .

The density of Al_2O_3 and ZrO_2 mixture is 2,2 - 2,4 g/cm^3 .

The mean pore diameter of macropores is determined by the milling time of Al_2O_3 (T1, hours) and ZrO_2 (T2, hours) and is equal to

| | |
|-----------------------------|---------------------|
| 0,2 μm | for T1=50 and T2=60 |
| 0,22 μm | for T1=50 and T2=70 |
| 0,14 and 0,20 μm | for T1=50 and T2=80 |
| 0,16 and 0,24 μm | for T1=50 and T2=90 |
| 0,15 and 0,18 μm | for T1=60 and T2=60 |
| 0,17 μm | for T1=60 and T2=70 |
| 0,19 μm | for T1=60 and T2=80 |
| 0,18 and 0,24 μm | for T1=60 and T2=90 |
| 0,14 and 0,21 μm | for T1=70 and T2=60 |
| 0,21 μm | for T1=70 and T2=70 |
| 0,15 μm | for T1=70 and T2=80 |
| 0,12 and 0,19 μm | for T1=70 and T2=90 |
| 0,15 μm | for T1=80 and T2=60 |
| 0,15 μm | for T1=80 and T2=70 |

0,16 and 0,21 μm for $T_1=80$ and $T_2=80$

0,16 μm for $T_1=80$ and $T_2=90$

The thickness of the mesoporous layer is determined by the milling time of ZrO_2 and is equal to 0 for 50 hours, 10 μm for 200 hours milling in a ball mill.

The pores of mesoporous outer layer have a mean pore diameter of 2,6 nm and 4 nm.

The drying the membrane precursor is carried out at 20°C during 3 days.

The calcination the membrane precursor is carried out 1300°C during 60 minutes. The heating rate to reach the calcination temperature is 100-110°C/hour.

Example 1

$\gamma\text{-Al}_2\text{O}_3$ and ZrO_2 stabilized with Y_2O_3 was heated at 900°C in a vacuum furnace for 2 hours in order to remove organic pollutants. This operation was followed by a separate milling in a wet ball mill using steel balls with a diameter of 15 mm. The oxide / balls / water ratio was maintained as close as possible to 1 / 2 / 1 throughout the whole milling operation. The milling time for Al_2O_3 was 80 hours and for ZrO_2 - 60 hours. The dense precipitate formed in the mill was placed into the polyethylene drum, 15 % water was added to it and the mixture was roller-stirred over 4 hours. The casting suspension was prepared by mixing milled Al_2O_3 and ZrO_2 in the same drum for 1 hour.

The composition of the casting suspension attributed to the best mechanical properties and highest chemical stability of resulting ceramic membranes was as follows:

Al_2O_3 - 70%

ZrO_2 - 29%

Y_2O_3 - 1%

The casting suspension was poured into specially designed tubular gypsum moulds where precursors for ceramic membranes formed during 1 min. The moulds were drained and membrane precursors were removed from them and placed into a drying chamber. The drying temperature was maintained at 20°C, the humidity at 40 %, the drying time was 3 days. After the drying operation the membrane precursors were placed in an oven, heated up to 1300°C at a heating rate of 100°C and calcined at this temperature during 1 hour.

The resulting ceramic membranes possessed uniform pore-size distribution in the macropore support layer with a mean pore diameter of 0,15 μm . A thin mesoporous layer was formed on the inner surface of the ceramic membranes. The mean pore diameters of mesopores in this layer were 2,6 and 4,0 nm.

Example 2

Milling time of Al_2O_3 - 50 h. Milling time of ZrO_2 - 100 h. Suspension composition 70% Al_2O_3 and ZrO_2 . Moulding casting time - 5 min. Air

drying of green body for 72 h. Temperature increase at $100^{\circ}\text{C h}^{-1}$ up to 1300°C , firing for 60 min.

Membrane thickness - 1 mm. Average pore diameter of support - $0,2\mu\text{m}$. Thickness of active layer - $10\mu\text{m}$. Average pore diameter of active layer - 4 nm.

Example 3

Milling time of Al_2O_3 - 50 h. Milling time of ZrO_2 - 200 h. Suspension composition 70% Al_2O_3 and 30% ZrO_2 . Moulding casting time - 5 min. Air drying of green body for 72 h. Temperature increase at $100^{\circ}\text{C h}^{-1}$ up to 1300°C , firing for 60 min.

Membrane thickness - 1 mm. Average pore diameter of support - $0,2\mu\text{m}$. Thickness of active layer - $20\mu\text{m}$. Average pore diameter of active layer - 4 nm.

Example 4

Milling time of Al_2O_3 - 100 h. Milling time of ZrO_2 - 100 h. Suspension composition 70% Al_2O_3 and 30% ZrO_2 . Moulding casting time - 5 min. Air drying of green body for 72 h. Temperature increase at $100^{\circ}\text{C h}^{-1}$ up to 1300°C , firing for 60 min.

Membrane thickness - 1 mm. Average pore diameter of support - $0,15\mu\text{m}$. Thickness of active layer - $15\mu\text{m}$. Average pore diameter of active layer - 4 nm.

Example 5

Milling time of Al_2O_3 - 50 h. Milling time of ZrO_2 - 100 h. Suspension composition 80% Al_2O_3 and 20% ZrO_2 . Moulding casting time - 5 min. Air drying of green body for 72 h. Temperature increase at $100^{\circ}\text{C h}^{-1}$ up to 1300°C , firing for 60 min.

Membrane thickness - 1 mm. Average pore diameter of support - $0,2\mu\text{m}$. Thickness of active layer - $12\mu\text{m}$. Average pore diameter of active layer - 4 nm.

Example 6

Milling time of Al_2O_3 - 50 h. Milling time of ZrO_2 - 100 h. Suspension composition 60% Al_2O_3 and 40% ZrO_2 . Moulding casting time - 5 min. Air drying of green body for 72 h. Temperature increase at $100^{\circ}\text{C h}^{-1}$ up to 1300°C , firing for 60 min.

Membrane thickness - 1 mm. Average pore diameter of support - $0,2\mu\text{m}$.

Thickness of active layer - $12\mu\text{m}$. Average pore diameter of active layer - 4 nm.

FIG. 1

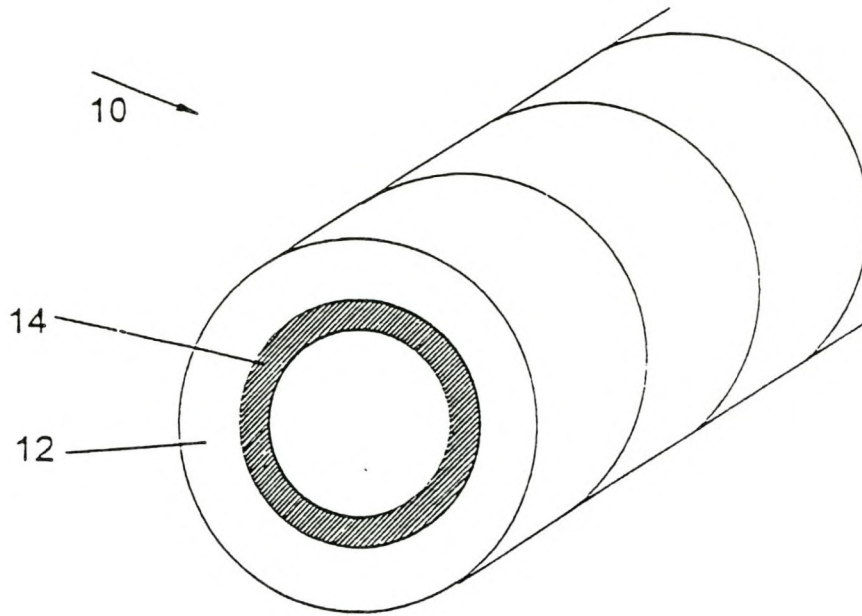






FIG 2

| | | $\frac{d_{min}}{d_{max}}$ | | | | |
|---|--------------|---------------------------|-------|-------|-------|-------|
| | | | d_1 | d_2 | d_3 | d_4 |
|  | $d = 0,155D$ | d_1 | 1,0 | 2,58 | 4,51 | 0,16 |
|  | $d = 0,4D$ | d_1 | 0,39 | 1,0 | 1,75 | 0,4 |
|  | $d = 0,7D$ | d_1 | 0,22 | 0,57 | 1,0 | 0,7 |
|  | $d = 1,0D$ | d_1 | 0,16 | 0,40 | 0,7 | 1,0 |

Appendix B: Raw Materials Specifications and Phase Diagrams.

Gamma Alumina, (γ -Al₂O₃), gamma aluminium oxide

Merck, 150013N

Powder

| | |
|----------------------------|----------------|
| Appearance | white powder |
| pH(10% aqueous suspension) | 8.5-9.5 |
| Minimum filtering range | 0.30ml/min. |
| Particle size (70%) | 0.063-0.200 mm |
| Specific Gravity | 3.2 |

Maximum Limits of Impurities

| | |
|-----------------------------|-------|
| Water-soluble matter | 0.5 % |
| Chloride (Cl) | 0.1% |
| Sulphate (SO ₄) | 0.1% |

BET Results

Analysis adsorptive: N₂

| | |
|--|----------------------------|
| BET Surface Area: | 167.6762 m ² /g |
| Average Pore Diameter (4V/A by BET): | 60.7879 A |
| BJH Adsorption Average Pore Diameter (4V/A): | 51.2851 A |
| BJH Desorption Average Pore Diameter (4V/A): | 51.2851 A |

Zirconia (ZrO₂), zirconium(IV) oxide

Aldrich, catalogue No.: 23,069-3, EEC No.: 215-227-2

Powder

| | |
|---------------------|--------------|
| Appearance | white powder |
| Particle size (99%) | < 5 micron |
| Relative density | 5.850 |

BET Results

Analysis adsorptive: N₂

| | |
|--|--------------------------|
| BET Surface Area: | 6.6551 m ² /g |
| Average Pore Diameter (4V/A by BET): | 120.4069 A |
| BJH Adsorption Average Pore Diameter (4V/A): | 133.9835 A |
| BJH Desorption Average Pore Diameter (4V/A): | 85.9523 A |

Yttria (Y₂O₃), Yttrium oxide

Aldrich, 20,516-8

Powder

| | |
|------------------|-------------------------|
| Appearance | white powder |
| Purity: | 99.99% |
| Formula weight | 225.81 |
| Specific Gravity | 5.010 |
| Titration | 78.9%Y (complexometric) |

Trace Analysis, ICP

Rare earth elements

| | |
|--------|---------|
| TB | 27 ppm |
| DY | 6 ppm |
| ER, YB | 1 ppm |
| SC | 0.3 ppm |

Other Elements

| | |
|----|--------|
| SI | 30 ppm |
| FE | 2 ppm |
| MG | 1 ppm |

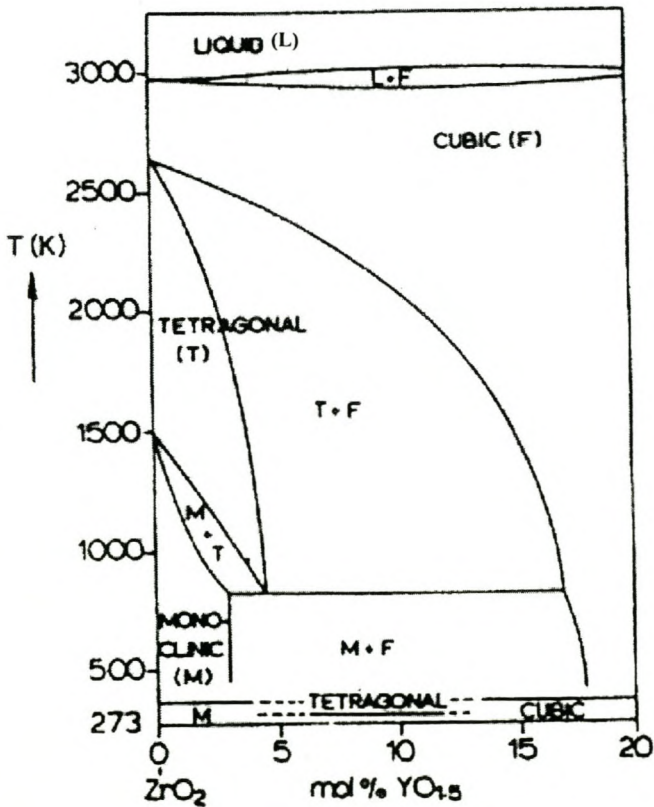


Figure B.1: Influence of yttria on zirconia phase diagram. [Source: Welles et al., 1988]

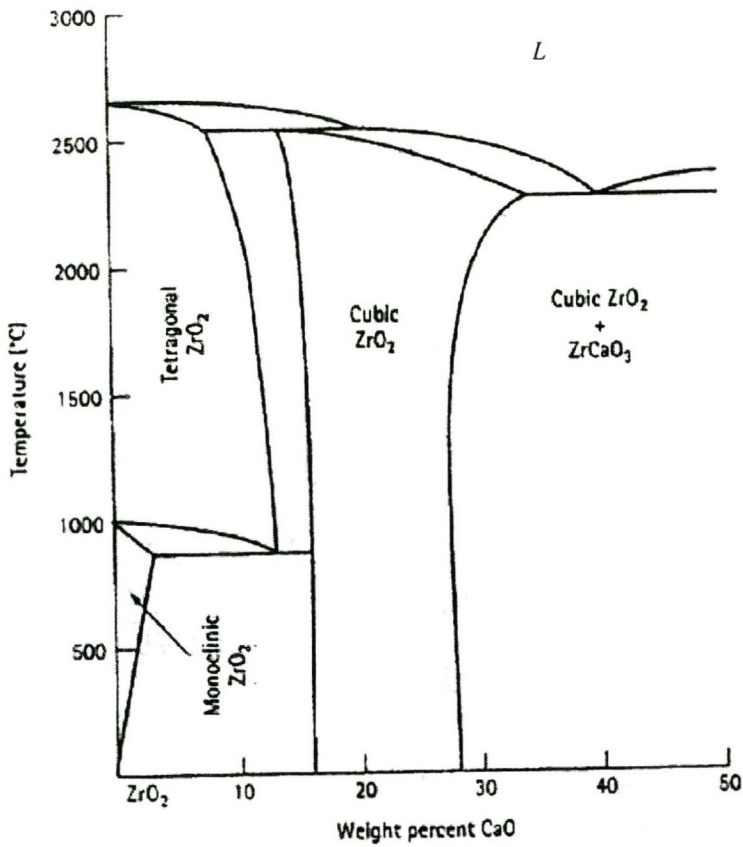
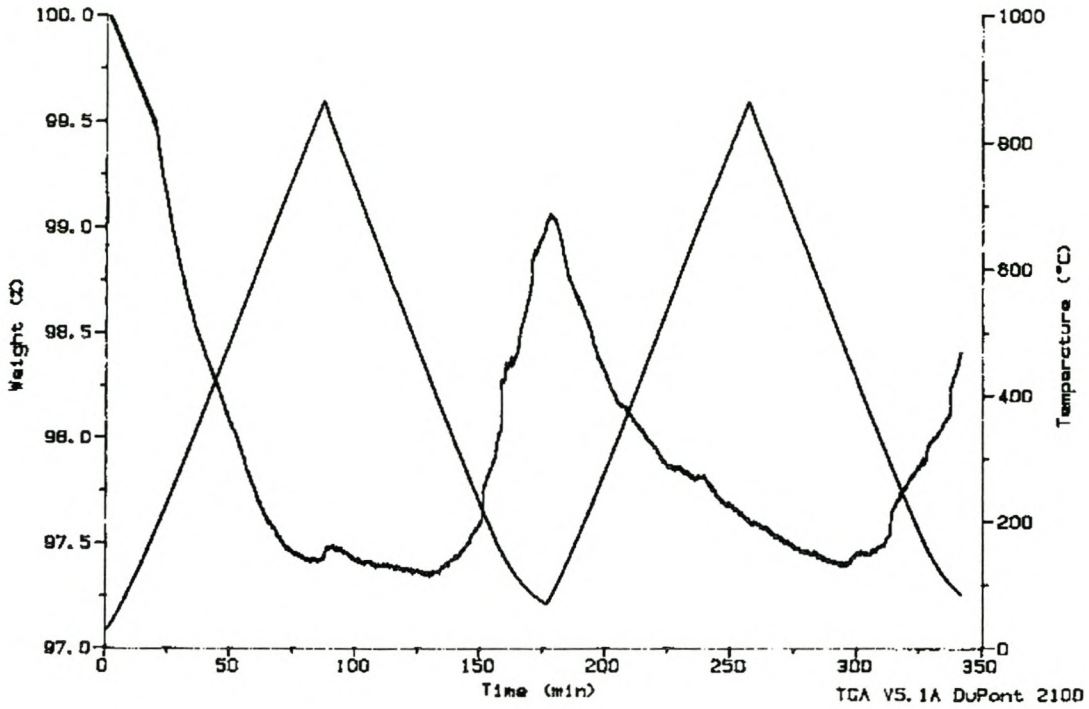


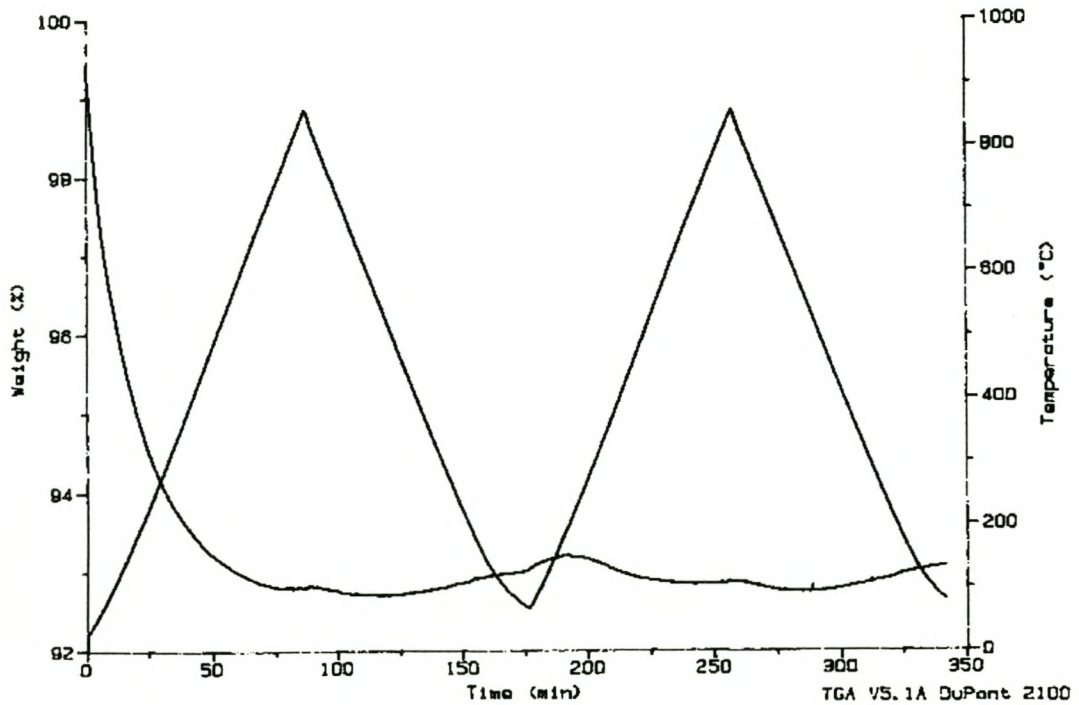
Figure B.2: The ZrO₂-CaO phase diagram. A polymorphic phase transformation occurs for pure ZrO₂. Adding 16 to 26% CaO produces a single cubic zirconia phase at all temperatures. [Source: D.R. Askeland, 1996]

Appendix C: TGA Results

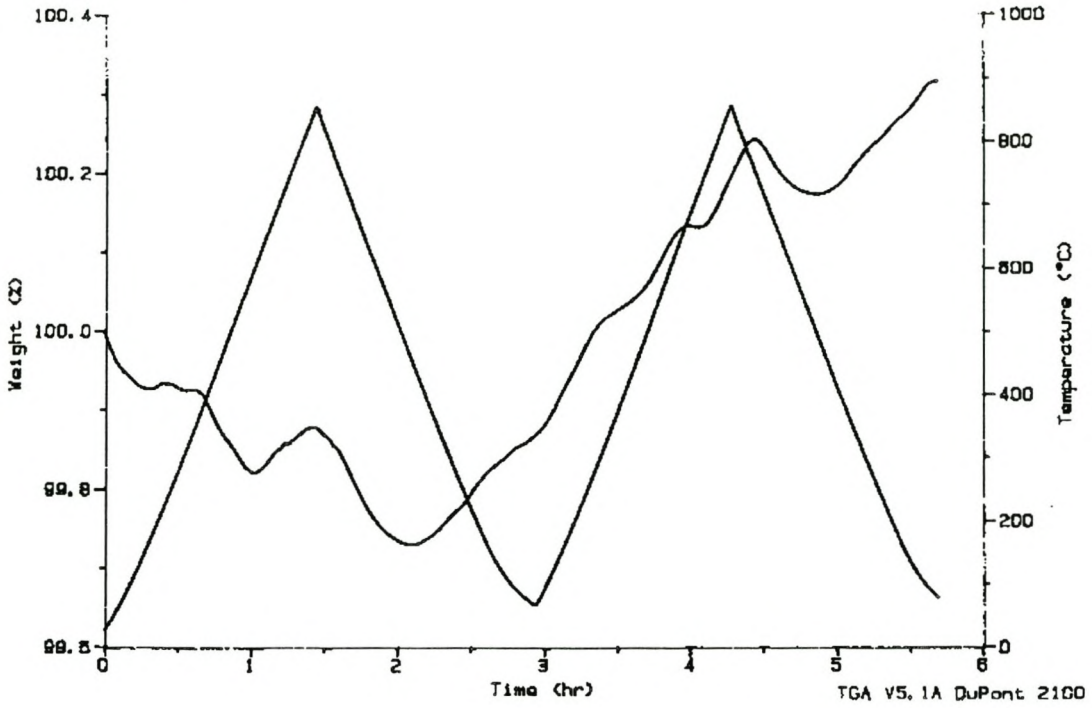
Sample: Alumina
Size: 19.0480 mg



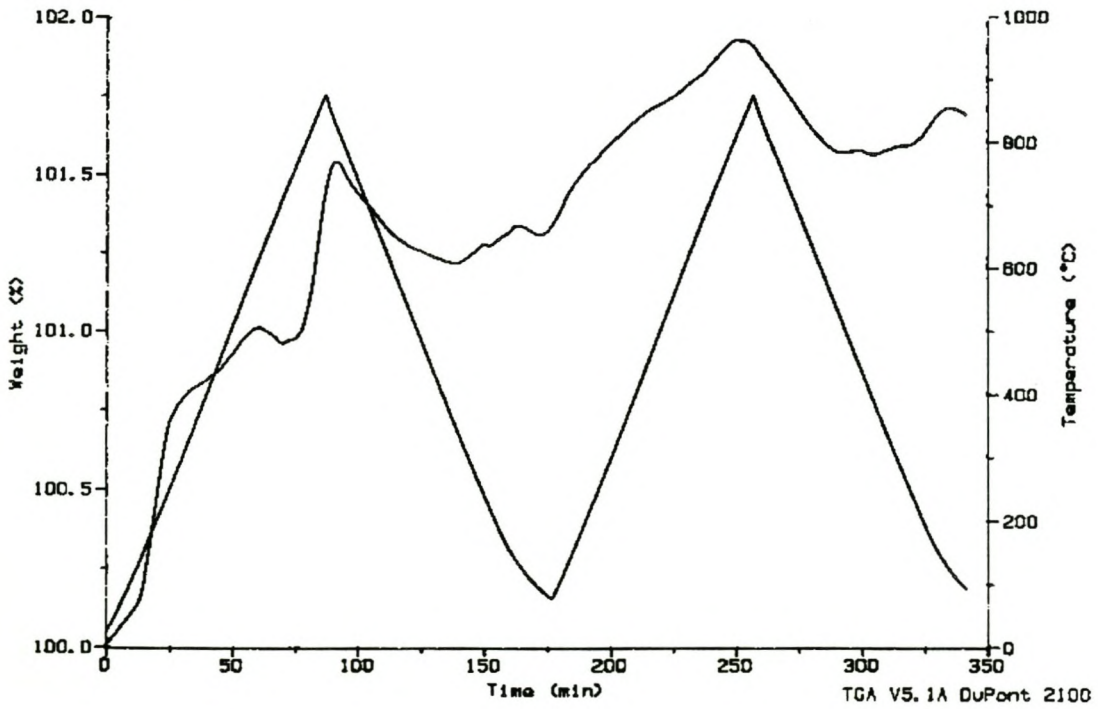
Sample: Alumina after vacuum heating treatment
Size: 17.1060 mg



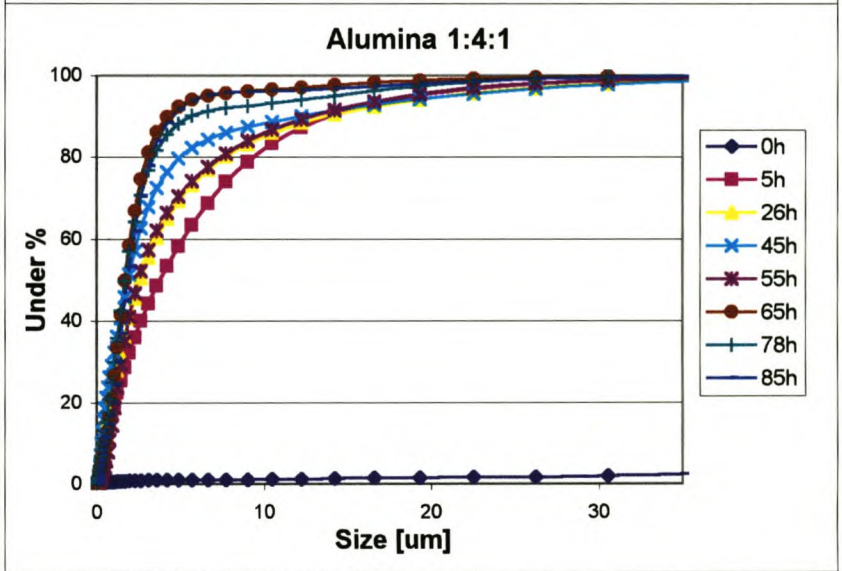
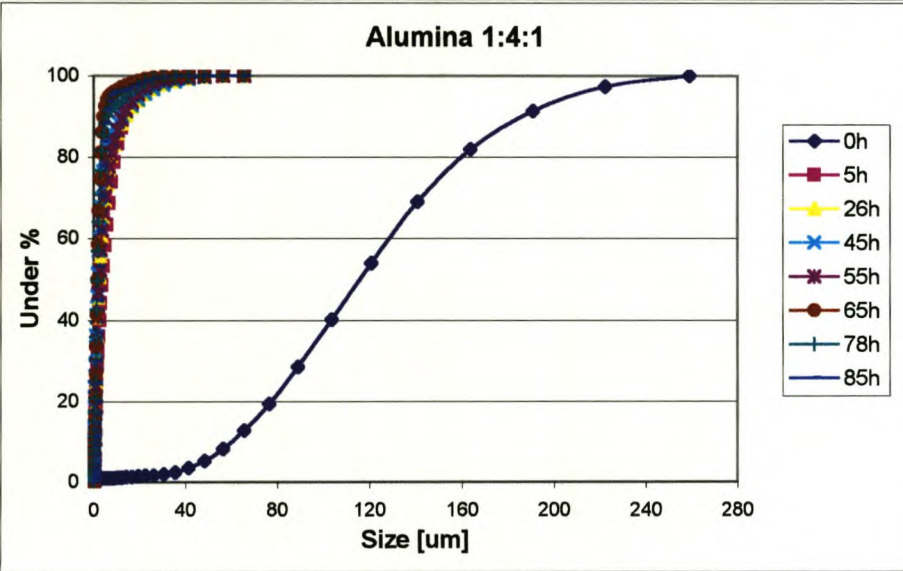
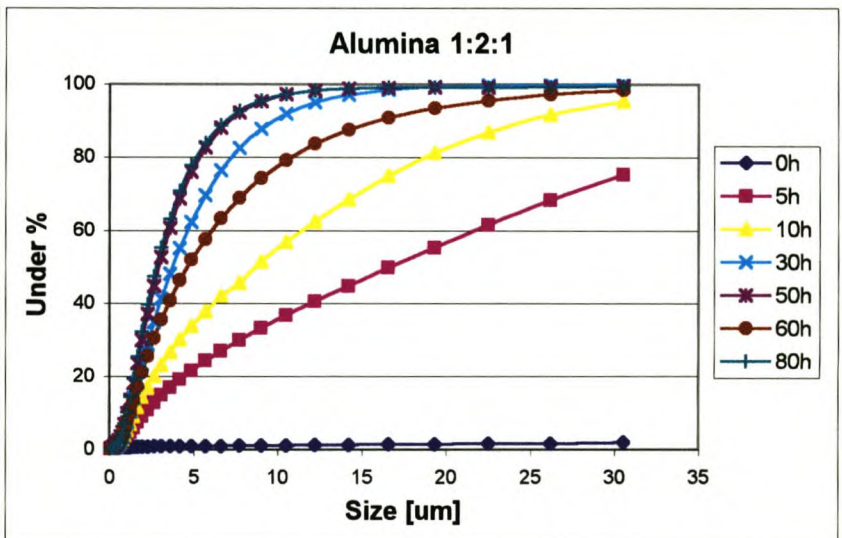
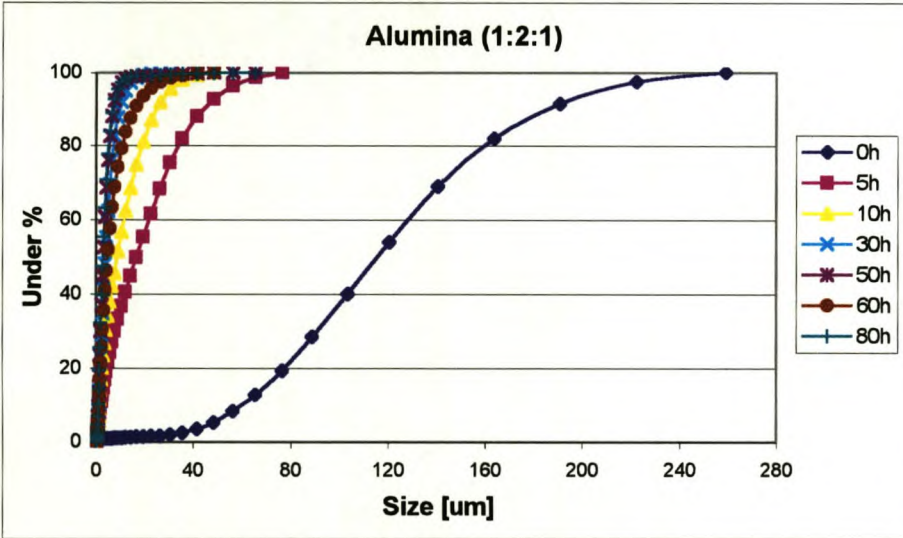
Sample: Zirconia
Size: 18.0210 mg

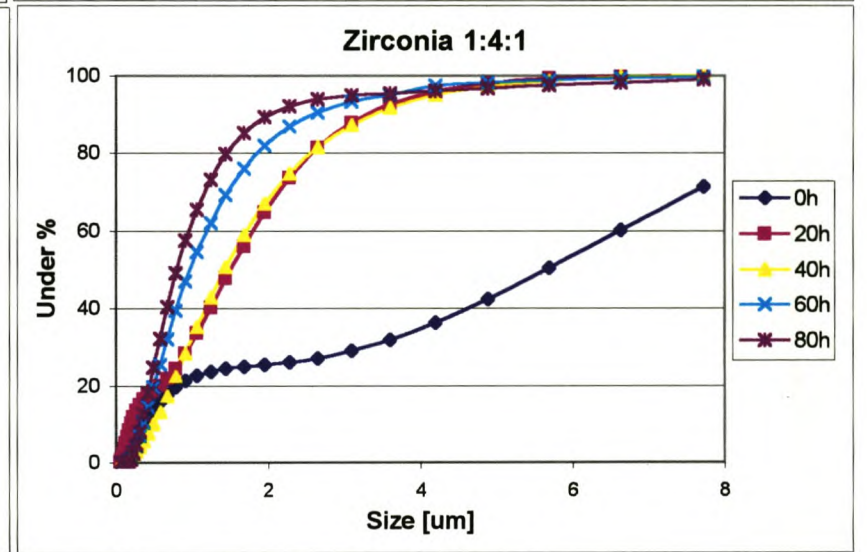
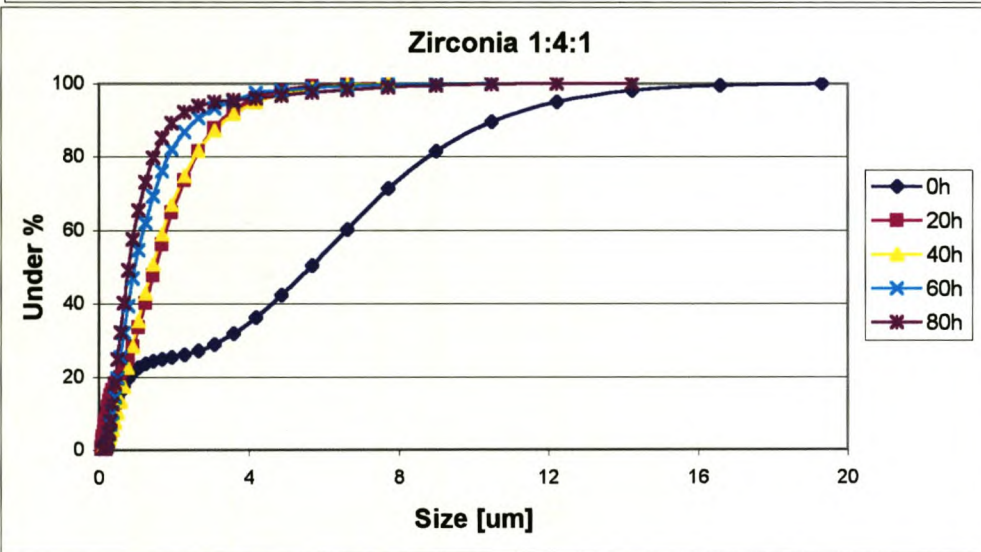
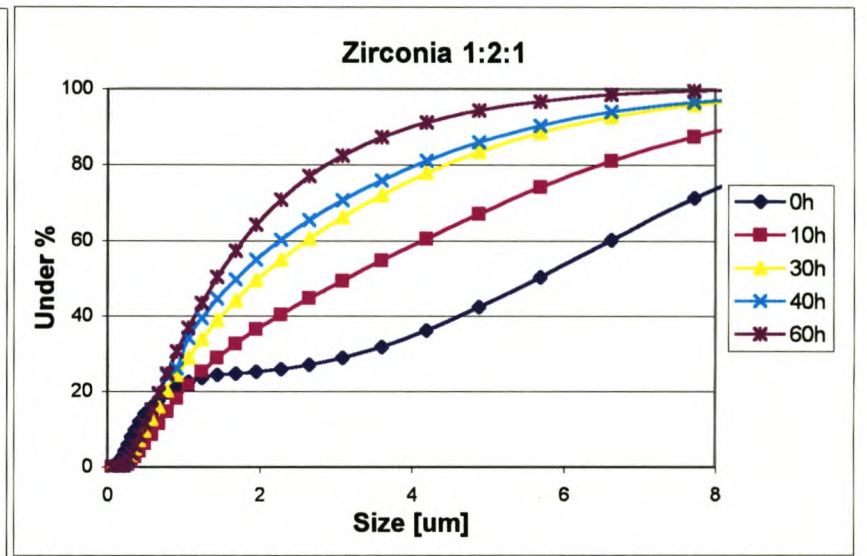
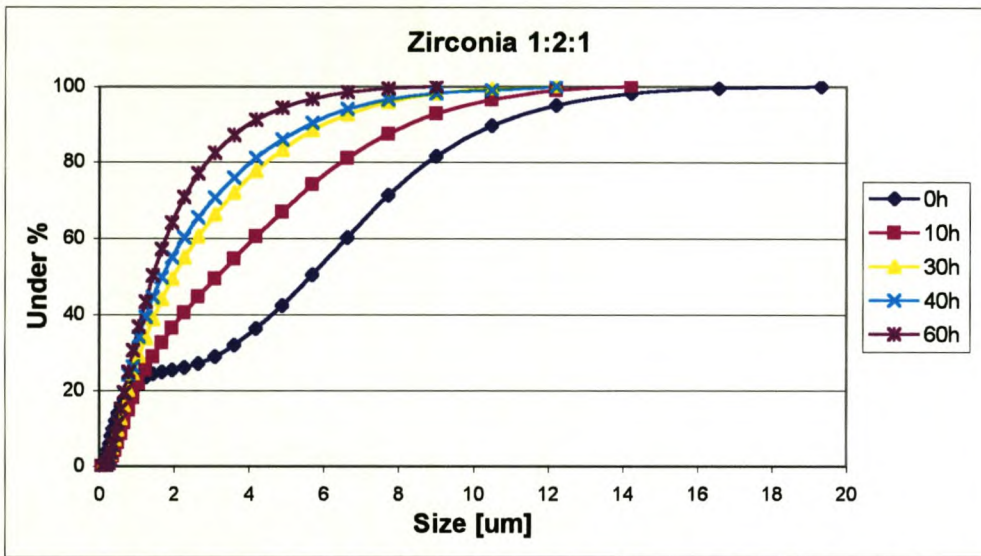


Sample: Zirconia after vacuum heating treatment
Size: 14.8950 mg



Appendix D: Particle Size Distribution





Appendix E: Slip Casting

Calcium Sulphate (plaster of Paris)

- Calcium Sulphate (plaster of Paris) chemically pure, 500 g
NT laboratory supplies (PTY) LTD.
- Calcium Sulphate Hemihydrate, 98%, CaSO₄ F.G.: 145.15, Aldrich.
- Calcium Sulphate (plaster of Paris) Approx. CaSO₄·^{1/2}H₂O (152 69 80) UniTek, Technical Grade
Saarchem (PTY) LTD.

To make gypsum, 40/50 g water per 100 g of calcined gypsum are required to obtain an optimally hardened product. The mixture generally expands somewhat (the linear expansion is about 0.4 % when 45 g H₂O en 100 g gypsum are used).

Hardened gypsum does not resist flowing water and for this reason gypsum is less suitable for use in places where it is exposed to wet conditions.

Hardened gypsum does not resist heat since it loses water when heated; because of this phenomenon gypsum protects objects against fire until the dehydration process is completed.

Problems encountered with the gypsum mould:

1) Release of the gypsum from the steel mould:

Plan A: The gypsum was poured into the steel mould. Then the gypsum was forced out of the mould. -this did not work, the gypsum broke.

Plan B: The inside of the steel mould was covered with vaseline to make the gypsum come loose from its mould. This did not work extremely well, but the gypsum came out of the mould some of the times.

Plan C: The outside part of the steel mould was then cut into two halves → This plan worked very well. The gypsum moulds became slightly oval.

2) How to get the ceramic membrane formed in the gypsum mould out of the gypsum.

-->According to the French patent obtained from Mr. Grangeon, the ceramic material will shrink so that it can easily be separated from the mould. This makes sense since the mould

will absorb water from the membrane which could make it come loose from the surface of the mould. This was indeed the case.

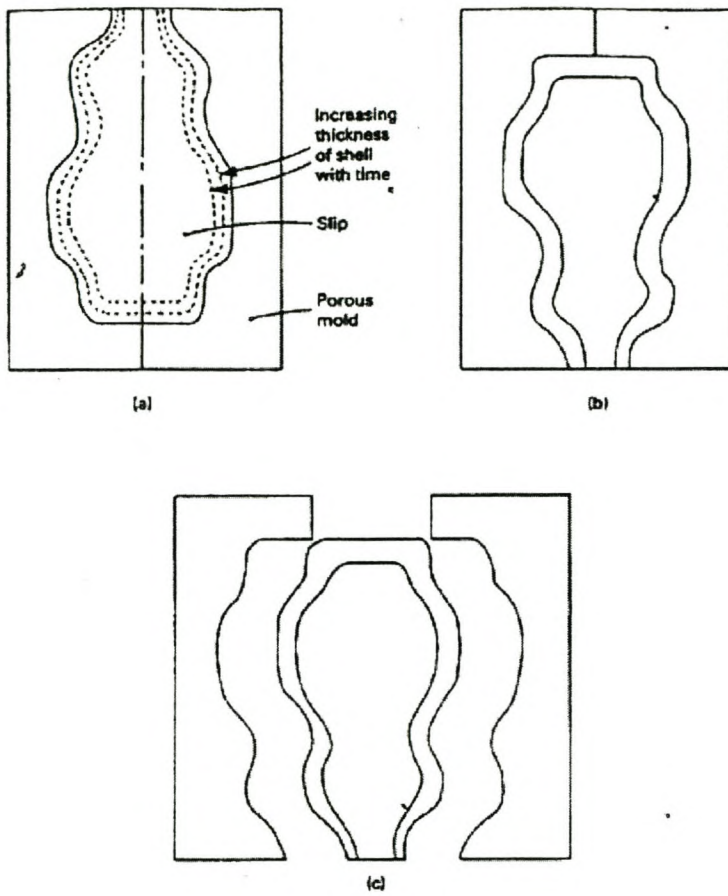


Figure E.1: Processing of hollow ceramic products by slip casting. (a) Pouring slip in mold and waiting for shell of required thickness to form. (b) Removing excess slip. (c) Removing green product out of mold in preparation for drying and firing. [Source: M.M. Farag, selection of Materials and Manufacturing Processes for Engineering Design]

Appendix F: List of Tested Manufactured Membranes

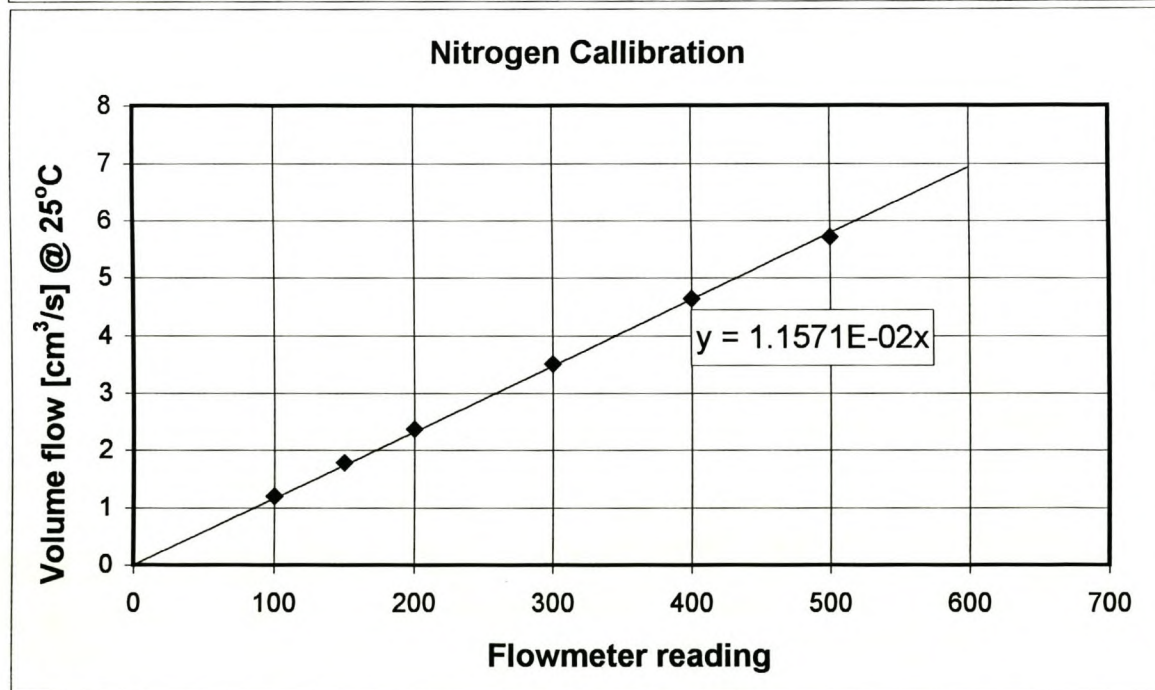
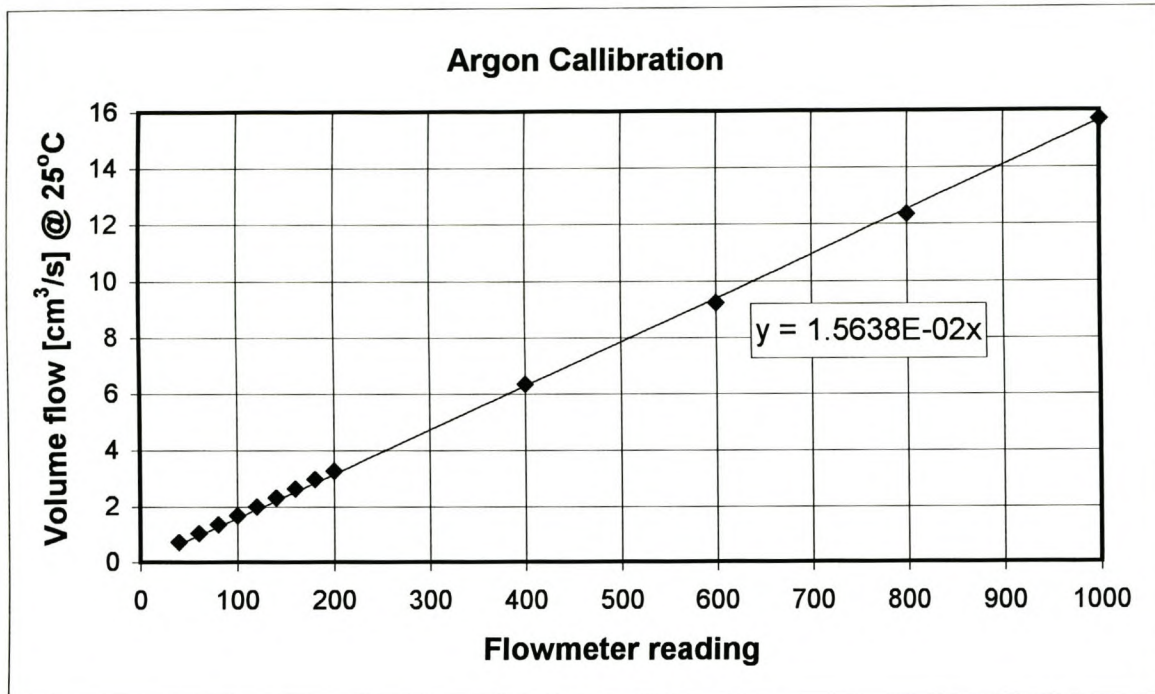
| Sintering Profile | | Memb. | W/O* Ratio | thickness th [mm] | Gas permeability, Fo | | | Selectivity | | | Gas permeability coefficient, Kg | | |
|-------------------|------------|-------|------------|-------------------|--------------------------|------------|------------|------------------------|-------------------------------------|------------------------|----------------------------------|------------------------|------------------------|
| time [h] | Temp. [°C] | | | | F H2 | F N2 | F Ar | S (H ₂ /Ar) | S (H ₂ /N ₂) | S (N ₂ /Ar) | K H2 [m ²] | K N2 [m ²] | K Ar [m ²] |
| | | | | | [mol/m ² sPa] | | | | | | | | |
| 0 | 1300 | M53d | 1.83 | 0.9 | 3.6205E-05 | 1.0066E-05 | 7.7439E-06 | 4.68 | 3.6 | 1.3 | 6.132E-15 | 3.609E-15 | 3.563E-15 |
| 0 | 1300 | M54 | 1.83 | 1.85 | 2.3337E-05 | 6.3764E-06 | 5.0217E-06 | 4.65 | 3.66 | 1.27 | 7.347E-15 | 4.304E-15 | 4.186E-15 |
| 0 | 1300 | M56a | 1.83 | 1.25 | 2.5385E-05 | 7.5444E-06 | 5.5187E-06 | 4.6 | 3.36 | 1.37 | 5.750E-15 | 3.532E-15 | 3.343E-15 |
| 0 | 1300 | M56c | 1.83 | 1.1 | 3.2755E-05 | 8.3194E-06 | 6.7488E-06 | 4.85 | 3.94 | 1.23 | 6.614E-15 | 3.611E-15 | 3.730E-15 |
| 0.5 | 1300 | M38b | 1.4 | 1.35 | 3.6218E-05 | 1.0182E-05 | 8.0065E-06 | 4.25 | 3.56 | 1.27 | 8.519E-15 | 5.235E-15 | 5.217E-15 |
| 0.5 | 1300 | M38c | 1.4 | 1.25 | 4.3458E-05 | 1.3413E-05 | 1.06E-05 | 4.1 | 3.24 | 1.27 | 9.623E-15 | 6.323E-15 | 6.342E-15 |
| 0.5 | 1300 | M39a | 2 | 0.75 | 3.987E-05 | 1.1288E-05 | 9.1227E-06 | 4.37 | 3.53 | 1.24 | 5.582E-15 | 3.303E-15 | 3.340E-15 |
| 0.5 | 1300 | M40 | 1.4 | 1.25 | 2.8413E-05 | 8.135E-06 | 6.4755E-06 | 4.39 | 3.49 | 1.26 | 6.401E-15 | 3.944E-15 | 4.244E-15 |
| 1 | 1300 | M21 | 1.8 | 1.18 | 5.2771E-05 | 1.5413E-05 | 1.2248E-05 | 4.31 | 3.42 | 1.26 | 1.075E-14 | 6.617E-15 | 6.626E-15 |
| 1 | 1300 | M24b | 1.45 | 1.15 | 3.2251E-05 | 9.3169E-06 | 7.111E-06 | 4.54 | 3.46 | 1.31 | 6.653E-15 | 4.180E-15 | 4.180E-15 |
| 1 | 1300 | M28a | 1.8 | 1.05 | 3.6595E-05 | 1.0531E-05 | 8.1719E-06 | 4.48 | 3.47 | 1.29 | 6.964E-15 | 4.321E-15 | 4.074E-15 |
| 1 | 1300 | M51a | 1.9 | 0.8 | 3.9319E-05 | 1.1496E-05 | 9.0532E-06 | 4.34 | 3.42 | 1.27 | 7.697E-15 | 4.753E-15 | 4.754E-15 |
| 1 | 1300 | M51b | 1.9 | 0.8 | 4.4842E-05 | 1.3739E-05 | 1.0389E-05 | 4.32 | 3.26 | 1.32 | 6.907E-15 | 4.182E-15 | 4.020E-15 |
| 1 | 1300 | M53a | 1.83 | 1 | 4.632E-05 | 1.3835E-05 | 1.077E-05 | 4.3 | 3.35 | 1.28 | 8.620E-15 | 5.309E-15 | 5.265E-15 |
| 1 | 1300 | M53c | 1.83 | 1 | 4.1151E-05 | 1.2536E-05 | 9.4203E-06 | 4.37 | 3.28 | 1.33 | 7.936E-15 | 4.731E-15 | 4.604E-15 |
| 1.5 | 1300 | M42 | 2 | 0.85 | 4.6442E-05 | 1.3386E-05 | 1.0397E-05 | 4.47 | 3.47 | 1.29 | 7.392E-15 | 4.396E-15 | 4.378E-15 |
| 1.5 | 1300 | M44 | 1.4 | 1.2 | 3.5646E-05 | 1.0272E-05 | 8.0676E-06 | 4.42 | 3.47 | 1.27 | 7.445E-15 | 4.597E-15 | 4.628E-15 |
| 1.5 | 1300 | M45 | 2 | 0.9 | 5.0327E-05 | 1.5829E-05 | 1.1259E-05 | 4.47 | 3.18 | 1.41 | 8.161E-15 | 5.121E-15 | 4.743E-15 |
| 2 | 1300 | M36a | 1.65 | 1.1 | 4.8825E-05 | 1.4592E-05 | 1.1032E-05 | 4.43 | 3.35 | 1.32 | 1.004E-14 | 6.221E-15 | 6.112E-15 |
| 2 | 1300 | M36d | 1.65 | 1 | 2.986E-05 | 9.6858E-06 | 7.8076E-06 | 3.82 | 3.08 | 1.24 | 4.836E-15 | 2.977E-15 | 2.972E-15 |
| 2 | 1300 | M37a | 1.85 | 1 | 5.0817E-05 | 1.5707E-05 | 1.2601E-05 | 4.03 | 3.24 | 1.25 | 9.018E-15 | 5.815E-15 | 5.782E-15 |
| 4 | 1300 | M46a | 1.8 | 1.05 | 4.4893E-05 | 1.263E-05 | 9.9056E-06 | 4.53 | 3.55 | 1.28 | 8.551E-15 | 5.031E-15 | 5.011E-15 |
| 4 | 1300 | M46b | 1.8 | 1.05 | 4.8483E-05 | 1.42E-05 | 1.1102E-05 | 4.37 | 3.41 | 1.28 | 9.422E-15 | 5.779E-15 | 5.751E-15 |
| 4 | 1300 | M47 | 1.8 | 1.05 | 4.1982E-05 | 1.2355E-05 | 9.5983E-06 | 4.37 | 3.4 | 1.29 | 8.125E-15 | 4.955E-15 | 4.934E-15 |
| 4 | 1300 | M49 | 1.65 | 1.1 | 3.4407E-05 | 1.012E-05 | 8.0527E-06 | 4.27 | 3.4 | 1.26 | 7.053E-15 | 4.423E-15 | 4.445E-15 |
| 1 | 1350 | M32c | 1.45 | 1.15 | 4.5269E-05 | 1.3182E-05 | 1.0539E-05 | 4.3 | 3.43 | 1.25 | 1.035E-14 | 6.398E-15 | 6.504E-15 |
| 1 | 1350 | M34b | 1.65 | 1.15 | 5.4781E-05 | 1.6561E-05 | 1.3024E-05 | 4.21 | 3.31 | 1.27 | 1.117E-14 | 7.053E-15 | 7.037E-15 |
| 1 | 1400 | M57a | 1.83 | 1.05 | 4.269E-05 | 1.2678E-05 | 1.0195E-05 | 4.19 | 3.37 | 1.24 | 8.273E-15 | 5.069E-15 | 5.120E-15 |
| 1 | 1400 | M57d | 1.83 | 1.3 | 4.5089E-05 | 1.3659E-05 | 1.0588E-05 | 4.26 | 3.3 | 1.29 | 1.051E-14 | 6.530E-15 | 6.455E-15 |
| 1 | 1400 | M57e | 1.83 | 1.7 | 3.274E-05 | 9.3959E-06 | 7.4567E-06 | 4.39 | 3.48 | 1.26 | 9.534E-15 | 5.961E-15 | 5.928E-15 |
| 1 | 1400 | M57f | 1.83 | 0.95 | 5.6319E-05 | 1.6526E-05 | 1.3464E-05 | 4.18 | 3.41 | 1.23 | 9.913E-15 | 6.112E-15 | 6.180E-15 |

* W/O Ratio is the Water/Oxides ratio.

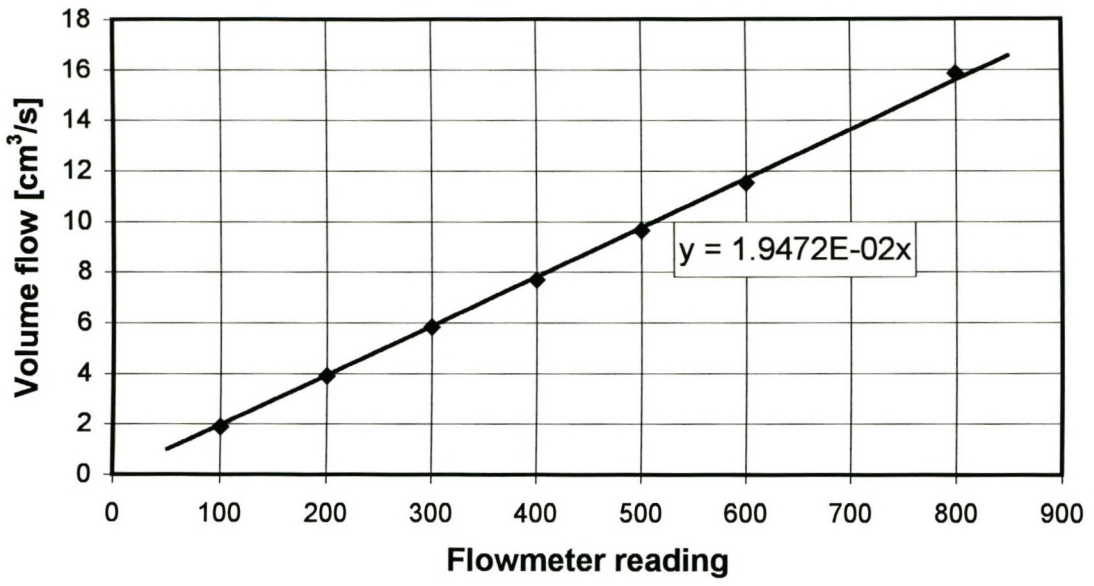
Appendix G: Gas Permeability Results

| | |
|--|------|
| G-I: Calibration | G1 |
| G-II: Results for each Membrane | G-3 |
| G-III: Averaged Results @ 105 kPa | G-13 |
| G-IV: Results for Linkovs Membrane | G17 |
| G-V: Selectivity Results | G-20 |
| G-VI: Gas Permeability Coefficient results | G-23 |

Appendix G-I: Permeability Tests-Calibration

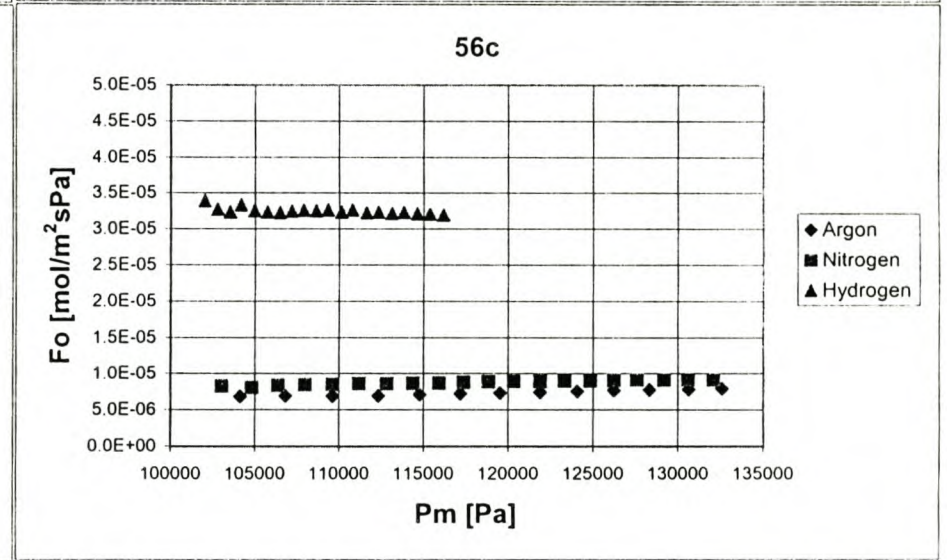
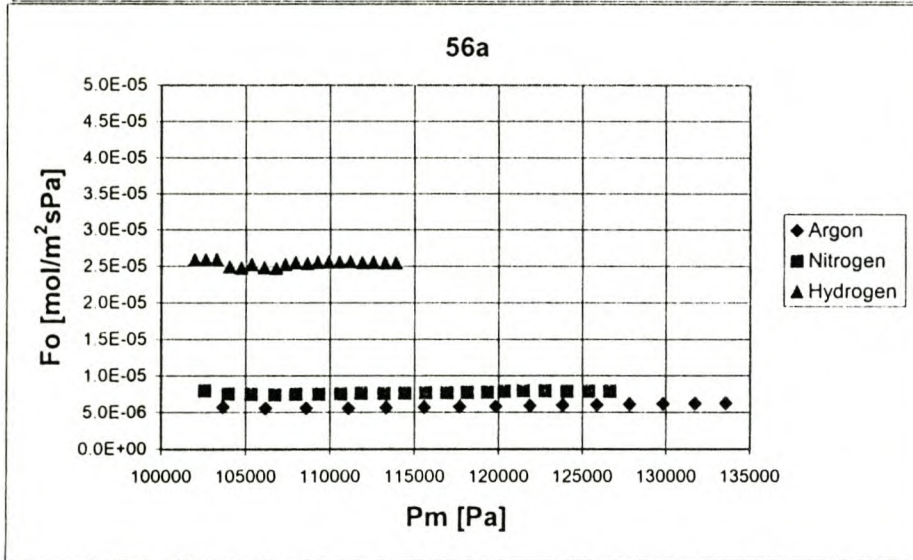
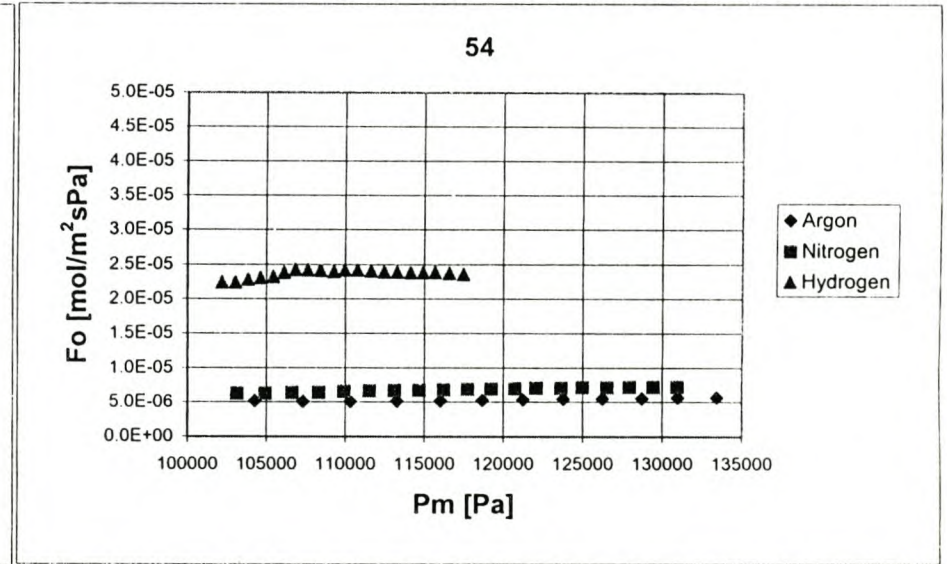
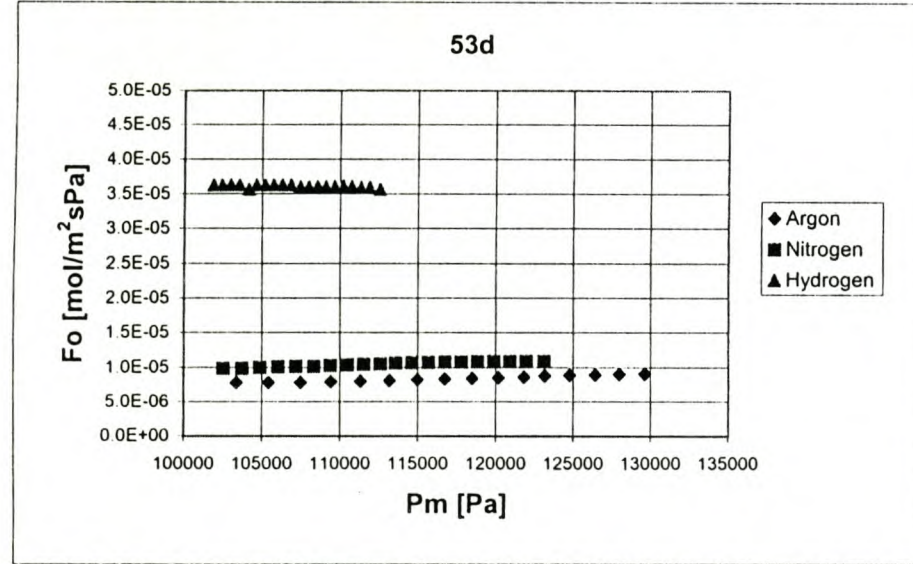


Hydrogen Calibration

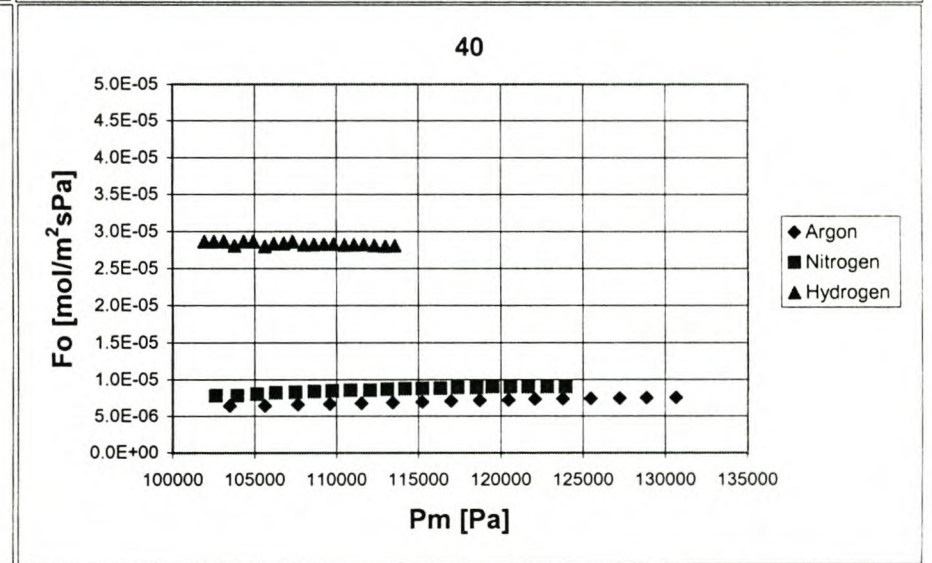
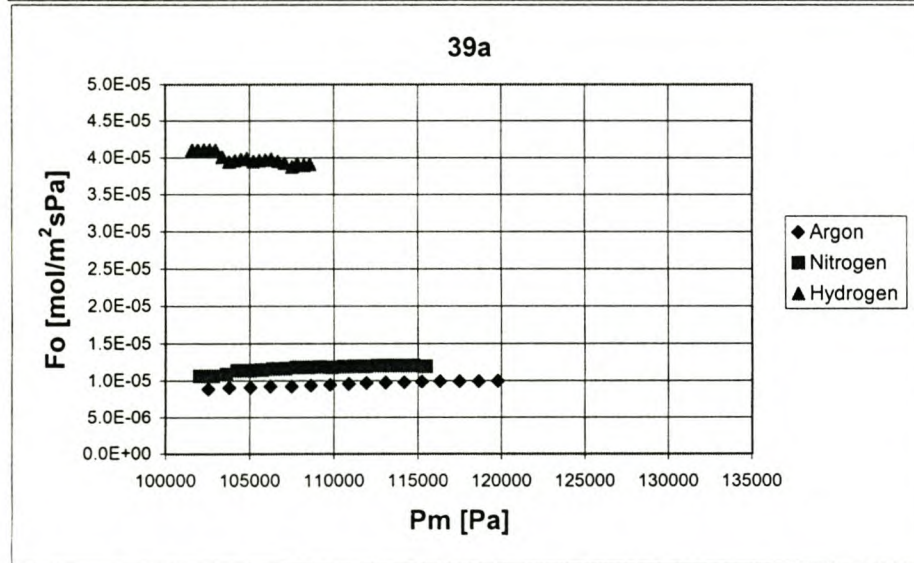
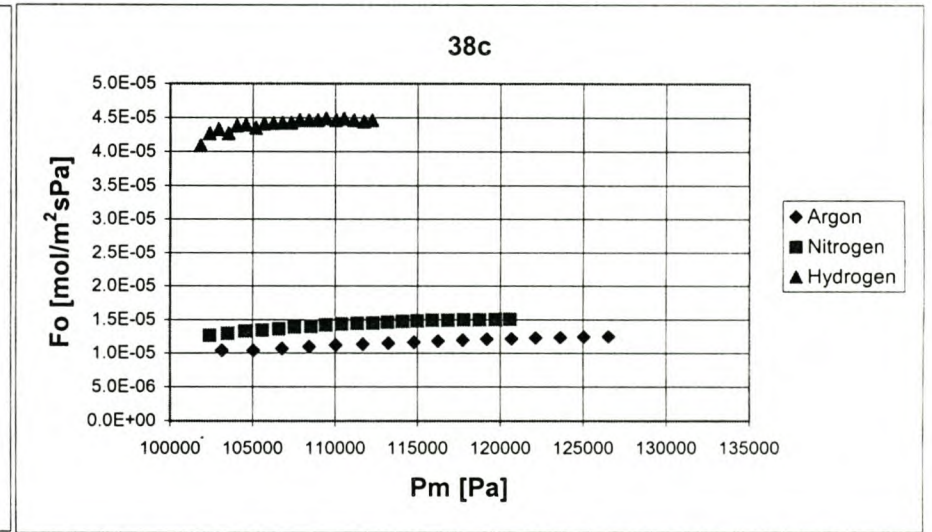
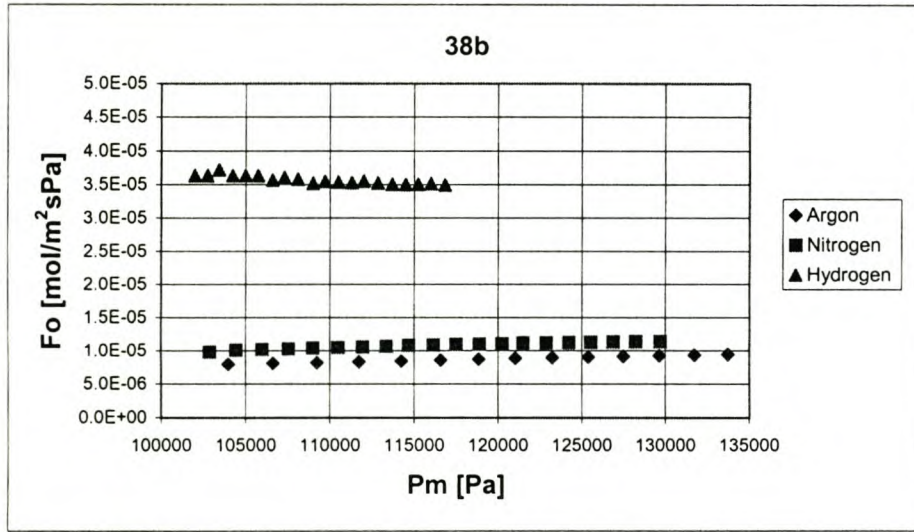


G-II: Results for each Membrane

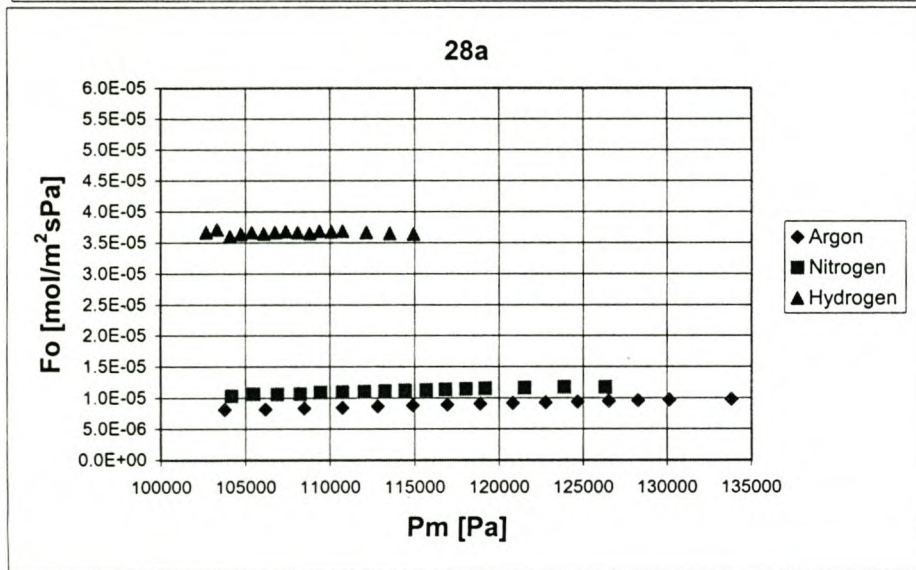
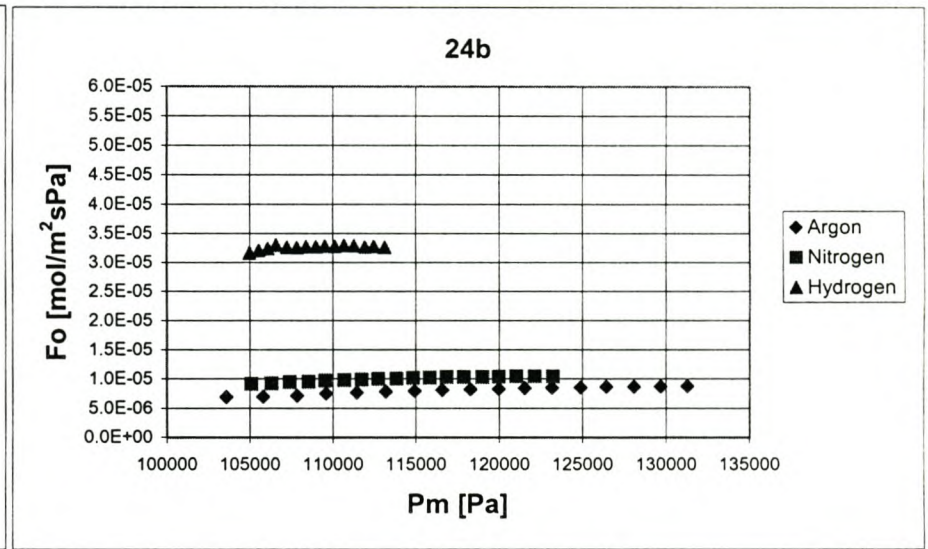
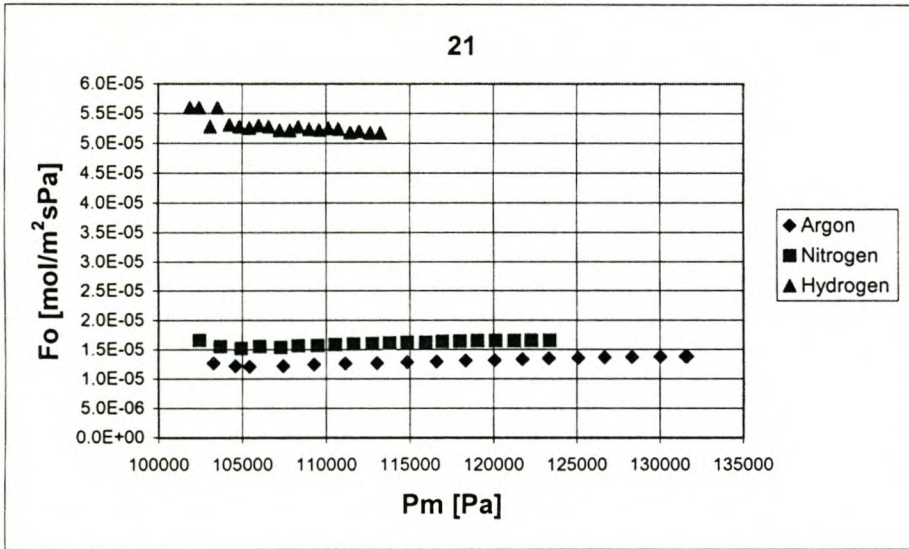
Gas Permeability Results for Manufactured Membranes Sintered for 0 h at 1300 °C



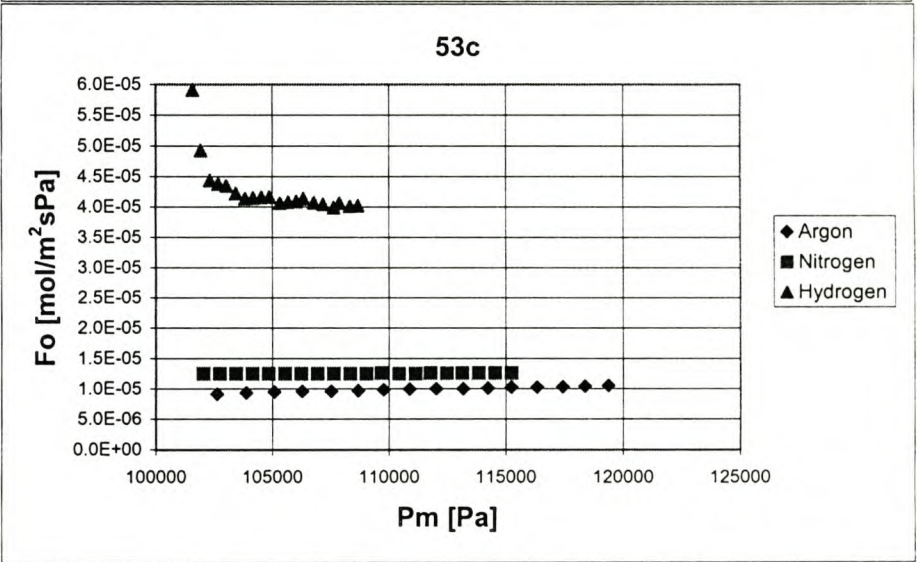
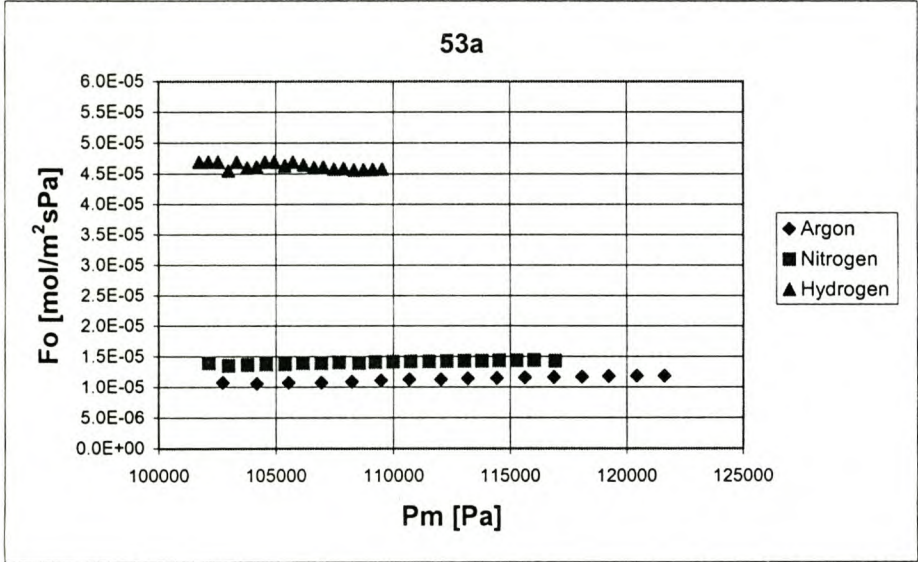
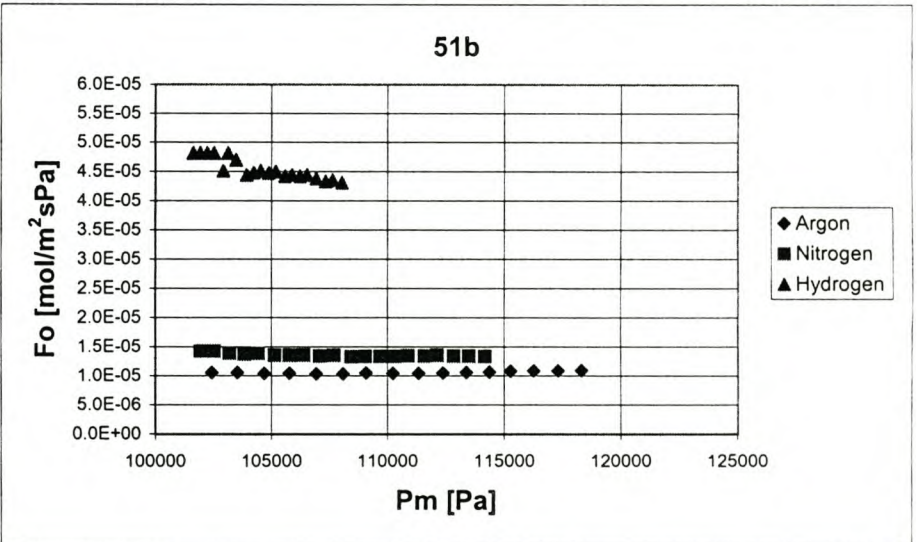
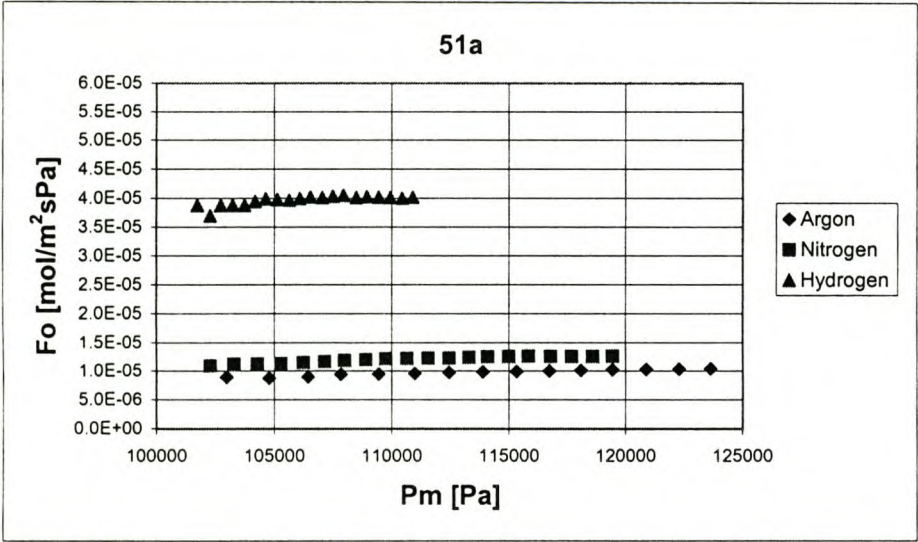
Gas Permeability Results for Manufactured Membranes Sintered for 0.5 h at 1300 °C



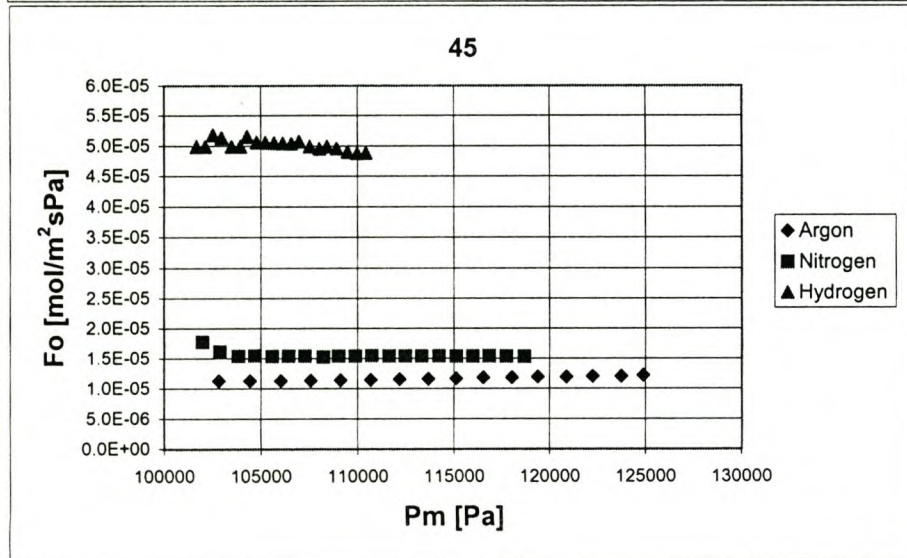
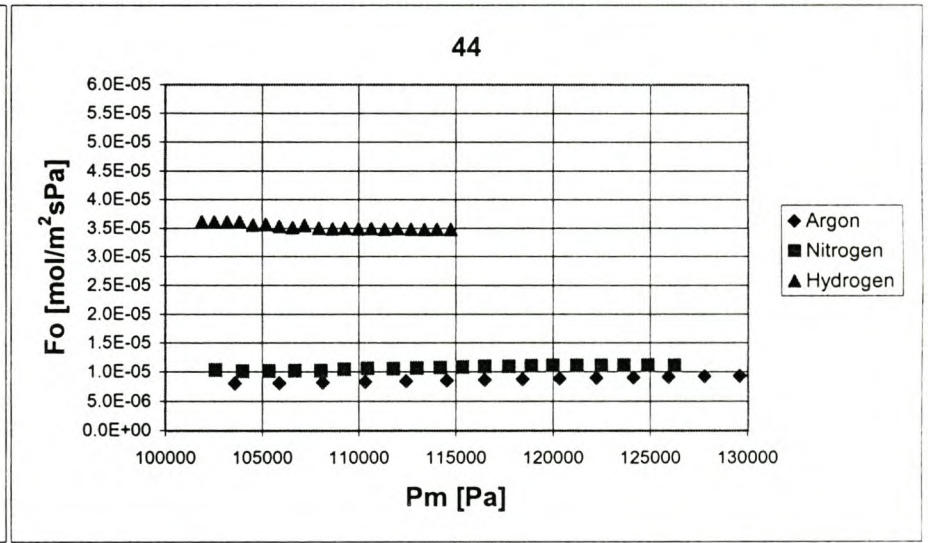
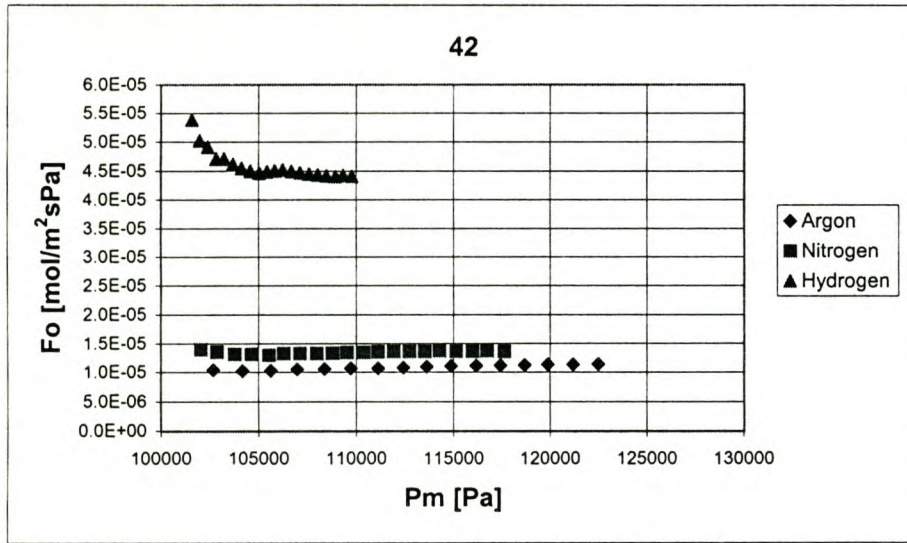
Gas Permeability Results for Manufactured Membranes Sintered for 1 h at 1300 °C



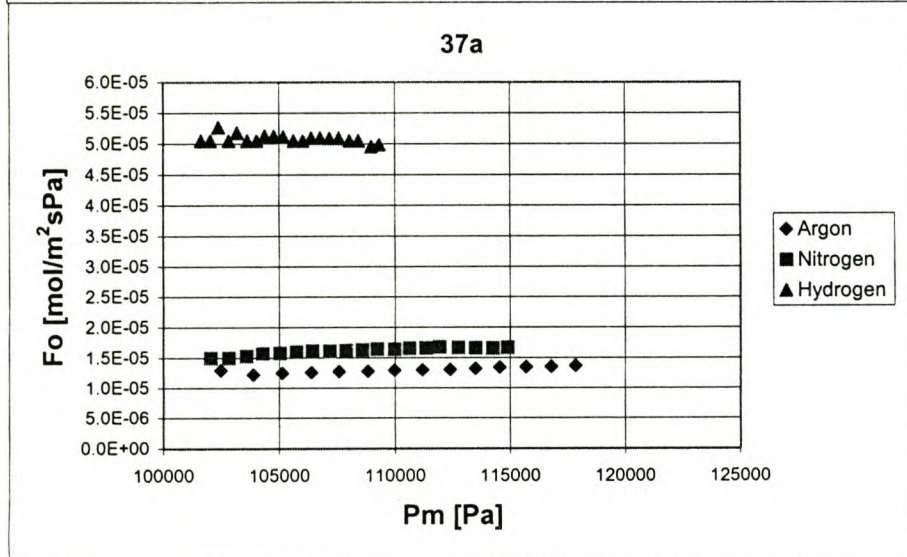
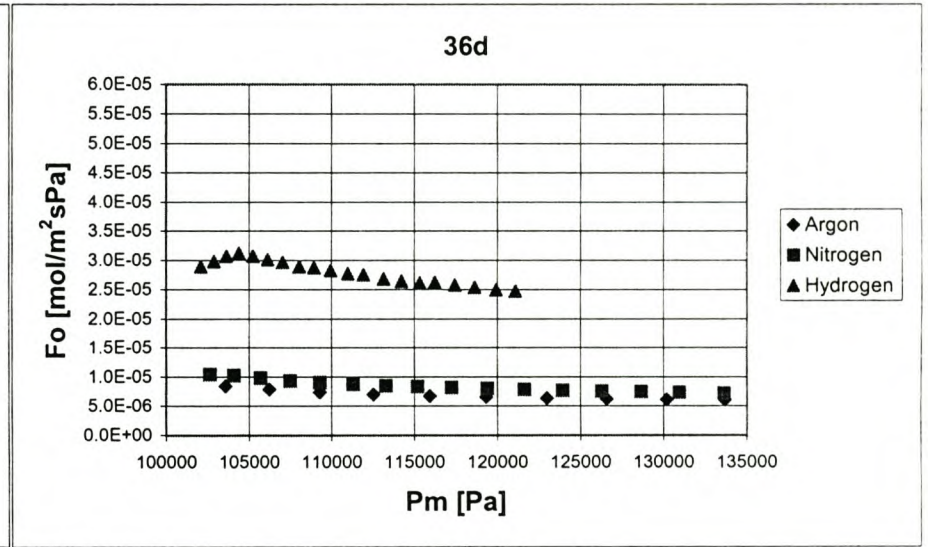
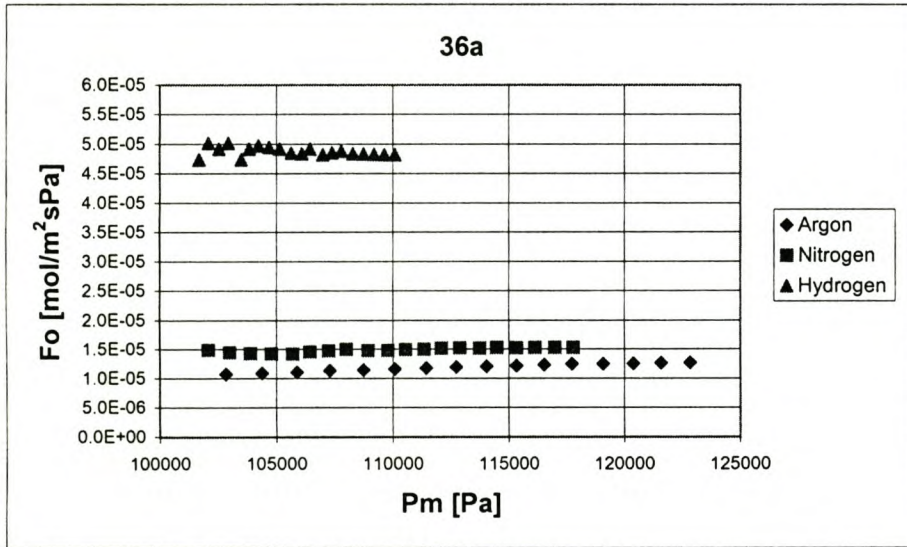
Gas Permeability Results for Manufactured Membranes Sintered for 1 h at 1300 °C



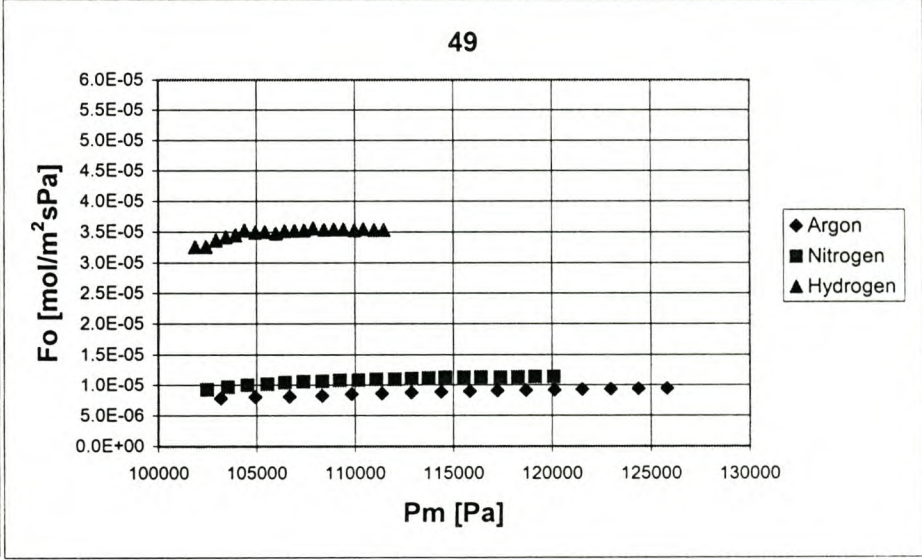
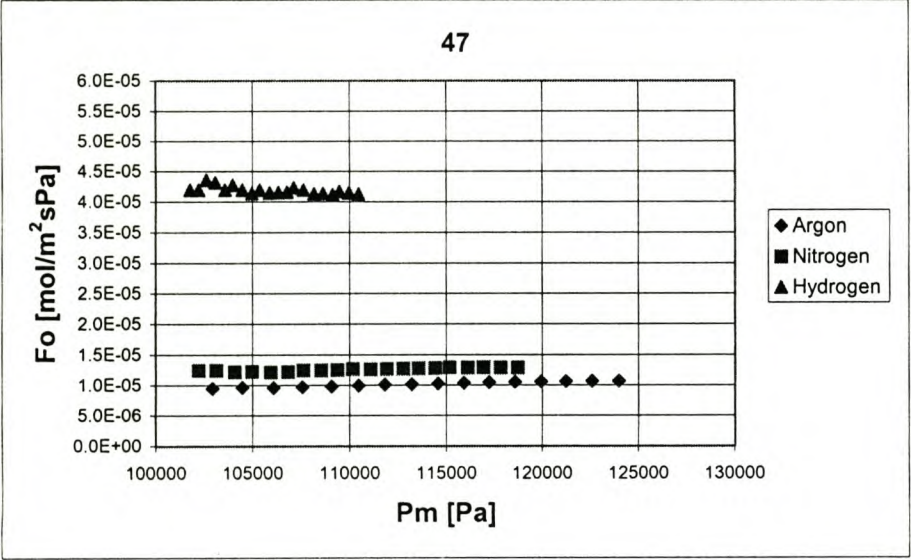
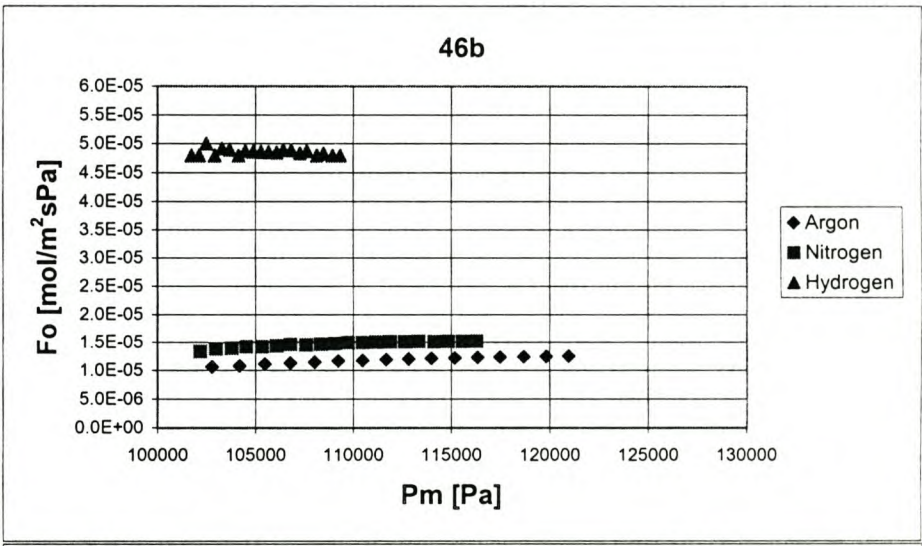
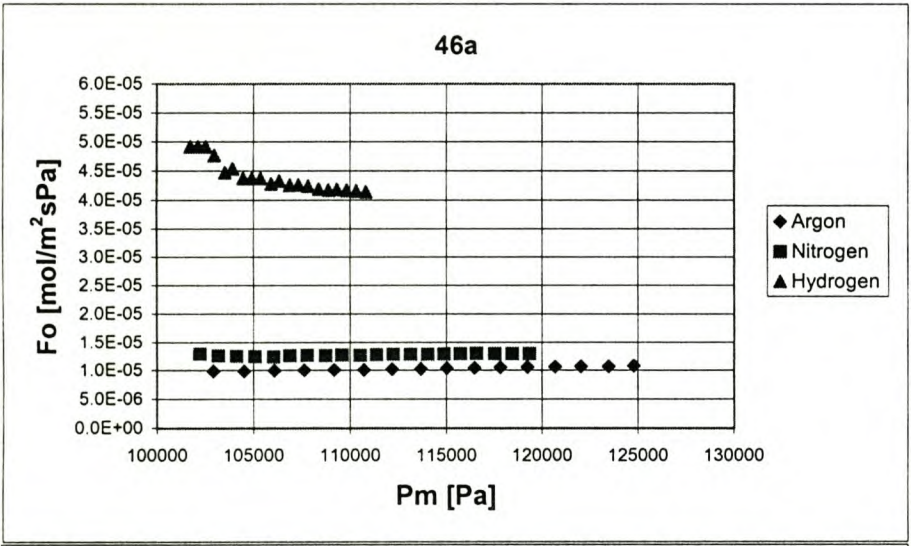
Gas Permeability Results for Manufactured Membranes Sintered for 1.5 h at 1300 °C



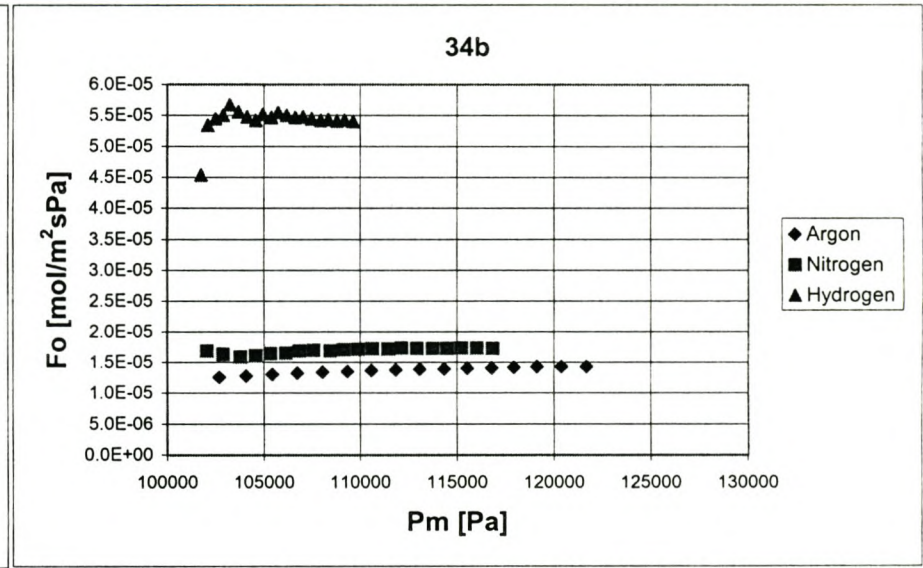
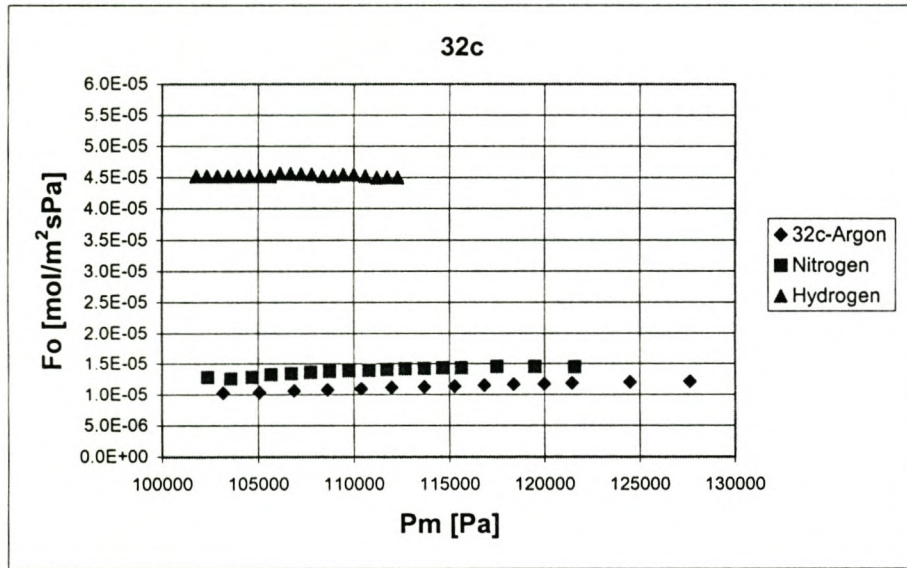
Gas Permeability results for Manufactured Membranes Sintered for 2 h. at 1300°C



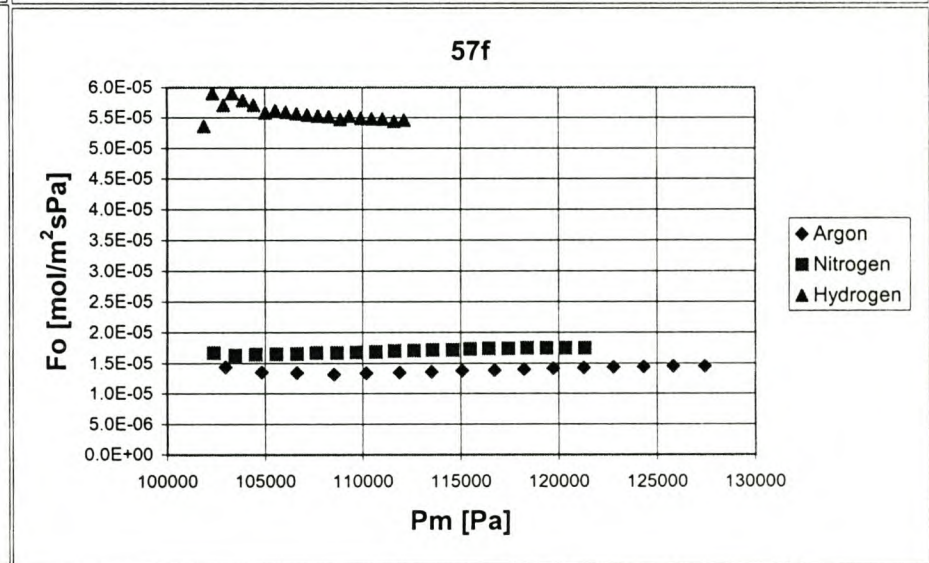
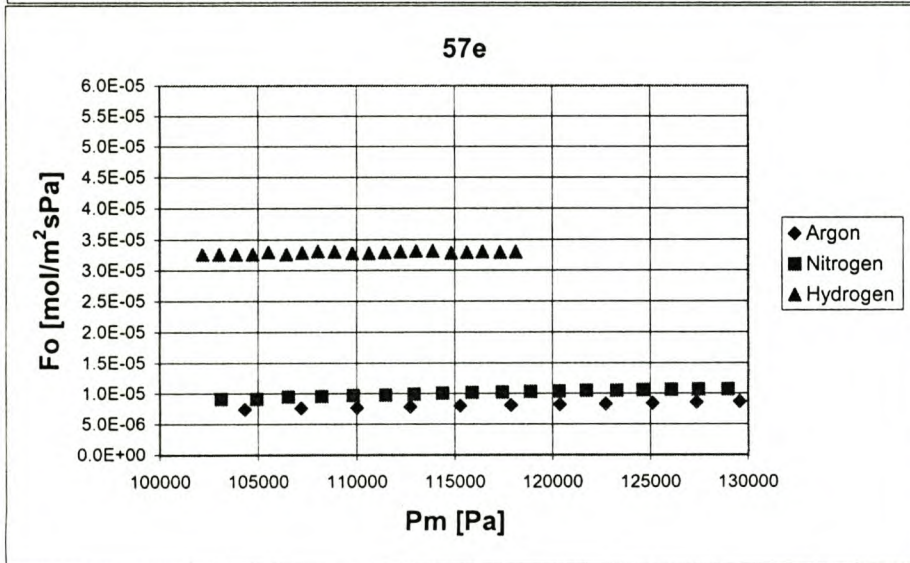
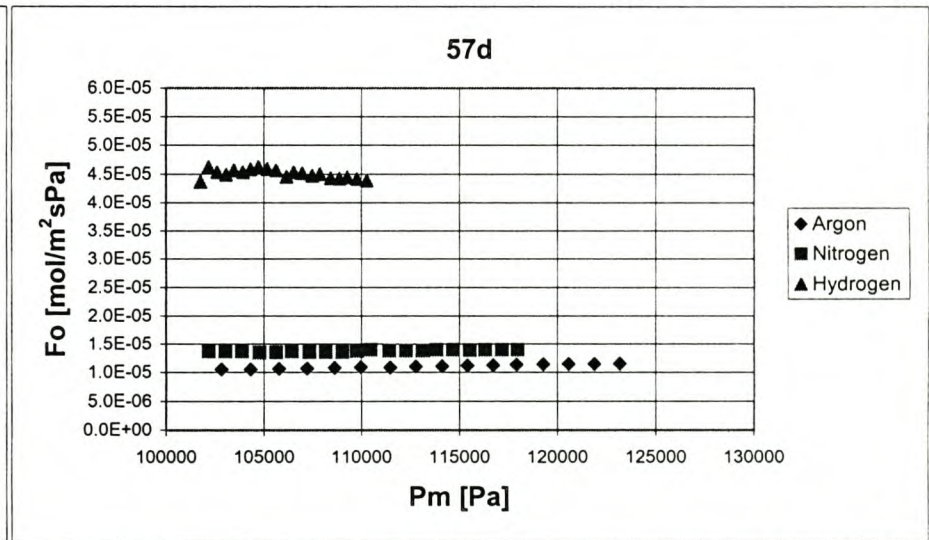
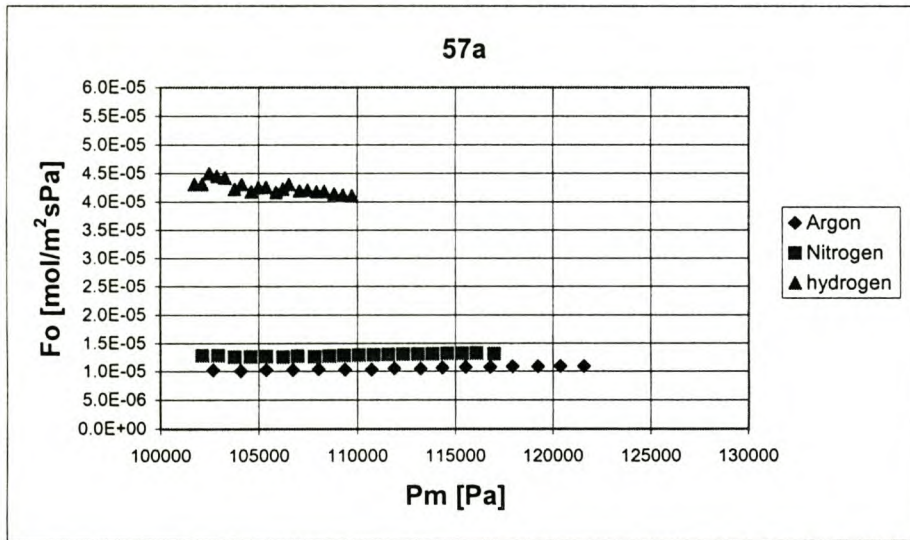
Gas Permeability results for Manufactured Membranes Sintered for 4 h. at 1300°C



Gas Permeability results for Manufactured Membranes Sintered for 1 h. at 1350°C



Gas Permeability results for Manufactured Membranes Sintered for 1 h at 1400°C



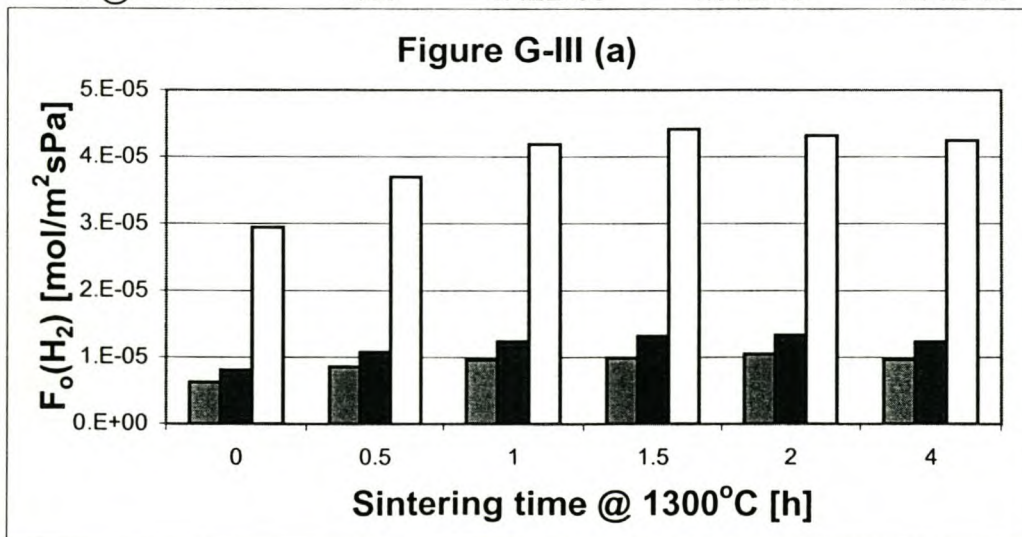
G-III: Average Results @ 105 kPa

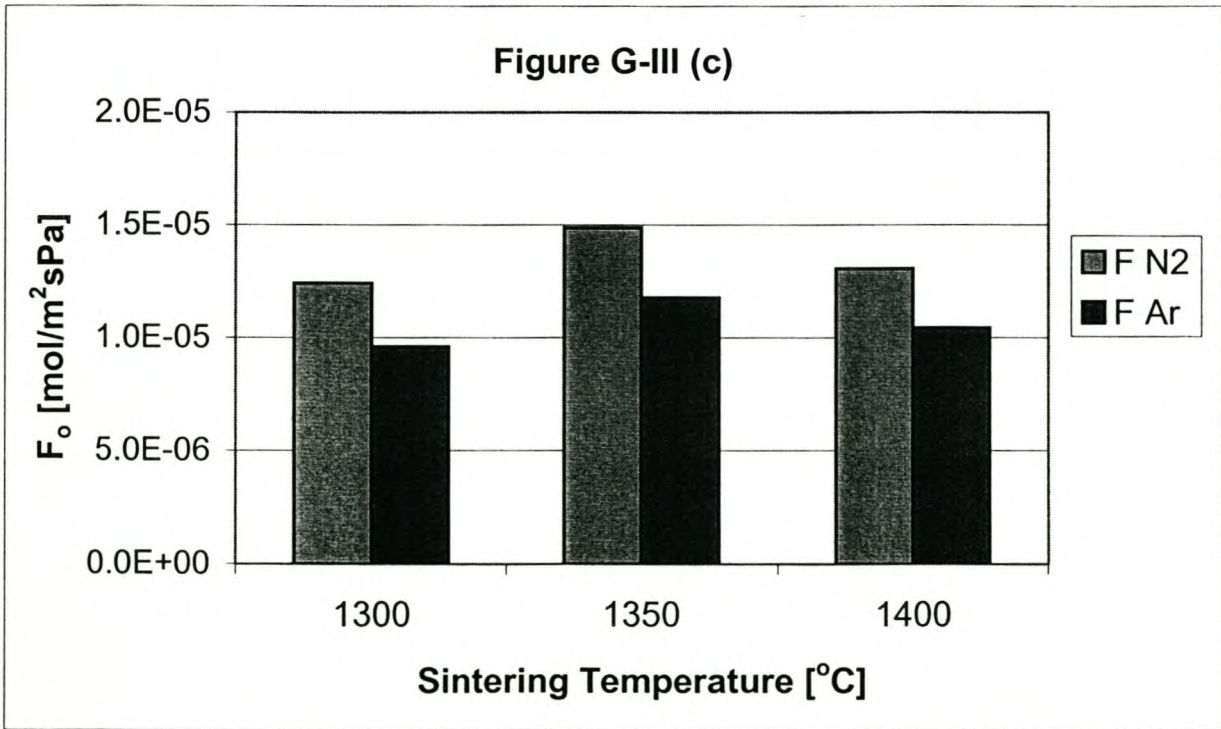
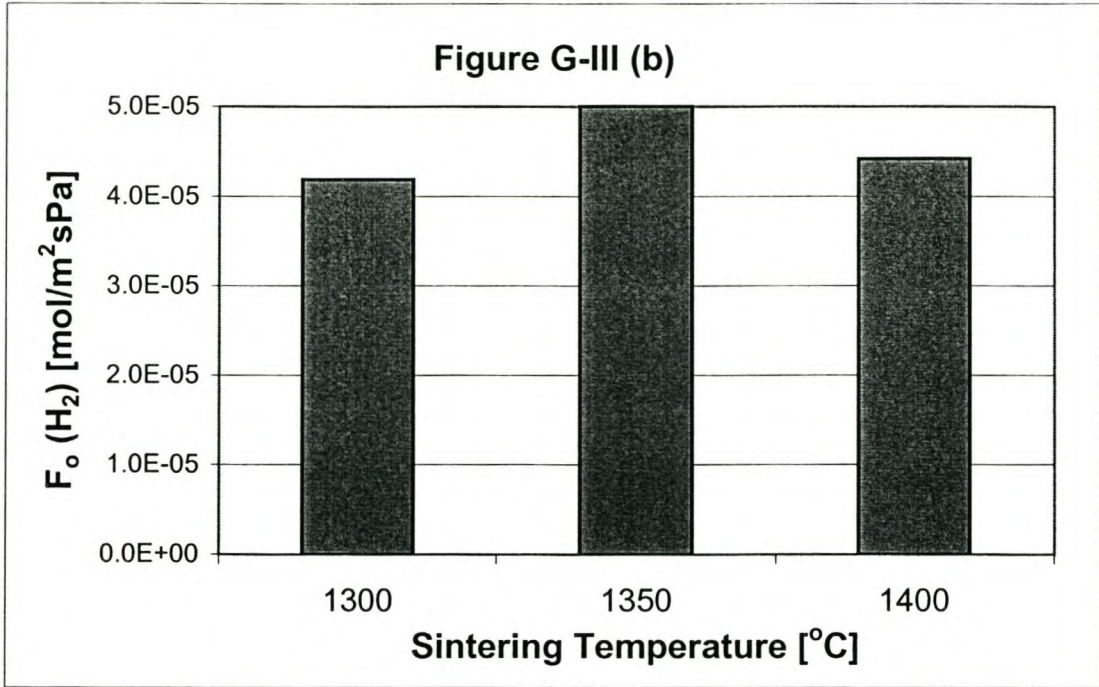
| t [h] | T [oC] | | membrane | | | |
|-------|--------|----------|----------|-----------|-----------|-----------|
| | 0 | 1300 | F H2 | F N2 | F Ar | |
| 0 | | | 53d | 3.621E-05 | 1.007E-05 | 7.744E-06 |
| | | | 54 | 2.334E-05 | 6.376E-06 | 5.022E-06 |
| | | | 56a | 2.538E-05 | 7.544E-06 | 5.519E-06 |
| | | | 56c | 3.275E-05 | 8.319E-06 | 6.749E-06 |
| | | | average: | 2.94E-05 | 8.08E-06 | 6.26E-06 |
| 0.5 | | 1300 | F H2 | F N2 | F Ar | |
| | | | 38b | 3.622E-05 | 1.018E-05 | 8.007E-06 |
| | | | 38c | 4.346E-05 | 1.341E-05 | 1.060E-05 |
| | | | 39a | 3.987E-05 | 1.129E-05 | 9.123E-06 |
| | | | 40 | 2.841E-05 | 8.135E-06 | 6.476E-06 |
| | | average: | 3.70E-05 | 1.08E-05 | 8.55E-06 | |
| 1 | | 1300 | F H2 | F N2 | F Ar | |
| | | | 21 | 5.277E-05 | 1.541E-05 | 1.225E-05 |
| | | | 24a | 1.834E-04 | 8.616E-05 | 5.697E-05 |
| | | | 24b | 3.225E-05 | 9.317E-06 | 7.111E-06 |
| | | | 28a | 3.659E-05 | 1.053E-05 | 8.172E-06 |
| | | | 51a | 3.932E-05 | 1.150E-05 | 9.053E-06 |
| | | | 51b | 4.484E-05 | 1.374E-05 | 1.039E-05 |
| | | | 53a | 4.632E-05 | 1.384E-05 | 1.077E-05 |
| | | | 53c | 4.115E-05 | 1.254E-05 | 9.420E-06 |
| | | | average: | 4.19E-05 | 1.24E-05 | 9.59E-06 |
| 1.5 | | 1300 | F H2 | F N2 | F Ar | |
| | | | 42 | 4.644E-05 | 1.339E-05 | 1.040E-05 |
| | | | 44 | 3.565E-05 | 1.027E-05 | 8.068E-06 |
| | | | 45 | 5.033E-05 | 1.583E-05 | 1.126E-05 |
| | | | average: | 4.41E-05 | 1.32E-05 | 9.91E-06 |
| 2 | | 1300 | F H2 | F N2 | F Ar | |
| | | | 36a | 4.883E-05 | 1.459E-05 | 1.103E-05 |
| | | | 36d | 2.986E-05 | 9.686E-06 | 7.808E-06 |
| | | | 37a | 5.082E-05 | 1.571E-05 | 1.260E-05 |
| | | | average: | 4.32E-05 | 1.33E-05 | 1.05E-05 |

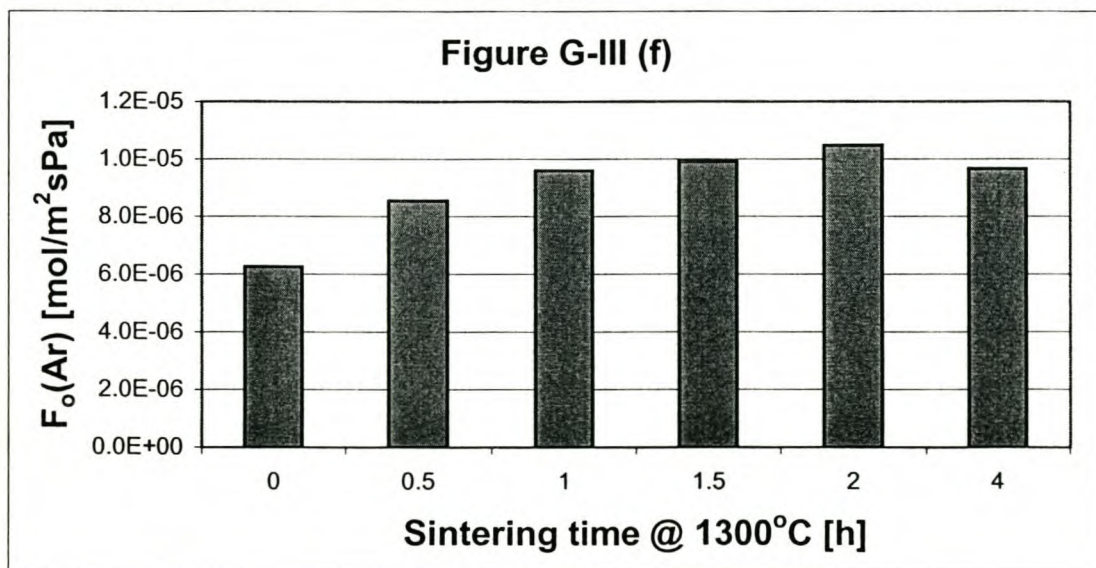
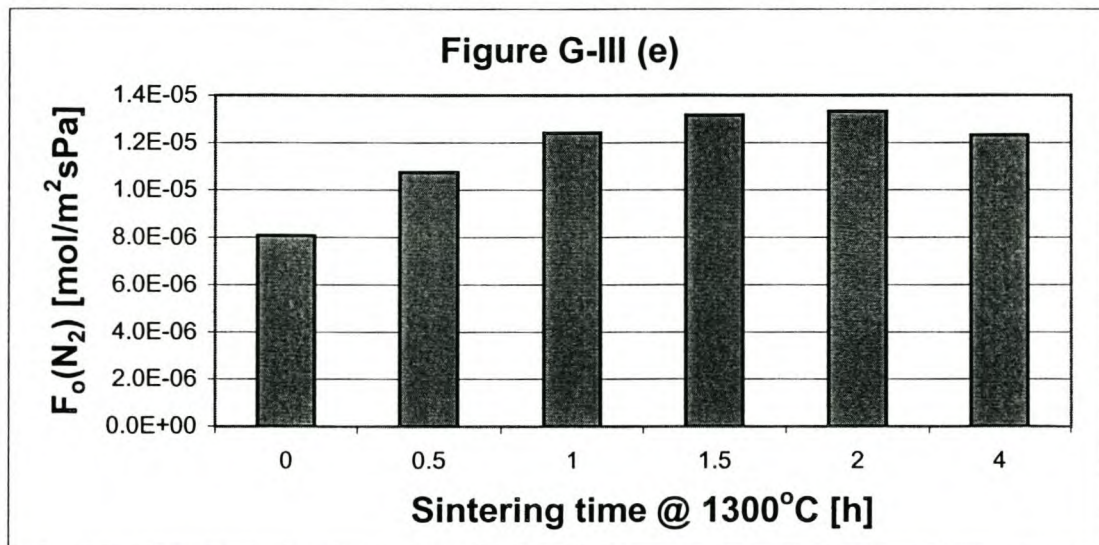
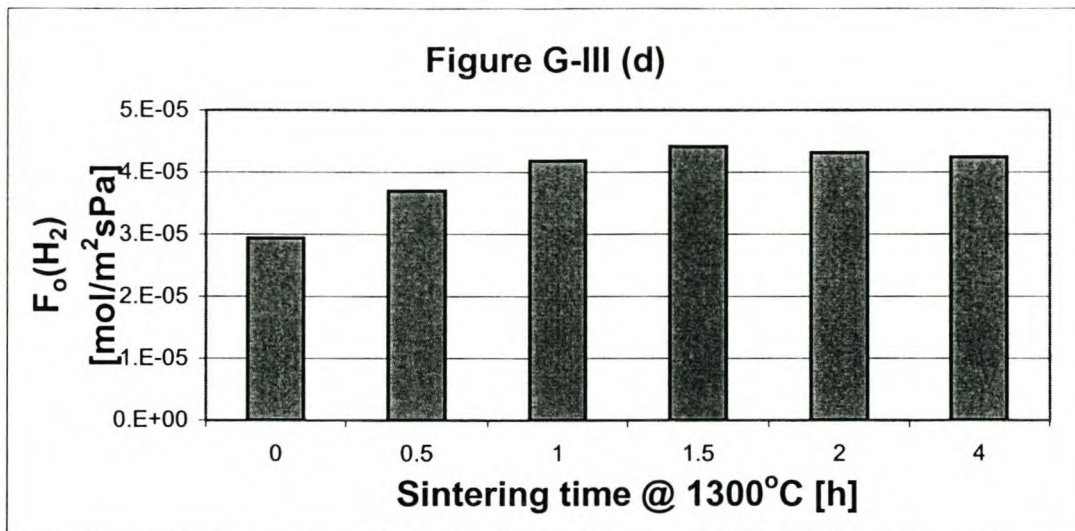
| | | | | |
|---|----------|-----------|-----------|-----------|
| 4 | 1300 | F H2 | F N2 | F Ar |
| | 46a | 4.489E-05 | 1.263E-05 | 9.906E-06 |
| | 46b | 4.848E-05 | 1.420E-05 | 1.110E-05 |
| | 47 | 4.198E-05 | 1.235E-05 | 9.598E-06 |
| | 49 | 3.441E-05 | 1.012E-05 | 8.053E-06 |
| | average: | 4.24E-05 | 1.23E-05 | 9.66E-06 |
| 1 | 1350 | F H2 | F N2 | F Ar |
| | 32c | 4.527E-05 | 1.318E-05 | 1.054E-05 |
| | 34b | 5.478E-05 | 1.656E-05 | 1.302E-05 |
| | average: | 5.00E-05 | 1.49E-05 | 1.18E-05 |
| 1 | 1400 | F H2 | F N2 | F Ar |
| | 57a | 4.269E-05 | 1.268E-05 | 1.019E-05 |
| | 57d | 4.509E-05 | 1.366E-05 | 1.059E-05 |
| | 57e | 3.274E-05 | 9.396E-06 | 7.457E-06 |
| | 57f | 5.632E-05 | 1.653E-05 | 1.346E-05 |
| | average: | 4.42E-05 | 1.31E-05 | 1.04E-05 |

Averages:

| | | | | |
|--------------|------|----------|----------|----------|
| @ 1300 oC | | F H2 | F N2 | F Ar |
| | 0 | 2.94E-05 | 8.08E-06 | 6.26E-06 |
| | 0.5 | 3.70E-05 | 1.08E-05 | 8.55E-06 |
| | 1 | 4.19E-05 | 1.24E-05 | 9.59E-06 |
| | 1.5 | 4.41E-05 | 1.32E-05 | 9.91E-06 |
| | 2 | 4.32E-05 | 1.33E-05 | 1.05E-05 |
| | 4 | 4.24E-05 | 1.23E-05 | 9.66E-06 |
| | | F H2 | F N2 | F Ar |
| 1h @ 1300 oC | 1300 | 4.19E-05 | 1.24E-05 | 9.59E-06 |
| 1h @ 1350 oC | 1350 | 5.00E-05 | 1.49E-05 | 1.18E-05 |
| 1h @ 1400 oC | 1400 | 4.42E-05 | 1.31E-05 | 1.04E-05 |







G-IV: Results for Linkov's Membrane

Membrane: L2
 A [m²] 0.00144 2 pirh
 Gas: Argon
 ni [Pas] 2.10E-05 r1 0.0051 m ID 0.0102
 Mi [kg/mol] 0.03994 r2 0.00585 m OD 0.0117
 R [J/Kmol] 8.3143 H 0.045 m
 T [T] 298
 Po [Pa] 101233

| Flowmeter Qar [cm ³ /s] | dP [mbar] | Qi [m ³ /s] | dP [Pa] | QiPo/AdP [m/s] | P~ [Pa] | rho [kg/m ³] | m [kg/s] | Kg [m ²] | 1/Pm [1/Pa] | Permselectivity | | |
|---------------------------------------|--------------|---------------------------|------------|-------------------|------------|-----------------------------|-------------|-------------------------|----------------|-----------------|--------------------------------|-----------|
| | | | | | | | | | | F [mol/s] | Fo [mol/m ² sPa] | |
| 40 | 0.626 | 86 | 6.26E-07 | 8600 | 0.0051 | 105533 | 1.701 | 1.06E-06 | 7.412E-16 | 9.476E-06 | 2.556E-05 | 2.061E-06 |
| 80 | 1.251 | 164 | 1.25E-06 | 16400 | 0.0054 | 109433 | 1.764 | 2.21E-06 | 7.773E-16 | 9.138E-06 | 5.112E-05 | 2.161E-06 |
| 100 | 1.564 | 202 | 1.56E-06 | 20200 | 0.0054 | 111333 | 1.795 | 2.81E-06 | 7.889E-16 | 8.982E-06 | 6.389E-05 | 2.194E-06 |
| 120 | 1.877 | 239 | 1.88E-06 | 23900 | 0.0055 | 113183 | 1.825 | 3.42E-06 | 8.001E-16 | 8.835E-06 | 7.667E-05 | 2.225E-06 |
| 140 | 2.189 | 276 | 2.19E-06 | 27600 | 0.0056 | 115033 | 1.854 | 4.06E-06 | 8.083E-16 | 8.693E-06 | 8.945E-05 | 2.248E-06 |
| 180 | 2.815 | 347 | 2.81E-06 | 34700 | 0.0057 | 118583 | 1.912 | 5.38E-06 | 8.266E-16 | 8.433E-06 | 1.150E-04 | 2.298E-06 |
| 200 | 3.128 | 382 | 3.13E-06 | 38200 | 0.0057 | 120333 | 1.940 | 6.07E-06 | 8.343E-16 | 8.310E-06 | 1.278E-04 | 2.320E-06 |
| 160 | 2.502 | 309 | 2.50E-06 | 30900 | 0.0057 | 116683 | 1.881 | 4.71E-06 | 8.251E-16 | 8.570E-06 | 1.022E-04 | 2.294E-06 |
| 220 | 3.440 | 417 | 3.44E-06 | 41700 | 0.0058 | 122083 | 1.968 | 6.77E-06 | 8.407E-16 | 8.191E-06 | 1.406E-04 | 2.338E-06 |
| 237 | 3.706 | 447 | 3.71E-06 | 44700 | 0.0058 | 123583 | 1.992 | 7.38E-06 | 8.449E-16 | 8.092E-06 | 1.514E-04 | 2.349E-06 |
| 240 | 3.753 | 454 | 3.75E-06 | 45400 | 0.0058 | 123933 | 1.998 | 7.50E-06 | 8.424E-16 | 8.069E-06 | 1.533E-04 | 2.342E-06 |
| 260 | 4.066 | 489 | 4.07E-06 | 48900 | 0.0058 | 125683 | 2.026 | 8.24E-06 | 8.473E-16 | 7.957E-06 | 1.661E-04 | 2.356E-06 |
| 280 | 4.379 | 527 | 4.38E-06 | 52700 | 0.0058 | 127583 | 2.057 | 9.01E-06 | 8.467E-16 | 7.838E-06 | 1.789E-04 | 2.354E-06 |
| 300 | 4.691 | 554 | 4.69E-06 | 55400 | 0.0059 | 128933 | 2.078 | 9.75E-06 | 8.629E-16 | 7.756E-06 | 1.917E-04 | 2.399E-06 |
| 340 | 5.317 | 616 | 5.32E-06 | 61600 | 0.0061 | 132033 | 2.128 | 1.13E-05 | 8.796E-16 | 7.574E-06 | 2.172E-04 | 2.446E-06 |
| 380 | 5.942 | 677 | 5.94E-06 | 67700 | 0.0062 | 135083 | 2.178 | 1.29E-05 | 8.945E-16 | 7.403E-06 | 2.428E-04 | 2.487E-06 |
| 385 | 6.021 | 689 | 6.02E-06 | 68900 | 0.0061 | 135683 | 2.187 | 1.32E-05 | 8.904E-16 | 7.370E-06 | 2.460E-04 | 2.476E-06 |
| | | | | | | | | | average: | 8.324E-16 | | |

Membrane: L2
 A [m²] 0.00144 2pirh, d=1,05cm, h=2.2cm
 Gas: Nitrogen
 ni [Pas] 1.70E-05 r1 0.0051 m ID 0.0102
 Mi [kg/mol] 0.02802 r2 0.0085 m OD 0.017
 R [J/Kmol] 8.3143 H 0.045 m
 T [T] 298
 Po [Pa] 101233

| Flowmeter Qar [cm ³ /s] | dP [mbar] | Qi [m ³ /s] | dP [Pa] | QiPo/AdP [m/s] | P~ [Pa] | rho [kg/m ³] | m [kg/s] | Kg [m ²] | 1/Pm [1/Pa] | Permselectivity | | |
|---------------------------------------|--------------|---------------------------|------------|-------------------|------------|-----------------------------|-------------|-------------------------|----------------|-----------------|--------------------------------|-----------|
| | | | | | | | | | | F [mol/s] | Fo [mol/m ² sPa] | |
| 40 | 0.463 | 67 | 4.63E-07 | 6700 | 0.00485 | 104583 | 1.182729 | 5.474E-07 | 5.699E-16 | 9.562E-06 | 1.891E-05 | 1.957E-06 |
| 80 | 0.926 | 109 | 9.26E-07 | 10900 | 0.005962 | 106683 | 1.206478 | 1.117E-06 | 7.006E-16 | 9.374E-06 | 3.782E-05 | 2.406E-06 |
| 100 | 1.157 | 129 | 1.16E-06 | 12900 | 0.006297 | 107683 | 1.217787 | 1.409E-06 | 7.399E-16 | 9.287E-06 | 4.728E-05 | 2.542E-06 |
| 140 | 1.620 | 176 | 1.62E-06 | 17600 | 0.006462 | 110033 | 1.244363 | 2.016E-06 | 7.593E-16 | 9.088E-06 | 6.619E-05 | 2.608E-06 |
| 180 | 2.083 | 220 | 2.08E-06 | 22000 | 0.006646 | 112233 | 1.269243 | 2.644E-06 | 7.81E-16 | 8.910E-06 | 8.510E-05 | 2.682E-06 |
| 200 | 2.314 | 242 | 2.31E-06 | 24200 | 0.006713 | 113333 | 1.281683 | 2.966E-06 | 7.889E-16 | 8.824E-06 | 9.455E-05 | 2.710E-06 |
| 240 | 2.777 | 285 | 2.78E-06 | 28500 | 0.006841 | 115483 | 1.305998 | 3.627E-06 | 8.038E-16 | 8.659E-06 | 1.135E-04 | 2.761E-06 |
| 280 | 3.240 | 327 | 3.24E-06 | 32700 | 0.006956 | 117583 | 1.329747 | 4.308E-06 | 8.173E-16 | 8.505E-06 | 1.324E-04 | 2.807E-06 |
| 300 | 3.471 | 349 | 3.47E-06 | 34900 | 0.006983 | 118683 | 1.342186 | 4.659E-06 | 8.205E-16 | 8.426E-06 | 1.418E-04 | 2.818E-06 |
| 340 | 3.934 | 389 | 3.93E-06 | 38900 | 0.0071 | 120683 | 1.364805 | 5.369E-06 | 8.343E-16 | 8.286E-06 | 1.607E-04 | 2.866E-06 |
| 380 | 4.397 | 431 | 4.40E-06 | 43100 | 0.007162 | 122783 | 1.388554 | 6.105E-06 | 8.416E-16 | 8.144E-06 | 1.797E-04 | 2.891E-06 |
| 400 | 4.628 | 452 | 4.63E-06 | 45200 | 0.007189 | 123833 | 1.400428 | 6.482E-06 | 8.447E-16 | 8.075E-06 | 1.891E-04 | 2.901E-06 |
| 440 | 5.091 | 491 | 5.09E-06 | 49100 | 0.007279 | 125783 | 1.422481 | 7.242E-06 | 8.554E-16 | 7.950E-06 | 2.080E-04 | 2.938E-06 |
| 480 | 5.554 | 530 | 5.55E-06 | 53000 | 0.007357 | 127733 | 1.444533 | 8.023E-06 | 8.645E-16 | 7.829E-06 | 2.269E-04 | 2.969E-06 |
| 500 | 5.786 | 549 | 5.79E-06 | 54900 | 0.007398 | 128683 | 1.455277 | 8.420E-06 | 8.693E-16 | 7.771E-06 | 2.364E-04 | 2.986E-06 |
| 540 | 6.248 | 589 | 6.25E-06 | 58900 | 0.007447 | 130683 | 1.477895 | 9.234E-06 | 8.751E-16 | 7.652E-06 | 2.553E-04 | 3.006E-06 |
| 580 | 6.711 | 627 | 6.71E-06 | 62700 | 0.007514 | 132583 | 1.499382 | 1.006E-05 | 8.83E-16 | 7.542E-06 | 2.742E-04 | 3.033E-06 |
| 600 | 6.943 | 644 | 6.94E-06 | 64400 | 0.007568 | 133433 | 1.508995 | 1.048E-05 | 8.893E-16 | 7.494E-06 | 2.837E-04 | 3.055E-06 |
| 640 | 7.405 | 683 | 7.41E-06 | 68300 | 0.007612 | 135383 | 1.531048 | 1.134E-05 | 8.944E-16 | 7.386E-06 | 3.026E-04 | 3.072E-06 |
| 680 | 7.868 | 722 | 7.87E-06 | 72200 | 0.007651 | 137333 | 1.5531 | 1.222E-05 | 8.99E-16 | 7.282E-06 | 3.215E-04 | 3.088E-06 |
| 700 | 8.100 | 740 | 8.10E-06 | 74000 | 0.007684 | 138233 | 1.563278 | 1.266E-05 | 9.029E-16 | 7.234E-06 | 3.309E-04 | 3.101E-06 |
| | | | | | | | | | average: | 8.207E-16 | | |

Membrane: L2

A [m²] 0.00144 2pirh, d=1,02cm, h=4.5cm

Gas: Hydrogen

ni [Pas] 8.40E-06 r1 0.0051 m ID 0.0102

Mi [kg/mol] 0.00202 r2 0.0085 m OD 0.017

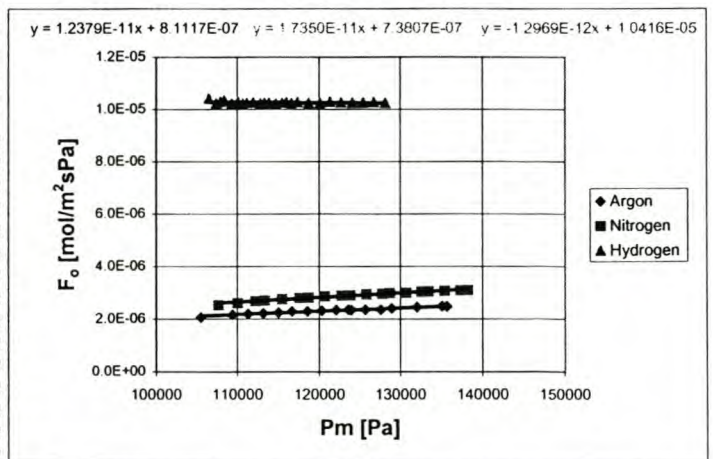
R [J/Kmol] 8.3143 H 0.045 m

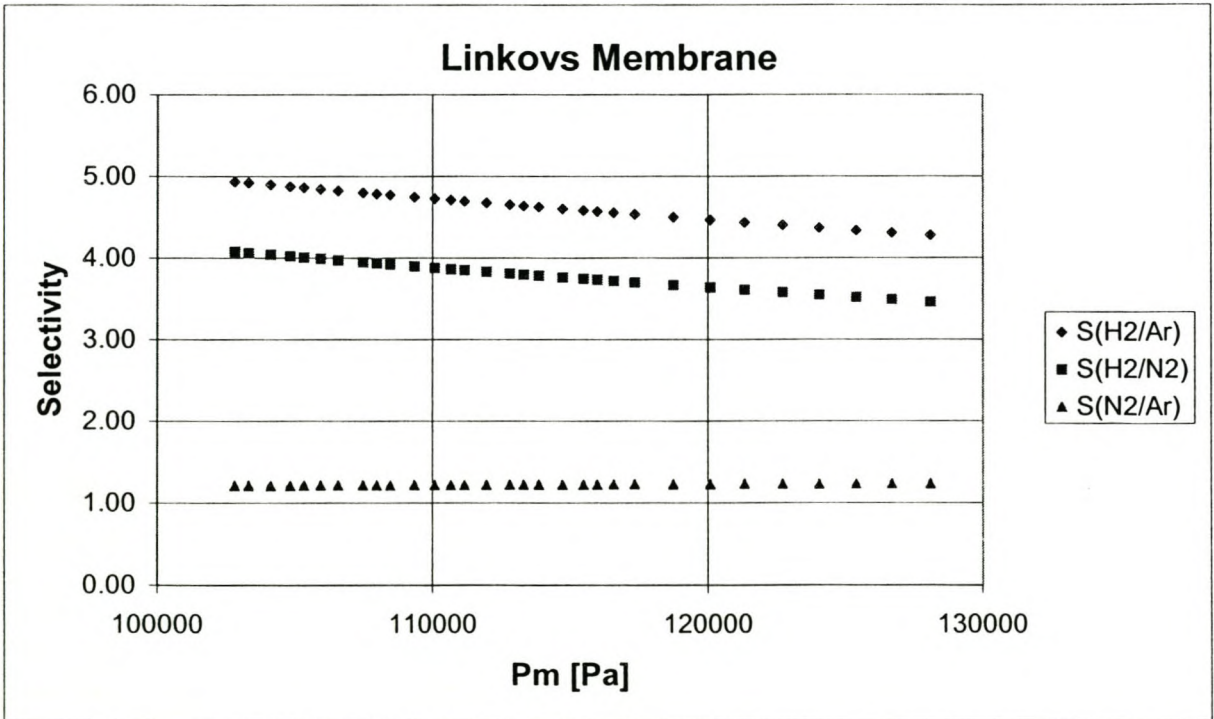
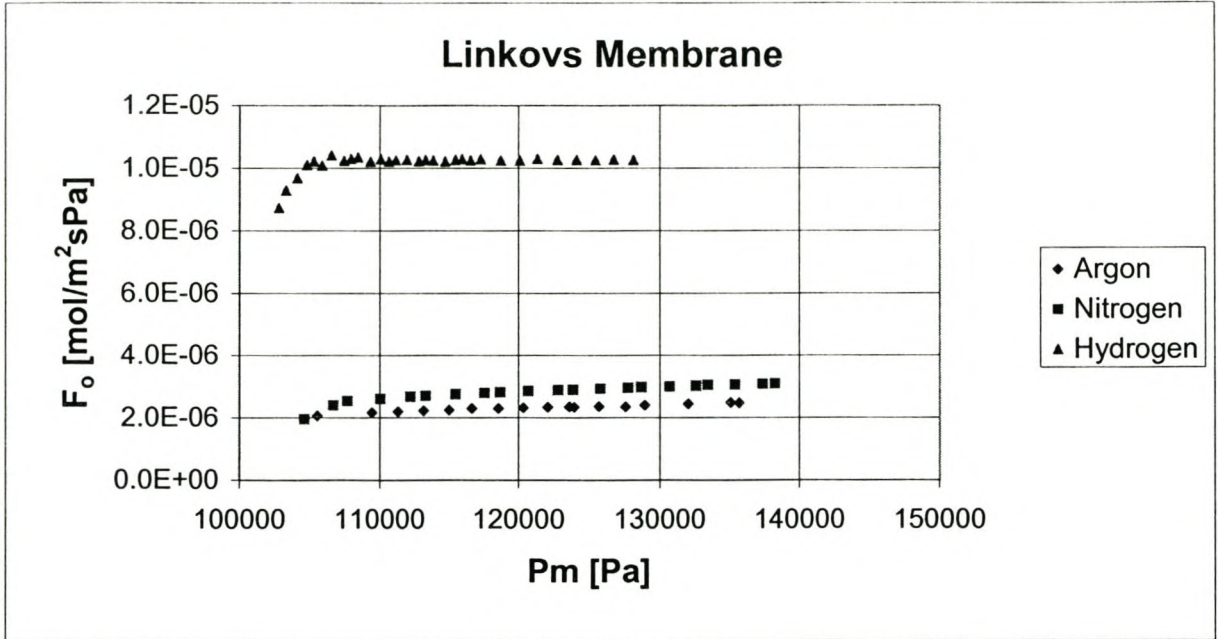
T [T] 298

Po [Pa] 101233

| Flowmeter Qar [cm ³ /s] | dP [mbar] | Qi [m ³ /s] | dP [Pa] | QiPo/AdP [m/s] | P- [Pa] | rho [kg/m ³] | m [kg/s] | Kg [m ²] | 1/Pm [1/Pa] | Permselectivity | | |
|---------------------------------------|--------------|---------------------------|------------|-------------------|------------|-----------------------------|-------------|-------------------------|----------------|-----------------|--------------------------------|-----------|
| | | | | | | | | | | F [mol/s] | Fo [mol/m ² sPa] | |
| 49 | 0.954 | 31 | 9.54E-07 | 3100 | 0.021607 | 102783 | 0.083631 | 7.979E-08 | 1.255E-15 | 9.729E-06 | 3.898E-05 | 8.721E-06 |
| 69 | 1.344 | 41 | 1.34E-06 | 4100 | 0.023006 | 103283 | 0.084038 | 1.129E-07 | 1.336E-15 | 9.682E-06 | 5.490E-05 | 9.285E-06 |
| 100 | 1.947 | 57 | 1.95E-06 | 5700 | 0.023982 | 104083 | 0.084689 | 1.649E-07 | 1.392E-15 | 9.608E-06 | 7.956E-05 | 9.679E-06 |
| 130 | 2.531 | 71 | 2.53E-06 | 7100 | 0.02503 | 104783 | 0.085258 | 2.158E-07 | 1.453E-15 | 9.544E-06 | 1.034E-04 | 1.010E-05 |
| 150 | 2.921 | 81 | 2.92E-06 | 8100 | 0.025315 | 105283 | 0.085665 | 2.502E-07 | 1.47E-15 | 9.498E-06 | 1.193E-04 | 1.022E-05 |
| 170 | 3.310 | 93 | 3.31E-06 | 9300 | 0.024988 | 105883 | 0.086153 | 2.852E-07 | 1.451E-15 | 9.444E-06 | 1.353E-04 | 1.009E-05 |
| 200 | 3.894 | 106 | 3.89E-06 | 10600 | 0.025792 | 106533 | 0.086682 | 3.376E-07 | 1.498E-15 | 9.387E-06 | 1.591E-04 | 1.041E-05 |
| 230 | 4.479 | 124 | 4.48E-06 | 12400 | 0.025356 | 107433 | 0.087415 | 3.915E-07 | 1.472E-15 | 9.308E-06 | 1.830E-04 | 1.023E-05 |
| 250 | 4.868 | 134 | 4.87E-06 | 13400 | 0.025504 | 107933 | 0.087821 | 4.275E-07 | 1.481E-15 | 9.265E-06 | 1.989E-04 | 1.029E-05 |
| 270 | 5.257 | 144 | 5.26E-06 | 14400 | 0.025631 | 108433 | 0.088228 | 4.639E-07 | 1.488E-15 | 9.222E-06 | 2.148E-04 | 1.034E-05 |
| 300 | 5.842 | 162 | 5.84E-06 | 16200 | 0.025315 | 109333 | 0.088961 | 5.197E-07 | 1.47E-15 | 9.146E-06 | 2.387E-04 | 1.022E-05 |
| 330 | 6.426 | 177 | 6.43E-06 | 17700 | 0.025486 | 110083 | 0.089571 | 5.756E-07 | 1.48E-15 | 9.084E-06 | 2.625E-04 | 1.029E-05 |
| 350 | 6.815 | 189 | 6.82E-06 | 18900 | 0.025315 | 110683 | 0.090059 | 6.138E-07 | 1.47E-15 | 9.035E-06 | 2.785E-04 | 1.022E-05 |
| 370 | 7.205 | 199 | 7.20E-06 | 19900 | 0.025417 | 111183 | 0.090466 | 6.518E-07 | 1.476E-15 | 8.994E-06 | 2.944E-04 | 1.026E-05 |
| 400 | 7.789 | 215 | 7.79E-06 | 21500 | 0.025433 | 111983 | 0.091117 | 7.097E-07 | 1.477E-15 | 8.930E-06 | 3.182E-04 | 1.026E-05 |
| 430 | 8.373 | 232 | 8.37E-06 | 23200 | 0.025337 | 112833 | 0.091808 | 7.687E-07 | 1.471E-15 | 8.863E-06 | 3.421E-04 | 1.023E-05 |
| 450 | 8.762 | 242 | 8.76E-06 | 24200 | 0.025419 | 113333 | 0.092215 | 8.080E-07 | 1.476E-15 | 8.824E-06 | 3.580E-04 | 1.026E-05 |
| 470 | 9.152 | 253 | 9.15E-06 | 25300 | 0.025395 | 113883 | 0.092663 | 8.480E-07 | 1.474E-15 | 8.781E-06 | 3.739E-04 | 1.025E-05 |
| 500 | 9.736 | 270 | 9.74E-06 | 27000 | 0.025315 | 114733 | 0.093354 | 9.089E-07 | 1.47E-15 | 8.716E-06 | 3.978E-04 | 1.022E-05 |
| 530 | 10.320 | 285 | 1.03E-05 | 28500 | 0.025421 | 115483 | 0.093965 | 9.697E-07 | 1.476E-15 | 8.659E-06 | 4.217E-04 | 1.026E-05 |
| 550 | 10.710 | 295 | 1.07E-05 | 29500 | 0.025486 | 115983 | 0.094372 | 1.011E-06 | 1.48E-15 | 8.622E-06 | 4.376E-04 | 1.029E-05 |
| 570 | 11.099 | 307 | 1.11E-05 | 30700 | 0.025381 | 116583 | 0.09486 | 1.053E-06 | 1.474E-15 | 8.578E-06 | 4.535E-04 | 1.024E-05 |
| 600 | 11.683 | 322 | 1.17E-05 | 32200 | 0.025472 | 117333 | 0.09547 | 1.115E-06 | 1.479E-15 | 8.523E-06 | 4.774E-04 | 1.028E-05 |
| 650 | 12.657 | 350 | 1.27E-05 | 35000 | 0.025387 | 118733 | 0.096609 | 1.223E-06 | 1.474E-15 | 8.422E-06 | 5.171E-04 | 1.025E-05 |
| 700 | 13.630 | 377 | 1.36E-05 | 37700 | 0.025382 | 120083 | 0.097708 | 1.332E-06 | 1.474E-15 | 8.328E-06 | 5.569E-04 | 1.024E-05 |
| 750 | 14.604 | 402 | 1.46E-05 | 40200 | 0.025504 | 121333 | 0.098725 | 1.442E-06 | 1.481E-15 | 8.242E-06 | 5.967E-04 | 1.029E-05 |
| 800 | 15.578 | 430 | 1.56E-05 | 43000 | 0.025433 | 122733 | 0.099864 | 1.556E-06 | 1.477E-15 | 8.148E-06 | 6.365E-04 | 1.026E-05 |
| 850 | 16.551 | 457 | 1.66E-05 | 45700 | 0.025426 | 124083 | 0.100962 | 1.671E-06 | 1.476E-15 | 8.059E-06 | 6.763E-04 | 1.026E-05 |
| 900 | 17.525 | 484 | 1.75E-05 | 48400 | 0.025419 | 125433 | 0.102061 | 1.789E-06 | 1.476E-15 | 7.972E-06 | 7.160E-04 | 1.026E-05 |
| 950 | 18.498 | 510 | 1.85E-05 | 51000 | 0.025464 | 126733 | 0.103118 | 1.908E-06 | 1.478E-15 | 7.891E-06 | 7.558E-04 | 1.028E-05 |
| 1000 | 19.472 | 538 | 1.95E-05 | 53800 | 0.025409 | 128133 | 0.104258 | 2.030E-06 | 1.475E-15 | 7.804E-06 | 7.956E-04 | 1.026E-05 |
| average: | | | | | | | | | 1.461E-15 | | | |

| Pm [Pa] | FH2 | FN2 | Far | S(H2/Ar) | S(H2/N2) | S(N2/Ar) |
|----------|-----------|-----------|-----------|----------|----------|----------|
| 102782.5 | 1.028E-05 | 2.521E-06 | 2.084E-06 | 4.94 | 4.08 | 1.21 |
| 103282.5 | 1.028E-05 | 2.530E-06 | 2.090E-06 | 4.92 | 4.06 | 1.21 |
| 104082.5 | 1.028E-05 | 2.544E-06 | 2.100E-06 | 4.90 | 4.04 | 1.21 |
| 104782.5 | 1.028E-05 | 2.556E-06 | 2.108E-06 | 4.88 | 4.02 | 1.21 |
| 105282.5 | 1.028E-05 | 2.565E-06 | 2.114E-06 | 4.86 | 4.01 | 1.21 |
| 105882.5 | 1.028E-05 | 2.575E-06 | 2.122E-06 | 4.84 | 3.99 | 1.21 |
| 106532.5 | 1.028E-05 | 2.586E-06 | 2.130E-06 | 4.83 | 3.97 | 1.21 |
| 107432.5 | 1.028E-05 | 2.602E-06 | 2.141E-06 | 4.80 | 3.95 | 1.22 |
| 107932.5 | 1.028E-05 | 2.611E-06 | 2.147E-06 | 4.79 | 3.94 | 1.22 |
| 108432.5 | 1.028E-05 | 2.619E-06 | 2.153E-06 | 4.77 | 3.92 | 1.22 |
| 109332.5 | 1.027E-05 | 2.635E-06 | 2.165E-06 | 4.75 | 3.90 | 1.22 |
| 110082.5 | 1.027E-05 | 2.648E-06 | 2.174E-06 | 4.73 | 3.88 | 1.22 |
| 110682.5 | 1.027E-05 | 2.658E-06 | 2.181E-06 | 4.71 | 3.86 | 1.22 |
| 111182.5 | 1.027E-05 | 2.667E-06 | 2.187E-06 | 4.70 | 3.85 | 1.22 |
| 111982.5 | 1.027E-05 | 2.681E-06 | 2.197E-06 | 4.67 | 3.83 | 1.22 |
| 112832.5 | 1.027E-05 | 2.696E-06 | 2.208E-06 | 4.65 | 3.81 | 1.22 |
| 113332.5 | 1.027E-05 | 2.704E-06 | 2.214E-06 | 4.64 | 3.80 | 1.22 |
| 113882.5 | 1.027E-05 | 2.714E-06 | 2.221E-06 | 4.62 | 3.78 | 1.22 |
| 114732.5 | 1.027E-05 | 2.729E-06 | 2.231E-06 | 4.60 | 3.76 | 1.22 |
| 115482.5 | 1.027E-05 | 2.742E-06 | 2.241E-06 | 4.58 | 3.74 | 1.22 |
| 115982.5 | 1.027E-05 | 2.750E-06 | 2.247E-06 | 4.57 | 3.73 | 1.22 |
| 116582.5 | 1.026E-05 | 2.761E-06 | 2.254E-06 | 4.55 | 3.72 | 1.22 |
| 117332.5 | 1.026E-05 | 2.774E-06 | 2.264E-06 | 4.53 | 3.70 | 1.23 |
| 118732.5 | 1.026E-05 | 2.798E-06 | 2.281E-06 | 4.50 | 3.67 | 1.23 |
| 120082.5 | 1.026E-05 | 2.822E-06 | 2.298E-06 | 4.47 | 3.64 | 1.23 |
| 121332.5 | 1.026E-05 | 2.843E-06 | 2.313E-06 | 4.43 | 3.61 | 1.23 |
| 122732.5 | 1.026E-05 | 2.867E-06 | 2.330E-06 | 4.40 | 3.58 | 1.23 |
| 124082.5 | 1.026E-05 | 2.891E-06 | 2.347E-06 | 4.37 | 3.55 | 1.23 |
| 125432.5 | 1.025E-05 | 2.914E-06 | 2.364E-06 | 4.34 | 3.52 | 1.23 |
| 126732.5 | 1.025E-05 | 2.937E-06 | 2.380E-06 | 4.31 | 3.49 | 1.23 |
| 128132.5 | 1.025E-05 | 2.961E-06 | 2.397E-06 | 4.28 | 3.46 | 1.24 |
| 105000 | 1.028E-05 | 2.560E-06 | 2.111E-06 | 4.87 | 4.02 | 1.21 |

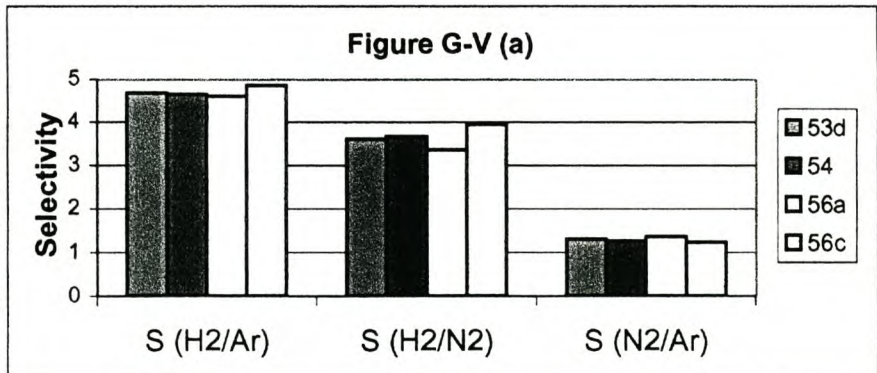




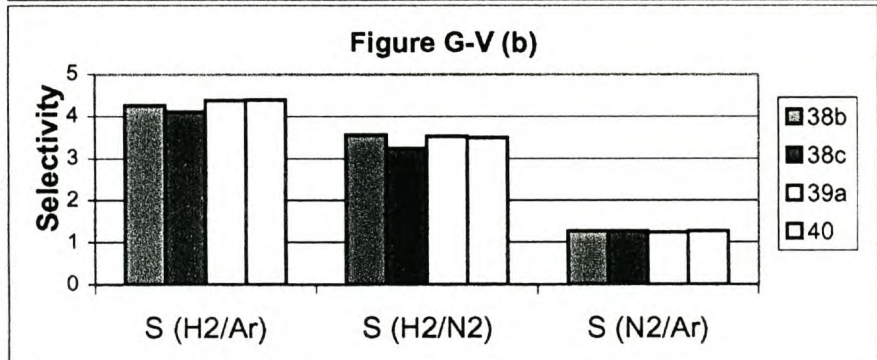
G-V: Selectivity Results

Selectivity @ 105 kPa

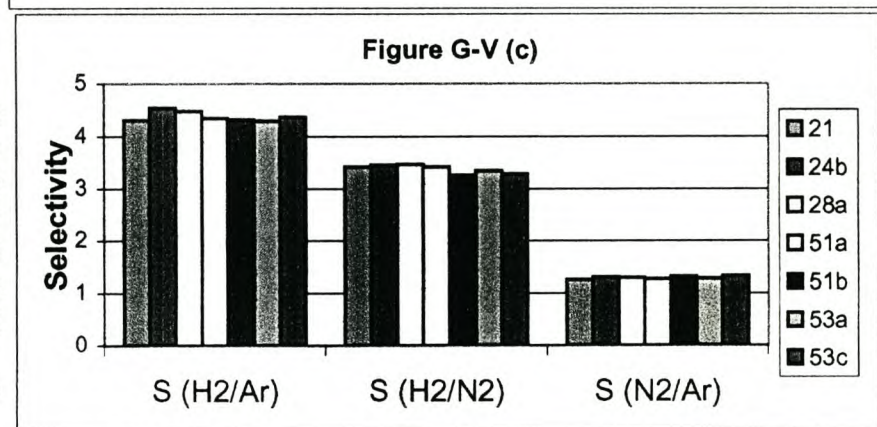
| time [h] | Temp [oC] | Membrane | S (H2/Ar) | S (H2/N2) | S (N2/Ar) |
|----------|-----------|----------|-----------|-----------|-----------|
| 0 | 1300 | 53d | 4.68 | 3.6 | 1.3 |
| | | 54 | 4.65 | 3.66 | 1.27 |
| | | 56a | 4.6 | 3.36 | 1.37 |
| | | 56c | 4.85 | 3.94 | 1.23 |
| | | Average: | 4.70 | 3.64 | 1.29 |



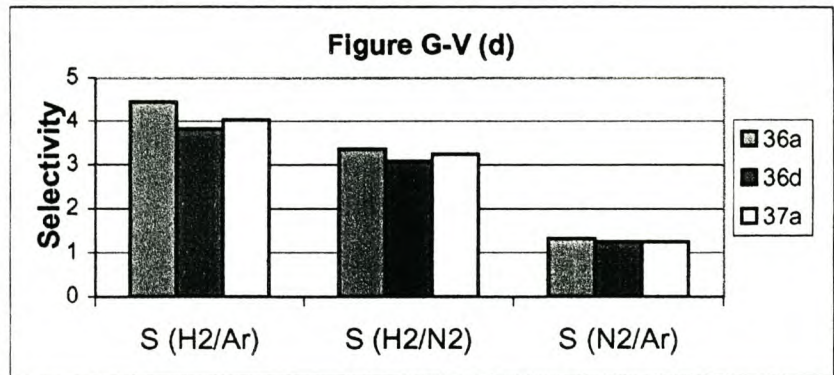
| time [h] | Temp [oC] | Membrane | S (H2/Ar) | S (H2/N2) | S (N2/Ar) |
|----------|-----------|----------|-----------|-----------|-----------|
| 0.5 | 1300 | 38b | 4.25 | 3.56 | 1.27 |
| | | 38c | 4.1 | 3.24 | 1.27 |
| | | 39a | 4.37 | 3.53 | 1.24 |
| | | 40 | 4.39 | 3.49 | 1.26 |
| | | Average: | 4.28 | 3.46 | 1.26 |



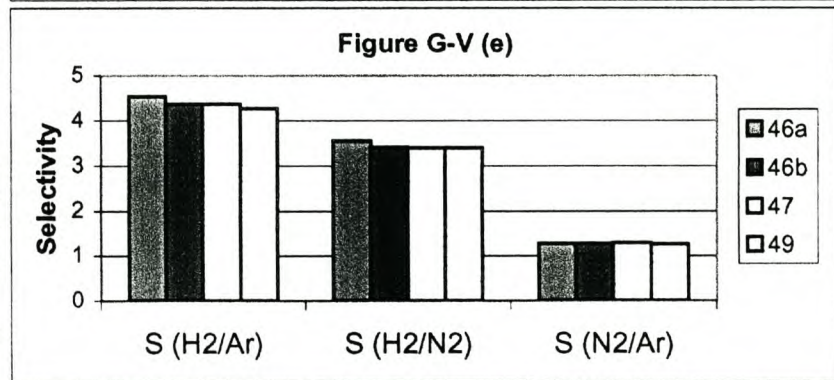
| time [h] | Temp [oC] | Membrane | S (H2/Ar) | S (H2/N2) | S (N2/Ar) |
|----------|-----------|----------|-----------|-----------|-----------|
| 1 | 1300 | 21 | 4.31 | 3.42 | 1.26 |
| | | 24b | 4.54 | 3.46 | 1.31 |
| | | 28a | 4.48 | 3.47 | 1.29 |
| | | 51a | 4.34 | 3.42 | 1.27 |
| | | 51b | 4.32 | 3.26 | 1.32 |
| | | 53a | 4.3 | 3.35 | 1.28 |
| | | 53c | 4.37 | 3.28 | 1.33 |
| | | Average: | 4.38 | 3.38 | 1.29 |



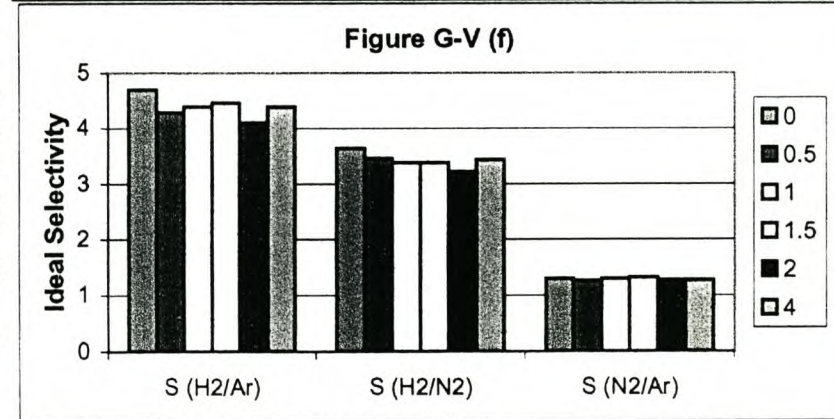
| 1.5 | 1300 | S (H2/Ar) | S (H2/N2) | S (N2/Ar) | |
|-----|----------|-----------|-----------|-----------|------|
| | | 42 | 4.47 | 3.47 | 1.29 |
| | | 44 | 4.42 | 3.47 | 1.27 |
| | | 45 | 4.47 | 3.18 | 1.41 |
| | Average: | 4.45 | 3.37 | 1.32 | |



| 2 | 1300 | S (H2/Ar) | S (H2/N2) | S (N2/Ar) | |
|---|----------|-----------|-----------|-----------|------|
| | | 36a | 4.43 | 3.35 | 1.32 |
| | | 36d | 3.82 | 3.08 | 1.24 |
| | | 37a | 4.03 | 3.24 | 1.25 |
| | Average: | 4.09 | 3.22 | 1.27 | |



| 4 | 1300 | S (H2/Ar) | S (H2/N2) | S (N2/Ar) | |
|---|----------|-----------|-----------|-----------|------|
| | | 46a | 4.53 | 3.55 | 1.28 |
| | | 46b | 4.37 | 3.41 | 1.28 |
| | | 47 | 4.37 | 3.4 | 1.29 |
| | | 49 | 4.27 | 3.4 | 1.26 |
| | Average: | 4.39 | 3.44 | 1.28 | |

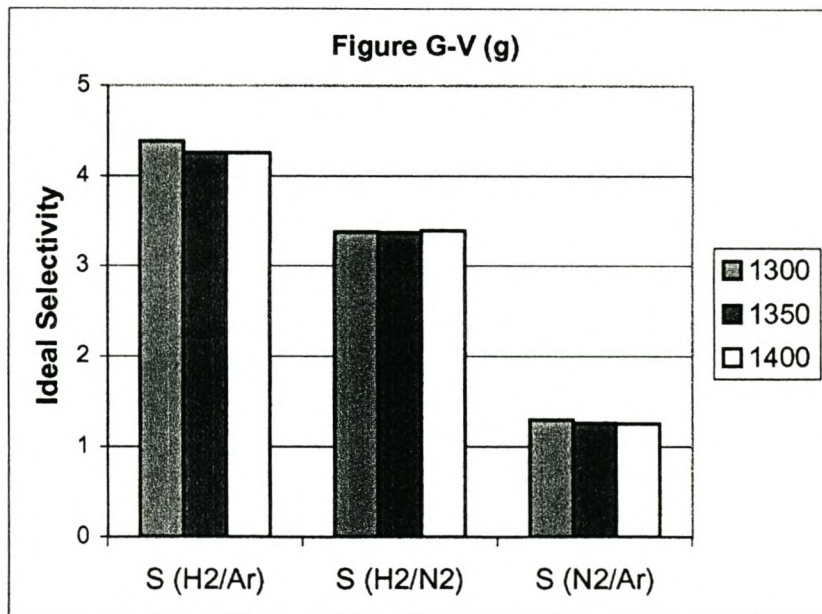


| time [h] | Average of: | S (H2/Ar) | S (H2/N2) | S (N2/Ar) |
|-----------|-------------|-----------|-----------|-----------|
| @ 1300oC: | | | | |
| 0 | | 4.70 | 3.64 | 1.29 |
| 0.5 | | 4.28 | 3.46 | 1.26 |
| 1 | | 4.38 | 3.38 | 1.29 |
| 1.5 | | 4.45 | 3.37 | 1.32 |
| 2 | | 4.09 | 3.22 | 1.27 |
| 4 | | 4.39 | 3.44 | 1.28 |
| 1 h @: | average: | 4.38 | 3.42 | 1.29 |

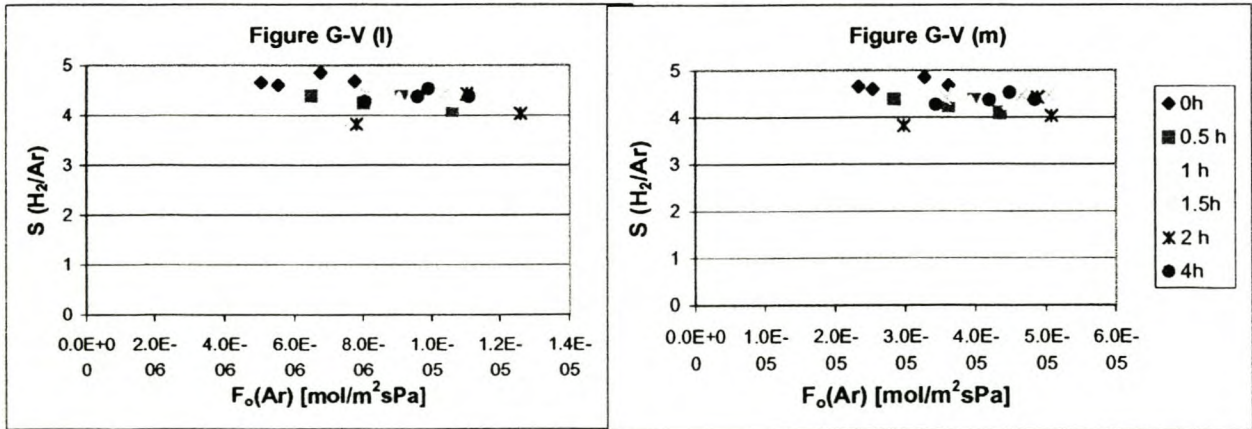
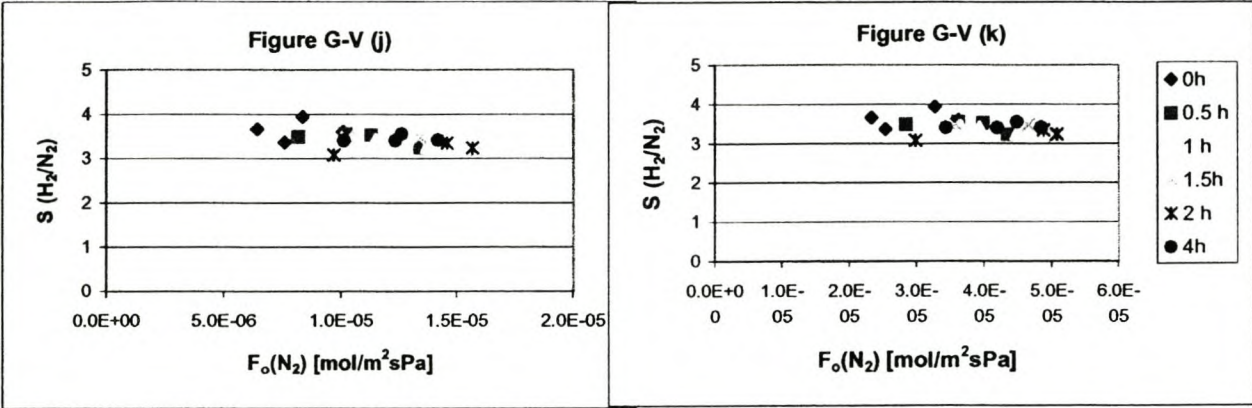
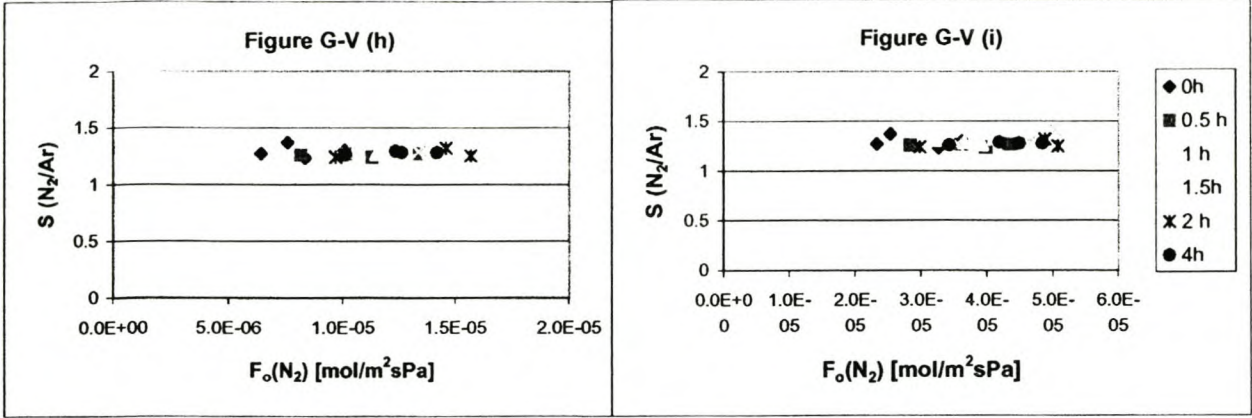
| 1350 | S (H2/Ar) | S (H2/N2) | S (N2/Ar) |
|----------|-----------|-----------|-----------|
| 32c | 4.3 | 3.43 | 1.25 |
| 34b | 4.21 | 3.31 | 1.27 |
| average: | 4.26 | 3.37 | 1.26 |

| 1400 | S (H2/Ar) | S (H2/N2) | S (N2/Ar) |
|----------|-----------|-----------|-----------|
| 57a | 4.19 | 3.37 | 1.24 |
| 57d | 4.26 | 3.3 | 1.29 |
| 57e | 4.39 | 3.48 | 1.26 |
| 57f | 4.18 | 3.41 | 1.23 |
| Average: | 4.26 | 3.39 | 1.26 |

| | S (H2/Ar) | S (H2/N2) | S (N2/Ar) |
|------|-----------|-----------|-----------|
| 1300 | 4.38 | 3.38 | 1.29 |
| 1350 | 4.26 | 3.37 | 1.26 |
| 1400 | 4.26 | 3.39 | 1.26 |



Ideal selectivities of each membrane plotted against the individual permeabilities



G-VI: Gas Permeability Coefficient Results

| t [h] | T [oC] | membrane | K H2 | K N2 | K Ar |
|-------|--------|----------|-----------|-----------|-----------|
| 0 | 1300 | | | | |
| | | 53d | 6.132E-15 | 3.609E-15 | 3.563E-15 |
| | | 54 | 7.347E-15 | 4.304E-15 | 4.186E-15 |
| | | 56a | 5.750E-15 | 3.532E-15 | 3.343E-15 |
| | | 56c | 6.614E-15 | 3.611E-15 | 3.730E-15 |
| | | average: | 6.46E-15 | 3.76E-15 | 3.71E-15 |
| 0.5 | 1300 | | | | |
| | | 38b | 8.519E-15 | 5.235E-15 | 5.217E-15 |
| | | 38c | 9.623E-15 | 6.323E-15 | 6.342E-15 |
| | | 39a | 5.582E-15 | 3.303E-15 | 3.340E-15 |
| | | 40 | 6.401E-15 | 3.944E-15 | 4.244E-15 |
| | | average: | 7.53E-15 | 4.70E-15 | 4.79E-15 |
| 1 | 1300 | | | | |
| | | 21 | 1.075E-14 | 6.617E-15 | 6.626E-15 |
| | | 24a | | | |
| | | 24b | 6.653E-15 | 4.180E-15 | 4.180E-15 |
| | | 28a | 6.964E-15 | 4.321E-15 | 4.074E-15 |
| | | 51a | 7.697E-15 | 4.753E-15 | 4.754E-15 |
| | | 51b | 6.907E-15 | 4.182E-15 | 4.020E-15 |
| | | 53a | 8.620E-15 | 5.309E-15 | 5.265E-15 |
| | | 53c | 7.936E-15 | 4.731E-15 | 4.604E-15 |
| | | average: | 7.93E-15 | 4.87E-15 | 4.79E-15 |
| 1.5 | 1300 | | | | |
| | | 42 | 7.392E-15 | 4.396E-15 | 4.378E-15 |
| | | 44 | 7.445E-15 | 4.597E-15 | 4.628E-15 |
| | | 45 | 8.161E-15 | 5.121E-15 | 4.743E-15 |
| | | average: | 7.67E-15 | 4.71E-15 | 4.58E-15 |
| 2 | 1300 | | | | |
| | | 36a | 1.004E-14 | 6.221E-15 | 6.112E-15 |
| | | 36d | 4.836E-15 | 2.977E-15 | 2.972E-15 |
| | | 37a | 9.018E-15 | 5.815E-15 | 5.782E-15 |
| | | average: | 7.97E-15 | 5.00E-15 | 4.96E-15 |

| t [h] | T [oC] | membrane | K H2 | K N2 | K Ar |
|--------------|----------|-------------|---------------------|---------------------|------------|
| 4 | 1300 | | | | |
| | | 46a | 8.551E-15 | 5.031E-15 | 5.011E-15 |
| | | 46b | 9.422E-15 | 5.779E-15 | 5.751E-15 |
| | | 47 | 8.125E-15 | 4.955E-15 | 4.934E-15 |
| | | 49 | 7.053E-15 | 4.423E-15 | 4.445E-15 |
| | average: | 8.29E-15 | 5.05E-15 | 5.04E-15 | |
| 1 | 1350 | | | | |
| | | 32c | 1.035E-14 | 6.398E-15 | 6.504E-15 |
| | | 34b | 1.117E-14 | 7.053E-15 | 7.037E-15 |
| | | average: | 1.08E-14 | 6.73E-15 | 6.77E-15 |
| 1 | 1400 | | | | |
| | | 57a | 8.273E-15 | 5.069E-15 | 5.120E-15 |
| | | 1.5 min 57d | 1.051E-14 | 6.530E-15 | 6.455E-15 |
| | | 2 min 57e | 9.534E-15 | 5.961E-15 | 5.928E-15 |
| | | 57f | 9.913E-15 | 6.112E-15 | 6.180E-15 |
| | | average: | 9.56E-15 | 5.92E-15 | 5.92E-15 |
| Averages: | | | K (H ₂) | K (N ₂) | K (Ar) |
| @ 1300 oC | 0 h | | 6.46E-15 | 3.76E-15 | 3.71E-15 |
| | 0.5 h | | 7.53E-15 | 4.70E-15 | 4.79E-15 |
| | 1 h | | 7.93E-15 | 4.87E-15 | 4.79E-15 |
| | 1.5 h | | 7.67E-15 | 4.71E-15 | 4.58E-15 |
| | 2 h | | 7.97E-15 | 5.00E-15 | 4.96E-15 |
| | 4 h | | 8.29E-15 | 5.05E-15 | 5.04E-15 |
| | | | K (H ₂) | K (N ₂) | K (Ar) |
| 1h @ 1300 oC | 1300 | | 7.93E-15 | 4.87E-15 | 4.79E-15 |
| 1h @ 1350 oC | 1350 | | 1.08E-14 | 6.73E-15 | 6.77E-15 |
| 1h @ 1400 oC | 1400 | | 9.56E-15 | 5.92E-15 | 5.92E-15 |
| | | | K H2 | K N2 | K Ar |
| | | Linkov | 1.461E-15 | 8.21E-16 | 8.3243E-16 |

Figure G-VI (a)

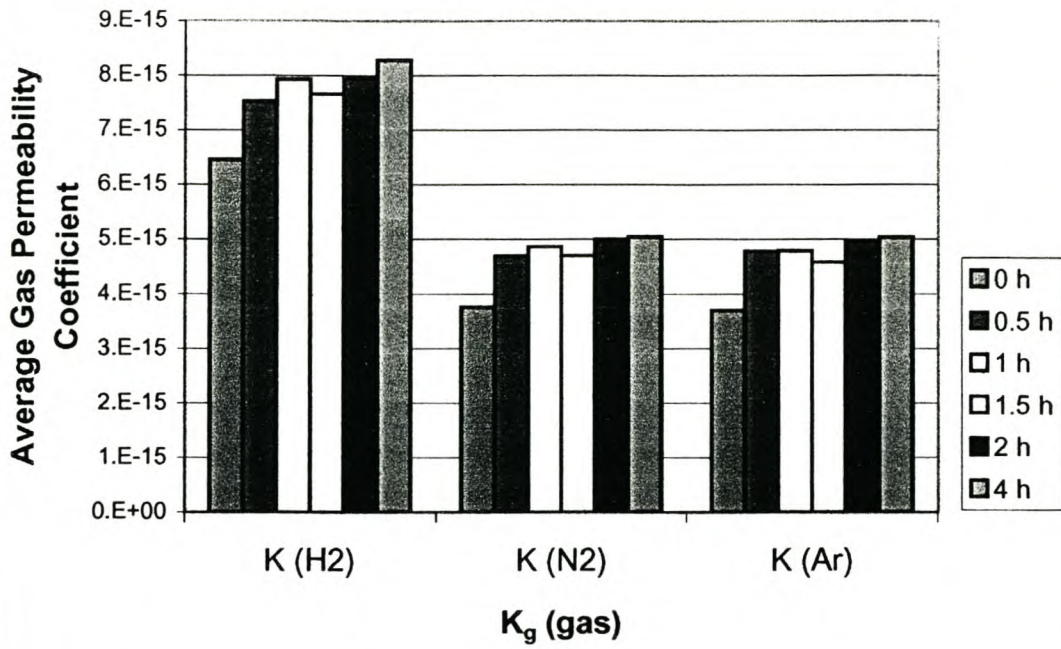
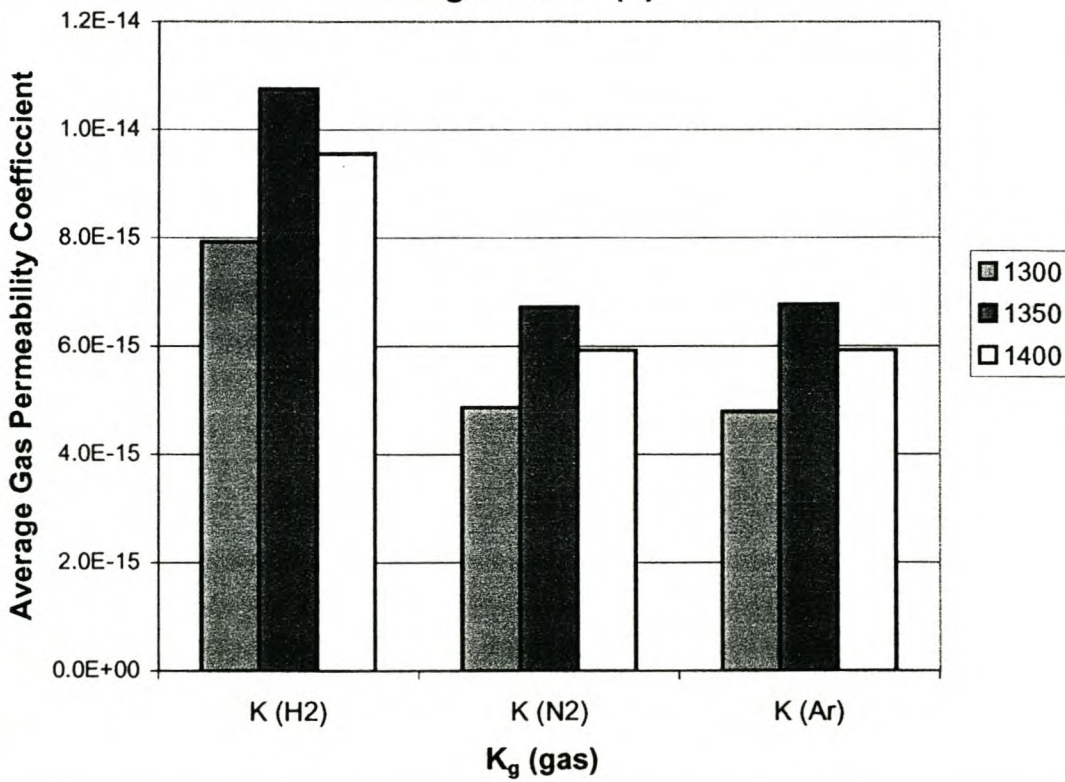


Figure G-VI (b)



Appendix H: Mathematical Derivation of K_l and K_g

Viscous flow of a Newtonian fluid through a cylindrical porous medium can be described by Darcy's law:

$$q = -\frac{k}{\mu} \cdot \frac{dP}{dr} = \frac{Q_m}{\rho} = \frac{\dot{m}}{A \cdot \rho} \quad (\text{H.1})$$

assumptions: - force fields such as gravity are neglected, and
- A uni-directional pressure gradient is assumed

This equation is valid for compressible as well as incompressible media.

Viscous flow through a porous medium starts with the equation of continuity and the equations of motion. When a stationary situation is assumed and the accumulation term neglected, for a cylindrical geometry this translates to:

$$\frac{d}{dr}(r \cdot Q_m) = 0 = \frac{d}{dr}\left(r \cdot \frac{\dot{m}}{A}\right) \quad (\text{H.2})$$

The area of a cylinder is: $A = 2\pi rH$, so

$$Q_m = \frac{\dot{m}}{A} = \frac{\dot{m}}{2 \cdot \pi \cdot r \cdot H} \quad (\text{H.3})$$

Substituting equation (H.3) into equation (H.1):

$$q = \frac{Q_m}{\rho} = -\frac{k}{\mu} \cdot \frac{dP}{dr} \quad (\text{H.4})$$

which becomes:

$$Q_m = -\frac{k \cdot \rho}{\mu} \cdot \frac{dP}{dr} \quad (\text{H.5})$$

Substituting equation (H.3) into equation (H.5):

$$\dot{m} = -\frac{k \cdot \rho \cdot 2 \cdot \pi \cdot H}{\mu} \cdot r \frac{dP}{dr} \quad (\text{H.6})$$

which becomes:

$$dP = -\frac{\dot{m} \cdot \mu}{k \cdot \rho \cdot 2 \cdot \pi \cdot H} \cdot \frac{dr}{r} \quad (\text{H.7})$$

Equation (H.7) is integrated between the inside of the membrane, where $r = r_1$ and $P = P_1$ and the outside of the membrane where $r = r_2$ and $P = P_2$ as follows:

$$\int_{P_1}^{P_2} (dP) = -\frac{\dot{m} \cdot \mu}{k \cdot \rho \cdot 2 \cdot \pi \cdot H} \int_{r_1}^{r_2} \left(\frac{1}{r} dr \right) \quad (\text{H.8})$$

which becomes:

$$[P]_{r_1}^{r_2} = -\frac{\dot{m} \cdot \mu}{k \cdot \rho \cdot 2 \cdot \pi \cdot H} [\ln(r)]_{r_1}^{r_2} \quad (\text{H.9})$$

$$(P_2 - P_1) = -\Delta P = -\frac{\dot{m} \cdot \mu}{k \cdot \rho \cdot 2 \cdot \pi \cdot H} \cdot (\ln(r_2) - \ln(r_1)) \quad (\text{H.10})$$

Which is:

$$\Delta P = \frac{\dot{m} \cdot \mu}{k \cdot \rho \cdot 2 \cdot \pi \cdot H} \cdot \ln\left(\frac{r_2}{r_1}\right) \quad (\text{H.11})$$

For a liquid, the dependence of density, ρ , and viscosity, μ , on pressure is minor and therefore neglected. After rearrangement of equation (H.11), the liquid permeability coefficient is thus expressed as follows:

$$K_l = \frac{\dot{m} \cdot \mu \cdot \ln\left(\frac{r_2}{r_1}\right)}{\rho \cdot 2 \cdot \pi \cdot H \cdot \Delta P} \quad (\text{H.12})$$

For a gas, i , which is a compressible medium, the density, ρ , is a function of pressure and after implementation of the ideal gas law:

$$\rho_i = \frac{P_m \cdot M_i}{R \cdot T} \quad (\text{H.13})$$

From the kinetic gas law it follows that the viscosity, μ , is independent of pressure for an ideal gas, while for a real gas, μ depends weakly on pressure for $P < 0.2 P_{\text{critical}}$. The viscosity of the gas is therefore considered independent of the pressure. Equation (H.13) is thus substituted into equation (H.11) and rearranged to obtain the following expression for the gas permeability coefficient:

$$K_g = \frac{\dot{m} \cdot \mu \cdot \ln\left(\frac{r_2}{r_1}\right) \cdot R \cdot T}{2 \cdot \pi \cdot H \cdot \Delta P \cdot P_m \cdot M_i} \quad (\text{H.14})$$

These equations, (H.12) and (H.14), are for viscous flow through a material with a constant permeability coefficient throughout and consisting of a single layer. The flow through an asymmetric membrane (consisting of several layers) is calculated likewise resulting in a "resistance-in-series" expression [Biesheuvel and Verweij, 1999]. Because the thicknesses of the "several layers" are not unknown and are impossible to obtain in case of the manufactured membranes, equation (H.12) and (H.14) are used as they are.

Water Permeability Results for Membrane 38b

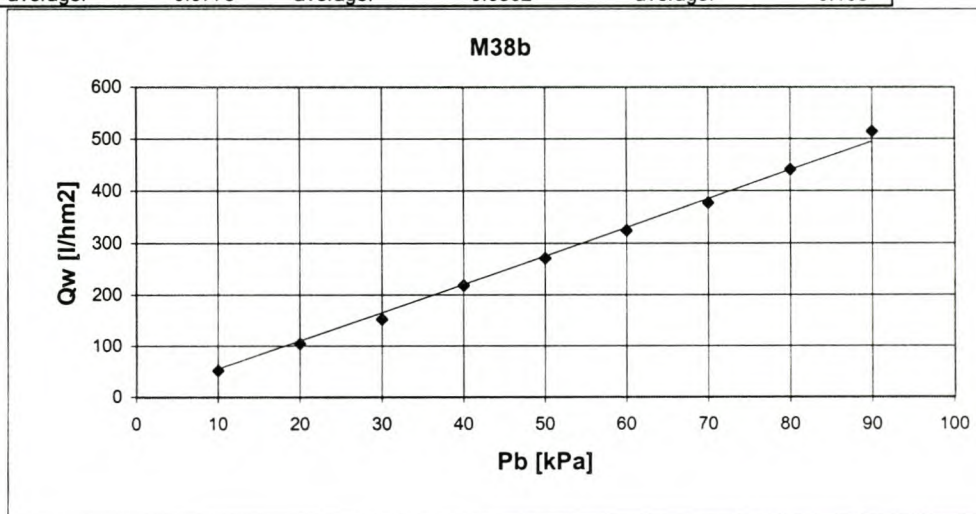
| P= 10 kPa | | | P= 20 kPa | | | P= 30 kPa | | | P= 40 kPa | | |
|-----------|------|--------|-----------|------|--------|-----------|------|--------|-----------|------|--------|
| t | m | m | t | m | m | t | m | m | t | m | m |
| [s] | [g] | [g/s] | [s] | [g] | [g/s] | [s] | [g] | [g/s] | [s] | [g] | [g/s] |
| 30.28 | 0.27 | 0.0089 | 30.25 | 0.62 | 0.0205 | 30.23 | 0.89 | 0.0294 | 30.1 | 1.3 | 0.0432 |
| 60.25 | 0.6 | 0.0100 | 60.28 | 1.23 | 0.0204 | 60.07 | 1.83 | 0.0305 | 60.23 | 2.66 | 0.0442 |
| 90.28 | 0.93 | 0.0103 | 90.25 | 1.89 | 0.0209 | 90.13 | 2.78 | 0.0308 | 90.13 | 4.02 | 0.0446 |
| 120.28 | 1.26 | 0.0105 | 120.31 | 2.56 | 0.0213 | 120.13 | 3.74 | 0.0311 | 120.07 | 5.37 | 0.0447 |
| 150.25 | 1.59 | 0.0106 | 150.07 | 3.22 | 0.0215 | 150.17 | 4.68 | 0.0312 | 150.19 | 6.73 | 0.0448 |
| 180.25 | 1.93 | 0.0107 | 180.29 | 3.87 | 0.0215 | 180.29 | 5.66 | 0.0314 | 180.31 | 8.06 | 0.0447 |
| average: | | 0.0106 | average: | | 0.0214 | average: | | 0.0312 | average: | | 0.0447 |

| P= 50 kPa | | | P= 60 kPa | | | P= 70 kPa | | | P= 80 kPa | | | P= 90 kPa | | |
|-----------|-------|--------|-----------|-------|--------|-----------|-------|--------|-----------|-------|--------|-----------|-------|-------|
| t | m | m | t | m | m | t | m | m | t | m | m | t | m | m |
| [s] | [g] | [g/s] | [s] | [g] | [g/s] | [s] | [g] | [g/s] | [s] | [g] | [g/s] | [s] | [g] | [g/s] |
| 30.17 | 1.65 | 0.0547 | 30.28 | 1.88 | 0.0621 | 30.29 | 2.28 | 0.0753 | 30.19 | 2.77 | 0.0918 | 30.28 | 3.21 | 0.106 |
| 60.17 | 3.35 | 0.0557 | 60.37 | 3.82 | 0.0633 | 60.14 | 4.62 | 0.0768 | 60.17 | 5.48 | 0.0911 | 60.25 | 6.37 | 0.106 |
| 90.17 | 5.01 | 0.0556 | 90.28 | 5.79 | 0.0641 | 90.2 | 6.95 | 0.0771 | 90.1 | 8.19 | 0.0909 | 90.19 | 9.54 | 0.106 |
| 120.23 | 6.65 | 0.0553 | 120.22 | 7.82 | 0.0650 | 120.23 | 9.28 | 0.0772 | 120.26 | 10.83 | 0.0901 | 120.13 | 12.65 | 0.105 |
| 150.17 | 8.32 | 0.0554 | 150.28 | 10.03 | 0.0667 | 150.14 | 11.59 | 0.0772 | 150.23 | 13.53 | 0.0901 | 150.19 | 15.78 | 0.105 |
| 180.3 | 10.08 | 0.0559 | 180.31 | 12.2 | 0.0677 | 180.47 | 14 | 0.0776 | 180.11 | 16.28 | 0.0904 | 180.61 | 18.89 | 0.105 |
| average: | | 0.0555 | average: | | 0.0665 | average: | | 0.0773 | average: | | 0.0902 | average: | | 0.105 |

Membrane: 38b

| | |
|----------------|---------------------------|
| Area: | 0.00074 [m ²] |
| μ | 0.001 [Pas] |
| ρ _w | 998 [kg/m ³] |
| r ₁ | 0.0043 [m] |
| r ₂ | 0.00565 [m] |
| H | 0.0273 [m] |

| P | m | Q _w | K _l | Permeability |
|----------|-------|----------------------|-------------------|--|
| [kPa] | [g/s] | [l/hm ²] | [m ²] | [L/hm ² Pa] [L/hm ² bar] |
| 10 | 0.011 | 51.7 | 1.69E-15 | 0.00517 516.8 |
| 20 | 0.021 | 104.4 | 1.71E-15 | 0.00522 522.2 |
| 30 | 0.031 | 152.4 | 1.66E-15 | 0.00508 508.1 |
| 40 | 0.045 | 218.2 | 1.78E-15 | 0.00546 545.5 |
| 50 | 0.056 | 271.1 | 1.77E-15 | 0.00542 542.2 |
| 60 | 0.066 | 324.5 | 1.77E-15 | 0.00541 540.8 |
| 70 | 0.077 | 377.0 | 1.76E-15 | 0.00539 538.6 |
| 80 | 0.090 | 440.1 | 1.80E-15 | 0.00550 550.1 |
| 90 | 0.105 | 514.5 | 1.87E-15 | 0.00572 571.7 |
| average: | | | 1.76E-15 | average: 537.4 |



Water Permeability Results for Membrane 53a

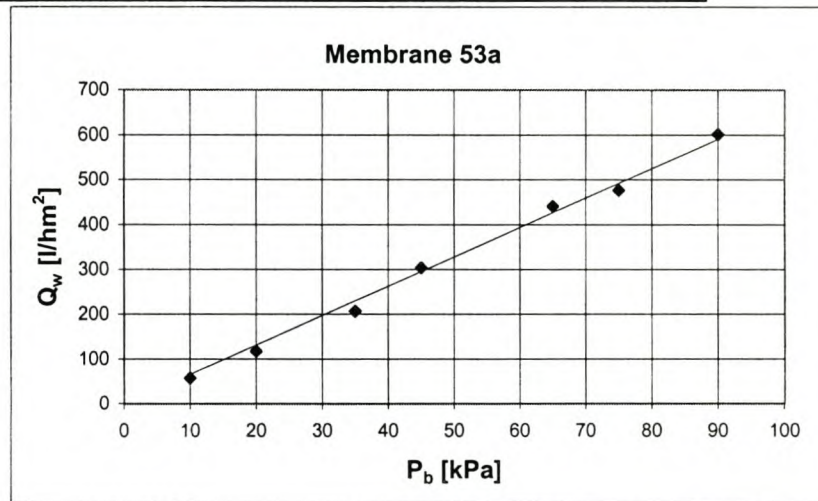
| P= 10 kPa | | | P= 20 kPa | | | P= 35 kPa | | |
|-----------------|------|--------|-----------------|------|--------|-------------------|-------|--------|
| t | m | m | t | m | m | t | m | m |
| [s] | [g] | [g/s] | [s] | [g] | [g/s] | [s] | [g] | [g/s] |
| 30.17 | 0.47 | 0.0156 | 30.3 | 0.98 | 0.0323 | 30.02 | 1.78 | 0.0593 |
| 60.17 | 0.98 | 0.0163 | 60.18 | 2.04 | 0.0339 | 60.27 | 3.61 | 0.0599 |
| 90.27 | 1.49 | 0.0165 | 90.9 | 3.1 | 0.0341 | 90.33 | 5.48 | 0.0607 |
| 120.2 | 2.03 | 0.0169 | 120.21 | 4.16 | 0.0346 | 120.83 | 7.36 | 0.0609 |
| 150.11 | 2.55 | 0.0170 | 150.21 | 5.18 | 0.0345 | 150.23 | 9.12 | 0.0607 |
| 180.3 | 3.11 | 0.0172 | 180.4 | 6.28 | 0.0348 | 180.09 | 10.98 | 0.0610 |
| average: 0.0169 | | | average: 0.0345 | | | average: 0.060814 | | |

| P= 45 kPa | | | P= 65 kPa | | | P= 75 kPa | | | P= 90 kPa | | |
|-----------------|-------|--------|-----------------|-------|--------|-------------------|-------|--------|----------------|-------|--------|
| t | m | m | t | m | m | t | m | m | t | m | m |
| [s] | [g] | [g/s] | [s] | [g] | [g/s] | [s] | [g] | [g/s] | [s] | [g] | [g/s] |
| 30.36 | 2.59 | 0.0853 | 30.13 | 3.85 | 0.1278 | 30.26 | 4.32 | 0.1428 | 30.23 | 5.25 | 0.1737 |
| 60.27 | 5.25 | 0.0871 | 60.22 | 7.79 | 0.1294 | 30.31 | 4.2 | 0.1386 | 60.19 | 10.61 | 0.1763 |
| 90.17 | 7.94 | 0.0881 | 90.13 | 11.69 | 0.1297 | 60.22 | 8.41 | 0.1397 | 90.23 | 15.99 | 0.1772 |
| 120.27 | 10.72 | 0.0891 | 120.25 | 15.61 | 0.1298 | 90.22 | 12.68 | 0.1405 | 120.13 | 21.29 | 0.1772 |
| 150.17 | 13.47 | 0.0897 | 150.28 | 19.41 | 0.1292 | 120.09 | 16.86 | 0.1404 | 150.23 | 26.63 | 0.1773 |
| 180.37 | 16.34 | 0.0906 | 180.37 | 23.48 | 0.1302 | 150.07 | 21.03 | 0.1401 | 180.19 | 31.81 | 0.1765 |
| average: 0.0894 | | | average: 0.1297 | | | average: 0.140397 | | | average: 0.177 | | |

Membrane: 53a

Area: 0.00106 [m²]
 μ : 0.001 [Pas]
 ρ_w : 998 [kg/m³]
 r_1 : 0.0047 [m]
 r_2 : 0.0057 [m]
 H : 0.0359 [m]

| P | m | Qw | Kl | Permeability |
|----------|-------|----------------------|-------------------|--|
| [kPa] | [g/s] | [l/hm ²] | [m ²] | [L/hm ² Pa] [L/hm ² bar] |
| 10 | 0.017 | 57.4 | 1.45E-15 | 0.00574 574.1 |
| 20 | 0.035 | 117.2 | 1.48E-15 | 0.00586 585.8 |
| 35 | 0.061 | 206.5 | 1.49E-15 | 0.00590 590.0 |
| 45 | 0.089 | 303.5 | 1.70E-15 | 0.00674 674.4 |
| 65 | 0.130 | 440.5 | 1.71E-15 | 0.00678 677.6 |
| 75 | 0.140 | 476.7 | 1.60E-15 | 0.00636 635.7 |
| 90 | 0.177 | 601.1 | 1.69E-15 | 0.00668 667.9 |
| average: | | | 1.59E-15 | average: 629.4 |



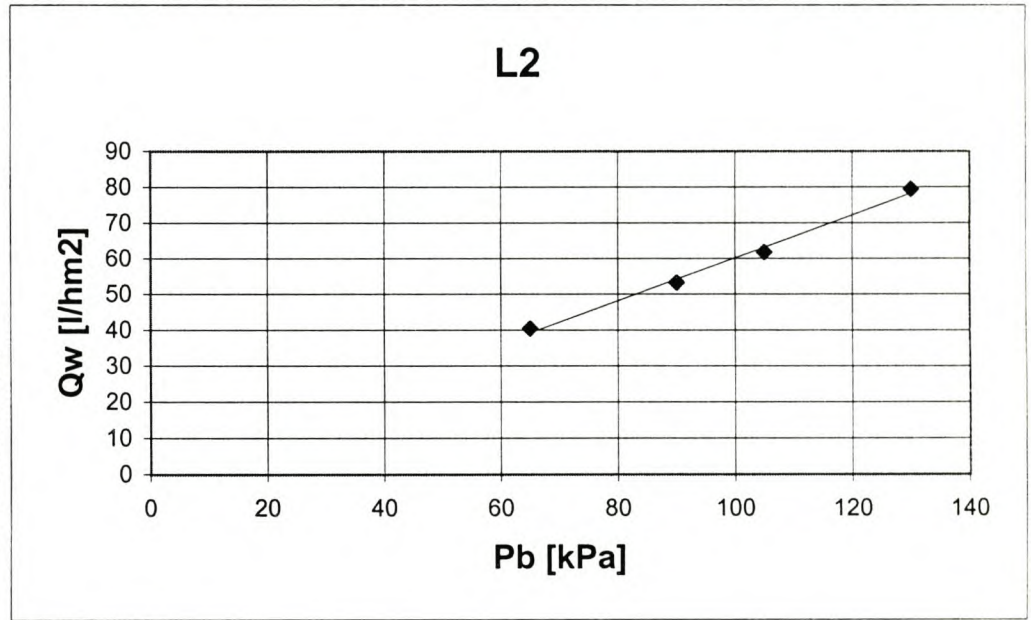
Water Permeability Results for Linkovs Membrane

| P= 65 kPa | | | P= 90 kPa | | | P= 110 kPa | | | P= 130 kPa | | |
|-----------------|------|--------|-------------------|------|--------|-----------------|------|--------|-----------------|------|--------|
| t | m | m | t | m | m | t | m | m | t | m | m |
| [s] | [g] | [g/s] | [s] | [g] | [g/s] | [s] | [g] | [g/s] | [s] | [g] | [g/s] |
| 30.19 | 0.44 | 0.0146 | 30.27 | 0.57 | 0.0188 | 30.17 | 0.67 | 0.0222 | 30.3 | 0.86 | 0.0284 |
| 60.25 | 0.89 | 0.0148 | 60 | 1.15 | 0.0192 | 60.14 | 1.33 | 0.0221 | 60.27 | 1.73 | 0.0287 |
| 90.25 | 1.34 | 0.0148 | 90.29 | 1.8 | 0.0199 | 90.11 | 2.01 | 0.0223 | 90.24 | 2.61 | 0.0289 |
| 120.07 | 1.78 | 0.0148 | 120.27 | 2.33 | 0.0194 | 120.17 | 2.74 | 0.0228 | 120.12 | 3.49 | 0.0291 |
| 150.25 | 2.29 | 0.0152 | 150.23 | 2.92 | 0.0194 | 150.23 | 3.43 | 0.0228 | 150.24 | 4.36 | 0.0290 |
| 210.83 | 3.26 | 0.0155 | 180.97 | 3.58 | 0.0198 | 180.33 | 4.16 | 0.0231 | 180.68 | 5.3 | 0.0293 |
| average: 0.0148 | | | average: 0.019531 | | | average: 0.0226 | | | average: 0.0291 | | |

Membrane: L2

Area: 0.00132 [m²]
 μ 0.001 [Pas]
 ρw 998 [kg/m³]
 r1 0.00525 [m]
 r2 0.006 [m]
 H 0.04 [m]

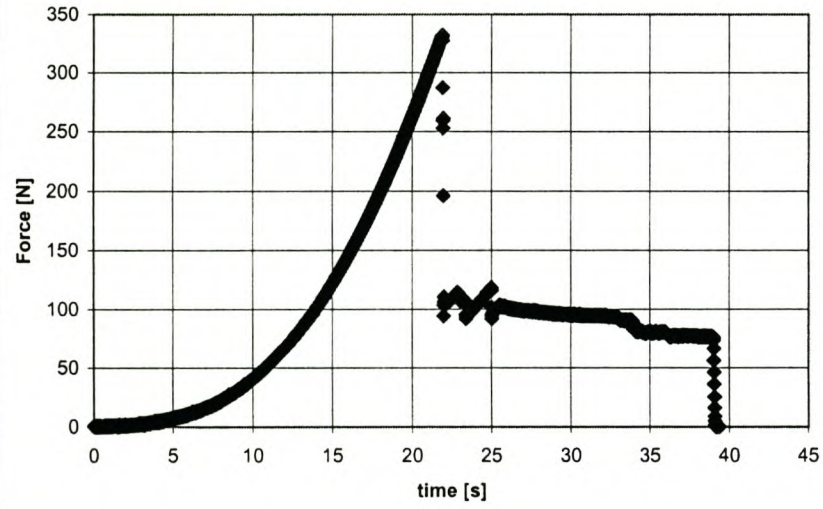
| P | m | Qw | KI | Permeability | |
|-------|--------|----------------------|-------------------|------------------------|-------------------------|
| [kPa] | [g/s] | [l/hm ²] | [m ²] | [L/hm ² Pa] | [L/hm ² bar] |
| 65 | 0.0148 | 40.4 | 1.21E-16 | 0.00062 | 62.2 |
| 90 | 0.0195 | 53.3 | 1.16E-16 | 0.00059 | 59.2 |
| 105 | 0.0226 | 61.8 | 1.15E-16 | 0.00059 | 58.8 |
| 130 | 0.0291 | 79.3 | 1.19E-16 | 0.00061 | 61.0 |
| | | average: | 1.18E-16 | average: | 60.3 |



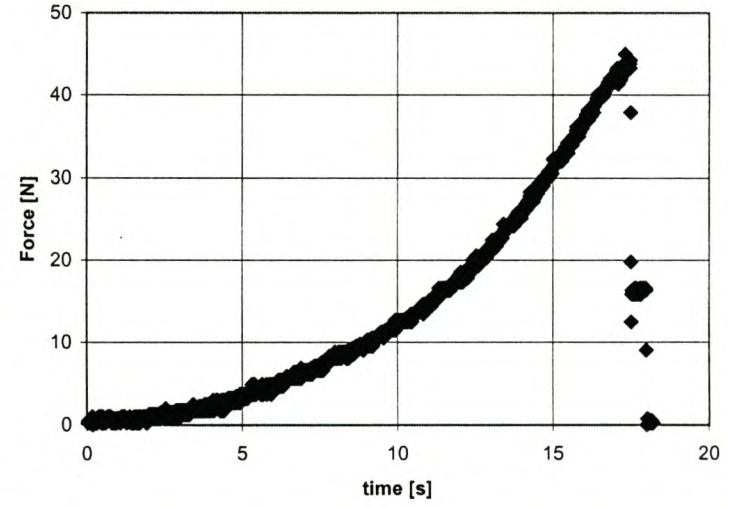
Appendix J: 3-Point Bend Test Results

| Typical Membrane: | | Membrane L2 | | Membrane M24b | | Membrane M46a | | Membrane M54 | |
|----------------------|-----------------------|----------------------|-------------------------|----------------------|-------------------------|----------------------|-------------------------|----------------------|-------------------------|
| d2 | 11 mm | d2 | 10.5 mm | d2 | 11.3 mm | d2 | 11.2 mm | d2 | 11.2 mm |
| d1 | 9 mm | d1 | 9.3 mm | d1 | 9.8 mm | d1 | 9.3 mm | d1 | 7.8 mm |
| r2 | 5.5 mm | r2 | 5.25 mm | r2 | 5.65 mm | r2 | 5.6 mm | r2 | 5.6 mm |
| 1/2 L | 14.5 mm | 1/2 L | 14.5 mm | 1/2 L | 14.5 mm | 1/2 L | 14.5 mm | 1/2 L | 14.5 mm |
| L | 29 mm | L | 29 mm | L | 29 mm | L | 29 mm | L | 29 mm |
| I = | 396.6 mm ⁴ | I = | 229.5 mm ⁴ | I = | 347.6 mm ⁴ | I = | 405.2 mm ⁴ | I = | 590.7 mm ⁴ |
| W = | 72.11 mm ³ | W = | 43.71 mm ³ | W = | 61.52 mm ³ | W = | 72.36 mm ³ | W = | 105.5 mm ³ |
| | | F _{max} = | 323 N | F _{max} = | 44 N | F _{max} = | 43 N | F _{max} = | 68 N |
| | | σ _{max} = | 107.2 N/mm ² | σ _{max} = | 10.37 N/mm ² | σ _{max} = | 8.617 N/mm ² | σ _{max} = | 9.348 N/mm ² |
| σ max | F | σ max | F | σ max | F | σ max | F | σ max | F |
| [N/mm ²] | [N] | [N/mm ²] | [N] | [N/mm ²] | [N] | [N/mm ²] | [N] | [N/mm ²] | [N] |
| 1 | 4.973 | 1 | 3.014 | 1 | 4.243 | 1 | 4.99 | 1 | 7.275 |
| 5 | 24.87 | 5 | 15.07 | 5 | 21.21 | 5 | 24.95 | 5 | 36.37 |
| 10 | 49.73 | 10 | 30.14 | 10 | 42.43 | 10 | 49.9 | 10 | 72.75 |
| 20 | 99.47 | 20 | 60.29 | 20 | 84.86 | 20 | 99.8 | 20 | 145.5 |
| 50 | 248.7 | 50 | 150.7 | 50 | 212.1 | 50 | 249.5 | 50 | 363.7 |
| 60 | 298.4 | 60 | 180.9 | 60 | 254.6 | 60 | 299.4 | 60 | 436.5 |
| 70 | 348.1 | 70 | 211 | 70 | 297 | 70 | 349.3 | 70 | 509.2 |
| 80 | 397.9 | 80 | 241.1 | 80 | 339.4 | 80 | 399.2 | 80 | 582 |
| 100 | 497.3 | 100 | 301.4 | 100 | 424.3 | 100 | 499 | 100 | 727.5 |
| 110 | 547.1 | 110 | 331.6 | 110 | 466.7 | 110 | 548.9 | 110 | 800.2 |

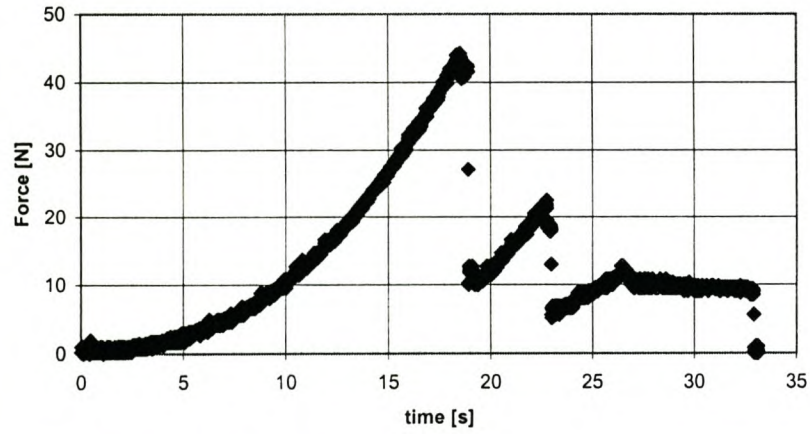
Linkov's Membrane



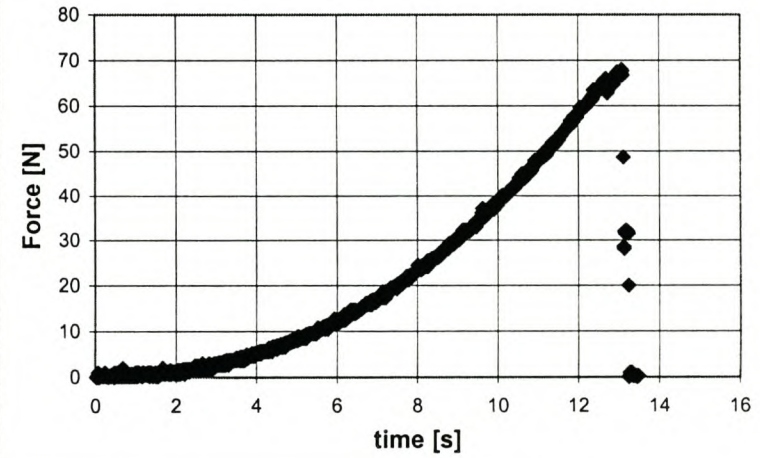
M24b

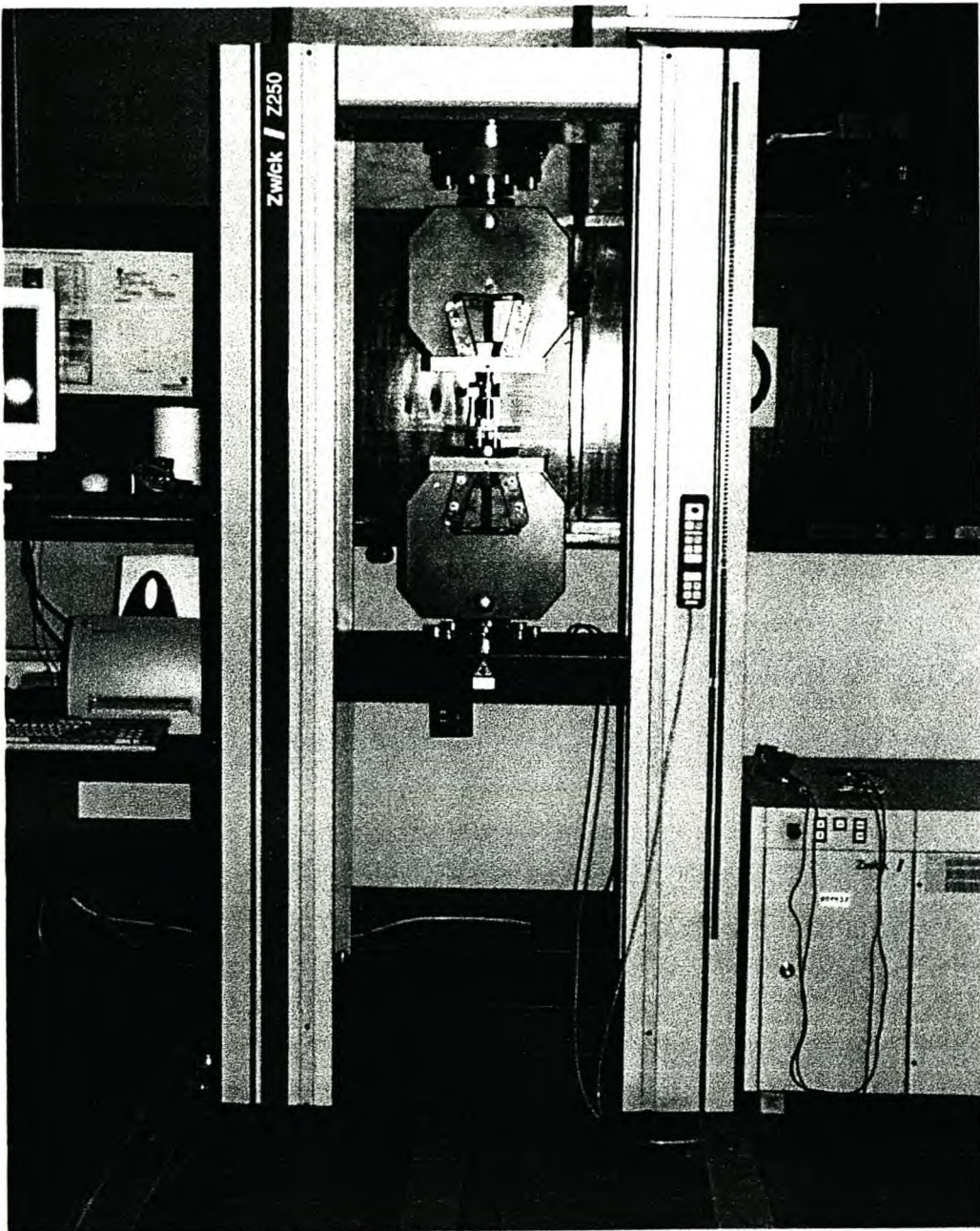


M46a

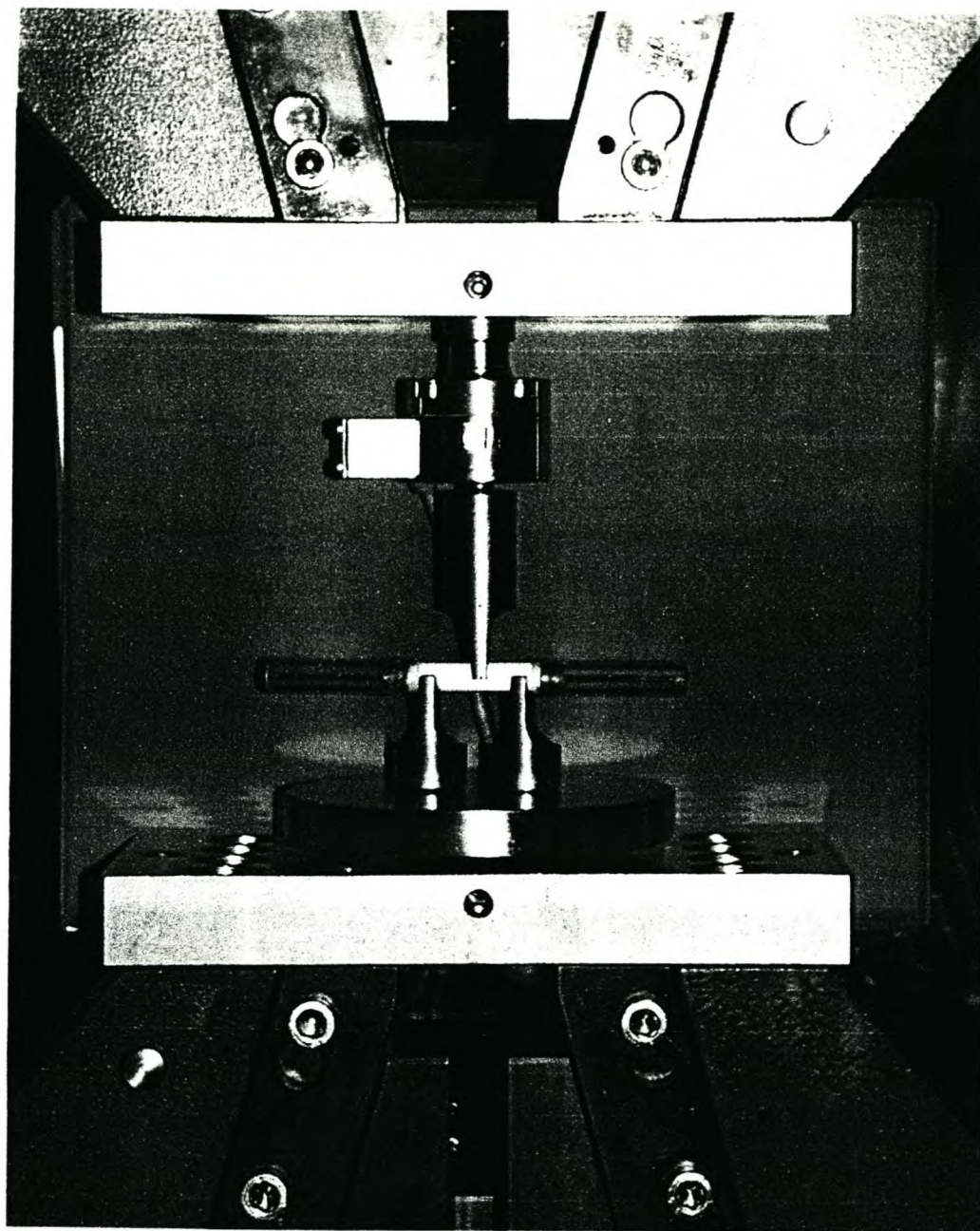


M54





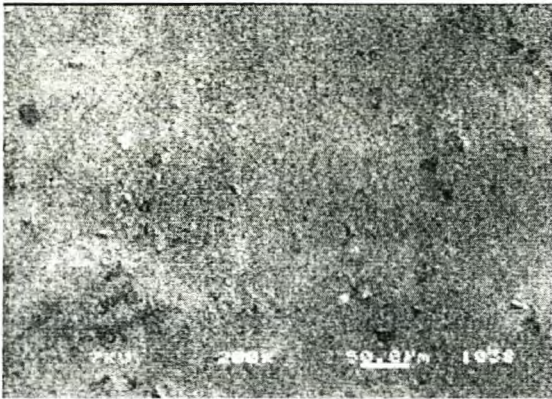
Picture J-1: Picture of the Zwick-bench used for the 3-point bend test. The actual bend test takes place in between the two horizontal bars and is also shown on **picture J-2**, on page J-4.



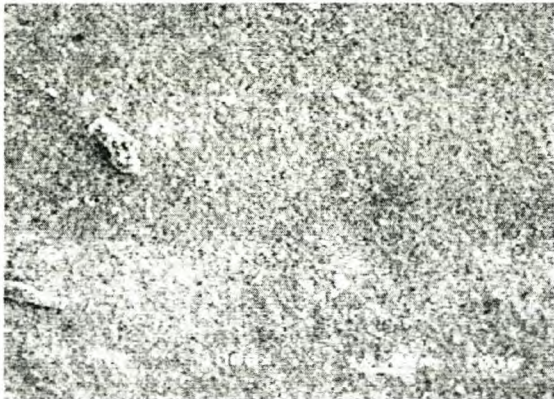
Picture J-2: Close-up picture of the bend test.

Appendix K: Some SEM Results

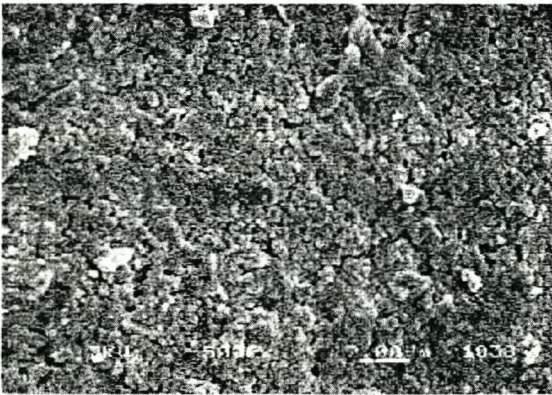
Membrane: Linkov, inside



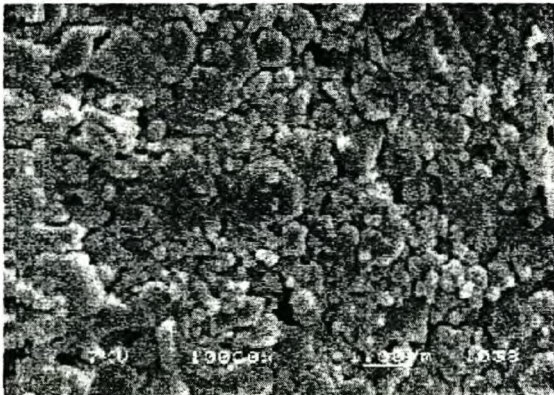
Bar = 50 micrometer



Bar = 10 micrometer

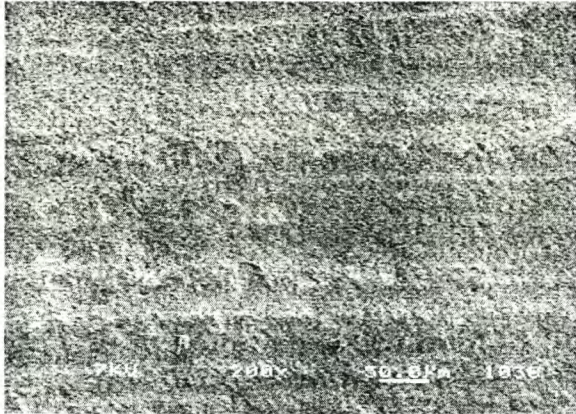


Bar = 2 micrometer



Bar = 1 micrometer

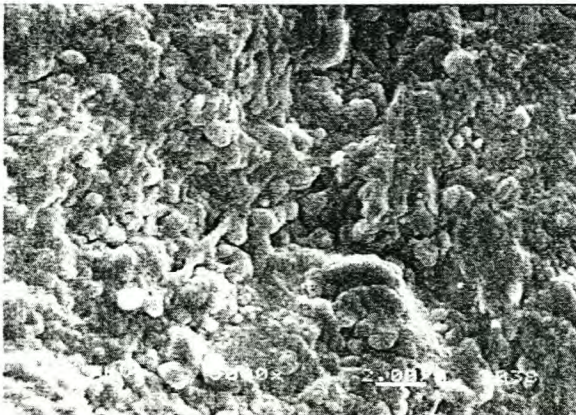
Membrane: Linkov, outside



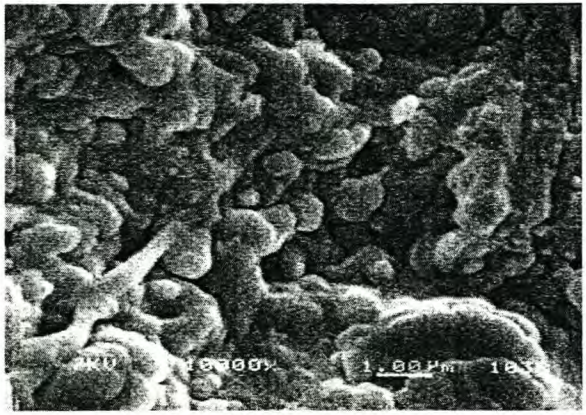
Bar = 50 micrometer



Bar = 10 micrometer

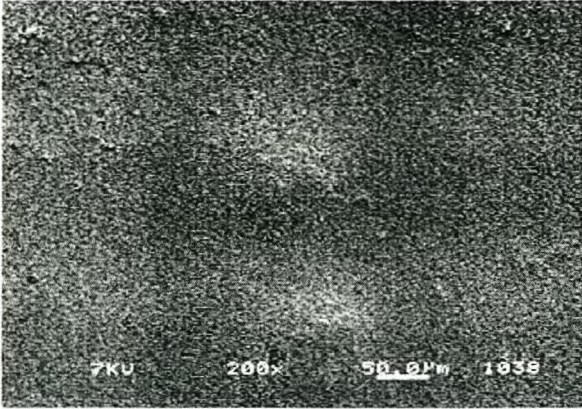


Bar = 2 micrometer

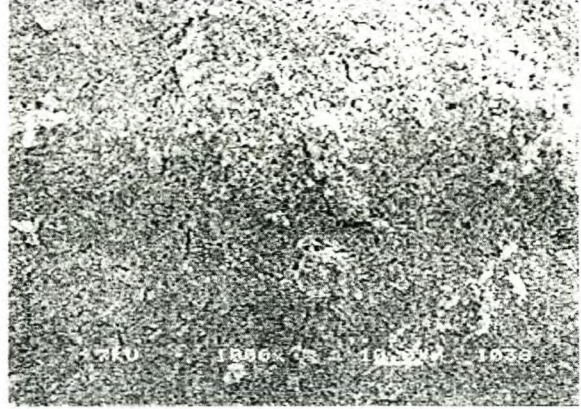


Bar = 1 micrometer

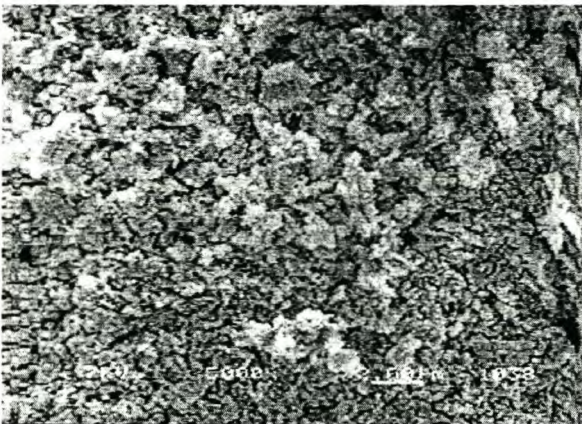
Membrane: M24b, inside



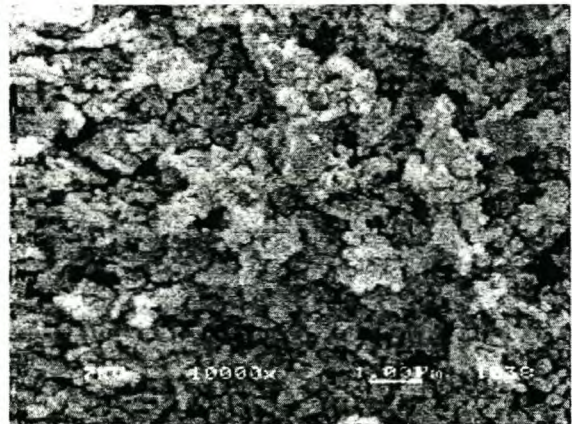
Bar = 50 micrometer



Bar = 10 micrometer



Bar = 2 micrometer



Bar = 1 micrometer

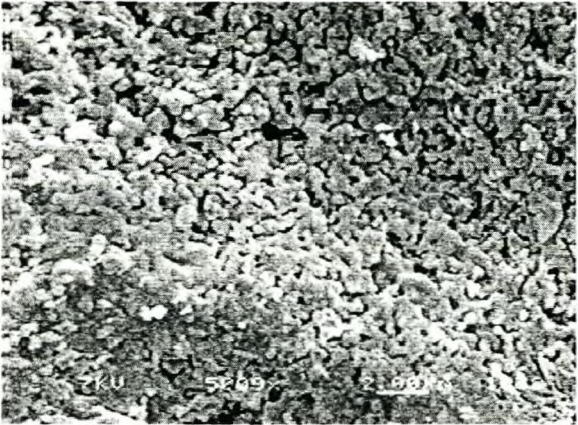
Membrane: M24b, outside



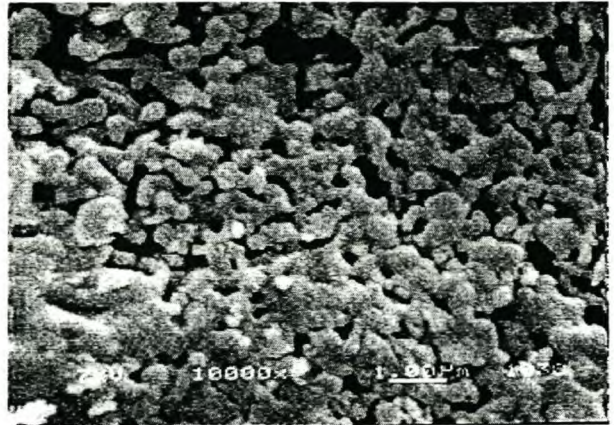
Bar = 50 micrometer



Bar = 10 micrometer



Bar = 2 micrometer



Bar = 1 micrometer

